RD&E CENTER

Technical Report

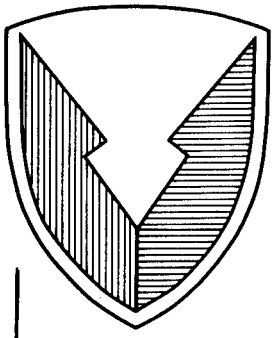

No. 13437

DEVELOPMENT OF DRIVER/VEHICLE STEERING INTERACTION MODELS FOR DYNAMIC ANALYSIS

CONTRACT DAAE07-85-C-R069

DECEMBER 1988

By Charles C. MacAdam
University of Michigan
Transportation Research Institute
2901 Baxter Road
Ann Arbor, MI 48109

U.S. ARMY TANK-AUTOMOTIVE COMMAND
RESEARCH, DEVELOPMENT & ENGINEERING CENTER
Warren, Michigan 48397-5000

NOTICES

This report is not to be construed as an official Department of the Army position.

Mention of any trade names or manufacturers in this report shall not be construed as an official endorsement or approval of such products or companies by the U. S. Government.

Destroy this report when it is no longer needed. Do not return it to the originator.

UMTRI The University of Michigan
Transportation Research Institute
2901 Baxter Road, Ann Arbor, Michigan 48109-2150

May 16, 1989

Commander
U.S. Army Tank-Automotive Command
ATTN: AMSTA-DDL (Technical Library)
Warren, MI 48397-5000

Subj: Development of Driver/Vehicle Steering Interaction Model for Dynamic Analysis, DAAE07-85-C-R069

Please find enclosed 14 copies of the final technical report for the subject contract. Two of the enclosed copies are for the TACOM Technical Library. Per instructions, the remaining copies are to be forwarded by you to:

Commander
Defense Technical Information Center
Bldg. 5, Cameron Station
ATTN: DDAC
Alexandria, Virginia 22304-9990

Thank you for your assistance.

Sincerely yours,

Charles C. MacAdam
Project Director

Enclosure

UNCLASSIFIED
SECURITY CLASSIFICATION OF THIS PAGE

REPORT DOCUMENTATION PAGE

Form Approved
OMB No. 0704-0188
Exp. Date: Jun 30, 1986

1a. REPORT SECURITY CLASSIFICATION	1b. RESTRICTIVE MARKINGS None
2a. SECURITY CLASSIFICATION AUTHORITY	3. DISTRIBUTION / AVAILABILITY OF REPORT Approved for public release. Distribution is unlimited.
2b. DECLASSIFICATION / DOWNGRADING SCHEDULE	
4. PERFORMING ORGANIZATION REPORT NUMBER(S) UMTRI-88-53	5. MONITORING ORGANIZATION REPORT NUMBER(S) 13437
6a. NAME OF PERFORMING ORGANIZATION The University of Michigan Transportation Research Instit.	6b. OFFICE SYMBOL (If applicable) UMTRI
	7a. NAME OF MONITORING ORGANIZATION U.S. Army Tank-Automotive Command
6c. ADDRESS (City, State, and ZIP Code) 2901 Baxter Road Ann Arbor, Michigan 48109	7b. ADDRESS (City, State, and ZIP Code) Warren, Michigan 48397-5000
8a. NAME OF FUNDING / SPONSORING ORGANIZATION	8b. OFFICE SYMBOL (If applicable)
	9. PROCUREMENT INSTRUMENT IDENTIFICATION NUMBER DAAE07-85-C-R069
8c. ADDRESS (City, State, and ZIP Code)	10. SOURCE OF FUNDING NUMBERS

PROGRAM ELEMENT NO.	PROJECT NO.	TASK NO.	WORK UNIT ACCESSION NO.

11. TITLE (Include Security Classification)
Development of Driver/Vehicle Steering Interaction Models for Dynamic Analysis. Final Technical Report.

12. PERSONAL AUTHOR(S)
MacAdam, Charles C.

13a. TYPE OF REPORT	13b. TIME COVERED	14. DATE OF REPORT (Year, Month, Day)	15. PAGE COUNT
Final	FROM 85 June TO 88 Nov	1988 December	290

16. SUPPLEMENTARY NOTATION

17. COSATI CODES			18. SUBJECT TERMS (Continue on reverse if necessary and identify by block number)
FIELD	GROUP	SUB-GROUP	Driver Model, Closed-Loop, Preview, Steering Control, Driver, Vehicle Dynamics, Directional Control, Braking Control, Man-Machine, Path Following, Simulation, Driver-Vehicle, (cont)

19. ABSTRACT (Continue on reverse if necessary and identify by block number)

This document reports on the development of a computer-based model of driver steering control which can be used to represent and predict realistic steering responses of human operators during path-following and obstacle-avoidance maneuvers. The model is intended to be used for controlling different types of land vehicles over a range of operating conditions. The model was validated through direct comparison with experimental measurements of driver-vehicle systems collected during this study. For conventional steering maneuvers, the model was shown capable of replicating most observed steering control behavior patterns through simple adjustment of two basic parameters. In addition, a set of special tests, conducted under unusual nonlinear operating conditions, produced new experimental results showing how drivers can stabilize and control vehicles operating beyond conventional boundaries ordinarily used to define the limits of vehicle directional stability.

20. DISTRIBUTION / AVAILABILITY OF ABSTRACT	21. ABSTRACT SECURITY CLASSIFICATION
☐ UNCLASSIFIED/UNLIMITED ☐ SAME AS RPT. ☐ DTIC USERS	Unclassified

22a. NAME OF RESPONSIBLE INDIVIDUAL	22b. TELEPHONE (Include Area Code)	22c. OFFICE SYMBOL
Mr. James Aardema / Dr. Roger Wehage	(313) 574-8680	AMSTA-RYA

DD FORM 1473, 84 MAR 83 APR edition may be used until exhausted. All other editions are obsolete.

SECURITY CLASSIFICATION OF THIS PAGE
UNCLASSIFIED

Block 18 (continued): Vehicle, Measurement, Human Operator, Bifurcation, Optimal Control, Handling, Braking, Dynamics.

PREFACE

The author gratefully acknowledges the assistance and cooperation of several key people who contributed to the success and support of this work. Mr. Michael Campbell of UMTRI deserves special credit for his technical expertise and strong contributions to the test program conducted during this project. Mr. Campbell not only served as the principal test driver during that program, but also supervised the technical aspects and instrumentation of the HMMWV and trailer test vehicles. Mr. Campbell also assisted in the data processing activities and acted as chief liaison with the Chrysler Proving Grounds staff. His cooperative efforts are greatly appreciated.

At TACOM, the cooperation and support of Mr. Cedric Mousseau, Dr. Roger Wehage, and Mr. James Aardema are gratefully acknowledged. Mr. Mousseau served as the primary technical representative for most of the project. Dr. Wehage and Mr. Aardema served in this same capacity during alternate periods. Messrs. Mousseau and Aardema provided the principal support for interfacing the developed driver model within the DADS simulation model at TACOM.

An unexpected but interesting development during the course of this project was the establishment of frequent cooperative efforts between the staff members at UMTRI and TACOM, not only on a level of technical exchange, but also on levels of mutual professional interest as well. A transfer of technology and expertise has flowed in both directions during this project, covering such topics as vehicle dynamics, field testing practices, and specialized vehicle simulation programs, with both organizations having benefited.

TABLE OF CONTENTS

Section		Page
1.0.	INTRODUCTION	15
2.0.	OBJECTIVE	15
3.0.	CONCLUSIONS	16
4.0.	RECOMMENDATIONS	17
5.0.	DISCUSSION	19
5.1.	Background and Overview	19
5.2.	The Preview Model Concept	23
5.3.	The Preview Model vs. Experimental Observations of Man/Machine Systems	24
5.4.	Mathematical Formulation of the Preview Control Model	27
5.5.	Application of the Preview Control Model to Steering of Basic Land Vehicles	36
5.6.	Driver / Vehicle Tests	57
5.6.1.	Inertial Parameter Measurements	57
5.6.2.	Tire Measurements	57
5.6.3.	HMMWV Test Maneuvers	63
5.6.4.	Data Acquisition Equipment	77
5.6.5.	Vehicle/Driver Measurements	77
5.7.	Driver Model Validation	79

Section **Page**

5.8. Implementation of the Driver Model in DADS 108

5.9. Path Planning and Obstacle Detection Algorithm 120

5.10. Driver Model Option for Closed-Loop Braking.....132

5.10.1. Closed-Loop Brake Application Strategy 132

5.10.2. Closed-Loop Brake Release Strategy.....137

LIST OF REFERENCES.....141

APPENDIX A. ARTICULATED VEHICLE EQUATIONS.....A-1

APPENDIX B. HMMWV TEST DATA.....B-1

APPENDIX C. HMMWV-TRAILER TEST DATA C-1

APPENDIX D. FORTRAN DRIVER MODEL SOURCE CODE.....D-1

APPENDIX E. FORTRAN DADS / DRIVER MODEL INTERFACE CODE E-1

APPENDIX F. PATH PLANNING / OBSTACLE DETECTION CODE F-1

APPENDIX G. BACKGROUND REFERENCES.....G-1

DISTRIBUTION LIST Dist-1

LIST OF ILLUSTRATIONS

Figure	Title	Page
Figure 5-1.	Driver Control Strategy: Minimize Previewed Path Error	20
Figure 5-2.	Driver Model Structure and Interface to Vehicle Model	21
Figure 5-3.	Typical Laboratory "Cross-Over Model" Measurements of Human Operators in Compensatory Tracking Task Experiments	25
Figure 5-4.	Typical Full Scale Road measurements of Driver/Vehicle Systems and Comparison with Laboratory Tracking Task Measurements	26
Figure 5-5.	TACOM Driver Model Predictions	28
Figure 5-6.	Sequence of Driver Model Calculations	30
Figure 5-7.	The Driver Model Shown in a Conventional Block Diagram Format	34
Figure 5-8.	The "Single-Point" Version of the Driver Model	37
Figure 5-9.	Three Control Schemes	39
Figure 5-10.	The Linearized Single-Unit Vehicle Model	41
Figure 5-11.	Interpretation of the Single-Unit Model Parameters when Steering an Articulated Vehicle	45
Figure 5-12.	Parameter Values for Example Calculations	46
Figure 5-13.	Driver Model Controlled Lane-Change Maneuver, front wheel only steering; k=0	48
Figure 5-14.	Driver Model Controlled Lane-Change Maneuver, front wheel only steering; k=0	49
Figure 5-15.	Driver Model Controlled Lane-Change Maneuver, front wheel and rear wheel steering; k=0.75	50
Figure 5-16.	Driver Model Controlled Lane-Change Maneuver, front wheel and rear wheel steering; k=0.75	51
Figure 5-17.	Driver Model Controlled Lane-Change Maneuver, Steering via an Applied Yaw Control Moment	53

Figure 5-18. Driver Model Controlled Lane-Change Maneuver, Steering via an Applied Yaw Control Moment 54

Figure 5-19. Driver Model Controlled Lane-Change Maneuver, Steering via an Applied Lateral Control Force 55

Figure 5-20. Driver Model Controlled Lane-Change Maneuver, Steering via an Applied Lateral Control Force 56

Figure 5-21. The M1037 Truck (HMMWV) 58

Figure 5-22. The M101 Trailer 59

Figure 5-23. HMMWV Tire: Influence of Tire Inflation Pressure 61

Figure 5-24. HMMWV Lateral Tire Force Measurements 62

Figure 5-25. Driver Controlled Constant Radius Turning Test 64

Figure 5-26. Path-Constrained Lane Change Maneuver 66

Figure 5-27. Unconstrained Lane Change Maneuver 67

Figure 5-28. Basic Obstacle Course Layout 68

Figure 5-29. Baseline Obstacle Course Layout Used in Tests 69

Figure 5-30. Driver Model Validation, Constrained Lane-Change 81

Figure 5-31. Driver Model Validation, Constrained Lane-Change 82

Figure 5-32. Constrained vs. Unconstrained Lane Change Test 85

Figure 5-33. Constrained vs. Unconstrained Lane-Change Test 86

Figure 5-34. Driver Model Validation, Obstacle Course, 40 mph 88

Figure 5-35. Driver Model Validation, Obstacle Course, 40 mph 89

Figure 5-36. HMMWV Entering the Obstacle Course 91

Figure 5-37. HMMWV Negotiating the First Obstacle 92

Figure 5-38. HMMWV Negotiating the Second Obstacle 93

Figure 5-39. HMMWV Exiting the Obstacle Course 94

Figure 5-40. Driver Model Validation, 500' Radius, 24.5 mph 96

Figure 5-41. Driver Model Validation, 500' Radius, 24.5 mph 97
Figure 5-42. Driver Model Validation, 500' Radius, 49 mph 98
Figure 5-43. Driver Model Validation, 500' Radius, 49 mph 99
Figure 5-44. Driver Model Validation, 500' Radius, 47 mph 101
Figure 5-45. Driver Model Validation, 500' Radius, 47 mph 102
Figure 5-46. Driver Model Validation, 500' Radius, 57 mph 103
Figure 5-47. Driver Model Validation, 500' Radius, 57 mph 104
Figure 5-48. Block Diagram of the DADS / Driver Model Interface 109
Figure 5-49. Initialization Sequence of Driver Model at Time = 0 112
Figure 5-50. Driver Model Calculations During Integration Loop 113
Figure 5-51. Example Lane-Change from DADS Simulation using the TACOM Driver Model 114
Figure 5-52. Example Lane-Change from DADS Simulation using the TACOM Driver Model 115
Figure 5-53. Example Circular Turn from DADS Simulation using the TACOM Driver Model 117
Figure 5-54. DADS / TACOM Driver Model for HMMWV Along Circular Turn at 50 mph 118
Figure 5-55. DADS / TACOM Driver Model for HMMWV Along Circular Turn at 50 mph 119
Figure 5-56. Example Path Planning Algorithm for the Driver Model (during integration loop) 121
Figure 5-57. Vehicle Entering Field of Obstacles and Corresponding Profile 123
Figure 5-58. Vehicle at Advanced Position and Corresponding Profile 124
Figure 5-59. Lane-Change Geometry for the Example Calculation using the Path Planning Algorithm 126

Figure 5-60. Example Calculation using the Path Planning Algorithm - Lane Change Maneuver....127

Figure 5-61. Example Calculation using the Path Planning Algorithm - Lane Change Maneuver....128

Figure 5-62. Obstacle Course Geometry for the Example Calculation using the Path Planning Algorithm....129

Figure 5-63. Example Calculation using the Path Planning Algorithm - Obstacle Course Maneuver....130

Figure 5-64. Example Calculation using the Path Planning Algorithm - Obstacle Course Maneuver....131

Figure 5-65. Example Prediction of Command Pressure from the Closed-Loop Driver Braking Model During a Controlled Stop....135

Figure 5-66. Comparison of Simple Driver Model Braking Expectation with Actual Retardation Properties....136

Figure 5-67. Command Pressure Modulation by the Driver Braking Model in Response to Front Axle Lock-ups....139

Figure A-1. Articulated Vehicle Model....A-4

Figure A-2. Example Calculations for a Simulated LVS....A-11

Figure B-1. HMMWV Test 50 mph Steady Turn....B-5

Figure B-2. HMMWV Test 50 mph Steady Turn....B-6

Figure B-3. HMMWV Test 25 mph Steady Turn....B-7

Figure B-4. HMMWV Test 25 mph Steady Turn....B-8

Figure B-5. HMMWV Test Braking-in-a-Turn, 132 ft....B-9

Figure B-6. HMMWV Test Braking-in-a-Turn, 132 ft....B-10

Figure B-7. HMMWV Test Braking-in-a-Turn, 195 ft....B-11

Figure B-8. HMMWV Test Braking-in-a-Turn, 195 ft....B-12

Figure B-9. HMMWV Test Lane-Change, 60 mph....B-13

Figure B-10. HMMWV Test Lane-Change, 60 mph B-14
Figure B-11. HMMWV Test Lane-Change, 30 mph B-15
Figure B-12. HMMWV Test Lane-Change, 30 mph B-16
Figure B-13. HMMWV Test Obstacle Course, short/short B-17
Figure B-14. HMMWV Test Obstacle Course, short/short B-18
Figure B-15. HMMWV Test Obstacle Course, long/long B-19
Figure B-16. HMMWV Test Obstacle Course, long/long B-20
Figure B-17. HMMWV Test Straight-Line Braking, 200 ft B-21
Figure B-18. HMMWV Test Straight-Line Braking, 145 ft B-22
Figure B-19. HMMWV Test Straight-Line Braking, 125 ft B-23
Figure B-20. HMMWV Test Random Steer Application B-24
Figure C-1. HMMWV / Trailer Lane-Change Test C-4
Figure C-2. HMMWV / Trailer Lane-Change Test C-5
Figure C-3. HMMWV / Trailer Lane-Change Test C-6
Figure C-4. HMMWV / Trailer Steady Turning Test C-7
Figure C-5. HMMWV / Trailer Steady Turning Test C-8
Figure C-6. HMMWV / Trailer Braking-in-a-Turn Test C-9
Figure C-7. HMMWV / Trailer Braking-in-a-Turn Test C-10
Figure C-8. HMMWV / Trailer Braking-in-a-Turn Test C-11
Figure C-9. HMMWV / Trailer "Divergence" Test C-12
Figure C-10. HMMWV / Trailer "Oscillation" Test C-13
Figure C-11. HMMWV / Trailer "Oscillation" Test C-14
Figure C-12. HMMWV / Trailer "Oscillation" Test C-15
Figure C-13. HMMWV / Trailer "Oscillation" Test C-16

LIST OF TABLES

Table	Title	Page
Table 5-1.	Parameter Measurements and Estimates for the HMMWV in its Test Condition	60
Table 5-2.	Log Sheet Summary of Driver-Vehicle Tests	70
Table 5-3.	Baseline Driver/Vehicle Parameters Used in Validation Calculations	80
Table A-1.	Articulated Vehicle Model - Parameter Definitions	A-5
Table A-2.	LVS Parameter Estimates	A-10

1.0. INTRODUCTION

This document constitutes the final technical report for the U.S. Army Tank-Automotive Command (TACOM) project entitled "Development of Driver/Vehicle Steering Interaction Models for Dynamic Analysis" conducted by the University of Michigan Transportation Research Institute (UMTRI) under contract DAAE07-85-C-R069. The purpose of the research conducted under this project was to develop a computer-based steering control model (or "driver model") of the human operator for use by TACOM within its large-scale vehicle simulation program. The model was to realistically represent steering control behavior of actual drivers during path-following and obstacle avoidance maneuvers. Predictions of driver steering control behavior by the model were to be subsequently validated by comparison with direct measurements of driver/vehicle tests conducted during the latter course of the project. The validation testing took place at the Chrysler Proving Grounds and involved a number of test maneuvers including negotiation of obstacle courses, lane-change maneuvers, steady turning along circular paths, and braking maneuvers. Data collected from these tests were used to correct any observed deficiencies in the initial model and to select parameter values for the driver model for representing realistic driver steering behavior.

The basis of the driver modelling effort was an UMTRI steering control model used previously to represent steering control behavior of passenger car drivers. It was proposed that the UMTRI model be modified and extended under this project to represent the steering behavior of drivers when controlling a broader and more unusual class of vehicles of interest to TACOM.

2.0. OBJECTIVE

The principal goal of this work was to develop a practical model of driver steering control which could be used to represent and predict realistic steering responses of human operators during path-following and obstacle-avoidance maneuvers. The model was intended to be used with a variety of different vehicle configurations and for a reasonable range of vehicle operating conditions.

An equally important objective was to validate the developed model through direct comparison with full-scale test data collected during the project. The test data would involve selected vehicles and drivers performing a variety of path-following and obstacle avoidance maneuvers. The initial project plan called for testing several different vehicle types including a steered-wheel vehicle (e.g. the HMMWV), an articulated vehicle (e.g. the LVS), and a tracked vehicle. However, because of the unavailability of the latter two

vehicle types during the proposed project testing, the HMMWV and a HMMWV-Trailer (M101) combination vehicle served as the primary test vehicles for the model validation.

3.0. CONCLUSIONS

A computer-based model used to steer, in a human-like manner, a wide variety of land vehicles was successfully developed and demonstrated under this work. Test data, collected to validate the driver model predictions, provided convincing evidence of the capabilities of the new model. Significant agreement between test track measurements and corresponding model predictions was demonstrated for a variety of path tracking and obstacle avoidance maneuvers.

A sequence of specialized tests, conducted under unusual nonlinear operating conditions, produced new experimental results clearly showing how drivers can stabilize and control vehicles operating beyond the conventional boundaries used to define the limits of vehicle directional stability. Investigation of this same phenomena during the project with the developed driver model produced a nearly identical result. This finding provided further evidence of the capabilities of the new model for predicting likely human operator steering responses under unusual maneuvering conditions.

With respect to the conventional steering maneuvers conducted under this project:

- The test drivers used in this test program reacted more quickly than what has been traditionally reported in the technical literature as typical for "average" drivers of passenger cars. The conclusion was that such differences in driver response characteristics can be attributed to differences in the directional response qualities of the controlled vehicles (i.e. a HMMWV versus most passenger cars). The observed change in driver responsiveness is assumed to represent typical human operator adaptation/compensation behavior frequently observed in most man-machine systems.

- A simplified vehicle representation was generally sufficient for describing the directional dynamics of the internal reference vehicle used by the driver model for estimating its future position.

- Adaptation by the driver model to changes in the controlled vehicle dynamics during more demanding ("high-g") maneuvers was found to be necessary, provided the changes to the vehicle dynamics lasted for an

extended period of time during the maneuver. Compensation by the driver model was less critical for maneuvers producing similar, but short-term, variations in the same vehicle properties.

- Regardless of the observed variations exhibited in driver steering behavior during this test program, or in what has been reported previously by others in the technical literature, the TACOM model appears to be quite capable of replicating most of these observed driver steering control behavior patterns through simple adjustment of two basic parameters.

Secondary tasks which were undertaken to supplement the basic features present in the steering control model, and which hold promise for further enhancing the present model capabilities, include the following:

- development of a path planning/obstacle avoidance algorithm for generating a path input to the steering control model based upon a simplified geometric description of the surrounding landscape

- development of a driver braking model to represent how human operators apply brake pedal force and control to vehicles during deceleration and stopping maneuvers

Lastly, a sequence of handling tests conducted with the HMMWV and M101 trailer produced no special problems for the test driver in controlling and stabilizing the combination vehicle, despite some significant payload alterations to the trailer and its dynamic behavior. Limiting the vehicle speed was the most effective means for controlling the more severe types of trailer oscillations introduced by extreme rearward placement of the trailer payload.

4.0. RECOMMENDATIONS

- Further tests involving a small group of vehicles are recommended to clarify certain interesting findings from this project which seem to suggest that a peculiar relationship may exist between the directional response of the controlled vehicle and the steering response of the driver. The two test drivers used in this test program responded more quickly during most of the steering maneuvers with the HMMWV test vehicle than that traditionally reported in the technical literature for similar tests with drivers of passenger cars. The relatively slow directional response of the HMMWV test vehicle,

when compared with a typical passenger car, may be the principal reason. However, without conducting a sequence of side-by-side tests with the same driver(s) and a group of vehicles having significantly different directional response qualities, this hypothesis will remain unproven. It is suggested that a brief follow-up test program be conducted to address this matter using the following group of three vehicles: 1) a directionally sluggish vehicle, 2) an empty HMMWV with directional response properties faster than those used in this test program, and 3) a directionally "quick" passenger car or comparable vehicle. The data collected should be analyzed in the same manner as performed under this project to clarify the results and observations reported here. This information would improve TACOM's ability to choose appropriate values of parameters for the developed driver model when used to steer vehicles having more unusual directional control properties.

- The path planning / obstacle detection model begun under this project should be extended and refined further to provide additional capabilities for TACOM in using the developed driver model with its present land vehicle *simulations*. Ideas and algorithms initiated here could also be combined with similar concepts residing in other navigation models, such as the NATO Mobility Model, to develop a more sophisticated computer-based land navigation capability. Specialized tests could be designed and conducted to help develop and validate such a model.

- The driver braking model concepts proposed in this report should be pursued further by TACOM to provide an enhanced capability for simulating representative driver braking behavior during vehicle stops or maneuvers involving controlled deceleration. Much of the test data collected under this project can be used as a good starting point for initial validation efforts.

- Lastly, use of the driver model developed here should be considered as a key ingredient for a basic research program involving autonomous vehicle and tele-operated vehicle applications. An on-board, silicon-based extension of this work appears as an obvious candidate for steering control of both autonomous and (a special class of) tele-operated land vehicles. Combined with existing remote sensing capabilities, a high performance "driver model on a chip" concept is very promising. Although previous research efforts have been hampered by time delays in remote sensing and image processing, improvements in the on-board steering controller and use of "image prediction" schemes can improve overall system performance for such vehicles.

5.0. DISCUSSION

5.1. Background and Overview

The starting point for the driver modelling research conducted under this project was a linear preview control model originally proposed by MacAdam [1, 2] in 1981. The primary conclusion from that work was that automobile driver steering control could be represented and modelled quite accurately as an optimal preview control strategy which attempts to minimize errors between a desired previewed path and the predicted future position of the vehicle being controlled. See Figure 5-1. The driver model incorporated knowledge of the vehicle dynamics (i.e. the vehicle being controlled) within its structure and could therefore project into the future an estimate of the vehicle position at an advanced point in time. Simultaneously, the use of preview permitted the driver model to observe directly (i.e. "look ahead at") the corresponding desired path to follow. See Figure 5-2. The difference between these two future projections (predicted vehicle position and previewed desired path) corresponded to the previewed error signal minimized by the steering controller. However, one additional refinement was proposed and found necessary in that original model to account for human operator limitations in reacting to external stimuli. This other ingredient was the presence of a pure time delay accounting primarily for the neuro-muscular transport delay of average human operators and generally observed in most tracking control task experiments of man-machine systems.[3, 4, 5, 6] When the proposed time delay property was added to the optimal preview control strategy outlined above, agreement between model predictions and actual driver/vehicle measurements for several different validations was found to be remarkably good.

Since that original paper, the driver model has been implemented in a number of UMTRI computer programs used to primarily simulate vehicle handling performance of passenger cars and commercial vehicles.[7, 8, 9] A number of technical papers have also been published since that time which utilized the original model to study problems associated with "closed-loop" or driver steering control of various vehicles.[10, 11, 12, 13, 14, 15]

In 1985, the research described within this report was begun and was aimed at extending the original UMTRI driver model to the TACOM vehicle simulation environment while simultaneously adding other features and capabilities not present in the original model. One primary goal of this research was to "generalize" the internal vehicle dynamics module of the driver model so that use of it with different vehicle configurations would be possible. That is, the driver model would be capable of representing, within its own internal vehicle dynamics structure, the dynamics of a four-wheel-steered vehicle or a tracked vehicle, for

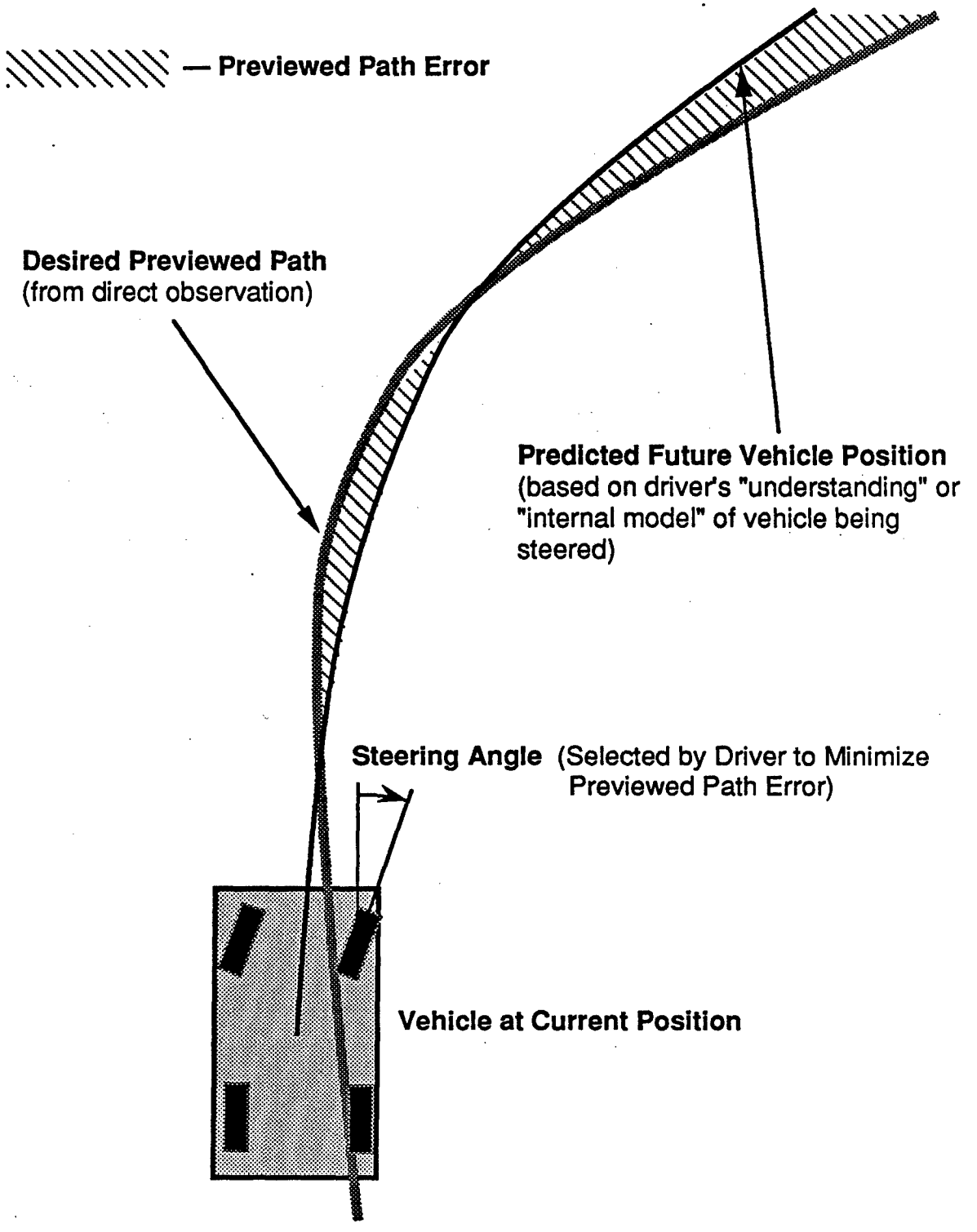

Figure 5-1. Driver Control Strategy: Minimize Previewed Path Error.

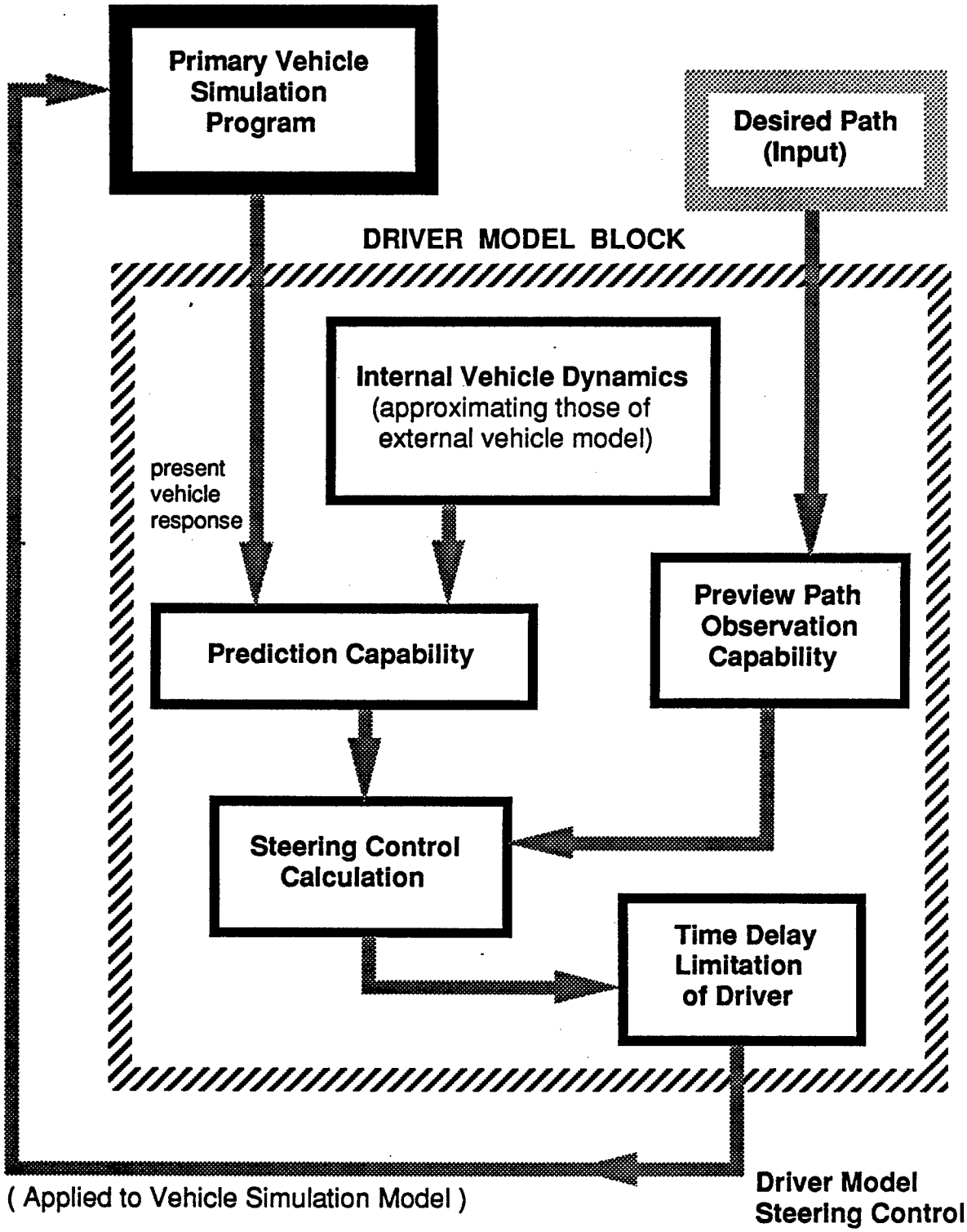

Figure 5-2. Driver Model Structure and Interface to Vehicle Model.

example, rather than just a basic passenger car with front-wheel-only steering. In addition, it was important that the resulting steering control predictions made by the driver model be representative of what actual drivers would likely produce under similar maneuvering scenarios.

Consequently, it was decided at the start of the project that an initial investigation would be first conducted to look at how the original UMTRI preview model could be adapted to a wider variety of vehicles than just passenger cars and conventional trucks — the type of vehicle it had been primarily used for up until that time. Because of the UMTRI model's demonstrated capability of accurately representing steering control behavior of passenger car drivers, it was reasoned that if its internal vehicle dynamics module could be generalized to account for a wider class of vehicles, it might also do a good job of simulating more diverse driver/vehicle systems as well. The results from that initial project task showed that generalization of the vehicle dynamics module for the UMTRI model would be possible and that doing so was a relatively straightforward process. Section 5.5 reports on that work.

Having found a means for adapting the driver model to a wider class of vehicles, the remaining basic goal was to validate the extended model through direct comparison with measurements from driver/vehicle tests. Testing was accomplished by performing a sequence of "closed-loop" driver/vehicle tests at the Chrysler Proving Grounds. Results from those tests and the subsequent model validation are reported on in Sections 5.6 and 5.7 respectively.

During the course of the project a number of additional topics arose which contributed to the further extension and refinement of the final model. These included:

- adaptation by the driver model to lateral acceleration due to maneuvering
- adaptation by the driver model to forward speed
- study of roll motion as an additional degree of freedom "sensed" by the driver model
- development of an optional "path planning / obstacle avoidance" algorithm capable of generating path inputs for the driver model based upon a previewed field of obstacles and terrain boundaries
- consideration of a proposed closed-loop braking model for future extensions to this work.

These topics are covered further within the discussion sections of 5.8 to 5.10.

Finally, installation of the developed driver model into the DADS simulation program used by TACOM is described in section 5.8. Computer code illustrating the interface procedure is listed in Appendices D and E.

5.2. The Preview Model Concept

The importance of utilizing a preview-based control concept to model the steering control strategy used by drivers of land-based vehicles cannot be over emphasized. Researchers and laymen alike know from simple observation and experience that path control of typical land vehicles relies heavily upon "looking ahead" to observe a desired path or direction of travel.[16, 17, 18, 19] Accordingly, preview or "look ahead" characteristics should seemingly be an inherent part of any mathematical model which attempts to represent the basic steering control characteristics of human operators. Thus, three key reasons are seen as arguments for a preview-based control approach to modelling the driver steering control process:

- Human operators are known to employ preview in their steering control strategy and therefore any corresponding model should include it.

- The use of preview allows the "physics" of the driving control process to be explained simply and directly in terms of regulating previewed path errors alone — something that anyone who has driven an automobile can relate to and understand.

- future extension of a preview-based model to incorporate path planning and navigation algorithms/models within a single overall driver model structure is a natural extension (physically and mathematically) of the project work reported on here.

References 20 - 23, 49 provide additional examples of preview-based driver modelling which have been published previously in the technical literature.

5.3. The Preview Model vs. Experimental Observations of Man/Machine Systems

A pertinent question is whether or not the developed preview control model is in fundamental agreement with known experimental measurements and findings regarding man/machine systems and their interactions. A well-known principle within the man/machine arena, and one used to describe the compensation / adaptation properties of human operators when interacting with different machines, is the so-called "cross-over model" principle.[4] This principle is really an experimental observation that when human subjects attempt to regulate simple first and second order plant dynamics during laboratory tracking task experiments, the measured transfer function of the combined man/machine system exhibits an invariant property within a certain range of frequencies. (The term "cross-over model" derives from the fact that a simple mathematical expression, $\omega_c e^{-j\omega\tau} / j\omega$, can be used to frequently curve fit the experimental measurements collected from such laboratory tests.) This invariant form of the combined man/machine transfer function is seen in Figure 5-3. The top portion of Figure 5-3 shows a block diagram depicting the typical laboratory tracking task experimental arrangement. In these experiments, human subjects are instructed to maintain an error signal, e, at a small or zero value by movement of a "joystick" controller, u. The error signal presented to the subject is simply the difference between a random input waveform, f, and the output of the plant, x, the subject is being asked to regulate.

When similar experiments are conducted with drivers in full-scale vehicle tests or sophisticated moving-base simulators,[24, 25, 26, 27] the complexity of the plant (vehicle) dynamics is now increased. Measurements then show that the same man/machine transfer function becomes altered to that seen in Figure 5-4. From this we note several things. First, the slope of the gain function at low frequencies is significantly increased from *that* of the laboratory tests; second, the low frequency phase lag is also increased, thereby producing a characteristic parabolic-like shape of the total phase plot; and finally, the cross-over frequency, ω_c, is increased. (The basic laboratory cross-over model result is included in the figure for direct comparison.) However, even though the frequency responses become altered and shifted, the shape of all the curves in the vicinity of their respective cross-over frequencies, ω_c, remains unchanged, with each maintaining a slope of -20 db/decade. The key point to be made here is that unless a driver model, regardless of its origin, can pass at least the elementary validation test of exhibiting "cross-over model"-like-behavior in the vicinity of its cross-over frequency, the model's legitimacy in terms of *its* ability to mimic human operator behavior will generally be held in question. Obviously, if a particular model can not only exhibit "cross-over model" behavior within the vicinity of its cross-over frequency, but can fit experimental measurements at other frequencies as well, its validity is further enhanced.

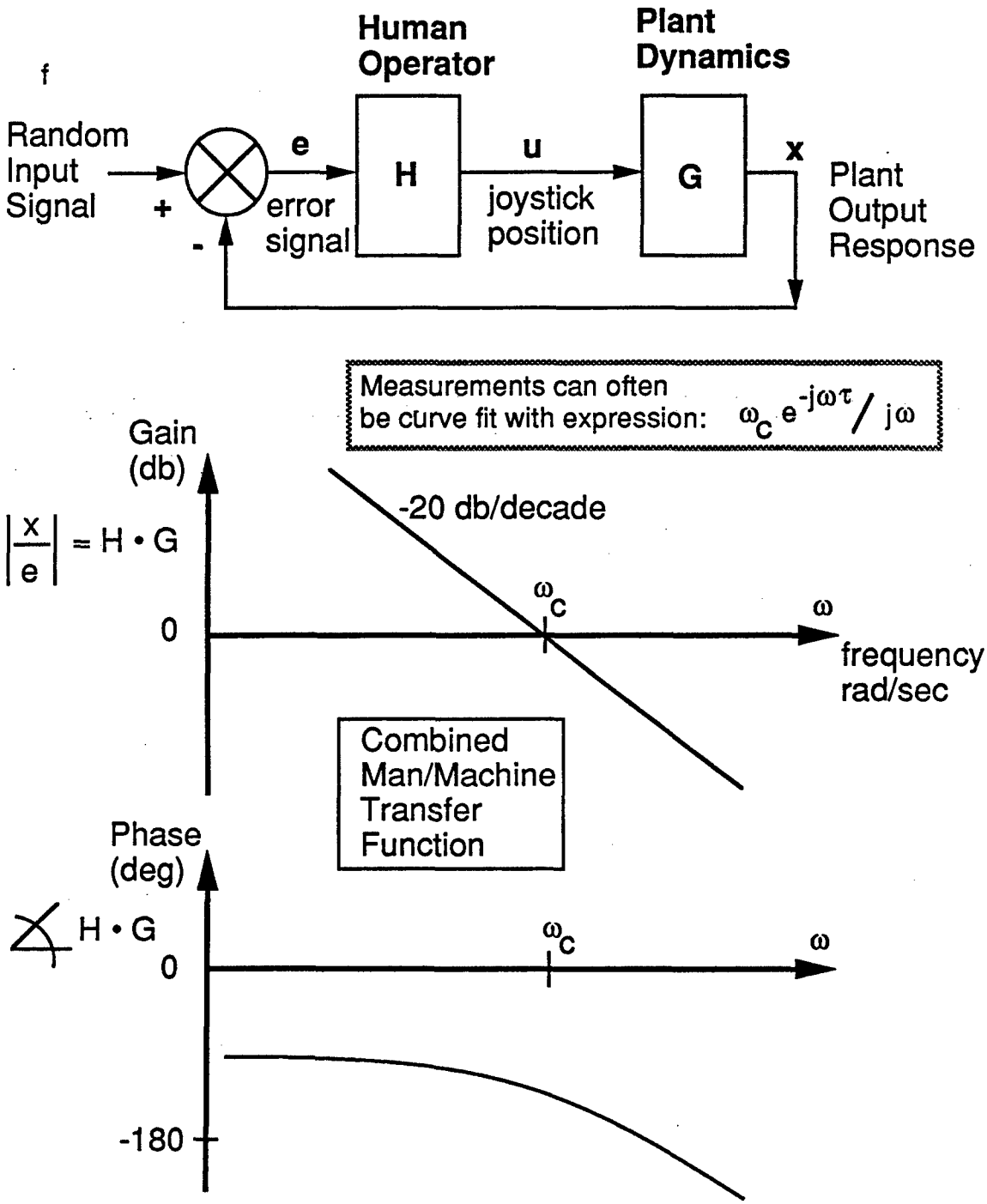

Figure 5-3. Typical Laboratory "Cross-Over Model" Measurements of Human Operators in Compensatory Tracking Task Experiments

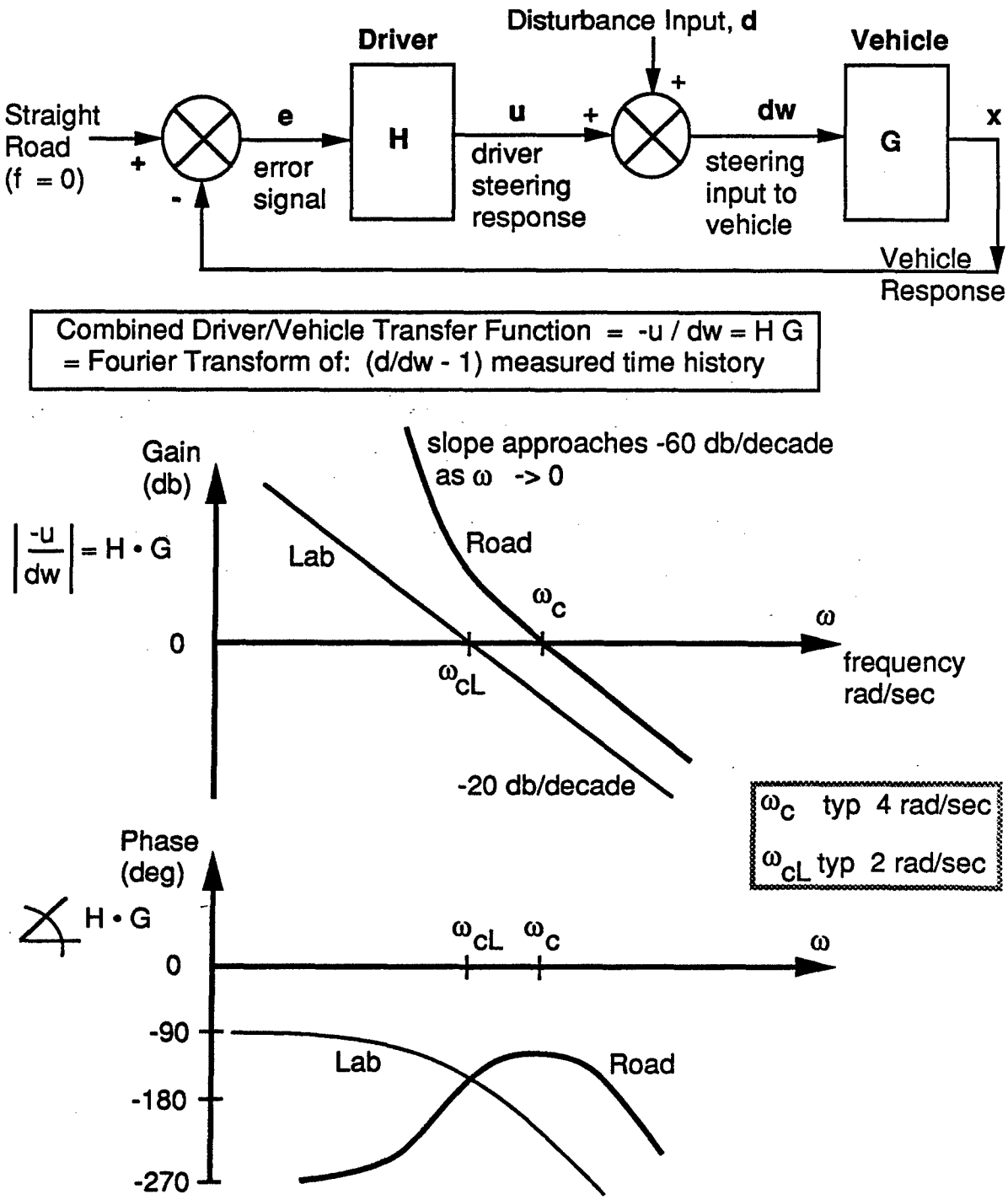

Figure 5-4. Typical Full Scale Road Measurements of Driver/Vehicle Systems and Comparison with Laboratory Tracking Task Measurements.

The importance of these observations for the TACOM driver model is that the very same transfer function characteristics seen for these full-scale experimental measurements are predicted by the TACOM model. To demonstrate, corresponding example calculations from the model are shown in Figure 5-5 using 1) a large passenger car (4000 lb), and 2) a loaded HMMWV (7500 lb) to represent the dynamics of the controlled vehicle in each case.

It can be shown [1], that adjustment of the transfer function characteristics seen in Figure 5-5 is easily controlled through two basic driver model parameters. The first parameter which determines the amount of preview or "look ahead" time used by the model, controls the slope of the low frequency end of the combined transfer function. Increasing the preview time decreases the slope at low frequencies and simultaneously decreases the corresponding phase lag as well. The other basic parameter determines the amount of neuromuscular time delay in the driver model and adjustment of it controls the frequency at which cross-over occurs in the combined transfer function plot. Consequently, a wide variety of basic man-machine behavior, as defined by such experimental measurements, can be accurately represented with this model through simple adjustment of only two basic parameters. Not surprisingly, the two model parameters that are key to controlling these adjustments are also parameters which represent the two central assumptions used in the development of the model: 1) recognition and use of preview within the model, and 2) presence of a driver time delay.

Prior to leaving this discussion, it should be noted that an analogous time-domain validation of the model is presented in Section 5.7 where driver/vehicle test track measurements for the HMMWV are compared with model predictions. Furthermore, a portion of those test/model comparisons show new results for a driver/vehicle system operating under unusual nonlinear operating conditions and which heretofore have not been reported in the general literature. The measurements presented there offer further experimental confirmation of the validity of the driver model in predicting steering control behavior of drivers operating at or near limit maneuvering conditions.

5.4. Mathematical Formulation of the Preview Control Model

The material in this section shows the mathematical development of the preview control model and closely follows that of reference 1. The basic "computational mechanics" of the model is to first calculate, at each point in time, the steering control, u^0, which will minimize the mean squared error between a desired path input, f, and the projected future lateral displacement of the vehicle, y, over a specified preview time interval, T. The "optimal" control, u^0, is then delayed in time by an amount τ seconds. The time delay is used to represent the effective neuromuscular lag and characteristic limitation of the human

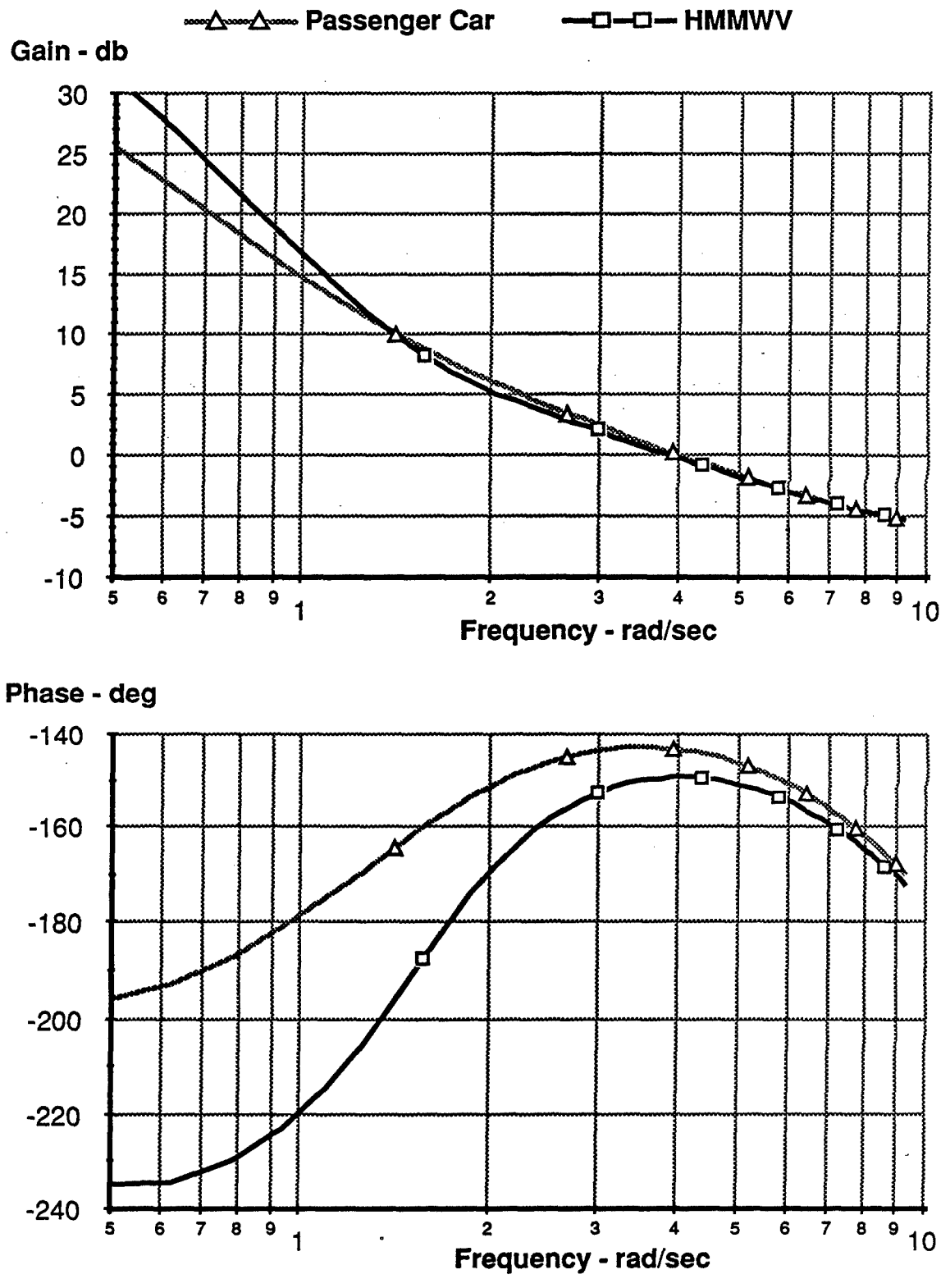

Figure 5-5. TACOM Driver Model Predictions.

operator in responding to external stimuli. The delayed steering control, u, is then used to steer the vehicle. This basic sequence is outlined in Figure 5-6.

As will be seen in the development which follows, the model is able to estimate the future response of the vehicle being controlled by utilizing an internal linearized dynamical representation of that vehicle within its own structure. Consequently, the driver model includes an internal "understanding" or "mapping" of the likely vehicle response resulting from a particular steering control input. Obviously, the better the internal linearized model is in representing the vehicle being controlled, the better will be the estimate of the projected vehicle response.

The resulting driver model then has certain basic features. First, the model incorporates preview to "look ahead" and anticipate the desired path to follow. Second, the driver model possesses an internal linearized representation of the vehicle being controlled and uses that dynamical representation to predict/estimate the vehicle position and response at future times. Third, the control strategy used by the model is to minimize the previewed error between the desired path input and the future estimated vehicle position. And finally, the steering control obtained from the error minimization calculation is delayed in time to account for human operator neuromuscular limitations in reacting to external stimuli.

These basic notions can all be expressed mathematically within the context of linear system theory. Following the mathematical formulation of the problem from references 1 and 2, we have for a given linear system,*

$$\dot{\mathbf{x}} = \mathbf{F}\,\mathbf{x} + \mathbf{g}\,u \tag{5.4-1}$$

$$y = \mathbf{m}^T\,\mathbf{x} \tag{5.4-2}$$

where,

- $\mathbf{x}$ is the n x 1 state vector
- y is the scalar output related to the state by the n x 1 $\mathbf{m}^T$ constant observer vector transpose
- $\mathbf{F}$ is the constant n x n system matrix
- $\mathbf{g}$ is the constant n x 1 control coefficient vector

and

- u is the scalar control variable.

* Bold face type denotes matrices and vectors.

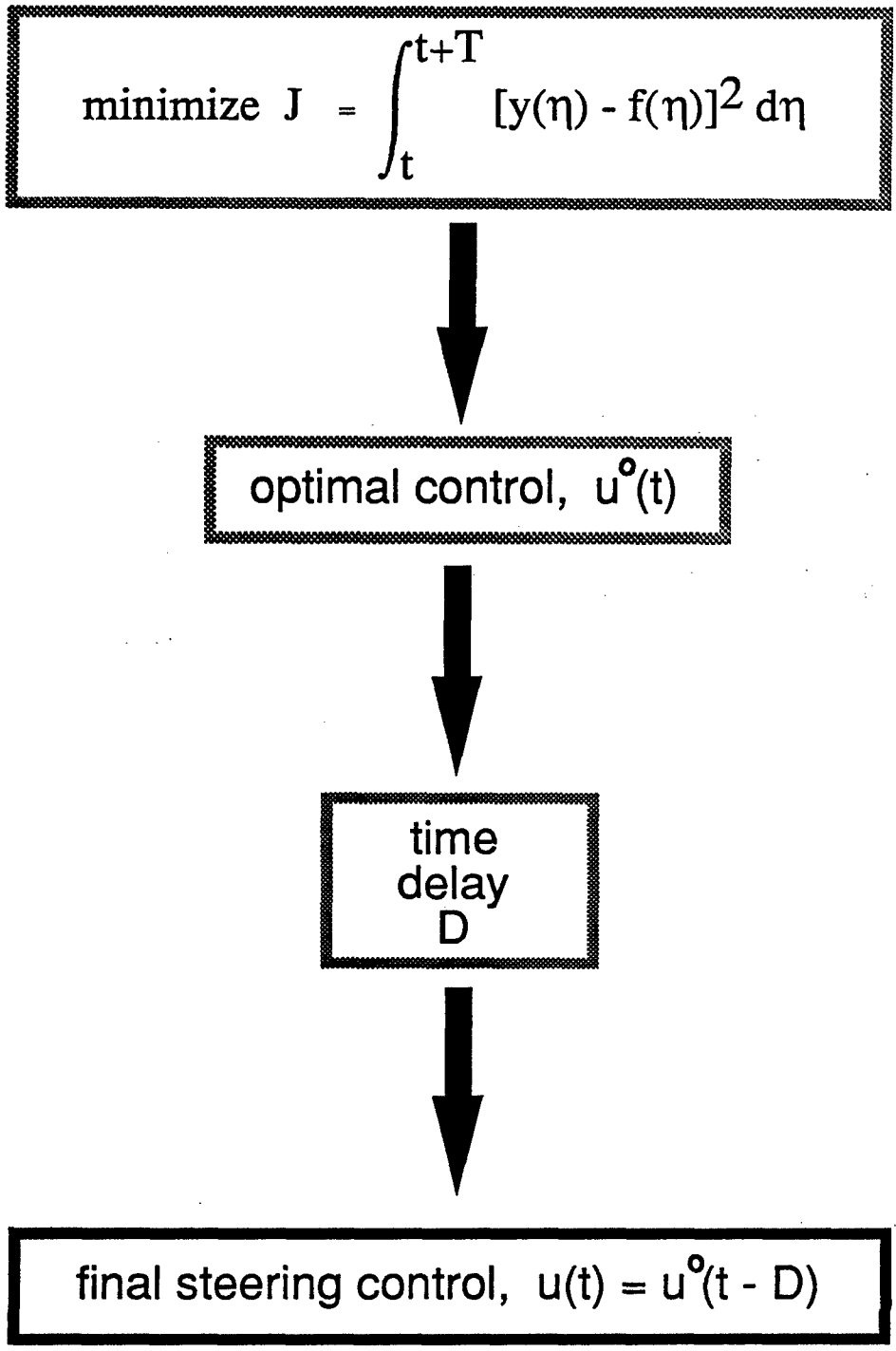

Figure 5-6. Sequence of Driver Model Calculations

We would like to find the control, $u^0(t)$, which minimizes a local performance index,

$$J = \frac{1}{T}\int_t^{t+T} \{[f(\eta) - y(\eta)]^2 W(\eta - t)\} d\eta \tag{5.4-3}$$

over the the current preview time interval (t, t + T) where,

W is an arbitrary weighting function over the preview interval (selected as a constant 1.0 for all of this discussion)

and,

f is the previewed input.

The previewed output, $y(\eta)$, is related to the current state, $\mathbf{x}(t)$, and fixed control, u(t), over the preview interval (t, t+T), by

$$y(\eta) = \mathbf{m}^T \left[\mathbf{I} + \sum_{n=1}^{\infty} \mathbf{F}^n (\eta - t)^n / n!\right] \mathbf{x}(t) + (\eta - t)\, \mathbf{m}^T \left[\mathbf{I} + \sum_{n=1}^{\infty} \mathbf{F}^n (\eta - t)^n / (n+1)!\right] \mathbf{g}\, u(t) \tag{5.4-4}$$

The matrix,

$$\mathbf{I} + \sum_{n=1}^{\infty} \mathbf{F}^n (\eta - t)^n / n!$$

is simply the state transition matrix for the linear system, **F**, and is frequently denoted as $\Phi(\eta, t)$.

When the above general formulation is applied to the driver/vehicle path following problem, **F** and **g** represent the dynamics of the controlled vehicle, f is associated with the desired path input, and y with the lateral displacement of the vehicle.

Returning to the general formulation, the necessary condition that the derivative of J with respect to the control variable, u, be zero, leads to the equation for the optimal control, u^0, given by,

$$u^0(t) = \left[\int_t^{t+T} \left\{ f(\eta) - \mathbf{m}^T \left[\mathbf{I} + \sum_{n=1}^{\infty} \mathbf{F}^n (\eta-t)^n / n! \right] \mathbf{x}(t) \right\} \right.$$

$$\left. \cdot \left\{ (\eta-t)\, \mathbf{m}^T \left[\mathbf{I} + \sum_{n=1}^{\infty} \mathbf{F}^n (\eta-t)^n / (n+1)! \right] \mathbf{g} \right\} W(\eta-t)\, d\eta \right]$$

$$/ \left[\int_t^{t+T} \left\{ (\eta-t)\, \mathbf{m}^T \left[\mathbf{I} + \sum_{n=1}^{\infty} \mathbf{F}^n (\eta-t)^n / (n+1)! \right] \mathbf{g} \right\}^2 W(\eta-t)\, d\eta \right]$$

(5.4-5)

Because of the need to subsequently apply this formulation to systems containing "imperfect" human operators which possess known reaction time limitations and cannot therefore be expected to exhibit optimal control behavior, an alternate but mathematically equivalent formulation of equation (5.4-5) is shown below. This alternate formulation directly involves the previewed error quantity, $e(\eta)$, which is being minimized in the original performance index of equation (5.4-3). The same optimal solution, $u^0(t)$, can therefore be expressed in terms of any current nonoptimal control, $u(t)$, and the previewed error, $e(\eta)$, as,

$$u^0(t) = u(t) + \frac{\displaystyle\int_t^{t+T} \varepsilon(\eta)\, A(\eta)\, W(\eta-t)\, d\eta}{\displaystyle\int_t^{t+T} A^2(\eta)\, W(\eta-t)\, d\eta}$$

(5.4-6)

where,

$$A(\eta) = (\eta-t)\, \mathbf{m}^T \left[\mathbf{I} + \sum_{n=1}^{\infty} \mathbf{F}^n (\eta-t)^n / (n+1)! \right] \mathbf{g}$$

and,

$$\varepsilon(\eta) = f(\eta) - \mathbf{m}^T \left[\mathbf{I} + \sum_{n=1}^{\infty} \mathbf{F}^n (\eta-t)^n / n! \right] \mathbf{x}(t) - u(t)\, A(\eta)$$

In this particular formulation, the current control is modified only in response to a nonzero function of the previewed output error, and thereby, is analogous to an integral controller. Note that the generality of the mathematics presented above allows it to be applied to a variety of control problems, assuming the controlled dynamical system can be expressed in terms of equations (5.4-1) and (5.4-2).

In order to apply this generalized formulation to the driver/vehicle path following problem, the **F** and **g** matrices must be associated with the directional dynamics of the vehicle being controlled. (In reference 1, **F** and **g** represent the directional dynamics of a two-degree-of-freedom automobile.) In addition, the resulting optimal control, $u^0(t)$, is assumed to be delayed an amount τ seconds to account for the known neuromuscular delay of the driver. From this, the steering control for the driver model finally becomes,

$$u(t) = u^0(t) \cdot e^{-s\tau} \tag{5.4-7}$$

where, $e^{-s\tau}$, is the driver time delay, and $u^0(t)$ is given by equation (5.4-5 or 5.4-6).

The final steering control law is noteworthy for several reasons. First, it shows a direct dependence upon the dynamics of the controlled system (vehicle) through the presence of **F** and **g** in equation (5.4-5). This is important for driver/vehicle systems since we know from experimental evidence that human operators, as part of man/machine systems, demonstrate great capacity for sensing and adapting to changes in the dynamics of the machine being controlled.[3, 22, 26, 28, 29, 30, 31, 32] Thus, when the driver model is used to steer different types of vehicles, or, when changes in the dynamics of the vehicle occur due to operating conditions, those vehicle-related effects are reflected directly in the driver model through the **F** and **g** matrices appearing in the control law. (For applications involving significant nonlinearities, or, parameters in the **F** and **g** matrices that may vary significantly over time, the **F** and **g** matrices may be updated continuously or intermittently to account for and represent the adaptive control behavior of drivers.) Secondly, the characteristic behavior of human operators to utilize preview as part of their control strategy, and the fact that human operators also have limited reaction times, are both incorporated in the model through the presence of the preview time parameter, T, and time delay parameter, τ, appearing in equation (5.4-5) and (5.4-7). Variations in these two parameters can markedly affect the response and stability properties of the closed-loop driver/vehicle system. Furthermore, as noted in section 5.3, adjustment of these same two parameters facilitates curve fitting the frequency response characteristics of the driver/vehicle model to experimental data in the frequency domain.

The driver model equations, (5.4-6) and (5.4-7), can also be expressed in terms of a conventional control system block diagram as seen in Figure 5-7. In this diagram, H

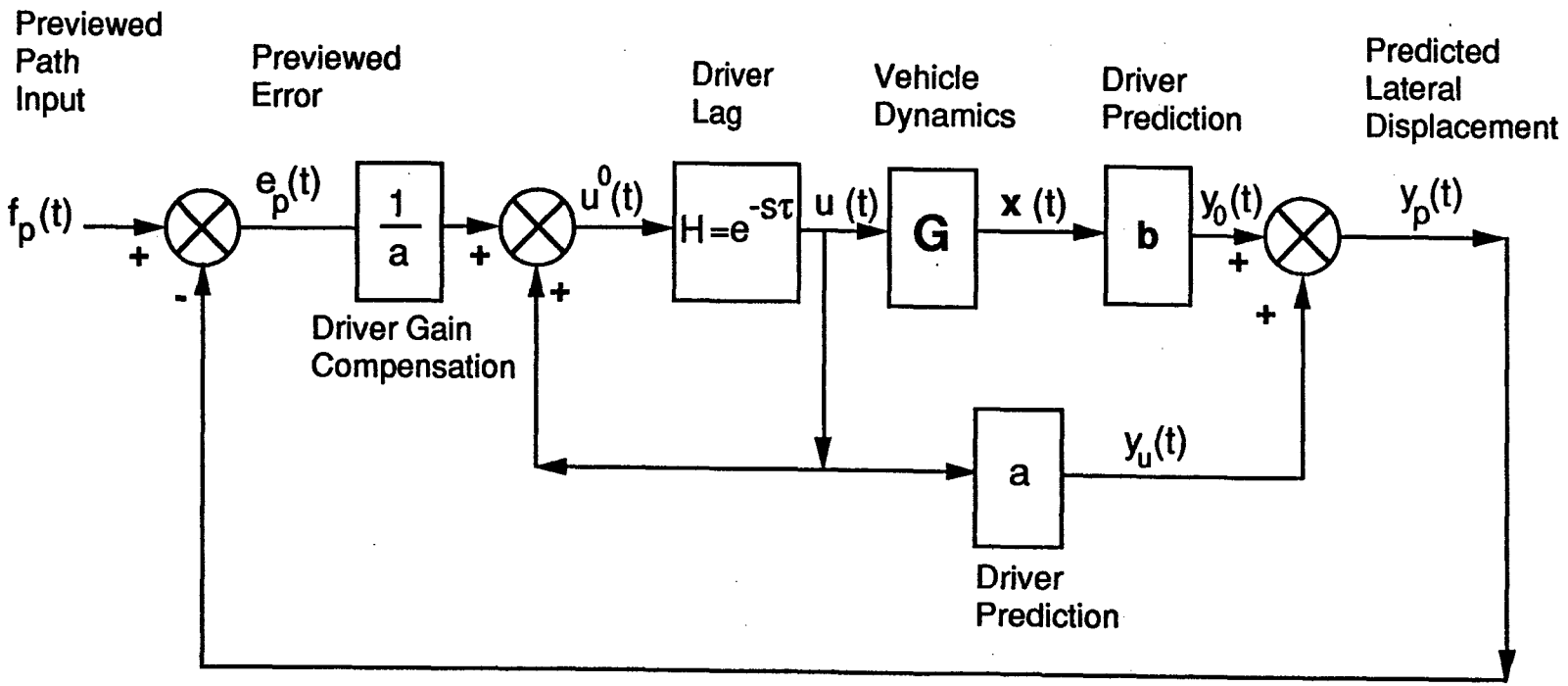

Figure 5-7. The Driver Model Shown in a Conventional Block Diagram Format

represents the time delay block of the human operator and is given by $H = e^{-s\tau}$. The block (vector) denoted as **G** represents the directional dynamics of the vehicle (internal to the driver model) and relates the vehicle state response, **x**, to the driver steering output, u. The scalar constant, a, appearing in two of the blocks is given by,

$$a = \frac{1}{T}\int_{t}^{t+T} \left\{ (\eta-t)\, \mathbf{m}^T \left[\mathbf{I} + \sum_{n=1}^{\infty} \mathbf{F}^n (\eta-t)^n / (n+1)!\right] \mathbf{g} \right\}^2 d\eta \Bigg] \tag{5.4-8}$$

and the constant gain vector, **b**, is given by the expression,

$$\mathbf{b} = \frac{1}{T}\int_{t}^{t+T} (\eta-t)\, \mathbf{m}^T \left[\mathbf{I} + \sum_{n=1}^{\infty} \mathbf{F}^n (\eta-t)^n / (n+1)!\right] \mathbf{g} \cdot \mathbf{m}^T \left[\mathbf{I} + \sum_{n=1}^{\infty} \mathbf{F}^n (\eta-t)^n / n!\right] d\eta \tag{5.4-9}$$

The scalar, a, represents the driver's ability to predict that component of the future response of the vehicle deriving only from the current steering control input. The constant gain vector, **b**, represents the driver's ability to predict that component of the future vehicle response deriving only from the present state of the vehicle.

The time history input to the block diagram, $f_p(t)$, is given by,

$$f_p(t) = \frac{1}{T}\int_{t}^{t+T} f(\eta)\, (\eta-t)\, \mathbf{m}^T \left[\mathbf{I} + \sum_{n=1}^{\infty} \mathbf{F}^n (\eta-t)^n / (n+1)!\right] \mathbf{g}\, d\eta \tag{5.4-10}$$

The quantities $y_0(t)$, $y_u(t)$, $y_p(t)$, $e_p(t)$, and $f_p(t)$ appearing in this diagram can then be interpreted as:

- $f_p(t)$ a weighted average of the previewed input (forcing function) over the preview interval (t, t+T)
- $y_0(t)$ a weighted average of the predicted output response over the preview interval due to the current system state, x(t)
- $y_u(t)$ a weighted average of the predicted output response over the preview interval due to the current control, u(t)

$y_p(t)$ a weighted average of the total predicted output response over the preview interval

$e_p(t)$ a weighted average of the previewed error over the preview interval

Note that the above block diagram and associated variables apply to the complete preview control formulation, wherein the minimization of the previewed error signal is occurring over the entire preview interval. If a simplification is introduced, so that the previewed error signal is being minimized or nulled out only at a single point, T* seconds ahead in time, the so-called "single-point" version of the preview model, as described in reference 1, is obtained. See the similar block diagram of Figure 5-8 for this model.

The "single-point" model is derived from the previous mathematical formulation by letting the arbitrary weight function, $W(\eta-t)$, be equal to the Dirac delta function, $\delta(T^*)$. In this diagram, the corresponding quantities $y(t+T^*)$, $f(t+T^*)$, and $e(t+T^*)$ are more directly and easily understood as the previewed plant output T* seconds ahead, the previewed input T* seconds ahead, and the previewed error signal T* seconds ahead, respectively. The corresponding constant gain, a*, is then provided by the somewhat simpler expression,

$$a^* = (T^*)\ \mathbf{m}^T \left[\mathbf{I} + \sum_{n=1}^{\infty} \mathbf{F}^n\ (T^*)^n / (n+1)!\right] \mathbf{g} \qquad (5.4\text{-}11)$$

and the constant feedback gain vector, **b***, is seen to be,

$$\mathbf{b}^* = \mathbf{m}^T \left[\mathbf{I} + \sum_{n=1}^{\infty} \mathbf{F}^n\ (T^*)^n / n!\right] \qquad (5.4\text{-}12)$$

The "single-point" model of Figure 5-8 is shown here primarily to present a simpler and more obvious version of the analogous diagram in Figure 5-7. Reference 1 also includes a similar version of the "single-point" model in its discussion.

5.5. Application of the Preview Control Model to Steering of Basic Land Vehicles

Attention is now turned to applying the generalized results of section 5.4 to the problem of directional and path control of land vehicles by human drivers. The vehicle directional dynamics equations (**F** and **g** matrices of section 5.4) appearing in the original UMTRI driver model [1] are extended here to provide for single-unit vehicles controlled by three possible schemes: a) control through steering of the front *and/or* rear wheels, b) control by

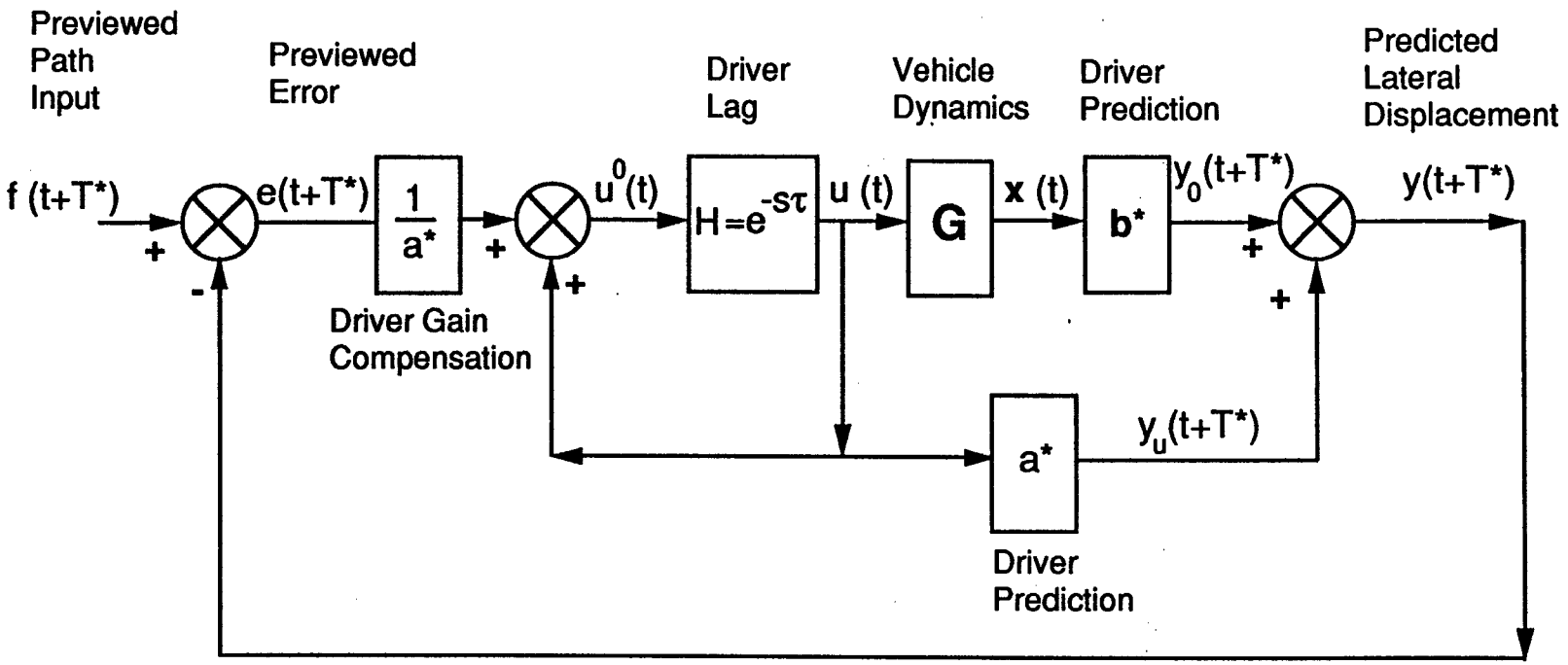

Figure 5-8. The "Single-Point" Version of the Driver Model

application of a pure yaw moment input, and c) control by means of both an applied lateral force and accompanying yaw moment. See Figure 5-9. Case a) applies to the conventional passenger car and single-unit vehicles such as the HMMWV. Case b) is primarily intended for applications involving tracked vehicles wherein the control torque, Mc, is applied by means of side-to-side longitudinal forces deriving from differential track speeds. Case c) is a generalized formulation intended to cover a broader range of future control possibilities as well as those represented by Cases a) and b).

For example, Case c) can duplicate a steered-wheel vehicle response by simply defining the control force as the product of the control variable and the tire cornering stiffness and then applying the control force at the forward non-steered wheel location. (The force control variable is in fact the steering magnitude, scaled by the cornering stiffness of the tire, of a an equivalent steerable wheel.) Likewise, Case c) can be used to duplicate a yaw moment control scheme, as given by Case b), by using a control force located at a very large forward distance, d, ahead of the mass center. This results in a sizeable yaw moment control accomplished through use of a very small lateral control force.

Looking first at the case of a single-unit vehicle having both front and rear wheel steering, the *linearized* vehicle dynamic equations are shown here:

$$y' = v + U\psi \tag{5.5-1}$$

$$v' = [\,-2(C_{af} + C_{ar}) / m\,U\,]\,v + [\,2(b\,C_{ar} - a\,C_{af}) / m\,U - U\,]\,r + (2\,C_{af} / m)\,\delta_f + (2\,C_{ar} / m)\,\delta_r \tag{5.5-2}$$

$$r' = [\,2(b\,C_{ar} - a\,C_{af}) / I\,U\,]\,v + [\,-2(a^2\,C_{af} + b^2\,C_{ar}) / I\,U\,]\,r + (2\,a\,C_{af} / I)\,\delta_f - (2\,b\,C_{ar} / I)\,\delta_r \tag{5.5-3}$$

$$\psi' = r \tag{5.5-4}$$

Directional Control Through Steering of Front and/or Rear Wheels

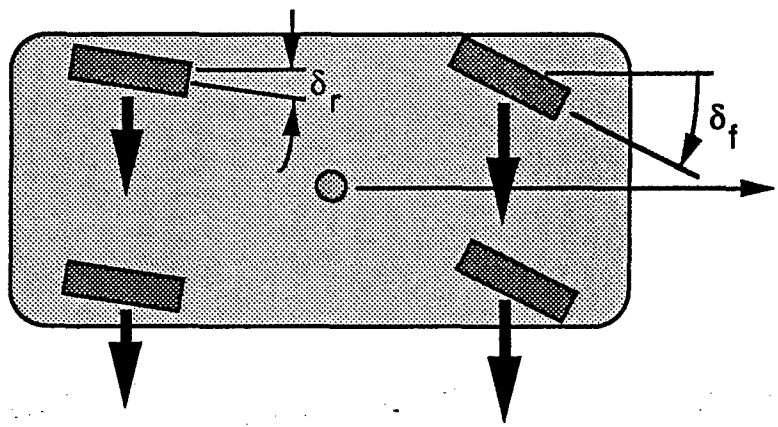

Directional Control Through Application of a Control Moment, M_c

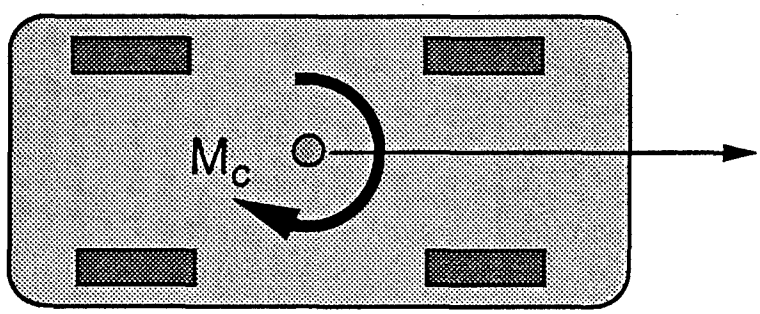

Directional Control Through Application of a Control Force, F_c

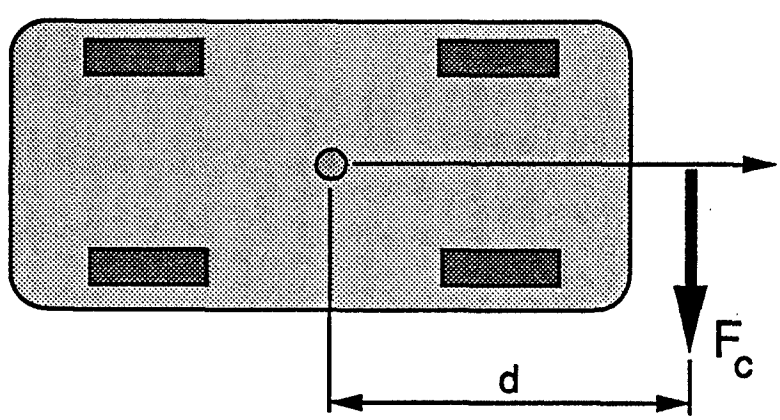

Figure 5-9. Three Control Schemes

where,

' denotes differentiation with respect to time

y is the inertial lateral displacement of the vehicle mass center

v is the lateral velocity in the vehicle body axis system

r is the yaw rate about the vertical body axis

ψ is the vehicle heading (yaw) angle

δ_f is the front tire steer angle, control variable

δ_r is the rear tire steer angle, control variable

and the parameters appearing in equations (5.5-1) -> (5.5-4) are:

U forward vehicle velocity

$C_{af,\,ar}$ front and rear tire cornering stiffnesses

a, b forward and rearward locations of tires from the vehicle mass center

m, I vehicle mass and yaw inertia

The diagram of Figure 5-10 further supplements these definitions.

The above equations can be simplified somewhat to represent rear wheel steering system implementations in which the rear wheels are proportionately *slaved* to the front wheel angle by a gain constant, **k**,

$$\delta_r = k\,\delta_f \qquad (5.5\text{-}5)$$

and thereby eliminating δ_{rw} as a second independent control input.

By also adding lateral force, $\boldsymbol{B}$ / m, and yaw moment, $\boldsymbol{D}$ / I, control terms, the equations (5.5-1) -> (5.5-4) can be written in a more general form that now encompasses all the cases shown in Figure 5-9:

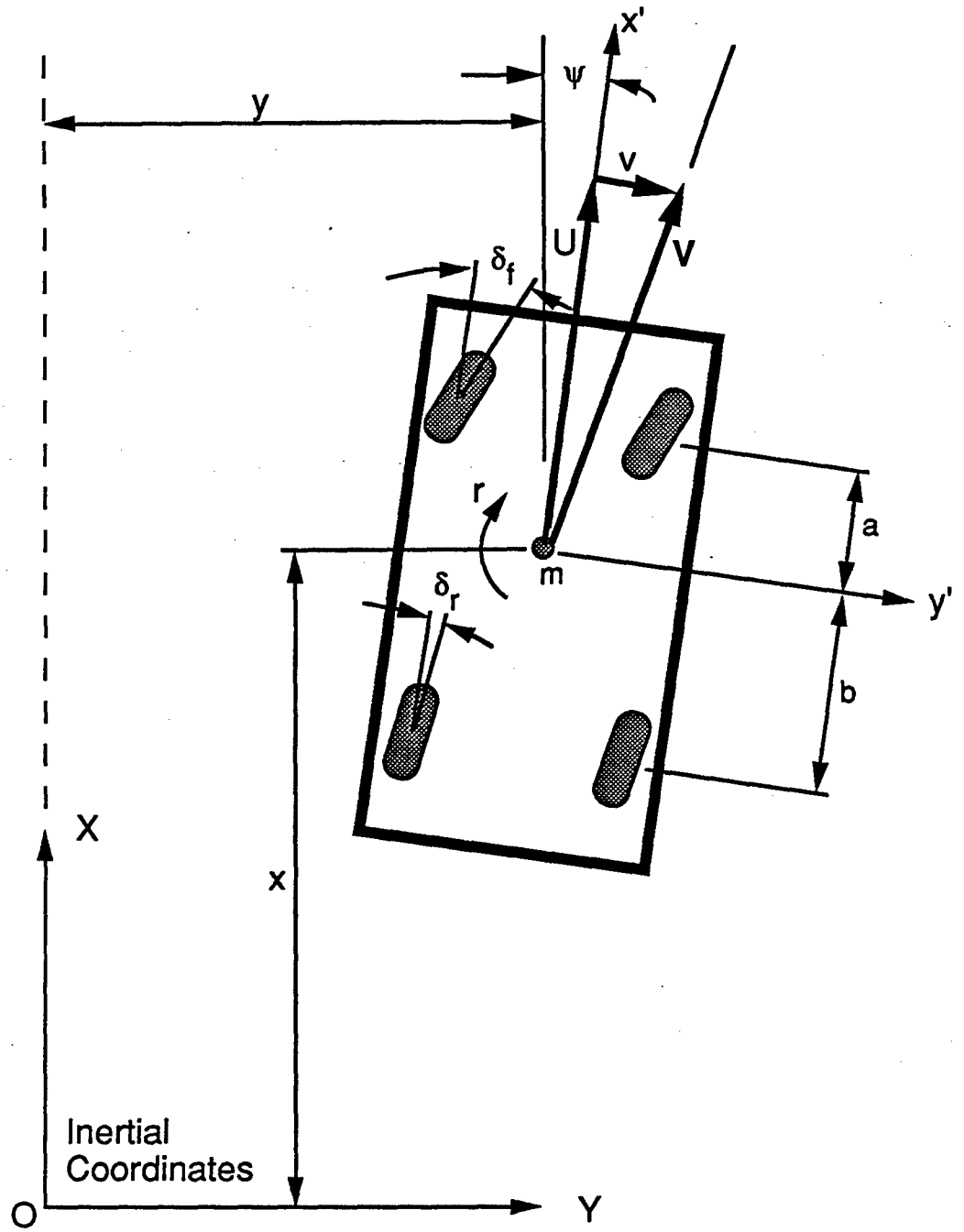

Figure 5-10. The Linearized Single-Unit Vehicle Model

$$y' = v + U\psi \tag{5.5-6}$$

$$v' = [\,-2(C_{af} + C_{ar}) / m\,U\,]\,v + [\,2(b\,C_{ar} - a\,C_{af}) / m\,U - U\,]\,r + \{\,\boldsymbol{A}\,[\,2(C_{af} + k\,C_{ar})/m\,] + \boldsymbol{B}/m\,\}\,u_c \tag{5.5-7}$$

$$r' = [\,2(b\,C_{ar} - a\,C_{af}) / I\,U\,]\,v + [\,-2(a^2\,C_{af} + b^2\,C_{ar}) / I\,U\,]\,r + \{\,\boldsymbol{C}\,[\,2(a\,C_{af} - k\,b\,C_{ar}) / I\,] + \boldsymbol{D}/I\,\}\,u_c \tag{5.5-8}$$

$$\psi' = r \tag{5.5-9}$$

where now,

u_c takes on the role of the general purpose control variable (u_c may be interpreted as either front wheel steer angle, lateral control force, or yaw moment control, depending upon the values of the control parameters $\boldsymbol{A}$, $\boldsymbol{B}$, $\boldsymbol{C}$, and $\boldsymbol{D}$).

and,

$\boldsymbol{A}$, $\boldsymbol{B}$, $\boldsymbol{C}$, and $\boldsymbol{D}$ are "control coefficients" specified to allow various types of control schemes to be represented in the above equations.

For example, by specifying $\boldsymbol{A}$ and $\boldsymbol{C}$ as 1.0 and $k = \boldsymbol{B} = \boldsymbol{D} = 0$, the conventional front wheel steered vehicle is represented with u_c interpreted as the front wheel *steer angle* control variable.

By specifying $\boldsymbol{A} = \boldsymbol{B} = \boldsymbol{C} = 0$ and $\boldsymbol{D}$ as 1.0, a vehicle controlled by a pure yaw moment control (e.g., a tracked vehicle) is represented with u_c now interpreted as the yaw moment control variable. In the case of the *tracked vehicle*, the sum of C_{af} and C_{ar} would be interpreted as an equivalent lateral force "cornering stiffness" of the track element due to track sideslip. Different fore-aft values of C_{af} and C_{ar} could be designated to move the center of track side force forward or rearward from the mid-wheelbase position, or equivalently, assign different levels of "front" and "rear" (single point) track side forces. The a and b parameters would be used to locate the tracked vehicle's fore-aft mass center location with respect to the equivalent "front" and "rear" side force locations. The resulting yaw moment control variable, u_c, calculated by the steering model could then be expressed, if desired, in terms of a driver steering control movement through knowledge of the steering control gain (e.g., inches or degrees of stick movement per differential *longitudinal* track force) and the lateral spacing of the tracks.

The last control option, for representing a lateral force control scheme, A and C are selected as 0, B = 1.0, and D is the distance forward of the vehicle mass center at which the lateral control force, u_c, acts.

Equations (5.5-6) -> (5.5-9) represent the internal set of vehicle dynamics utilized by the driver model for the category of single-unit vehicles. (The FORTRAN driver model code appearing in Appendix D utilizes these equations as the basis for its internal vehicle dynamics model.) The above equations can be expressed in state space terminology by defining the **F**, **g**, **x**, and **m** matrices of section 5.4 as,

$$\mathbf{F} = \begin{bmatrix} 0 & 1 & 0 & U \\ 0 & -2(C_{af}+C_{ar}) / m U & 2(b C_{ar} - a C_{af}) / m U - U & 0 \\ 0 & 2(b C_{ar} - a C_{af}) / I U & -2(a^2 C_{af} + b^2 C_{ar}) / I U & 0 \\ 0 & 0 & 1 & 0 \end{bmatrix}$$

$$\mathbf{g} = \begin{bmatrix} 0 \\ A\,[2\,(C_{af} + k\,C_{ar})\,/\,m] + B\,/\,m \\ C\,[2\,(C_{af} - k\,b\,C_{ar})\,/\,I] + D\,/\,I \\ 0 \end{bmatrix} \qquad \mathbf{x} = \begin{bmatrix} y \\ v \\ r \\ \psi \end{bmatrix} \qquad \mathbf{m} = \begin{bmatrix} 1 \\ 0 \\ 0 \\ 0 \end{bmatrix}$$

For the case of an articulated vehicle, a similar but lengthier set of equations is produced and is shown in Appendix A. The equations in Appendix A are for a linear, constant velocity articulated vehicle having front steerable wheels as well as an articulation joint torque as control variables — similar in concept to a simplified LVS (MK48 Series). These equations could be used in a manner identical to those just presented to represent the internal vehicle model of the driver if greater accuracy was required, for example, to study driver steering interactions with, or dependencies upon, the dynamics of the rear unit. In this way, the more extensive set of articulated vehicle equations could be used to represent a driver's more complete "understanding" of the contributions of the rear unit (or even the articulation controller torque) to the directional control of the total vehicle.

In general though, driver steering control of most articulated vehicles can be adequately represented by the single-unit equations presented above. When doing so, the following interpretations and modifications of the vehicle parameters in the single-unit equations need to be applied:

- the mass, m, and yaw inertia, I, now represent the mass and inertia of the lead unit *plus* that "contributed" by the static vertical hitch load from the second unit

- the a and b parameters locating the fore/aft positions of the front and rear suspension centerlines, must now be altered to reflect the additional static vertical hitch load from the second unit

- the tire cornering stiffness parameters need to reflect any changes resulting from the increased vertical loads

Referring to Figure 5-11, we see that the nominal single-unit parameters appearing at the top of the figure, become altered to those in the bottom portion of the figure due to the presence of the vertical hitch load contributed from the second unit. The driver model is then viewed as steering a single-unit vehicle having a total mass, mg + Fh, with a new "total c.g." location given by the modified parameters a' and b'. The tire cornering stiffnesses that now apply should also correspond to the new vertical tire loads Fz1' and Fz2'. (A more sophisticated and accurate method for representing the coupled inertial effects of multiple masses is described by Wehage.[33])

If a vehicle has more than one tire per side at a front or rear suspension location, the particular front/rear cornering stiffness parameter used in the model (C_{af} or C_{ar}) should represent the sum of all the tire cornering stiffnesses per side at the front/rear suspension location. Similarly, the a and b parameters locating the total mass center of the vehicle should be from the *centerline* of the axle set for a particular front or rear suspension.

To illustrate the types of responses that are representative of the driver model when steering a single unit vehicle, a sequence of example calculations are now presented for two single unit vehicles having significantly different sets of vehicle directional dynamics. The first vehicle is a conventional compact passenger car weighing 3000 lb; the other vehicle is a HMMWV loaded to a total gross weight of 7500 lb. The baseline maneuver for the examples that follow is a conventional 12-foot lane-change performed at a speed of 50 mph (73.3 ft/sec) over a forward travel distance of 100 feet. The driver model was used to steer the vehicle over this desired course and utilized a preview parameter of 1.50 seconds. The driver time delay parameter was fixed at 0.25 seconds. Figure 5-12 lists each of these parameters and shows a diagram of the desired path used in the example calculations. The vehicle parameter values seen in Figure 5-12 are based upon measurements and reasonable estimates.[34]

Identical calculations were performed for each vehicle for four different control cases corresponding to the following: A) control through front wheel steering only, A) control through front *and* rear wheel steering, with the front-to-rear-wheel ratio parameter, **k**, set at 0.75, C) control by means of an applied yaw control torque, and D) control through means

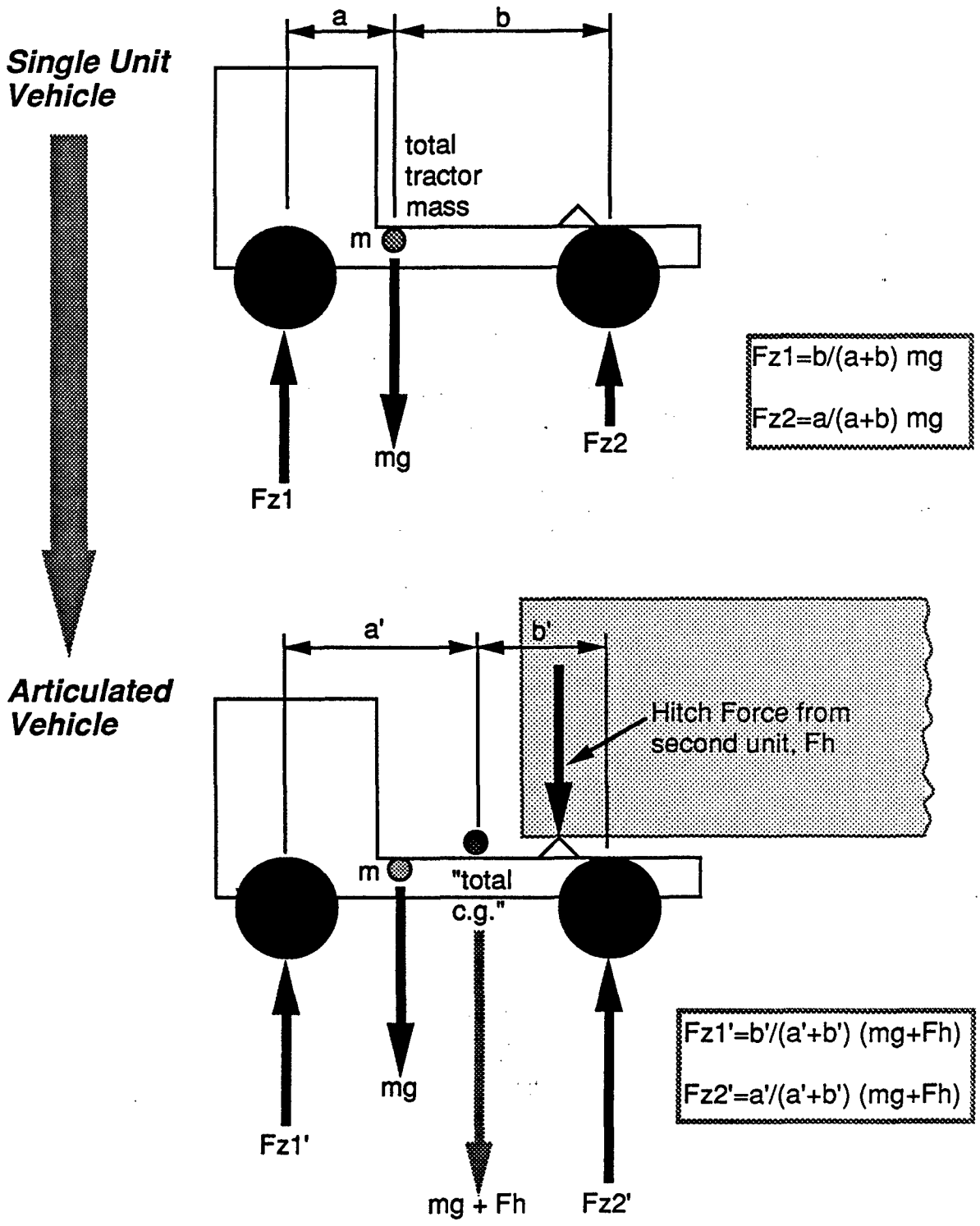

Figure 5-11. Interpretation of the Single-Unit Model Parameters when Steering an Articulated Vehicle.

"Desired" Path Input for Example Lane-Change Maneuver:

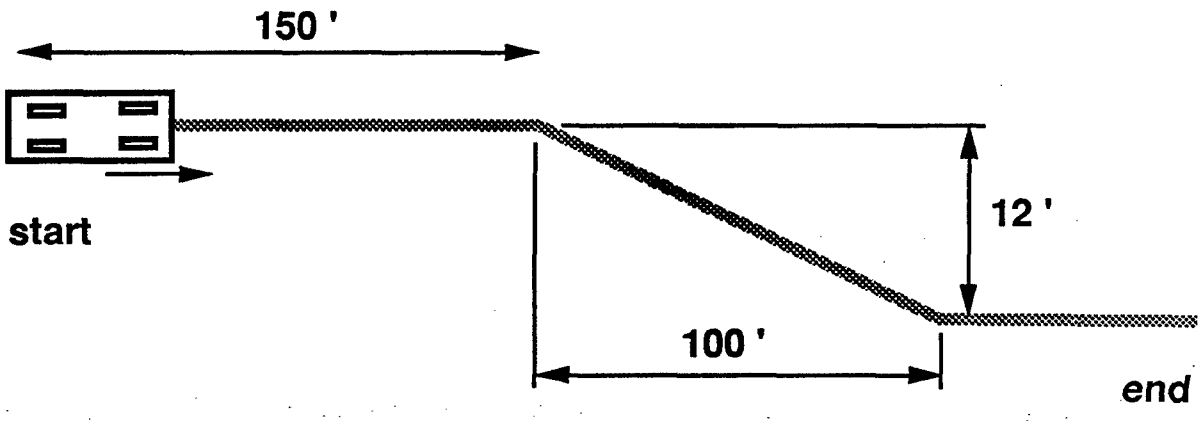

Driver Model Parameters: Preview Time = 1.50 sec

Time Delay = 0.25 sec

Baseline Vehicle Parameter Values

Passenger Car	
m	93.17 slugs
I	1500 slug-ft
Caf	11,460 lb/radian
Car	14,327 lb/radian
a	4.03 ft
b	4.55 ft
U	73.3 ft/sec

HMMWV	
m	232.9 slugs
I	7500 slug-ft
Caf	14,325 lb/radian
Car	19,196 lb/radian
a	6.80 ft
b	4.00 ft
U	73.3 ft/sec

Figure 5-12. Parameter Values for Example Calculations

of an applied lateral control force. In cases C and D, none of the wheels are steered. The above cases correspond closely with those seen earlier in Figure 5-9. (The HMMWV is a specific front-only steering vehicle and reference to it in these other example cases is for the purpose of only providing a distinctly different set of directional dynamics for comparison with the passenger car directional dynamics.) Additional analyses appear in the 1986 Interim Technical Report [35] for this project.

The example calculations which follow utilize equations (5.5-6) - (5.5-9) for simulating the vehicle directional dynamics, and equations (5.4-6) - (5.4-7) for simulating the driver steering control. The equations were implemented in a digital simulation. Referring to Figures 5-13 and 5-14, example time history results are seen for the case of conventional front wheel only steering. The earlier "control coefficients" (***A, B, C, D***) seen in the vehicle dynamics equations have the values here of 1.0, 0.0, 1.0, and 0.0 respectively. Also, the front-to-rear-wheel steering ratio, **k**, is set equal to 0.0 in this first example. As seen in Figure 5-13, the trajectories of both simulated driver/vehicle systems track the desired path quite well (bottom portion of the figure), even though significantly different steering control waveforms are required by the driver model for each vehicle (top portion). This is characteristic of the adaptive properties of the driver model (and most drivers) since the directional dynamics of each vehicle are completely different but still accounted for by the driver model. The corresponding time histories of Figure 5-14 show lateral acceleration and heading (yaw) angle results for each vehicle during the course of the simulated maneuver. The reduced level of damping exhibited by the HMMWV-driver system, in comparison to the passenger car-driver system, is not unusual since the HMMWV directional dynamics are significantly more oversteer (-3 deg/g) than the passenger car (1.2 deg/g), and such tendencies are frequently observed in closed-loop experimental tests. In practice, a driver could add more damping to the system by extending his/her preview time to a larger value.

In Figures 5-15 and 5-16 the same maneuver is repeated for both vehicles, with each now modified to include rear wheel steering (**k** = 0.75). In the top portion of Figure 5-15, the front wheel steering commands calculated by the driver model are seen for each vehicle, along with the corresponding rear wheel steering values (slaved at 75%, in this example, of the front wheel steer commands). The calculated vehicle trajectories are seen on the lower portion of the figure. Again, as in Figure 5-13, the driver model manages to track the desired path quite accurately, even though significantly different steering control inputs are required for each vehicle by the driver model. The use of rear wheel steering is seen to increase the required level of steering from the previous example, while decreasing the peak amplitudes of vehicle yaw angle and lateral acceleration (Figure 5-16). Both driver-vehicle systems also exhibit a greater degree of damping when rear wheel steering is present. This

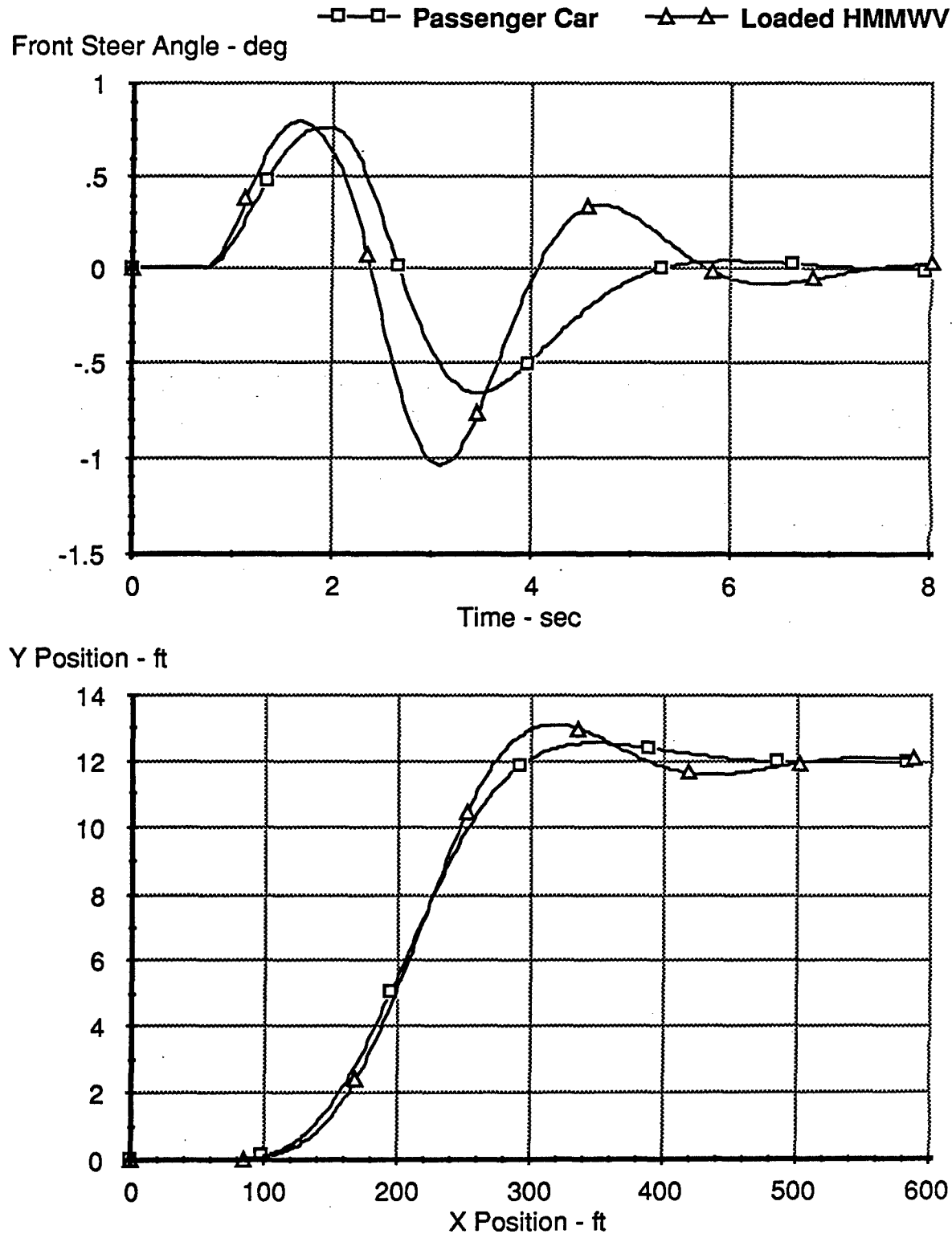

Figure 5-13. Driver Model Controlled Lane-Change Maneuver, front wheel only steering; k= 0

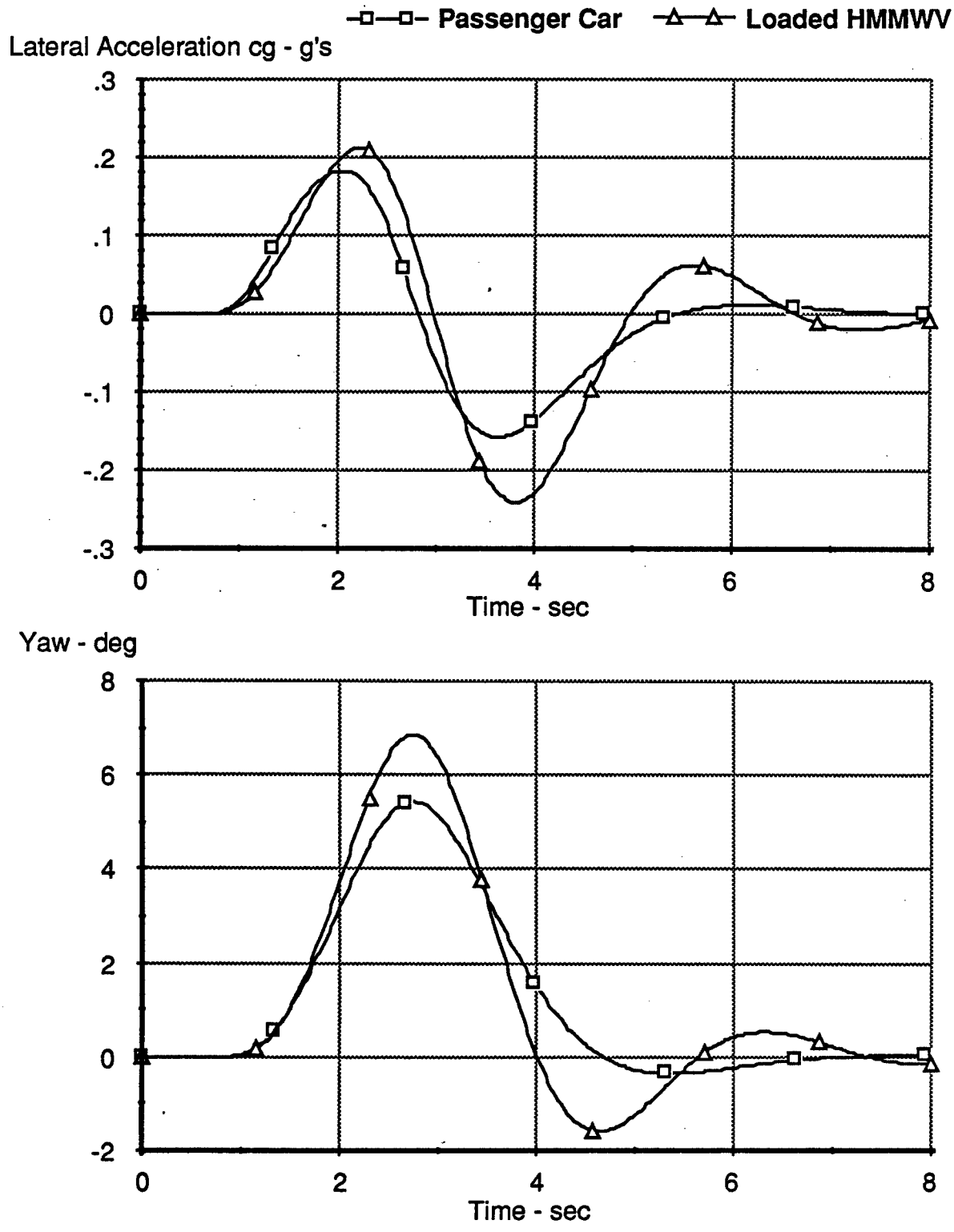

Figure 5-14. Driver Model Controlled Lane-Change Maneuver, front wheel only steering; k= 0

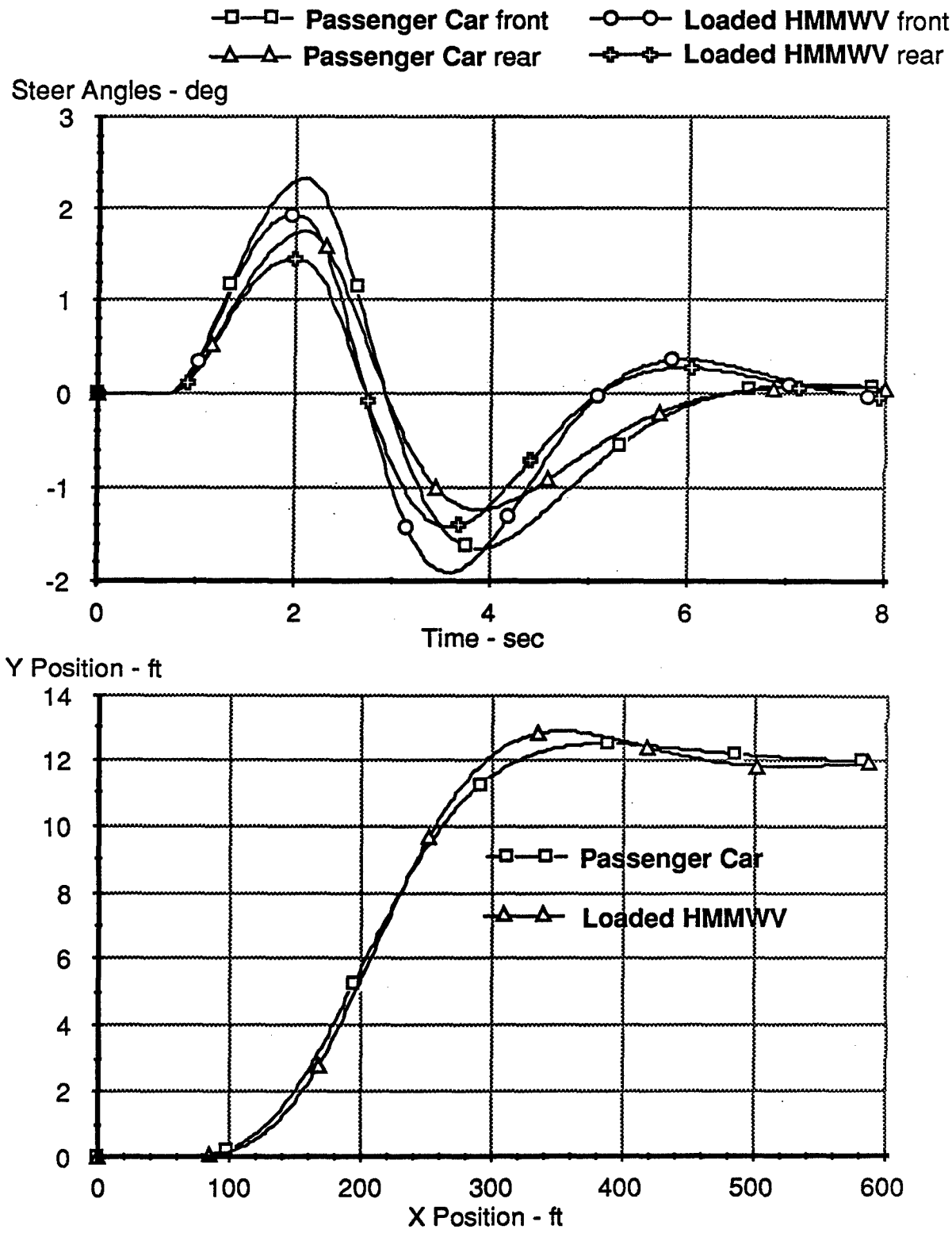

Figure 5-15. Driver Model Controlled Lane-Change Maneuver, front and rear wheel steering; k = 0.75

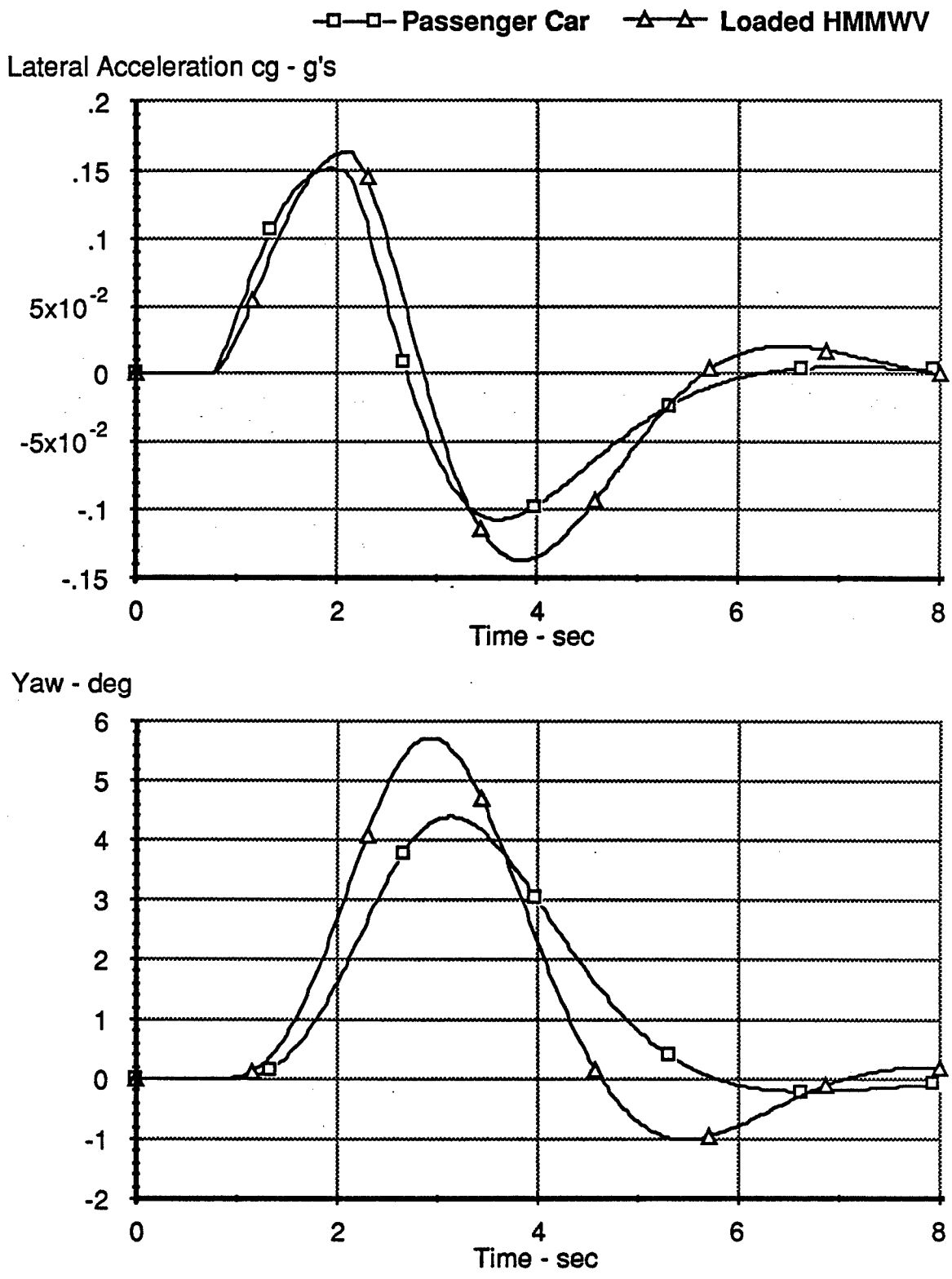

Figure 5-16. Driver Model Controlled Lane-Change Maneuver, front and rear wheel steering; k = 0.75

observation is also supported by recent experimental tests of four wheel steering passenger cars.[36, 37, 38, 39]

The next example calculation, seen in Figures 5-17 and 5-18 are for the same maneuver, but the two vehicles are now steered by means of an applied yaw moment control torque. Neither the front nor the rear wheels are steered in this example. Lateral motion is instead accomplished, as it is for a tracked vehicle, by rotating the vehicle in yaw through application of an applied moment to a certain sideslip condition, whereupon the non-steered wheels (or tracks) generate side force in reponse to sideslip. In this example, it is assumed that a physical mechanism is available (such as differential track speeds) *which can* generate an applied yaw control torque. The "control coefficients" in the previous equations then become: $A = 0$, $B = 0$, $C = 0$, and $D = 1$ with the control variable, u_C, now interpreted as torque, instead of steer angle.

The calculations show that the preview model is quite capable of steering each of the example vehicles along the desired trajectory by means of the applied control torque. Time histories for the required yaw control torques for each vehicle are seen in the upper portion of Figure 5-17 and the corresponding trajectories in the lower portion of the figure. The difference in control torque magnitudes is due to the difference in mass and dynamics of the two vehicles. The results seen here are quite similar to those seen earlier in Figures 5-13 and 5-14 for the front steer only example calculations.

The final example calculation, seen in Figures 5-19 and 5-20, is similar to the previous one but employs a lateral control force, instead of a yaw control torque, for steering each vehicle. In this example, the control force is applied at a distance of 2 feet ahead of the mass center of each vehicle. Consequently the "control coefficients" become: $A = 0$, $B = 1$, $C = 0$, and $D = 2$. Again, the control force magnitude differences seen in the top portion of Figure 5-19 are primarily due to the mass and inertia differences of the two vehicles and the placement of the control force relative to the vehicle mass center. Locating the applied control force further ahead of the vehicle mass center scales down the required control force. Placing it very far ahead results in a near zero applied control force accompanied by an increased yaw moment, thereby approximating the previous case of control by means of an applied yaw moment only.

If the control force is applied right at the front axle position, the case of front wheel only steering is duplicated. The required control force in that case is equal to the product of the front tire cornering stiffness and the steering angle required from a steerable front wheel.

Regardless of the particular vehicle control mechanism used, the above examples demonstrate that as long as the preview control driver model has a simple means of

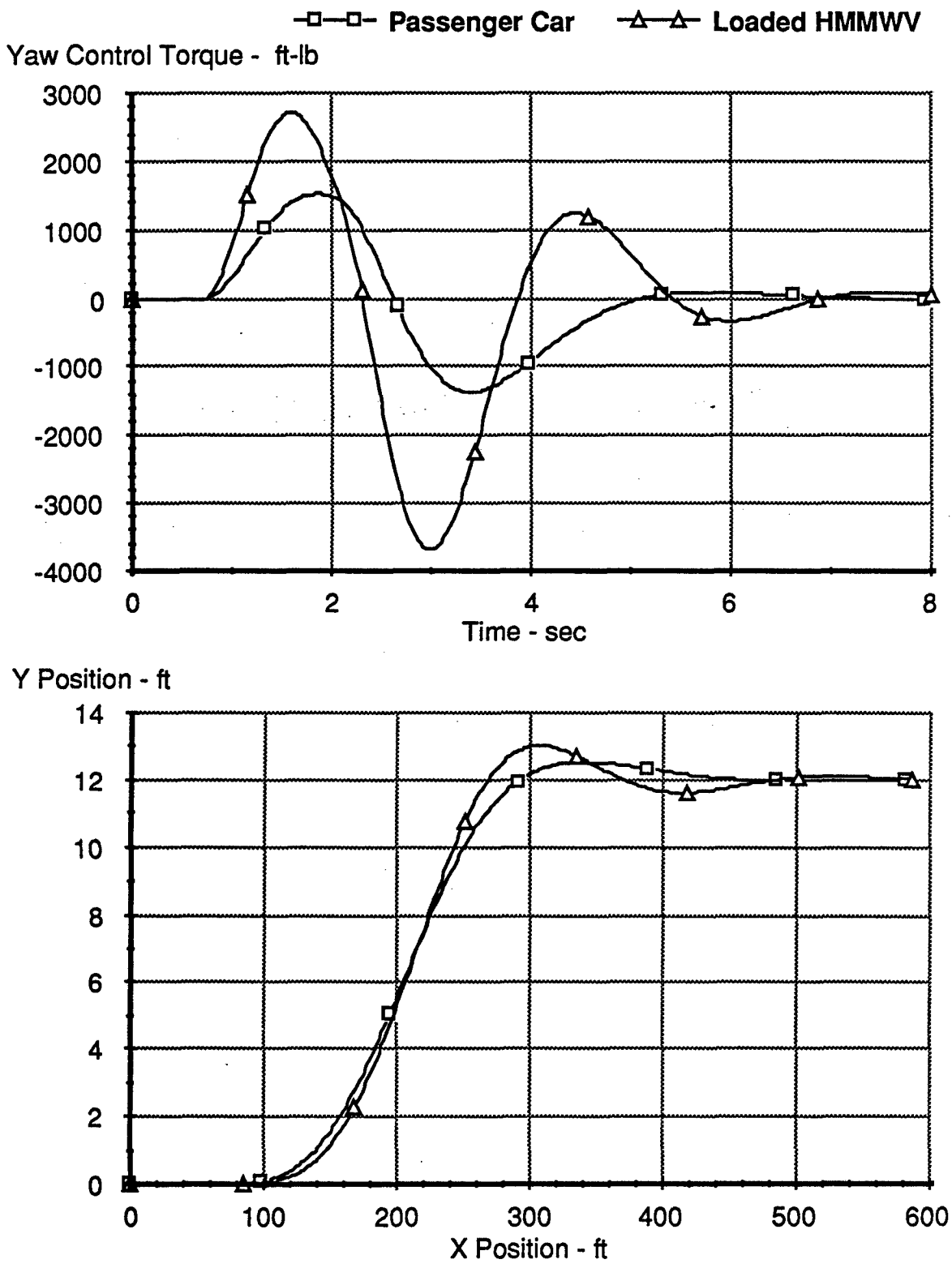

Figure 5-17. Driver Model Controlled Lane-Change Maneuver, Steering via an Applied Yaw Control Moment

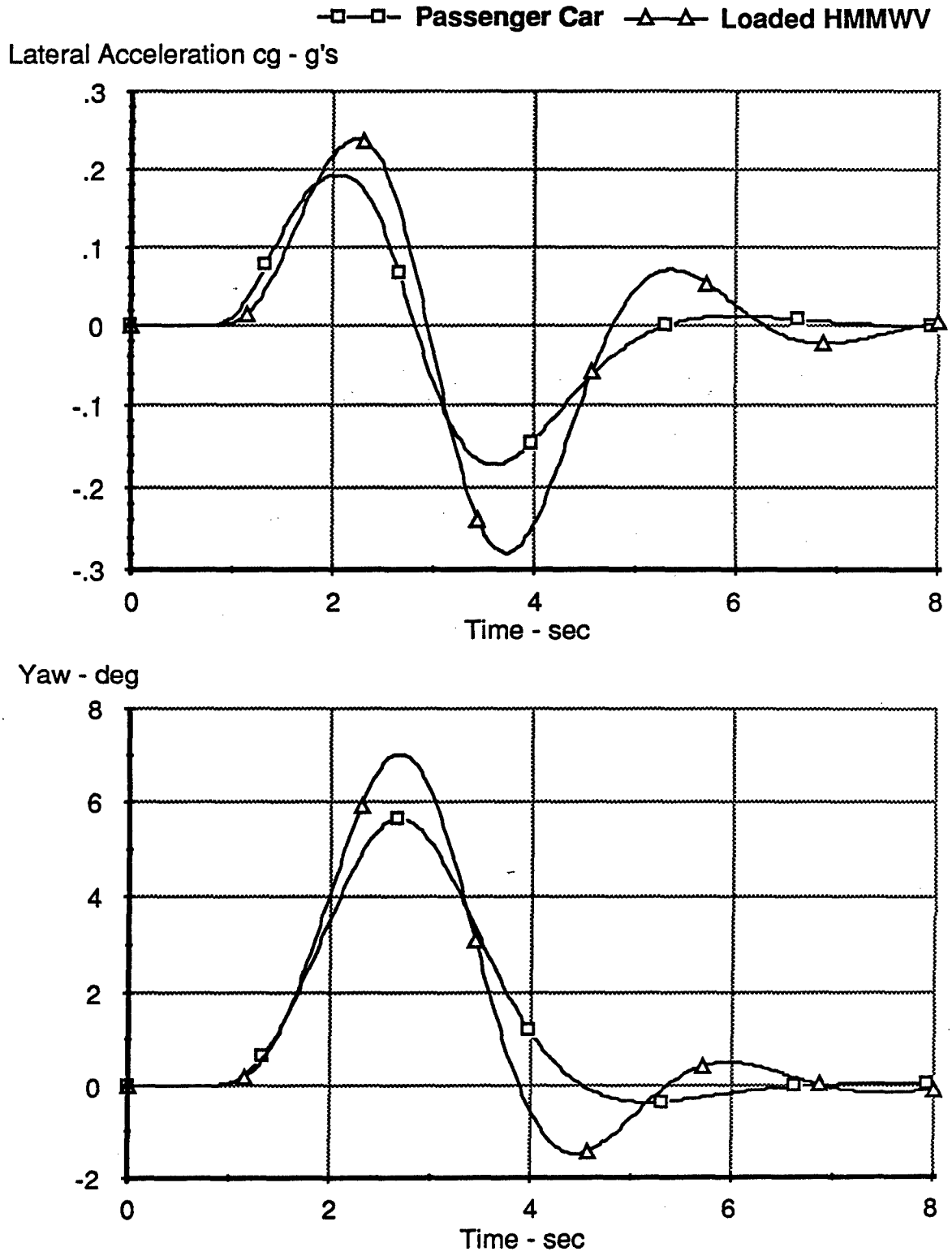

Figure 5-18. Driver Model Controlled Lane-Change Maneuver, Steering via an Applied Yaw Control Moment

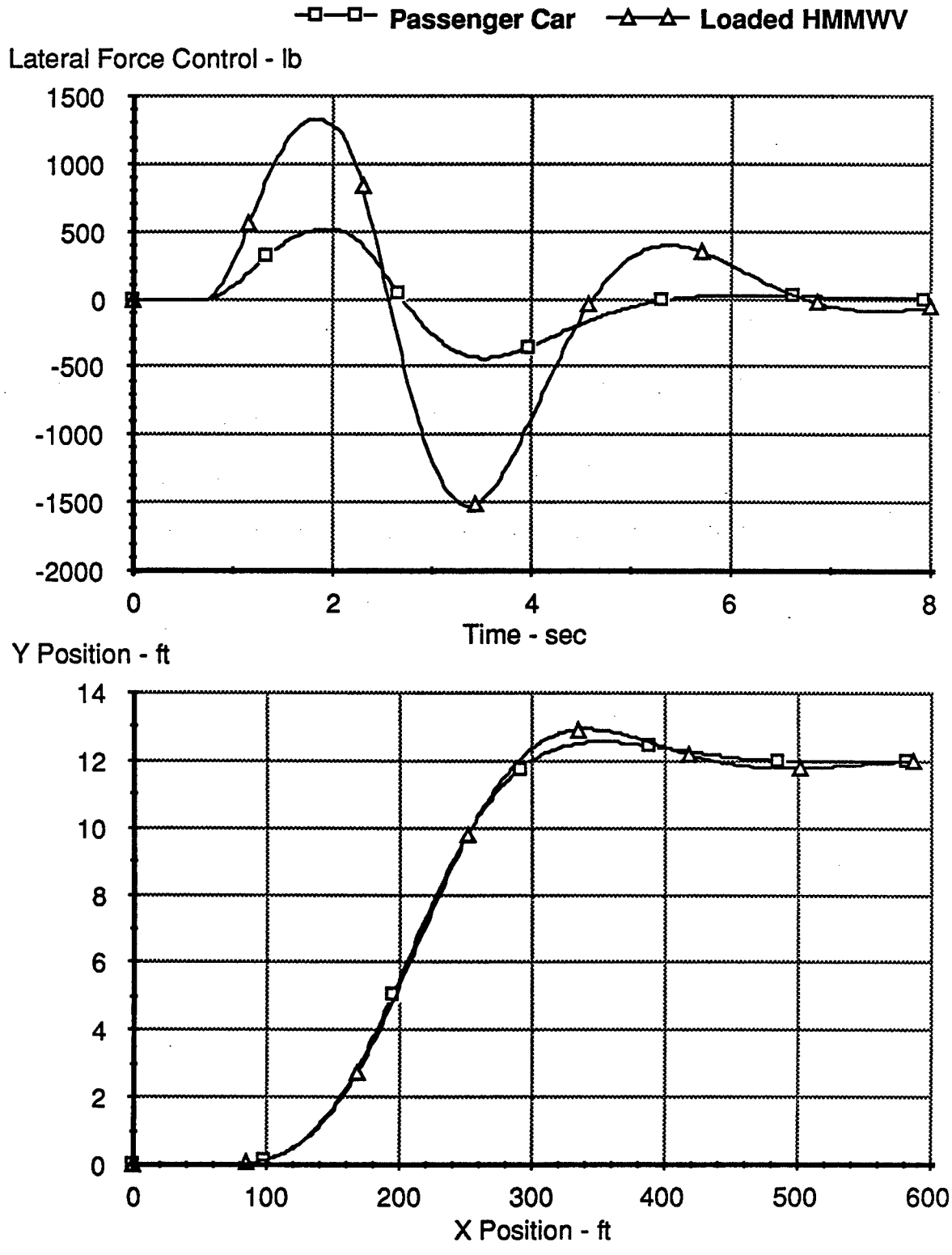

Figure 5-19. Driver Model Controlled Lane-Change Maneuver, Steering via an Applied Lateral Control Force

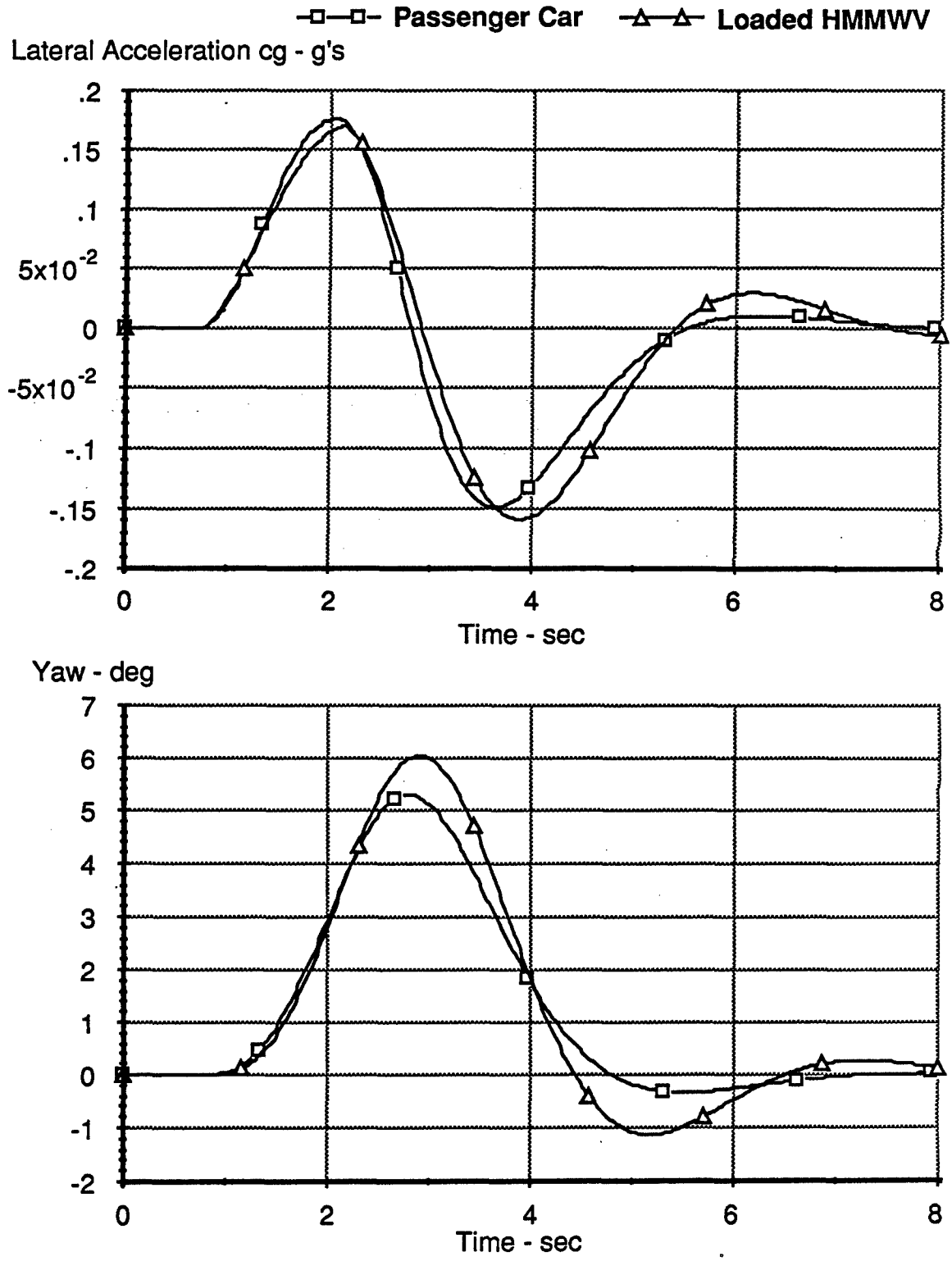

Figure 5-20. Driver Model Controlled Lane-Change Maneuver, Steering via an Applied Lateral Control Force

representing the dynamics of the vehicle and its control mechanism (via an internal vehicle model), it is capable of calculating an appropriate control variable time history which causes the vehicle to follow a prescribed path — and do so in a manner consistent with how actual human operators would steer a similar vehicle. To underscore this latter point, the following two sections of the report will present test data collected during the project, as well as direct comparisons between selected examples of that test data and corresponding predictions from the driver model.

5.6. Driver / Vehicle Tests

Closed-loop driver/vehicle tests were conducted during the project at the Chrysler Corporation Proving Grounds in Chelsea, Michigan. The primary vehicle used in these tests was an M1057 Truck also known as the HMMWV. The HMMWV was carrying a 3000 lb payload bringing its total weight to 7500 lb. Figure 5-21 shows a sketch of the basic HMMWV used in these tests. The 3000 lb payload was located directly over the rear axle thereby positioning the total mass center (of the vehicle and payload) at a point approximately 4 ft ahead of the rear axle and 4 ft above the ground.

A short sequence of additional tests were conducted with the same HMMWV pulling an M101 trailer. In these tests, the HMMWV's weight remained at 7500 lb and the total trailer weight was 3160 lb (1600 lb of payload). The trailer mass center was slightly ahead of its axle, producing a vertical hitch load of 176 lb on to the HMMWV. Figure 5-22 shows a sketch of the M101 trailer.

5.6.1. Inertial Parameter Measurements. The HMMWV was weighed in its test condition (with instrumentation and driver) to obtain front and rear tire loads and total weight. Estimates of yaw, pitch, and roll inertias were estimated or obtained from previous inertial measurements of the same vehicle at UMTRI. Likewise, total center of gravity height was estimated from previous empty vehicle inertial measurements and the known payload location. Measurements of wheelbase, wheel track, suspension locations, and overall geometry were also performed. Table 5-1 shows the parameter measurements and estimates for the HMMWV in its test condition.

5.6.2. Tire Measurements. One tire (size: 36 x 12.50 - 16.5 LT) from the HMMWV test vehicle was tested on the UMTRI flat-bed tire test machine to obtain lateral tire force measurements at four different nominal loads (1000, 2000, 3000, and 4000 lb) and eight slip angles (-1, 0, +1, 2, 3, 4, 6, and 12 degrees). See Figures 5-23 and 5-24. Tire cornering stiffness parameters needed by the driver model in subsequent model/test

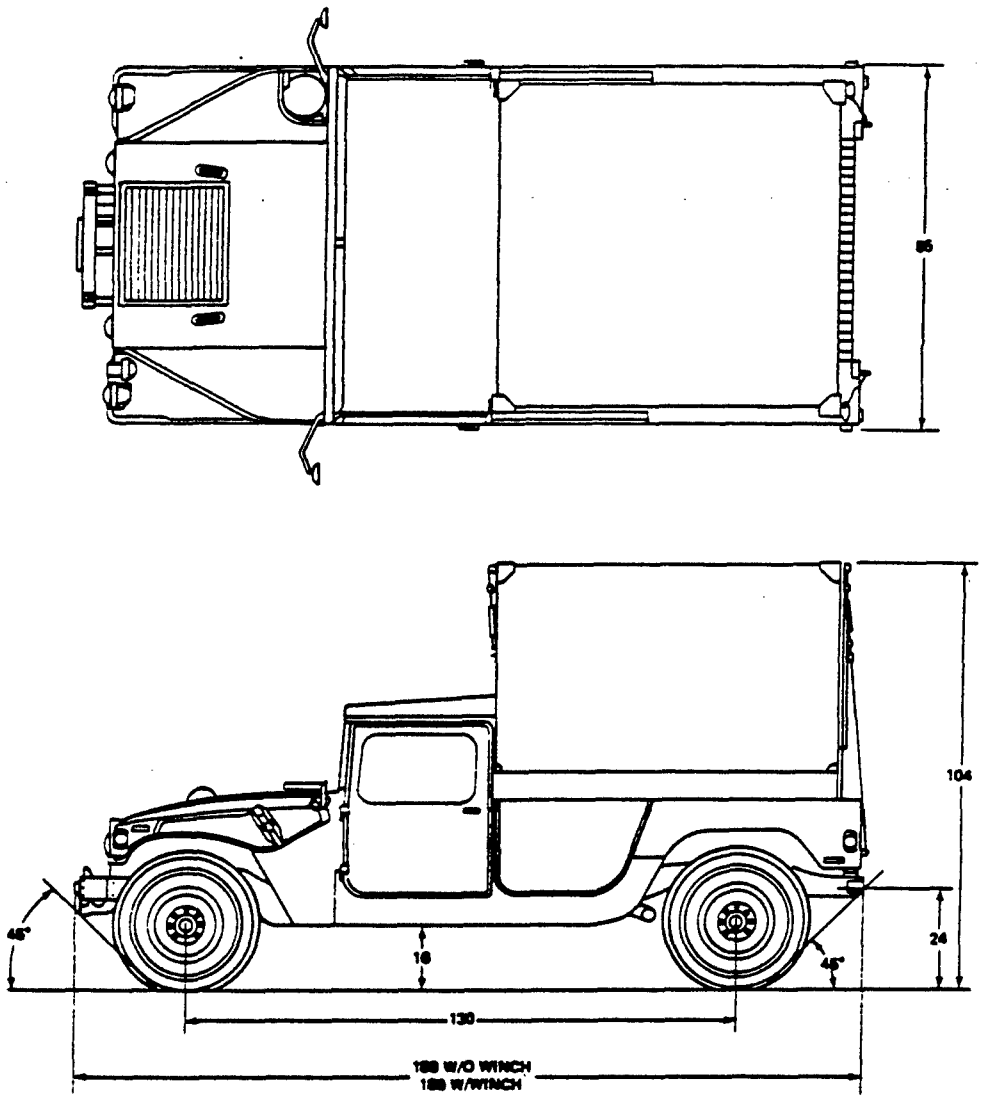

Figure 5-21. The M1037 Truck (HMMWV)

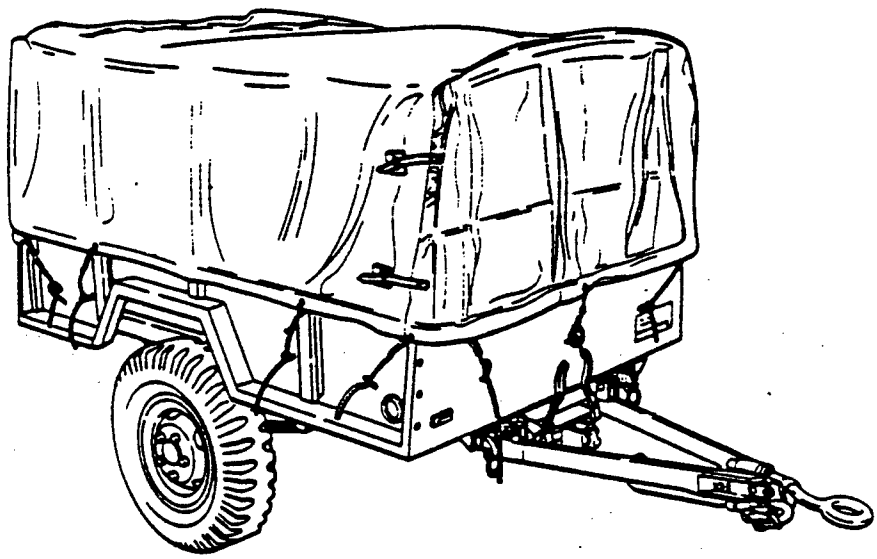

NOTE:
ALL DIMENSIONS ARE IN INCHES.

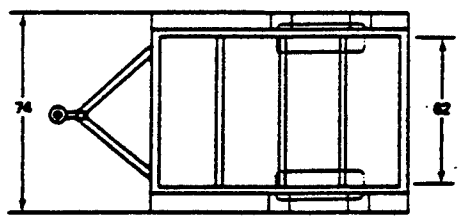

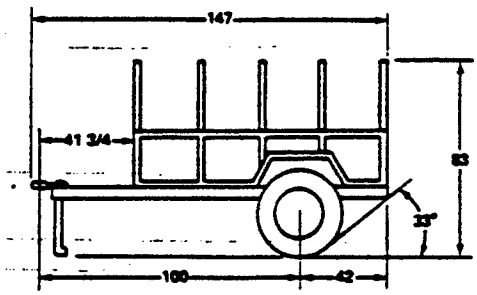

Figure 5-22. The M101 Trailer

Table 5-1. Parameter Measurements and Estimates for the HMMWV in its Test Condition

Total Weight	7460	lb
Wheelbase	130	in
Front Axle Load	2920	lb
Rear Axle Load	4540	lb
Distance from Total c.g Location to Rear Axle	50.9	in
Total Yaw Moment of Inertia	70000	in-lb-sec^2
Total Pitch Moment of Inertia	60000	in-lb-sec^2
Total Roll Moment of Inertia	13200	in-lb-sec^2
Front Tire Cornering Stiffness (@ static load)	270	lb/deg
Rear Tire Cornering Stiffness (@ static load)	335	lb/deg
Total c.g. Height Above Ground	48	in

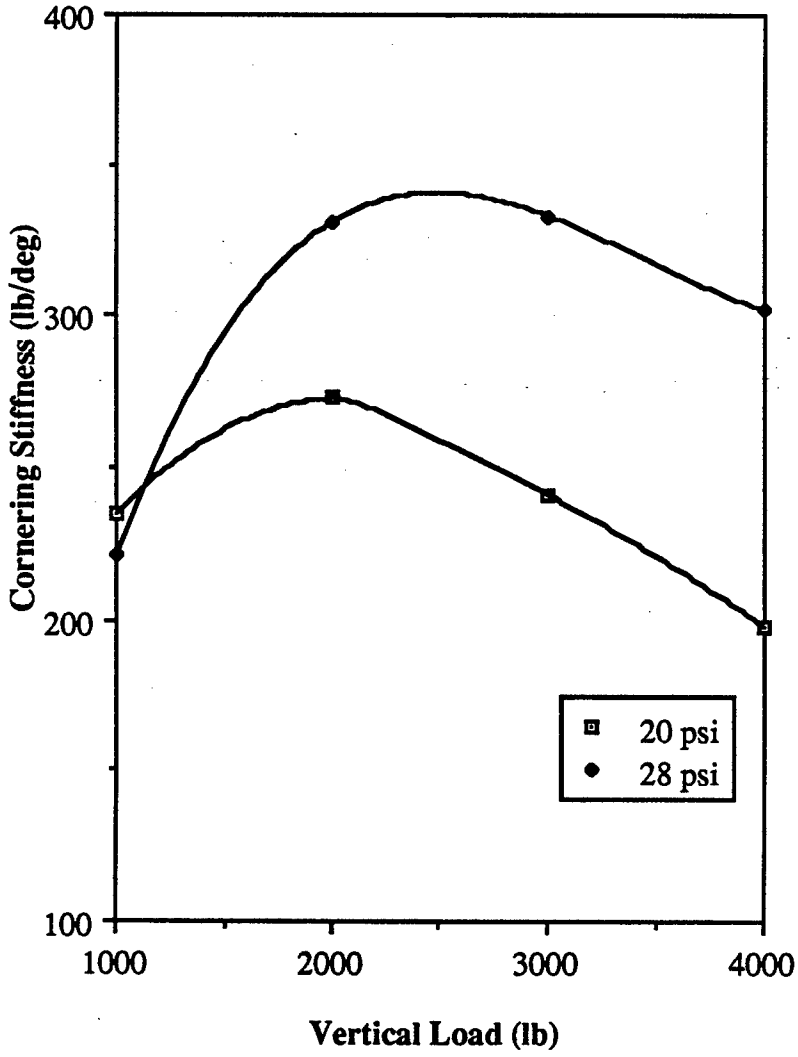

Figure 5-23. HMMWV Tire: Influence of Tire Inflation Pressure.

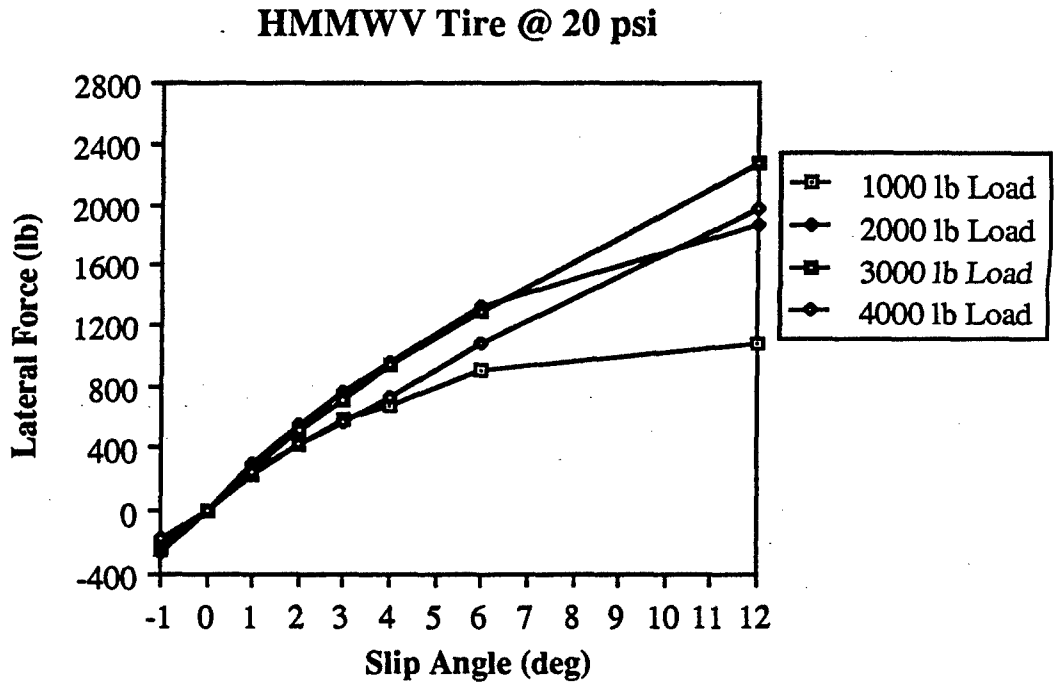

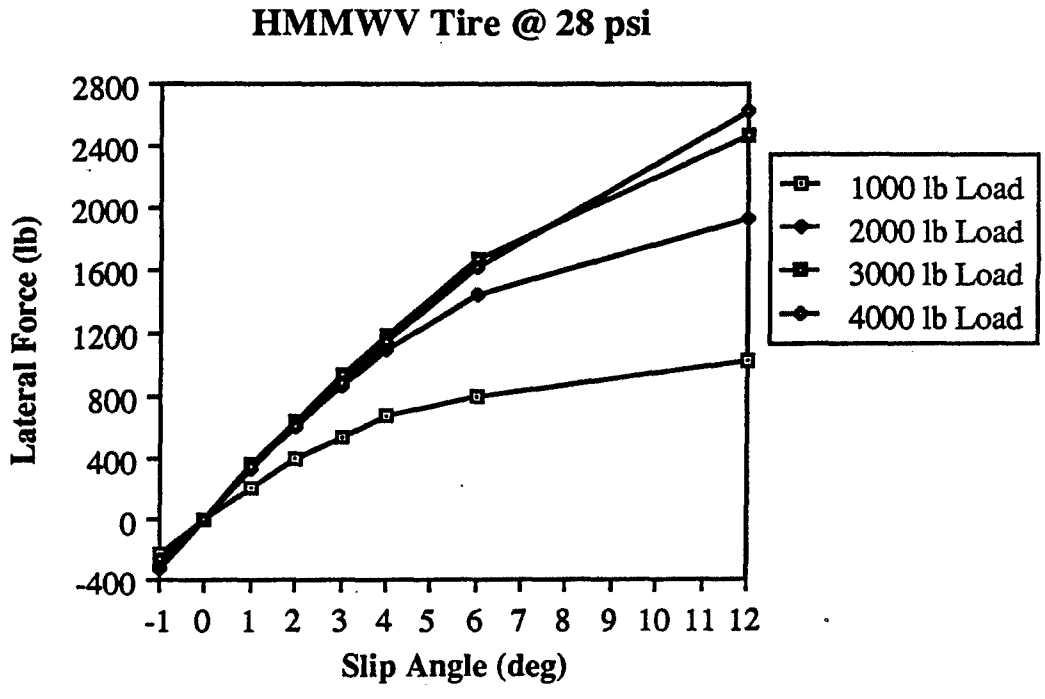

Figure 5-24. HMMWV Lateral Tire Force Measurements

validation activities, as well as complete lateral tire force representation within the DADS model [40], were based upon these measurements.

5.6.3. HMMWV Test Maneuvers. Three basic sets of driver/vehicle maneuvers were conducted during the test program with the HMMWV test vehicle. (1) The first test maneuver was simple steady turning by a driver along a circular path. The purpose of this test was to obtain estimates of the vehicle understeer and basic cornering properties, as well as, driver closed-loop steering control behavior into and during the steady turning maneuver under different conditions. (2) The second maneuver was similar to the first, but braking was applied during the turning maneuver by the driver so as to bring the vehicle to a stop at randomly selected points along the curve. (3) The third type of maneuver was to drive through a set of different obstacle courses, as defined by a pattern of traffic cones. These tests are explained more fully in the following.

- **Driver-Controlled Constant Radius Turning Tests.** The turning tests were conducted at 25, 50, and 60 mph with the test driver attempting to track a cone-marked turn of fixed radius (500 '). (A radius of 500 feet produces a lateral acceleration of 0.33 g's at 50 mph and was easily accommodated on the 800' x 800' Chrysler skid pad area.) The maneuver was begun by having the driver approach the circular turn along a straight tangent and, then, track the curve at constant speed. See Figure 5-25. Transient driver/vehicle response information due to entering the curve, as well as steady-state driver/vehicle response information due to tracking the curve, was gathered from these tests. Influence of forward speed and lateral acceleration upon system damping was obtained by conducting the same tests at the three different speeds. Vehicle turning properties, such as understeer level and steering control gains, were also derived from the steady turning data in these tests. Further, since both front wheel angles and steering wheel angle were being measured, estimates of the effective steering gear ratio and steering system compliance properties were available from these tests.

- **Driver-Controlled Braking-in-a-Turn Tests.** The braking-in-a-turn tests were all conducted from an initial speed of 50 mph with the test driver attempting to stop the vehicle in a fixed distance. The stopping distances were varied randomly, thereby requiring the driver to achieve different deceleration levels during each stop. This type of test served as a closed-loop braking control task for the driver, while simultaneously, yielding information on the basic braking performance capabilities of the test vehicle. Wheel lock-up occurrences were recorded for the shorter stopping distance cases. The driver brake pressure responses and corresponding deceleration time histories would be used to evaluate and outline a proposed closed-loop braking algorithm for the driver, augmenting the driver steering control model.

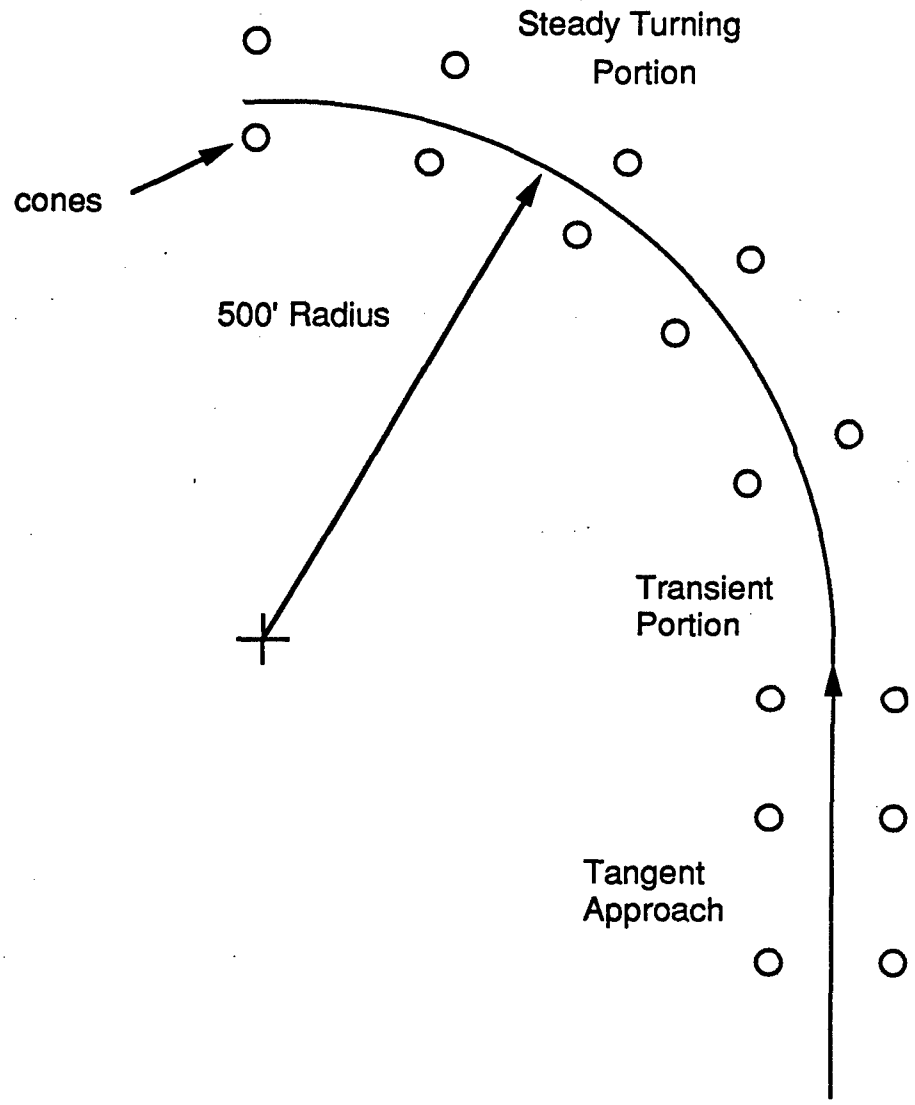

Figure 5-25. Driver Controlled Constant Radius Turning Test

• **Obstacle Course Tests.** The purpose of these tests was to gather transient driver/vehicle response data for both path-following and obstacle avoidance maneuvers. The basic type of maneuver consisted of performing various lane-to-lane movements with the vehicle as it traverses a cone-marked course. Tests were conducted at different speeds from 30 to 60 mph. Three basic obstacle course patterns were layed out and are shown in Figures 5-26 through 5-28:

A) Simple Path-Constrained Lane Change (Figure 5-26)

B) Simple Unconstrained Lane Change (Figure 5-27)

C) Obstacle Course (Figure 5-28)

The first two cases were included primarily to evaluate the influence of path constraints on driver steering control behavior. The constrained lane width in each of these tests was maintained at 12 feet, leaving the driver with about 2.5 feet of lateral maneuvering space with the vehicle centered in the lane. The remainder of the obstacle course tests took place with the layout shown in Figure 5-28. In these tests, the fore-aft distances between the 12' x 12' square obstacles were varied randomly from test to test.

In the lane-change tests, the baseline geometry, with the shoot-to-shoot forward travel distance (L) set at 100 feet, produced approximately 0.30 g's of peak lateral acceleration during the 60 mph maneuvers. The same course geometry was used for the 30 mph tests in order to evaluate the influence of forward speed upon driver preview and system damping.

In the obstacle course tests, the baseline geometry seen in Figure 5-29 produced peak lateral acceleration levels of about 0.4 g's with the obstacles located in their normal baseline positions. Tests were repeated several times, with the distances L1, L2, and L3 varied in a random-like sequence. The values of L1, L2, and L3 were set to 100 feet in the baseline course geometry. L1 and L2 were then varied forward or rearward by 20 feet to produce a 'short' or 'long' variation respectively from the nominal baseline geometry. The test driver continuously drove the vehicle dynamics oval — encountering a different obstacle course layout each time around the track. Data collection began several seconds prior to the beginning of the obstacle course and ended several seconds after the end of the obstacle course.

Table 5-2 is a listing of the log sheets from the test program. Run numbers and speeds are seen in the first two columns. Column 3 defines the test maneuver. Column 4 contains

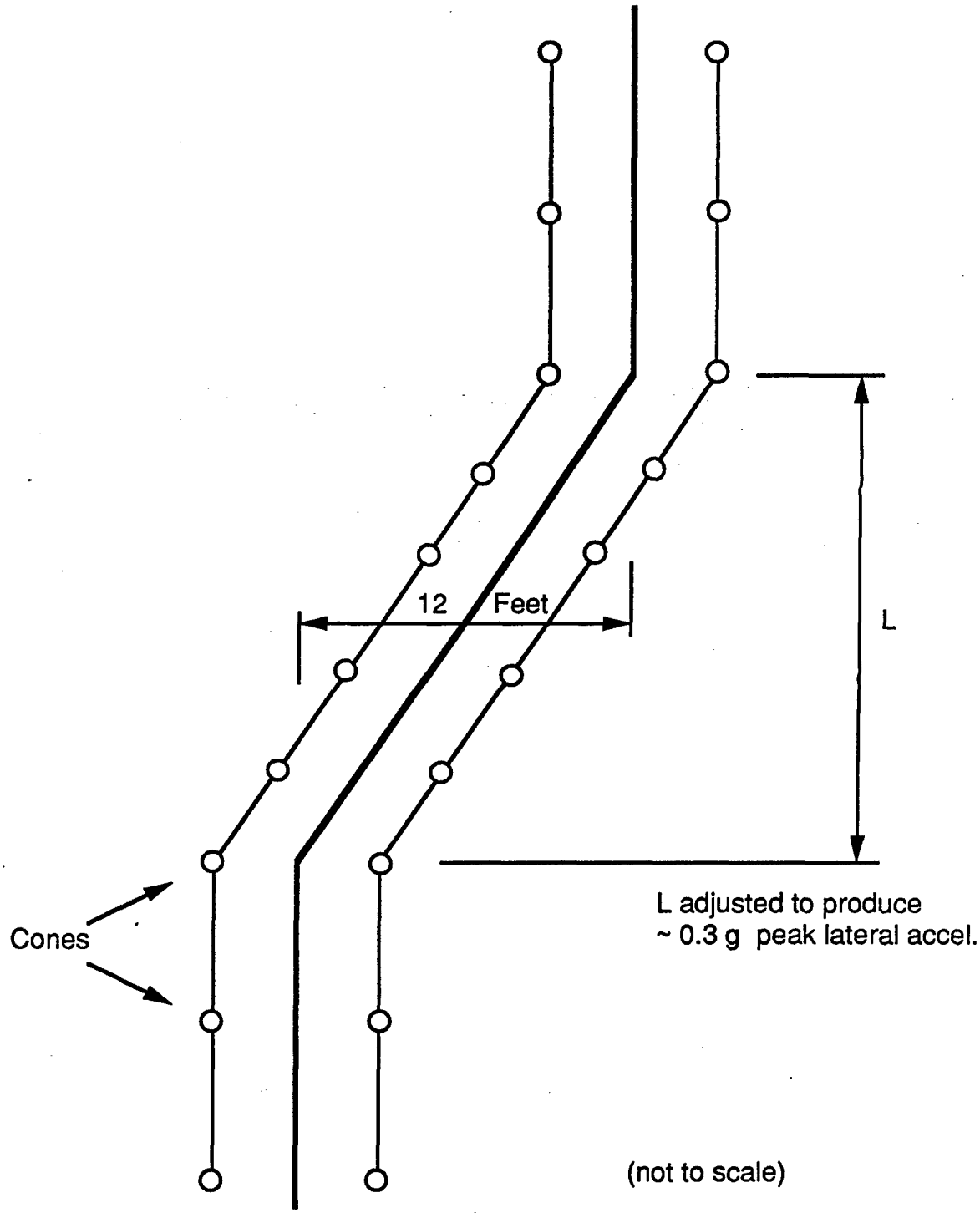

Figure 5-26. Path-Constrained Lane Change Maneuver

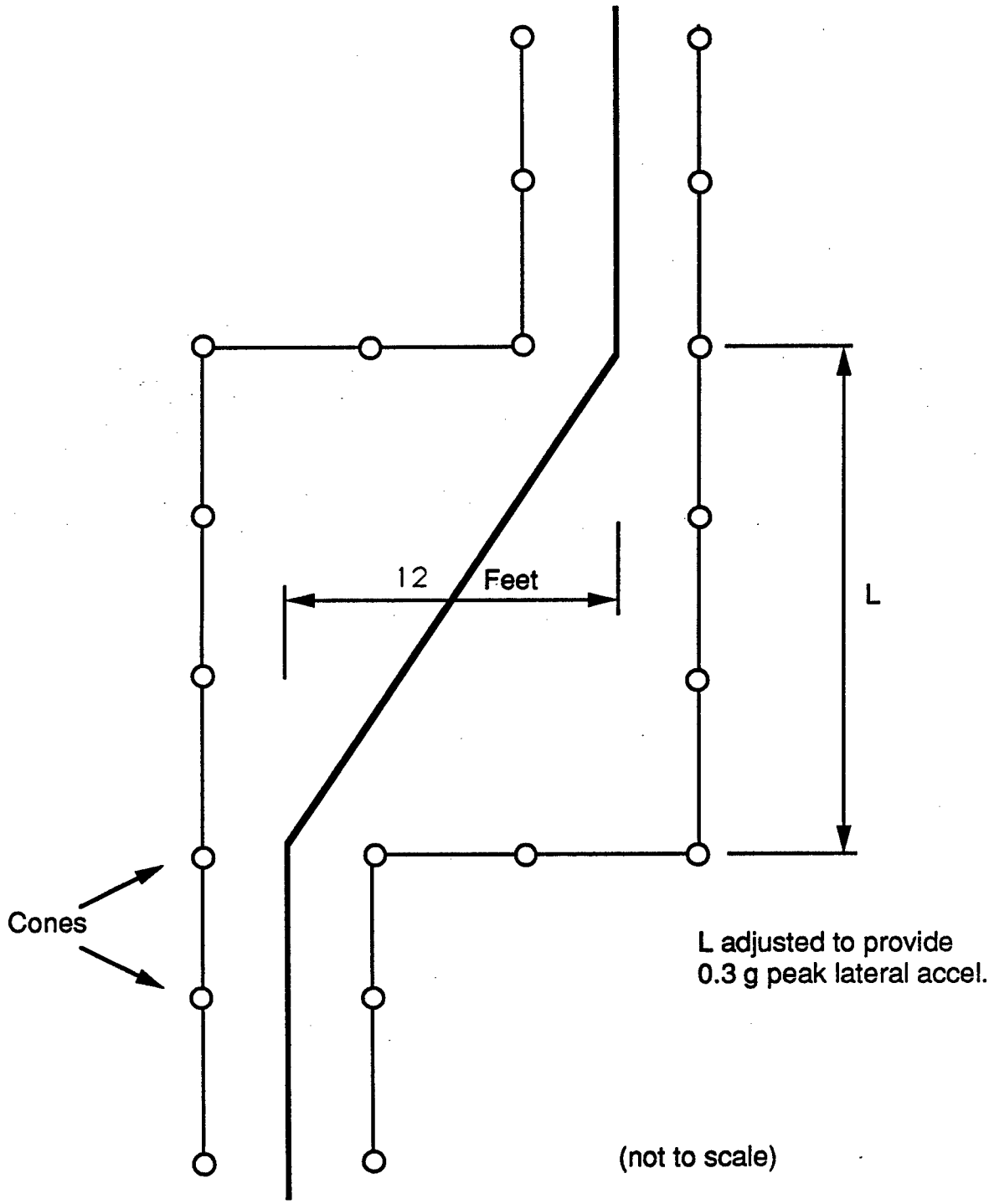

Figure 5-27. Unconstrained Lane Change Maneuver

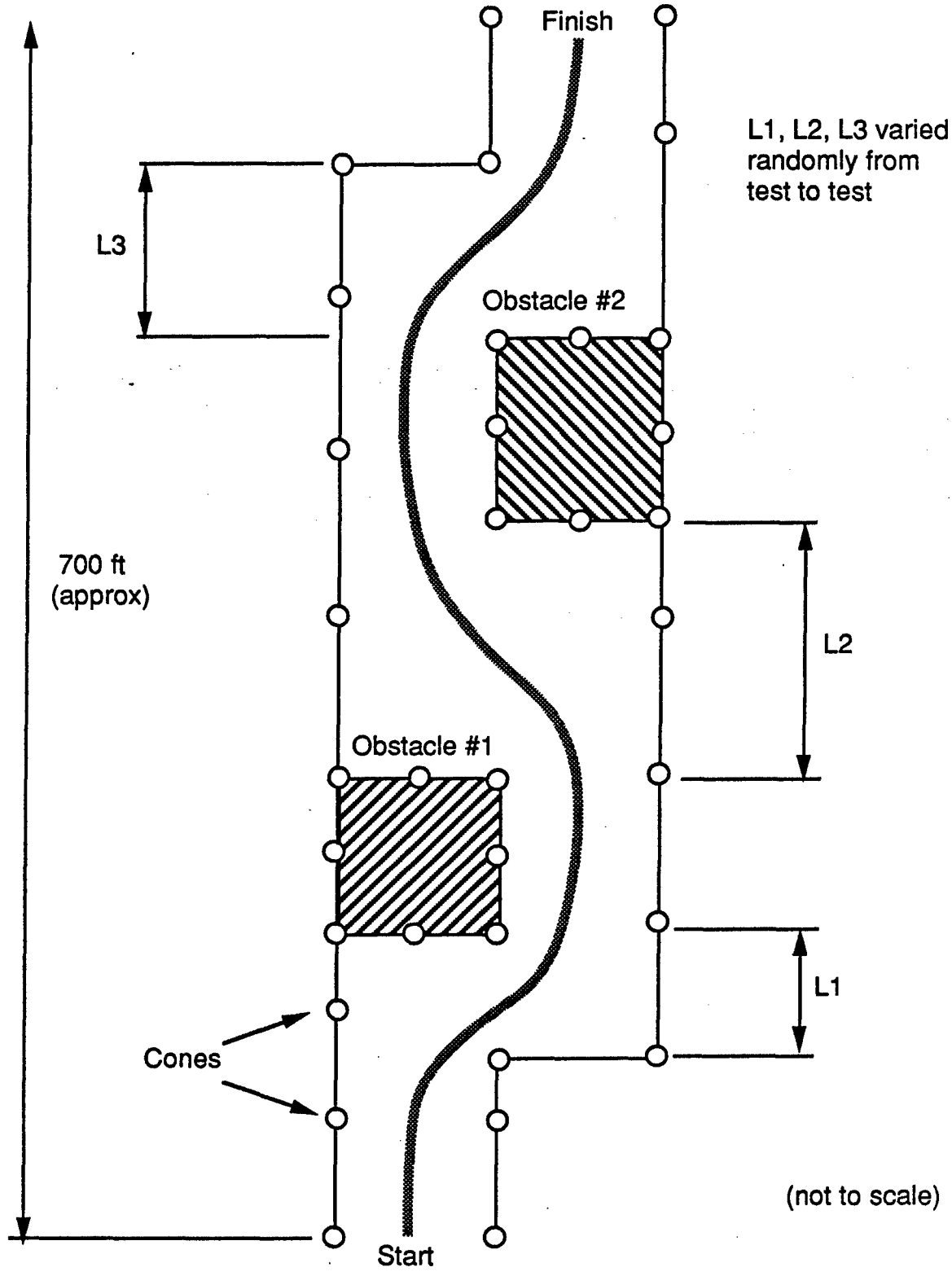

Figure 5-28. Basic Obstacle Course Layout

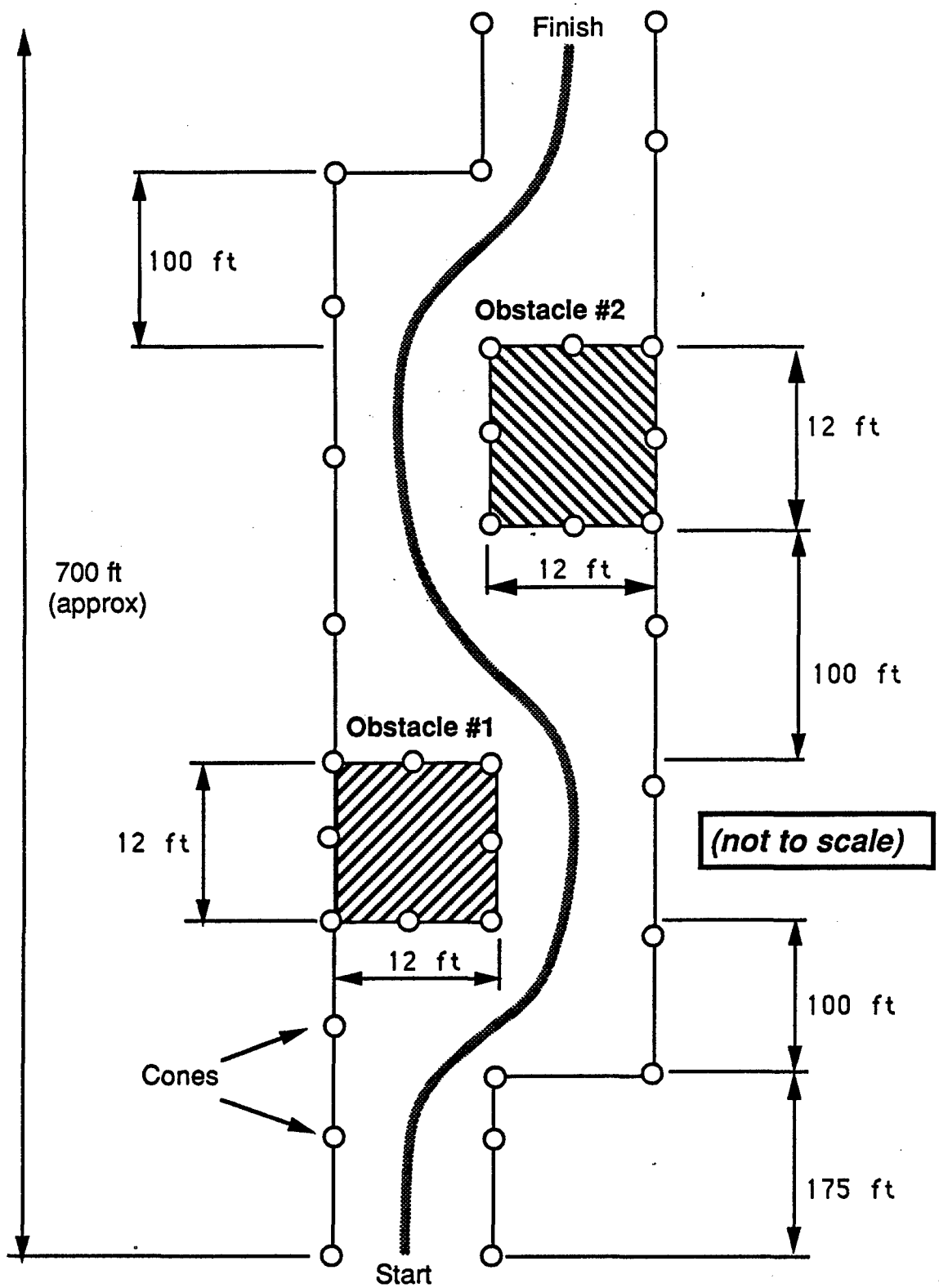

Figure 5-29. Baseline Obstacle Course Layout Used in Tests

Table 5-2. Log Sheet Summary of Driver-Vehicle Tests

Run #	Speed (mph)	Maneuver	Comments
101	50	Steady Turning	28 psi tire pressures, driver #1
102	50	"	
103	50	"	
104	50	"	
105	50	"	sign of Ay changed to proper SAE convention
106	25	"	
107	25	"	some swerving
108	25	"	5 mph fast at end
109	25	"	
110	25	"	
111	55	"	
112	55	"	lost velocity signal during run
113	55	"	lost yaw rate during run
114	50	Braking in a Turn	215' stopping distance
115	50	"	170 '
116	50	"	195'
117	50	"	145'
118	50	"	132'
119	50	"	195'
120	50	"	195'
121	50	"	130', left rear wheel locked, 37' of skid
122	50	"	140'
123	50	"	130'
124	50	"	125', left rear wheel locked, 34' of skid
125	50	Constrained Lane Change	12' x 100' , 28 psi tire pressures
126	60	"	
127	"	"	
128	"	"	
129	"	"	
130	"	"	lost velocity signal at end of run
131	"	"	
132	"	"	
133	"	"	
134	"	"	re-fueled
135	30	"	
136	"	"	
137	"	"	
138	"	"	
139	"	"	

Table 5-2. Log Sheet Summary of Driver-Vehicle Tests (continued)

Run #	Speed (mph)	Maneuver	Comments
140	30	Constrained Lane Change	
141	"	"	driver #2
142	"	"	driver #2
143	40	"	driver #2
144	50	"	driver #2
145	60	"	driver #2
146	30	Unconstrained Lane-Change	12' x 100', driver #1, no cones hit
147	30	"	"
148	30	"	"
149	60	"	"
150	60	"	"
151	60	"	"
152	60	"	driver #2, hit numerous cones
153	60	"	driver #2, no cones hit
154	30	Temporary Obst Course	driver #1
155	30	"	"
156	30	"	"
157	30	"	"
158	40	Obstacle Course	see Fig 5.6-6, driver #1, center/center
159	50	Obstacle Course	"
160	40	"	"
161	40	"	"
162	"	"	"
163	"	"	center/center, hit obstacle #2 on right
164	"	"	center/short
165	"	"	center/long
166	"	"	center/long
167	"	"	center/short
168	"	"	center/center
169	"	"	short/center
170	"	"	long/short, hit second obstacle
171	"	"	long/center
172	"	"	short/long, (obst #2 width=9.5')
173	"	"	center/long (obst #2 width=9.5')
174	"	"	long/long, (obst #2 width=9.5')
175	"	"	long/long
176	"	"	center/short
177	"	"	short/short, clipped obst #2
178	"	"	center/center
179	"	"	long/center, clipped obst #2
180	"	"	long/short, hit obst #2

Table 5-2. Log Sheet Summary of Driver-Vehicle Tests (continued)

Run #	Speed (mph)	Maneuver	Comments
181	40	Obstacle Course	long/short, hit obst #2, clipped cone on exit
182	"	"	center/center, clipped obst #2
183	"	"	center/center
184	"	"	short/short
185	"	"	long/long
186	30	Random Steer Tests	driver #2
187	30	"	"
188	30	"	"
189	50	"	"
190	60	"	"
191	"	"	"
192	"	"	"
193	"	"	"
194	"	"	"
195	30	"	"
196	30	"	
197	60	"	speed low
198	60	"	"
199	45	"	"
200	45	"	"
201	30	"	"
202	60	"	"
203	50	Straight-Line Braking	143' stopping distance
204	"	"	120', short lockup F & R
205	"	"	170'
206	"	"	195'
207	"	"	130', all locked, slight drift to right
208	"	"	140'
209	"	"	150'
210	"	"	200', short lock at end
211	"	"	170'
212	"	"	150'
213	"	"	200'
214	"	"	125', F & R lock
215	"	"	145'
216	"	"	150'
217	"	"	175'

Table 5-2. Log Sheet Summary of Driver-Vehicle Tests (continued)

Run #	Speed (mph)	Maneuver	Comments
218	25	Steady Turning	all tires at 28 psi
219	"	"	"
220	"	"	"
221	"	"	"
222	50	"	"
223	"	"	"
224	"	"	"
225	30	Random Steer Test	all tires at 28 psi
226	30	"	"
227	30	"	"
228	60	"	"
229	60	"	" (start tape seg 5)
230	60	"	"
231	60	"	"
232	30	Random Steer tests	all tires set to 22 psi HOT (were 29-32)
233	30	"	"
234	30	"	"
235	55	"	"
236	60	"	"
237	60	"	"
238	60	"	"
239	60	"	"
240	25	Steady Turning	all tires set at 20 psi HOT
241	25	"	"
242	25	"	"
243	50	"	"
244	50	"	"
245	50	"	"
246	60	"	gradual heating of tires during this sequence
247	60	"	"
248	"	"	"
249	"	"	"
250	"	"	"
251	"	"	"
252	"	"	tire pressures up to 24-26 psi
253	"	"	rear tire pressures set back to 22 psi HOT

Table 5-2. Log Sheet Summary of Driver-**Vehicle Tests** (continued)

Run #	Speed (mph)	Maneuver	Comments
254	30	Constrained Lane-Change	all tires set at 28 psi
255	30	"	"
256	30	"	"
257	60	"	"
258	60	"	"
259	60	"	tires up to 32 psi HOT
260	30	"	all tires reduced to 20 psi HOT
261	30	"	"
262	30	"	"
263	30	"	"
264	60	"	"
265	60	"	" (tape segment 6)
266	60	"	"
267	60	"	"
271	25	Constrained Lane Change	**HMMWV & Trailer, 30 psi / 82 psi**
272	25	"	"
273	25	"	"
274	25	"	"
275	35	"	"
276	43	"	"
277	48	"	"
278	48	"	"
279	46	"	"
280	4?	"	"
281	50	"	"
282	48	"	"
283	48	"	"
284	25	"	21 psi / 30 psi / 82 psi
285	25	"	"
286	25	"	"
287	45	"	"
288	48	"	"
289	46	"	"
290	48	"	"

Table 5-2. Log Sheet Summary of Driver-Vehicle Tests (continued)

Run #	Speed (mph)	Maneuver	Comments
291	25	Steady Turning	**HMMWV & Trailer, 30 psi/ 82 psi**
292	25	"	"
293	25	"	"
294	35	"	"
295	38	"	"
296	42	"	"
297	41	"	"
298	45	"	hit some cones
299	43	"	"
300	44	"	"
301	45	"	"
302	46	"	"
303	45	Braking in a Turn	180' stopping distance, wheel lock
304	45	"	220'
305	50	"	170'
306	50	"	180', hummer locked all, 50' skid marks
307	50	"	143'
308	50	"	169'
309	50	"	147', intermittent lockups, 25' skid marks
310	48	"	145'

Table 5-2. Log Sheet Summary of Driver-Vehicle Tests (continued)

Run #	Speed (mph)	Maneuver	Comments
320	45	Divergence Tests	HMMWV & Trailer, Divergence Tests
321	45	"	", video #3
322	48	"	", video #4
323	x	"	"
324	45	"	"
325	50	"	"
326	50	"	"
327	55	"	"
328	55	"	"
329	58	"	"
330	60	"	"
331	57	"	"
332	58	"	", video #8
333	62	"	"
334	63	"	"
335	63	"	"
336	40	Oscillation tests	HMMWV & Trailer, Oscillation Tests
337	40	"	
338	40	"	speed not constant
339	40	"	
340	45	"	
341	40	"	"small" steer input disturbance
342	40	"	"medium" steer input disturbance
343	40	"	"large" steer input disturbance
344	35	"	"small" steer input disturbance
345	35	"	"medium" steer input disturbance
346	35	"	"large" steer input disturbance
347	accel	"	"
348	accel	"	"

additional comments specific to each test. Two additional test maneuvers for the HMMWV are listed in the log sheets of Table 5-2 as "Random Steer Tests" and "Straight-line Braking". These tests were conducted initially as "additional" tests to provide further data on the directional dynamics and braking characteristics of the HMMWV. It turned out that the information provided by these additional tests was not subsequently needed in the model validation. However, the data from these additional tests are available as part of the entire collection of test data being delivered to TACOM and can be used as a source of additional information. The "Straight-line Braking" tests were conducted in the same manner as the braking-in-a-turn baseline tests (but without any turning) with the stopping point varied in a random manner. The stopping distances are noted in the log sheets of Table 5-2. The "Random Steer" tests were conducted during straight-line driving with the test driver producing a random-like steering input to purposely excite the vehicle directional dynamics across a range of steering input frequencies. Fourier transforms can be performed on these measured vehicle responses and the steering input to obtain frequency response characteristics for the open-loop directional dynamics of the vehicle.

Example measurements from each of these basic test maneuvers appear in Appendix B. The total set of data collected during the test program are being delivered to TACOM on floppy disks in a standardized UMTRI format.

5.6.4. Data Acquisition Equipment. Test data was collected using the UMTRI portable data acquisition system. The system consists of a Texas Instruments TM 990 microprocessor, signal-conditioning units, programmable filters, and analog/digital converters. A CRT unit and keyboard were used to operate and control the system. Data were stored on high capacity digital tape cartridges for subsequent post-processing. Simple statistical calculations and background calibrations could be performed in the field. Spot checks of the collected data would occur periodically throughout the duration of the test program to guard against undetected instrumentation failures. All of the test data collected during the program were transferred to hard disks and floppies in an UMTRI standard format for subsequent plotting and analysis.

5.6.5. Vehicle / Driver Measurements. The vehicle was instrumented with appropriate transducers and the UMTRI data acquisition package to measure the following signals and vehicle responses:

- Lateral Acceleration
- Longitudinal Acceleration
- Vehicle Velocity

- Yaw Rate
- Roll Angle
- Front Wheel Steer Angles (left and right)
- Steering Wheel Angle
- Brake Pedal Pressure

The UMTRI stable platform was used to measure the vehicle lateral and longitudinal accelerations, as well as the yaw rate and roll angle, relative to a horizontal plane oriented normal to the gravity vector. A conventional fifth wheel was used to measure forward velocity. Front wheel angles were measured with linear potentiometers, driver steering wheel angle with a rotary potentiometer, and driver brake pedal force with a hydraulic pressure transducer.

5.6.6. Special HMMWV-Trailer Tests. A sequence of baseline articulated vehicle tests were also conducted using the single-axle M101 trailer attached to the HMMWV via its rear pintle-hook. The trailer load was located approximately over the trailer axle, producing a vertical hitch load of 176 lbs at the HMMWV pintle hook. The dynamics of the trailer, and its possible effect upon driver steering control activity, were evaluated during a repeat of several of the lane-change and circular turning tests. Using the test data collected under this project, Mousseau in a TACOM technical report,[41] fully analyzed the HMMWV-trailer combination vehicle using the DADS simulation.[40]

In addition to the baseline tests studied by Mousseau, a short series of straight-line stability tests were also conducted with the trailer payload located in an adverse rearward location, thereby exciting a limit-cycle response in the articulation motion. The resulting driver steering action in response to the limit cycle motion was later analyzed and compared with results from comparable simulation runs. A short technical paper [42] reporting on some of these special tests appears in Appendix G of this report.

Example measurements from the HMMWV-Trailer test program appear in Appendix C. As in the case of the HMMWV data, all the trailer test results are being delivered to TACOM on floppy disks in a standardized format.

During all of these tests, the M101 trailer was instrumented with three additional transducers to measure the following vehicle responses:

- Trailer Lateral Acceleration

- HMMWV-Trailer Articulation Angle

and

- Trailer Roll Angle

The last portion of Table 5-2 lists the HMMWV-trailer tests. Tests 271-310 correspond to the HMMWV-trailer in its normal loading state as reported on by Mousseau.[41] Tests 336-348 ("Oscillation Tests") correspond to the straight-line stability tests with the trailer loaded in an adverse rearward manner in order to excite the limit cycle trailer oscillations. Tests 320-335 ("Divergence Tests") had the trailer payload located in the far forward position, but produced no significant instability or difficulty for the driver. A video tape was also produced at the time of these tests to record several of the trailer oscillation responses for later analysis.

5.7. Driver Model Validation

The material presented in this section of the report validates the developed steering control model by comparing example test results directly with corresponding predictions from the model. In most of these comparisons, the driver model is used in conjunction with a linear vehicle model.[43] In cases involving significant nonlinearities, fully nonlinear vehicle models [7, 40] are used with the same driver model to represent the vehicle. The parameters selected for the vehicle model were based upon the measured and estimated values obtained during the course of the project as reported in the previous section and by Mousseau.[41] Table 5-3 lists the basic vehicle and driver parameters used in most of these validation calculations. Any changes in speed, tire properties, or driver parameters for the individual comparisons that follow are noted and explained in the corresponding discussions for each case.

The first series of tests examined are for the *constrained lane-change maneuver* at the nominal speed of 60 mph. Figures 5-30 and 5-31 show a comparison between experimental measurements and predictions from the TACOM driver model. Tests 126, 127, 129, and 130 represent four repeated runs by the test driver through the constrained lane-change test course seen in Figure 5-26 at 60 mph. The driver steering wheel angle and lateral acceleration signals seen in these two figures are direct measurements. The experimental lateral displacement and yaw angle signals are obtained from the measured data by doubly integrating the lateral acceleration and singly integrating the yaw rate measurements respectively over the time interval shown. The thick dark line represents the output from the model using an identical 12-ft by 100-ft lane-change course as that used in the tests for its desired path input. Preview time and driver lag values were selected as 1.1

Table 5-3. Baseline Driver/Vehicle Parameters Used in Validation Calculations

Driver Model Preview Time	1.1	sec
Driver Model Delay Time	0.1	sec
Total Vehicle Weight	7500	lb
Wheelbase	130	in
Front Axle Load	2932	lb
Rear Axle Load	4568	lb
Distance from Total c.g Location to Rear Axle	50.8	in
Total Yaw Moment of Inertia	70000	in-lb-sec^2
Total Pitch Moment of Inertia	60000	in-lb-sec^2
Total Roll Moment of Inertia	13200	in-lb-sec^2
Front Tire Cornering Stiffness (@ static load)	270	lb/deg
Rear Tire Cornering Stiffness (@ static load)	335	lb/deg
Total c.g. Height Above Ground	48	in

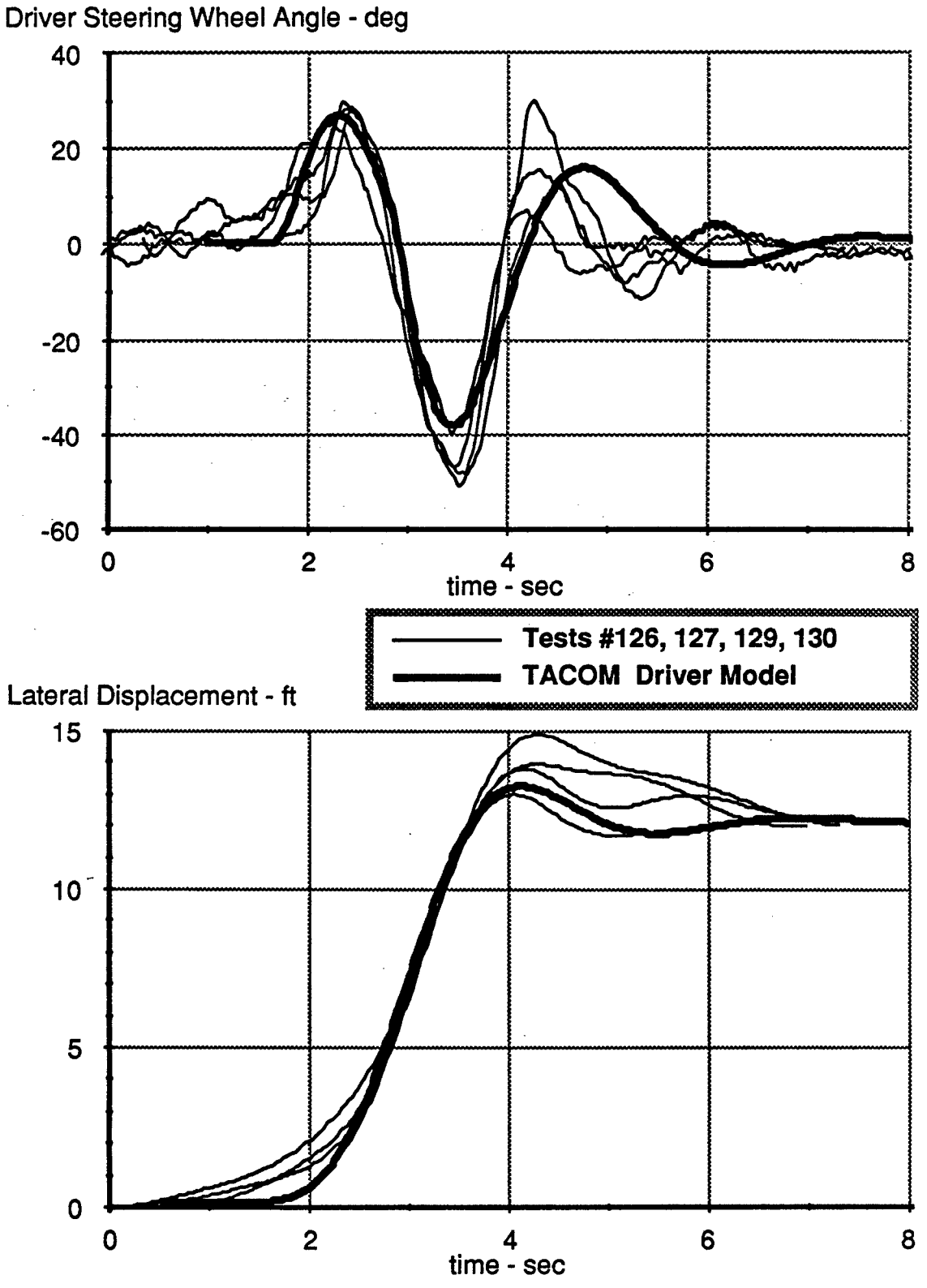

Figure 5-30. Driver Model Validation, Constrained Lane-Change

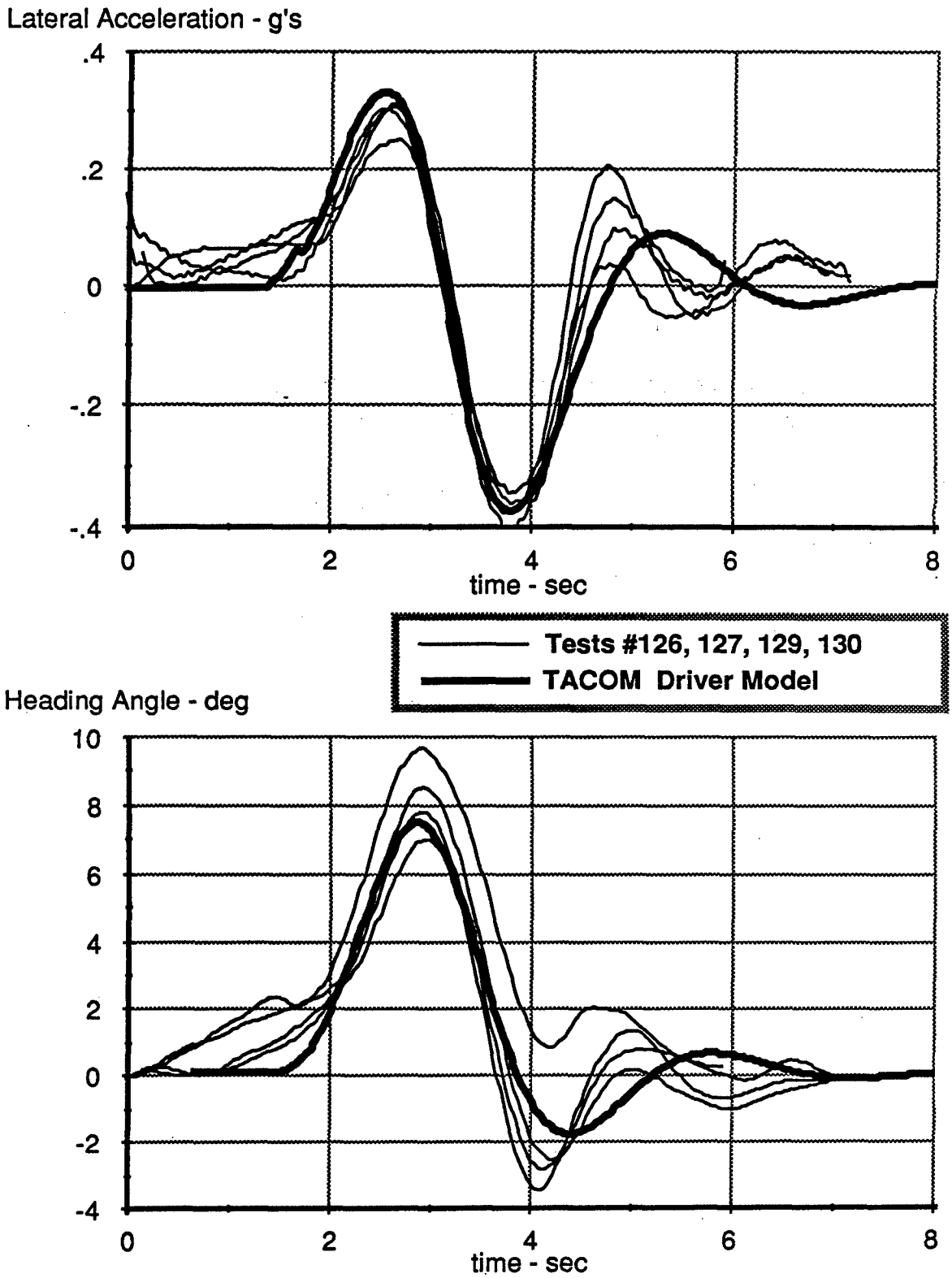

Figure 5-31. Driver Model Validation, Constrained Lane-Change

seconds and 0.1 seconds respectively to provide the degree of matching observed in Figures 5-30 and 5-31.

The relatively small value of the driver time delay parameter (0.1 seconds) is an interesting result. Recall from section 5.3 that most previous research involving random excitation of driver vehicle systems suggests that the TACOM driver model can best match such data by using a value of approximately 0.25 seconds ($1/\omega_c$, or, 1/4 rad/sec) for this parameter. However, these results are based upon closed-loop tests involving passenger cars. One explanation of this apparent conflict may be that because the HMMWV is more sluggish in its directional dynamics than a conventional passenger car, the driver of a HMMWV is required to provide more lead time and anticipation in order to perform a comparable maneuver. Another explanation may be that the lane-change tests conducted here were highly repeatable and easily predicted by the driver. Consequently, the "processing time" required by the driver to obtain an appropriate steering input for these tests may be considerably less than if the path input was less predictable. A reduction in driver processing time would then be reflected in the driver model by a smaller value of the driver time lag parameter. However, a previous study [1, 44] which examined lane-change tests with drivers of passenger cars and then represented the results with a similar version of the TACOM model, concluded that values of 0.2 to 0.3 seconds were appropriate in representing driver steering control time delay characteristics for that vehicle in a nearly identical lane-change maneuver. This would then seem to suggest that the differences raised here in driver time delay characteristics are somehow related to the directional dynamics of the controlled vehicle.

To illustrate this point further by example, if a driver model time lag value of 0.25 seconds is used instead of the 0.1 second value for the same HMMWV calculation just presented, the preview time parameter must correspondingly be increased to maintain the same degree of damping shown in the test data. This then results in a somewhat more sluggish response from the model with most of the resulting waveforms having a longer period than that seen in the test data. Figures 5-13 and 5-14, for example, previously showed a calculation for the HMMWV using a larger set of time delay and preview time parameters. The result was a considerably more sluggish response than that seen in Figures 5-30 and 5-31.

The suggestion that the TACOM driver model time delay parameter should be reduced in certain cases to values less than those previously suggested by random disturbance tests [1, 24, 25, 26] is an important result. This finding may suggest that drivers of land vehicles having more sluggish directional dynamics are required to be more responsive during typical steering maneuvers in order to compensate for the increased lag of the vehicle. Intuitively, this makes sense, but heretofore, this observation about the responsiveness of

drivers and the directional responsiveness of vehicles has not been adequately established and linked to experimental evidence from full-scale tests of driver/vehicle systems.

A less obvious suggestion that driver/vehicle systems are not necessarily any more stable with shortened driver lags follows from the observation that the preview time is apparently reduced "in step" with the driver lag for the lane-change data collected here. (Ordinarily, experimental measurements obtained from random disturbance tests [26] of passenger car / driver systems would suggest values of the time delay parameter on the order of 0.25 seconds, and values of the preview time on the order of 1.5 to 3.0 seconds.[1]) Recall that reductions in stability occur in the model for either an increased driver time lag or a reduced driver preview time. Consequently, similar stability margins can be maintained in the model to some extent by compensating increases in one parameter with increases in the other parameter. Any such apparent "correlation" between driver time delay and preview time thereby allows the driver to maintain approximately the same level of closed-loop system stability as a corresponding, but less responsive, driver/vehicle system having a larger time delay and longer preview time. It may be that drivers, under tight maneuvering conditions, only look far enough ahead to negotiate the next immediate "obstacle," thereby requiring a shortening of their preview time during such maneuvers. In order to maintain a desired level of stability, drivers may then decrease their time delay cycle through faster information processing under such circumstances.

Along this line, MacAdam [11] in 1983 hypothesized that drivers could possibly "trade off" directional stability for improved path tracking capabilities. This work however assumed that the driver time delay parameter (e.g. 0.25 seconds) was largely invariant based upon the measurements of the previous research using random disturbance input testing. The findings reported here, however, seem to suggest instead, that depending upon the vehicle being controlled, drivers have more control over their time delay characteristics than previously observed, and, that no such "trade off" between directional stability and path tracking performance need necessarily occur.

To further support the observation linking reduced driver time lag characteristics and the HMMWV test vehicle, the *unconstrained* lane-change maneuvers also conducted during this testing clearly demonstrated that both test drivers (during the sequence of lane-change tests 125 through 153; constrained and unconstrained) exhibited even more responsive behavior when the lane-change course was unconstrained than when the course was constrained. The basic observation was that the test drivers acted with more of an "open-loop" steering manner in initiating the unconstrained lane-change maneuver, moving quickly from the initial lane to the second lane. This was then followed by a more apparent "closed-loop" steering control pattern to stabilize the vehicle in the second lane. To illustrate this point, Figure 5-32 shows a comparison of steering and lateral displacement

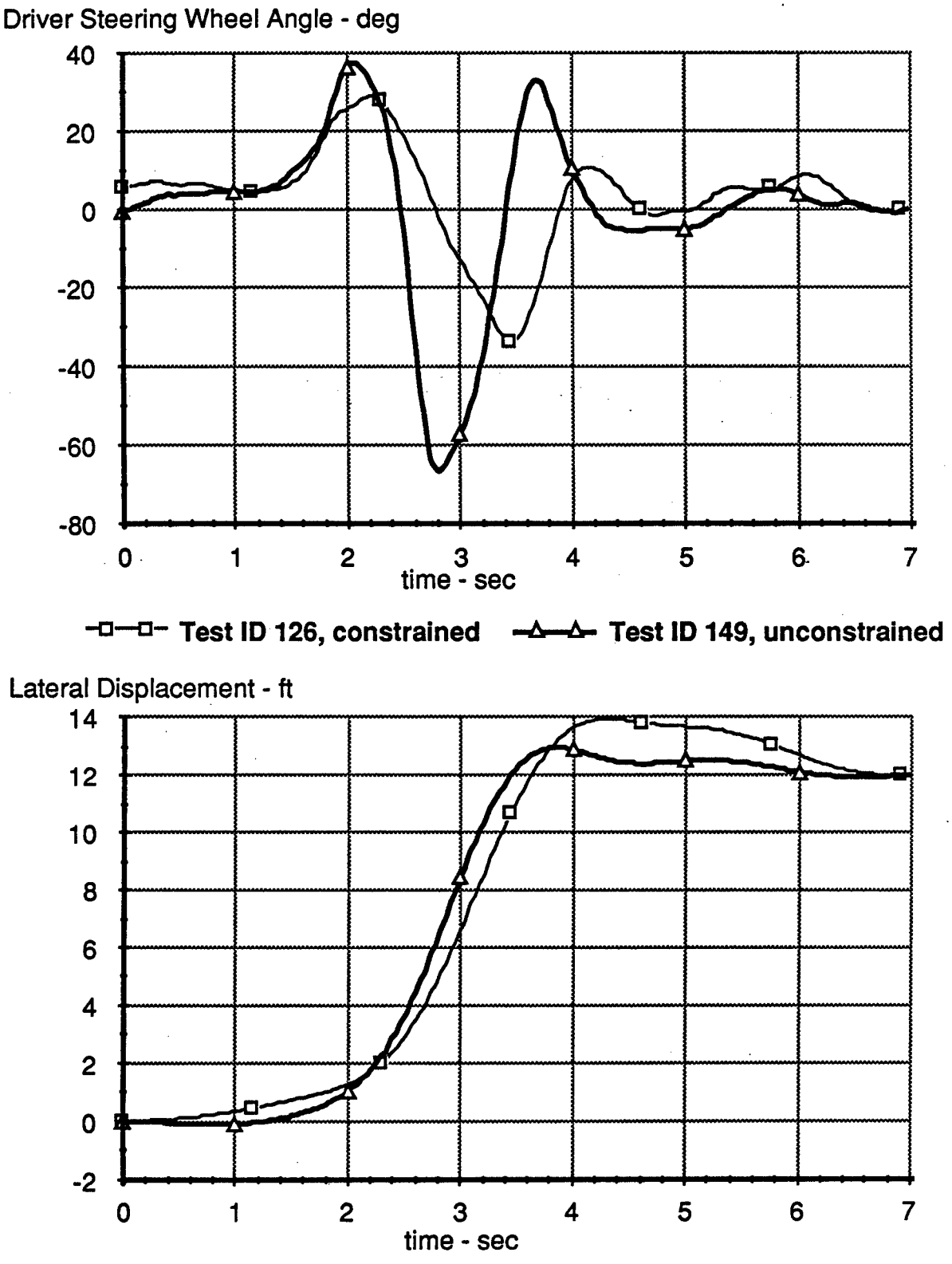

Figure 5-32. Constrained vs. Unconstrained Lane-Change Test

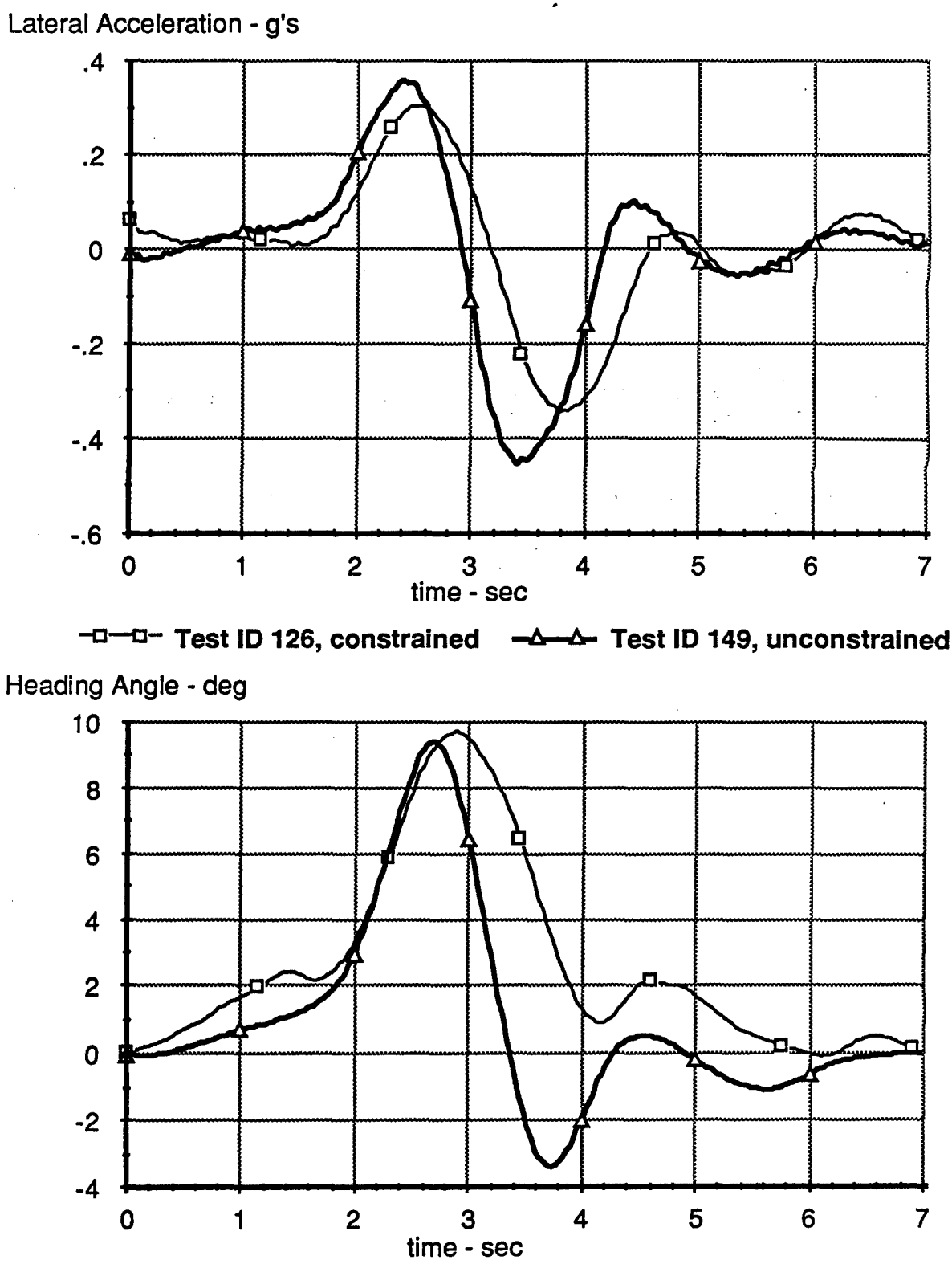

Figure 5-33. Constrained vs. Unconstrained Lane-Change Test

time histories for test 126 (constrained) and test 149 (unconstrained). Note the more responsive and aggressive behavior exhibited during the unconstrained test. This appeared to be a typical trend for most of the constrained vs. unconstrained comparisons. Figure 5-33 shows corresponding lateral acceleration and yaw angle comparisons from the same two tests. Again, the unconstrained response is more rapid, particularly during the reversal and correction phase of the maneuver. It was also visually apparent to observers at the time of these experiments that the test drivers were performing the unconstrained lane-changes more quickly and aggressively.

This observed behavior pattern during the unconstrained lane-change maneuvers seems to raise the question for users of the driver model as to what an "appropriate" desired path input should be in cases where portions of the desired trajectory are ill-defined. In the case of the constrained lane-change maneuver, the 12-ft x 100-ft trajectory is quite obvious since it represents the centerline of the constrained course. However, when the middle of the course is opened up, as in the unconstrained case, a corresponding desired path is not as obvious. Based on the above test results though, it appears that a more rapid lane-change path input is appropriate in such cases, for example, a 12-ft x 75-ft, or possibly, a 12-ft x 50-ft trajectory. In any event, a "bandwidth limit" for the driver-vehicle system will eventually be reached as the trajectory approaches a step-like input with the corresponding driver-vehicle reponse representing the bound for the system. Ordinarily, matching of the model with such data can be accommodated by selecting appropriate path inputs in combination with a representative set of driver time lag and preview time parameters. In the unconstrained example just seen, a 12-ft x 50-ft trajectory would better permit the model to reproduce the responses observed in the test data.

The next example of validating the driver model predictions is presented in Figures 5-34 and 5-35 for the baseline *obstacle course maneuver* of Figure 5-29. In this maneuver, the vehicle speed is maintained at 40 mph as the driver steers the vehicle from the left lane to the right lane around the first obstacle. The vehicle is then steered back to the left, around the second obstacle, and then to the right lane again to exit the course (positive values of lateral displacement in Figure 5-34 are to the right on the test course). In this example comparison, runs for the "center/center" positioning of the obstacles were selected (test numbers 168, 178, 182, and 183 from the log sheets of Table 5-2). The "center/center" obstacle arrangement had equal longitudinal gaps of 100 ft between each of the obstacles, as well as at the entrance and exit portions of the course (i.e., L1 = L2 = L3 = 100' in Figure 5-28). Figures 5-34 and 5-35 show an overlay of the four "center/center" tests and the predicted response from the driver model. Also seen in the trajectory overlay portion of Figure 5-34 are the locations of the two obstacles.

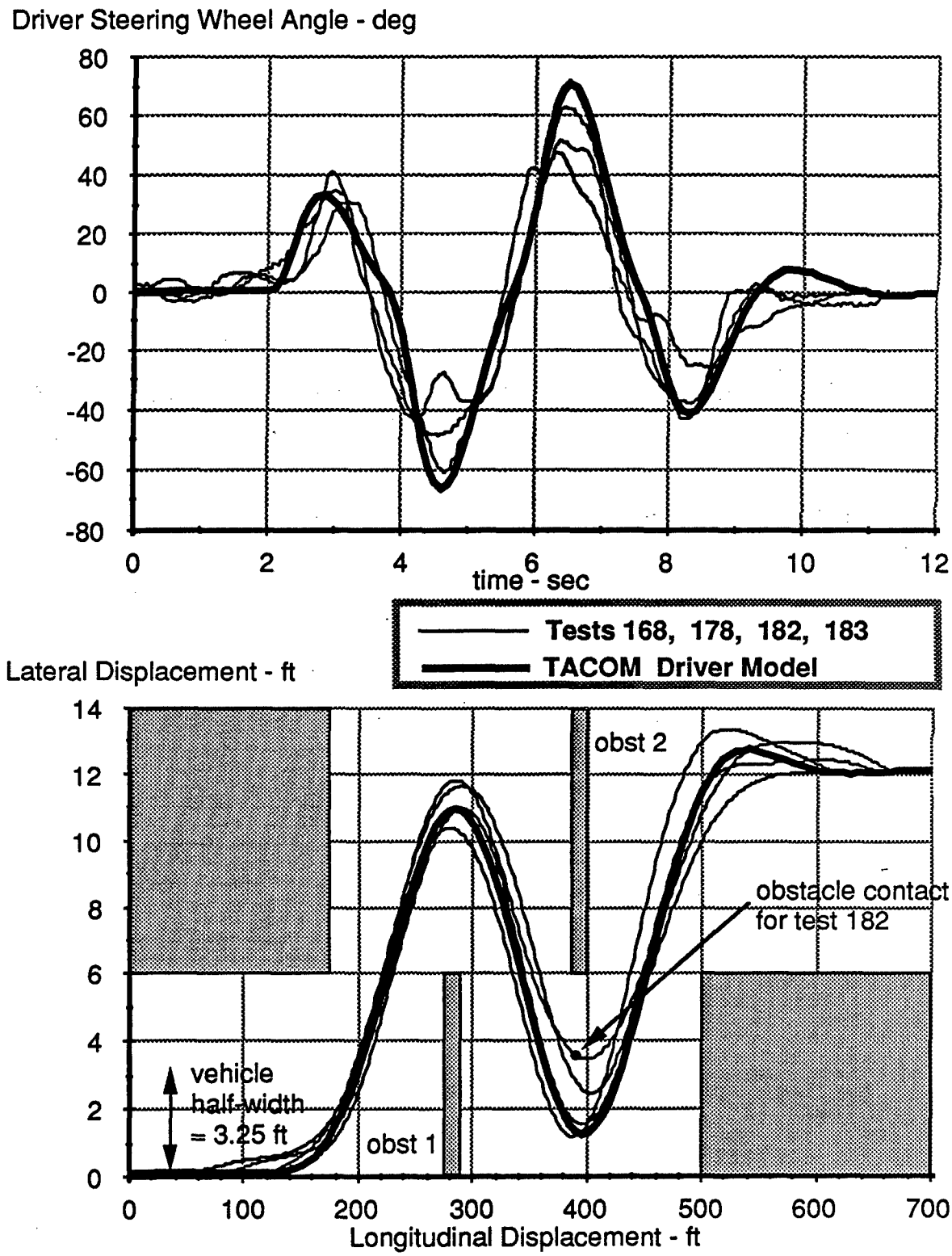

Figure 5-34. Driver Model Validation, Obstacle Course, 40 mph

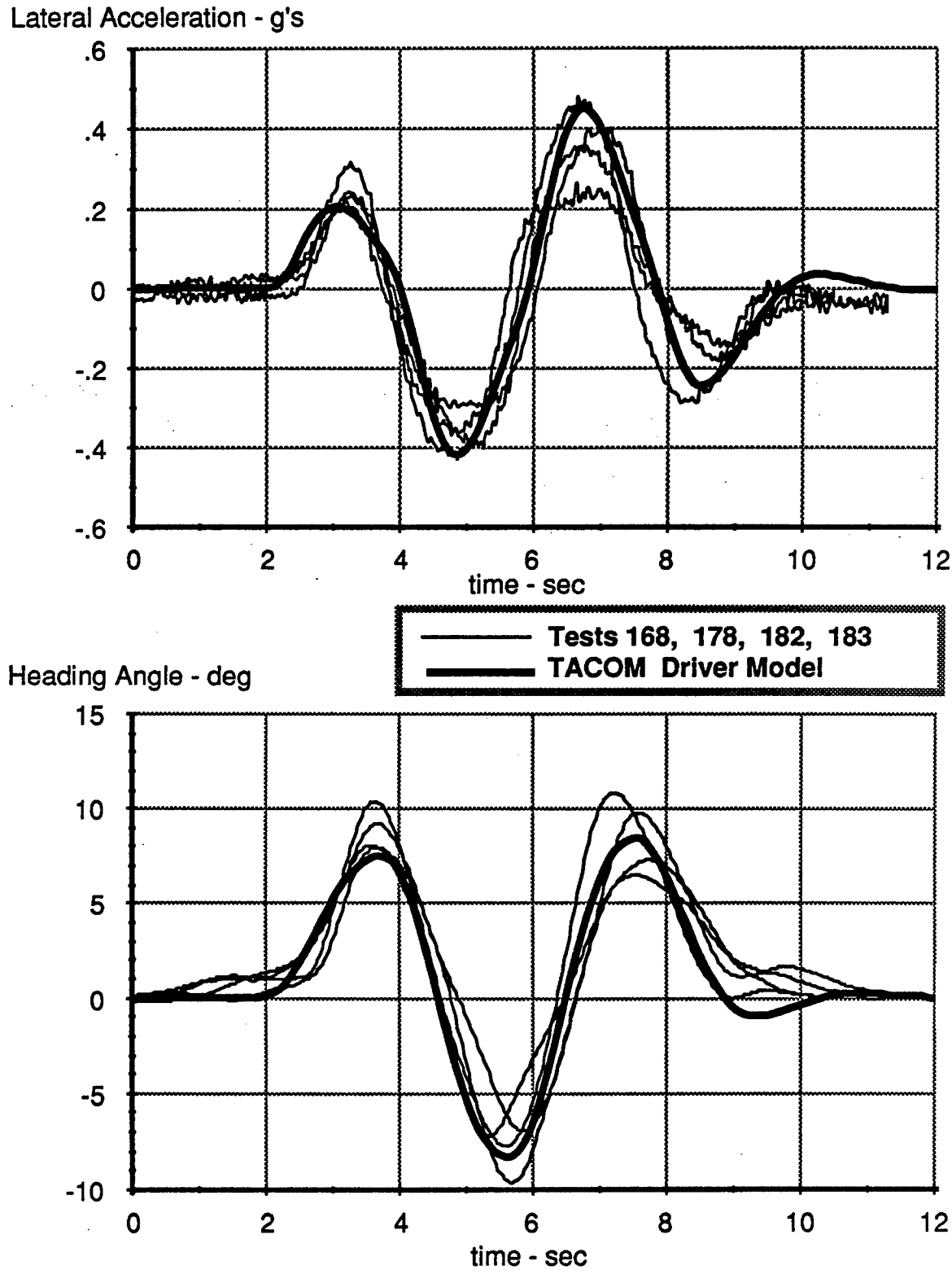

Figure 5-35. Driver Model Validation, Obstacle Course, 40 mph

Unlike the previous lane-change tests in which the course geometry remained static, the geometry of the obstacle course was varied to some extent from test to test by random longitudinal placement of the two obstacles. The exact placement of the obstacles was unknown to the test driver until the vehicle entered the obstacle course. Despite this, the test driver was still able to replicate with some accuracy the same basic response during each of the tests seen in Figures 5-34 and 5-35.

The driver model preview time and time delay parameters used for the *obstacle course* validation calculations were the same values used in the previous lane-change validation (1.1 and 0.1 seconds respectively). The desired path used as the input to the driver model was simply taken as the "center-line" of the course and defined here as seven straight-line segments:

x	y	
0.0	0.0	<— 175' straight-line to entrance of course
175.0	0.0	<— entrance point of course
275.0	12.0	<— 100' gap to first obstacle
287.0	12.0	<— 12' width of first obstacle
387.0	0.0	<— 100' gap to second obstacle
399.0	0.0	<— 12' width of second obstacle
499.0	12.0	<— 100' gap to exit of course
999.0	12.0	<— straight-line exit out of course

As seen in these figures, the model predictions are in very good agreement with the measured responses. Again, as in the previous comparison, the lateral displacement and yaw angle measurements were obtained from integration of the lateral acceleration and yaw rate measurements over the length of the course. The longitudinal displacement signal (Figure 5-34) was obtained by integration of the fifth-wheel forward speed measurement.

In the "Comments" field of the log sheets (Table 5-2) for run #182, it is noted that obstacle #2 was "clipped" during this test. This can be seen as well in the test data of Figure 5-34 in which one of the test trajectories (from run #182) records a value of lateral displacement of about 3.5-ft at the 390-ft mark of longitudinal displacement. Since the half-width of the HMMWV is about 3.25-ft at the outside of the tires and an indicated clearance of only 2.5 is seen at the point shown, this particular trajectory would produce wheel or body contact with obstacle #2.

Finally, a sequence of frames from a simplified computer animation program is shown in Figures 5-36 through 5-39 to illustrate the response and trajectory of the vehicle during the obstacle course maneuver. The frame number and time (corresponding to that in Figures 5-34 and 5-35) are noted in the upper left corner of each frame. The location and orientation

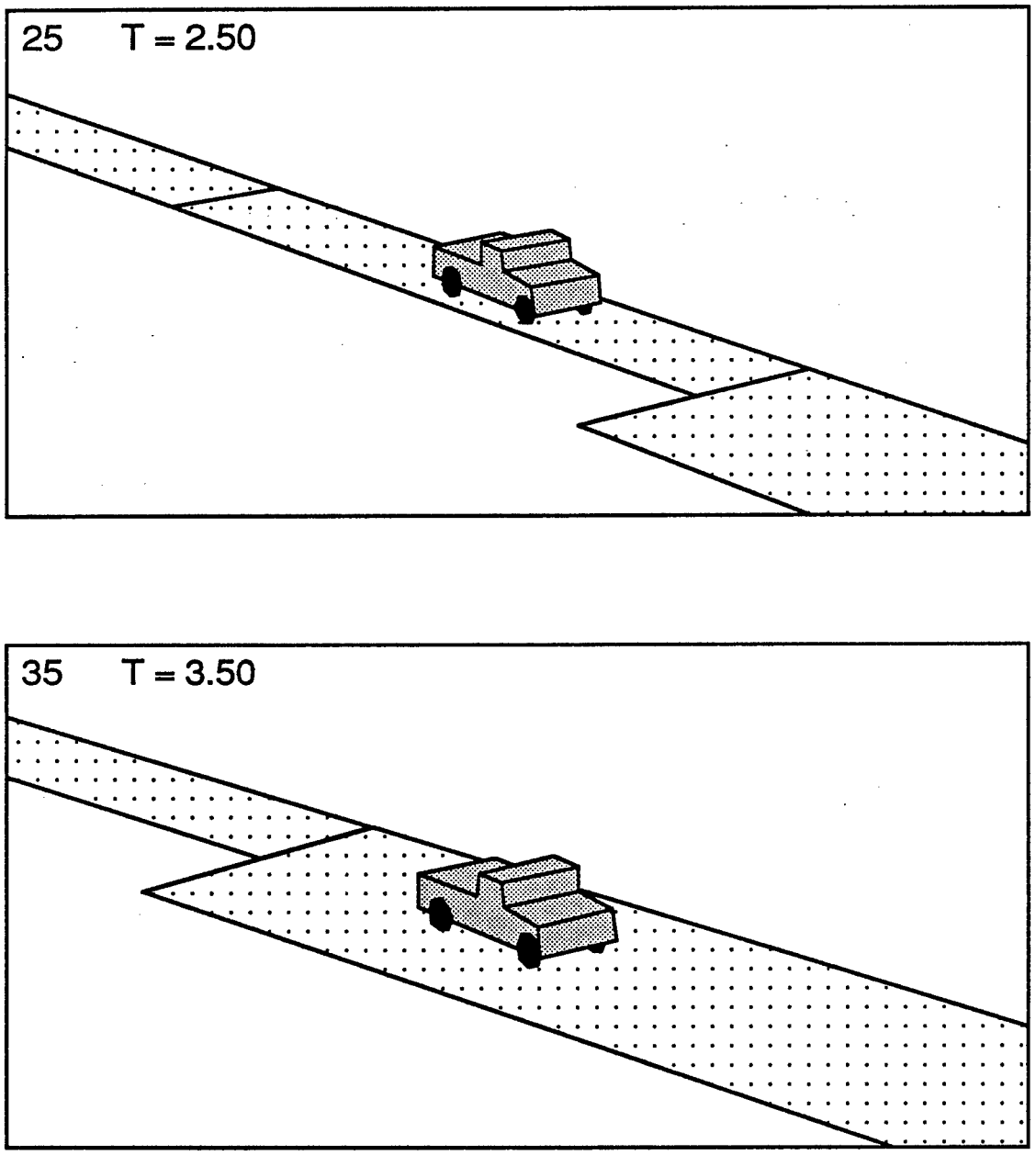

Figure 5-36. HMMWV Entering the Obstacle Course

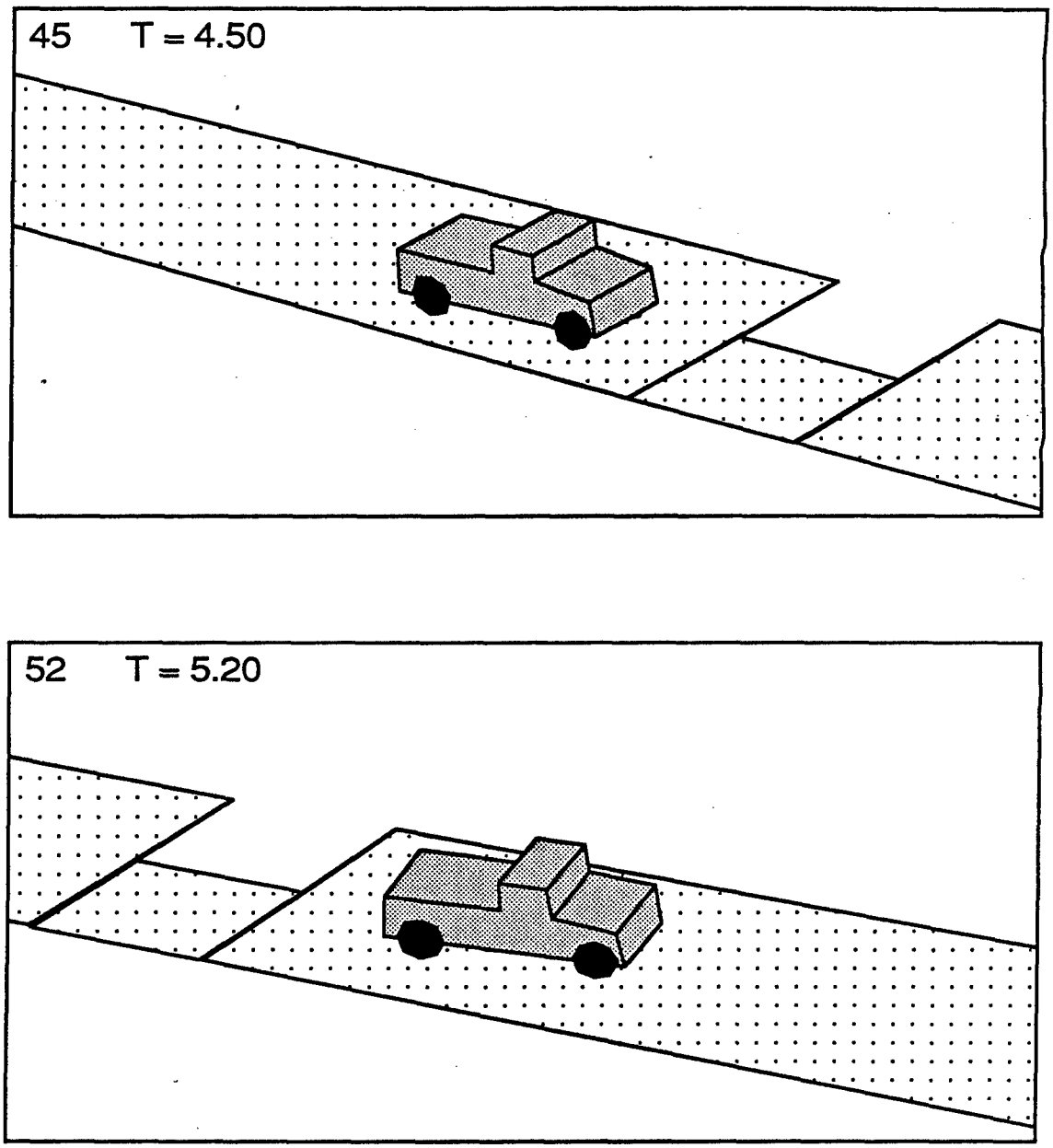

Figure 5-37. HMMWV Negotiating the First Obstacle

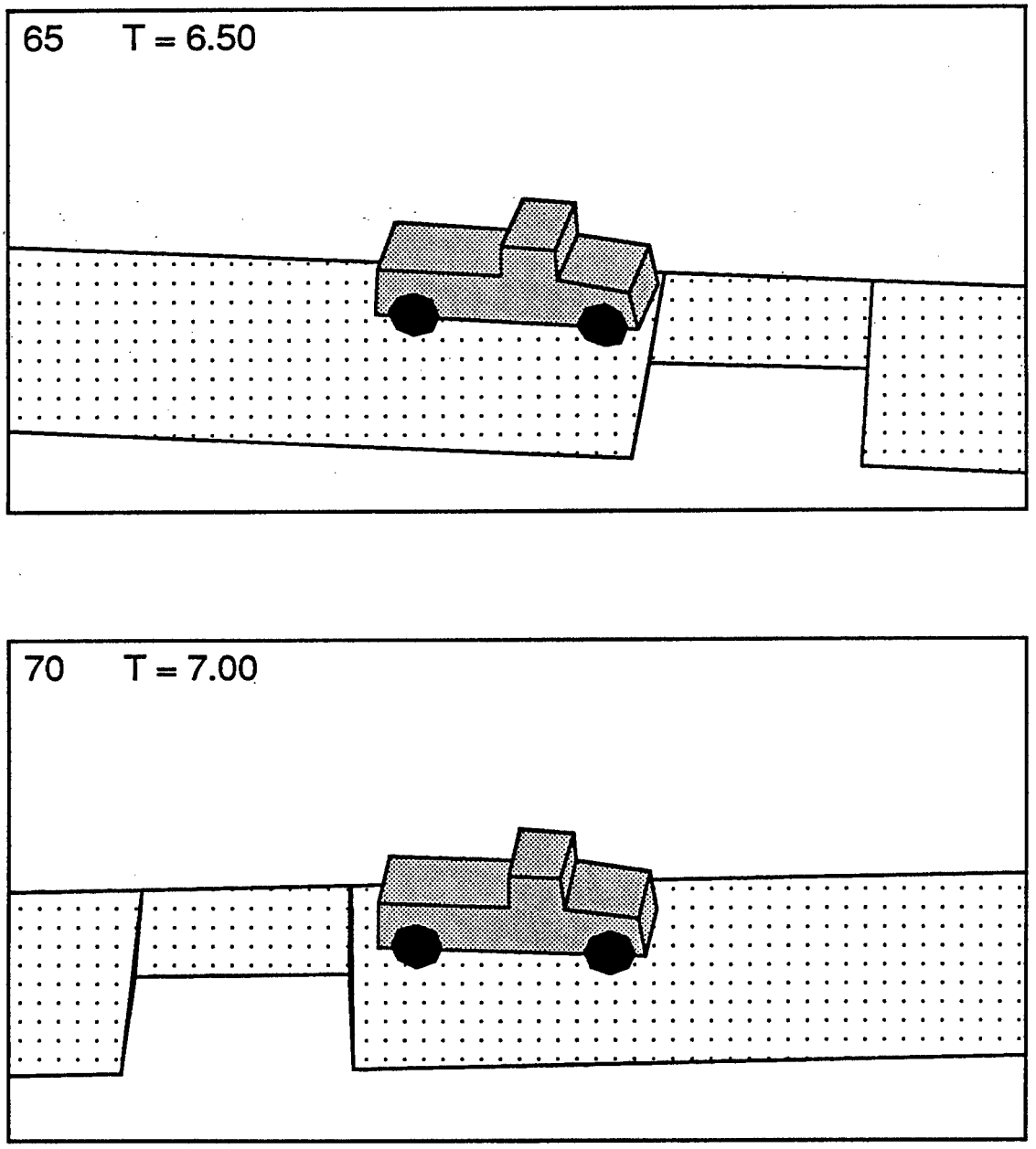

Figure 5-38. HMMWV Negotiating the Second Obstacle

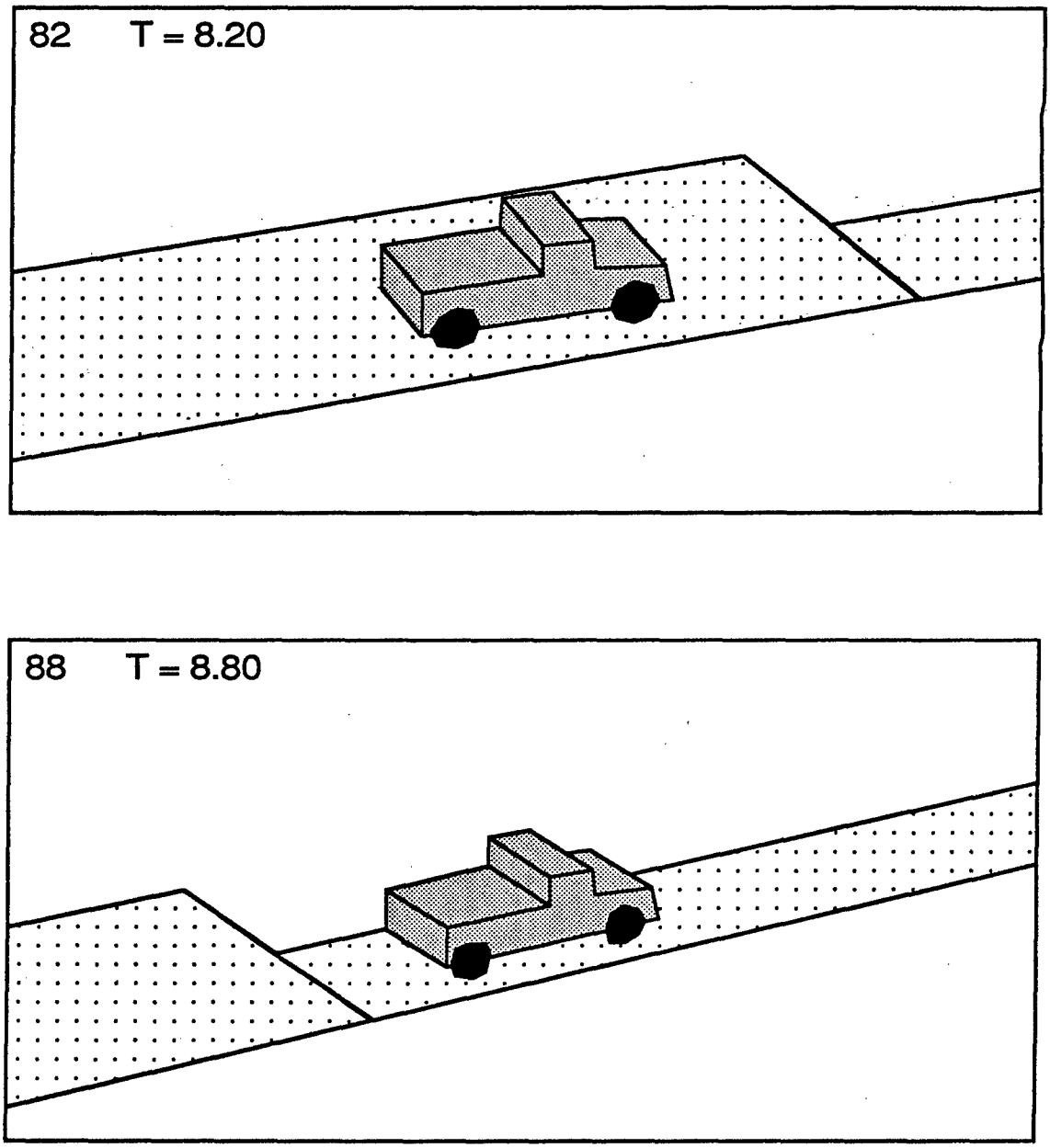

Figure 5-39. HMMWV Exiting the Obstacle Course

of the vehicle at each of the animation positions can be coordinated with the time histories of Figures 5-34 and 5-35 through the time parameter shown in each frame. The observer during this animation sequence is at a forward position of 400 ft, a lateral position of 200 ft, and an elevation of 100 ft.

The next maneuver examined during the validation exercise is that of *steady turning* (to the left) along a circular arc of 500 ft radius. As noted in section 5.6, tests were conducted at different speeds and tire inflation pressures in order to study the response of the driver/vehicle system under different lateral acceleration conditions and for different sets of vehicle directional dynamics. A sequence of figures is presented in the following discussion which compares the predicted response of the TACOM driver model and simulated vehicle with corresponding measurements from a number of steady turning tests.

The first comparison, shown in Figures 5-40 and 5-41, is for a low speed (24.5 mph), low lateral acceleration operating condition. Figure 5-40 shows the steering wheel angle input from the driver and the left front wheel angle at the road. Figure 5-41 shows the corresponding lateral acceleration and yaw rate relative to a stable platform oriented normal to the gravity vector. The HMMWV was loaded as before in its baseline configuration with all tires inflated to 28 psi. Measured signals from tests 219, 220, and 221 are shown overlayed with the prediction from the TACOM driver model. The same linear vehicle model [43] was used to represent the HMMWV dynamics. As seen in these two figures, the three test results and the model predictions are in close agreement. Since, the vehicle is turning on a circular arc and at low lateral acceleration, the front wheel angles should be close to the Ackerman steer angle, L/R, equal here to (130/12) / (500) • 57.3 degrees, or, 1.24 degrees. The test data and the model both indicate measured values in that range. The measured and predicted values are slightly smaller than the Ackerman value due to the modest oversteer condition of the vehicle and the 0.08 g's of lateral acceleration present during the test.

The next comparison is for the driver/vehicle system performing the same maneuver at a higher speed and lateral acceleration condition. Figures 5-42 and 5-43 show the same four driver/vehicle responses compared for the driver model and tests 223 and 224. The speed was maintained at an approximately constant value of 49 mph during these tests. Again, the basic predicted and measured responses are in good agreement. Note that despite the increase in lateral acceleration level for this maneuver, the driver input at the steering wheel is about the same. This is a direct result of the steering system compliance. The vehicle, with respect to the steering wheel input, could then be considered to be approximately neutral steer with the steering system compliance contributing about 2 deg/g of understeer, thereby cancelling out the opposite buy equal oversteer condition of the vehicle at the road wheels. Since the road wheel steer angle requirement *decreased* by approximately 0.5

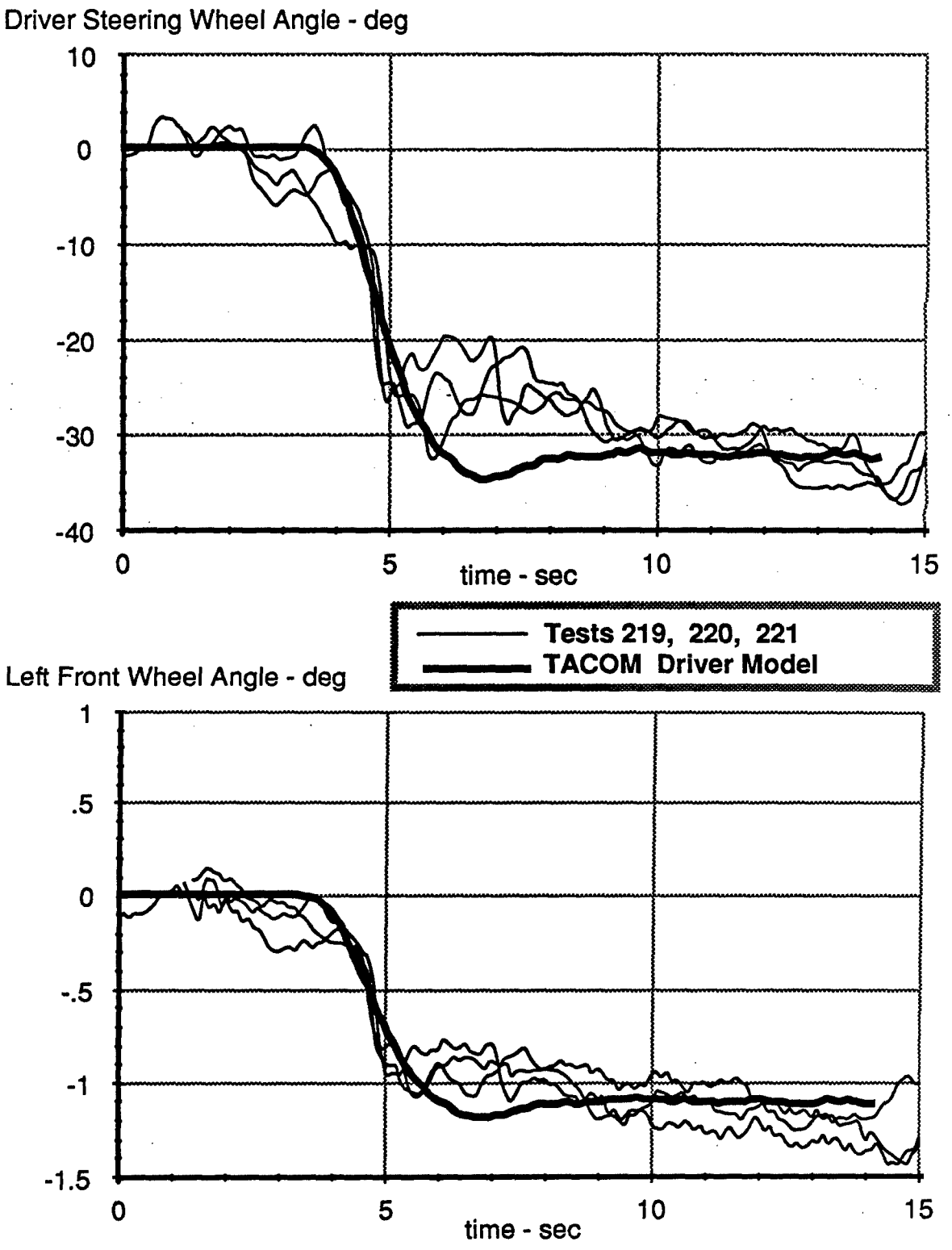

Figure 5-40. Driver Model Validation, 500' Radius, 24.5 mph

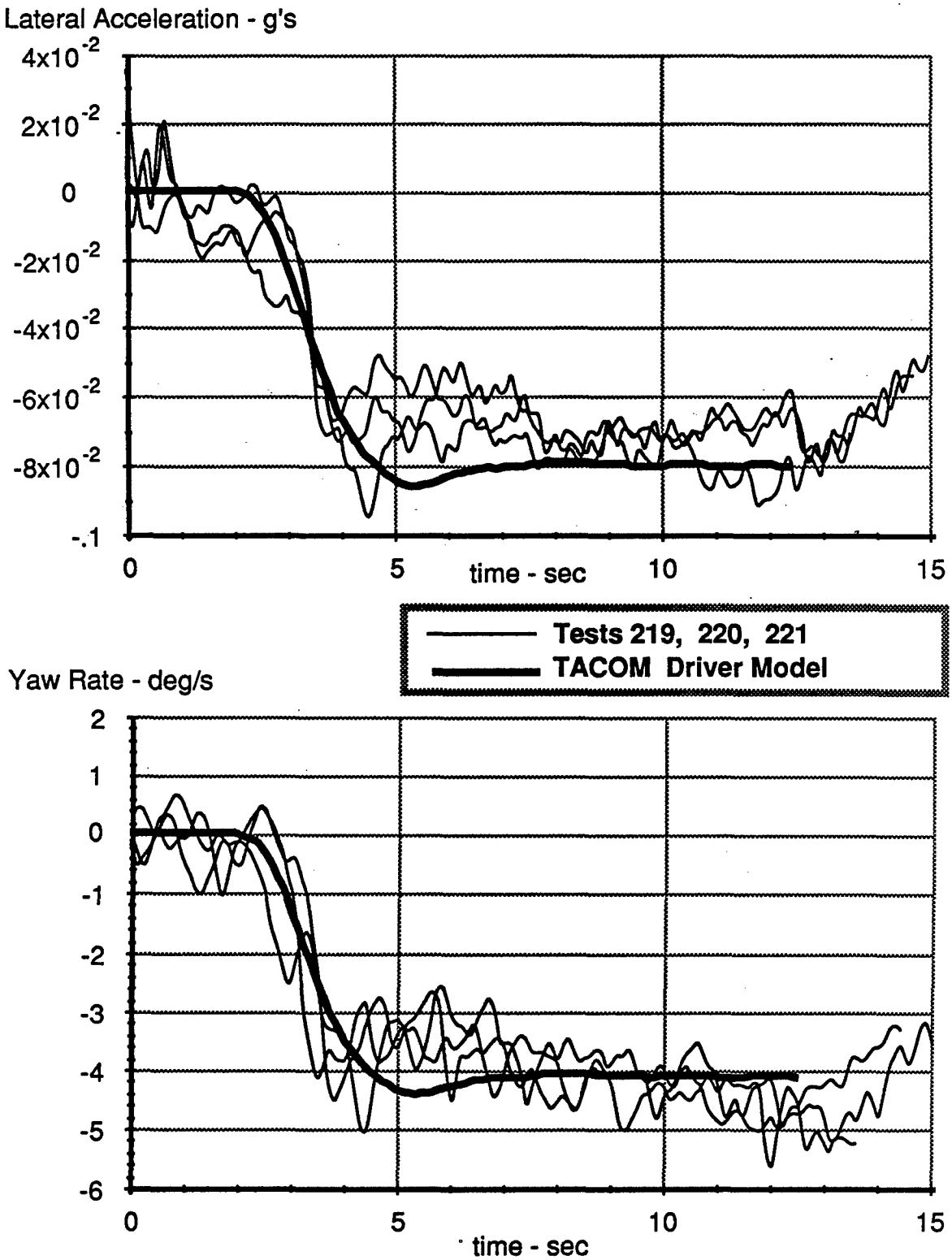

Figure 5-41. Driver Model Validation, 500' Radius, 24.5 mph

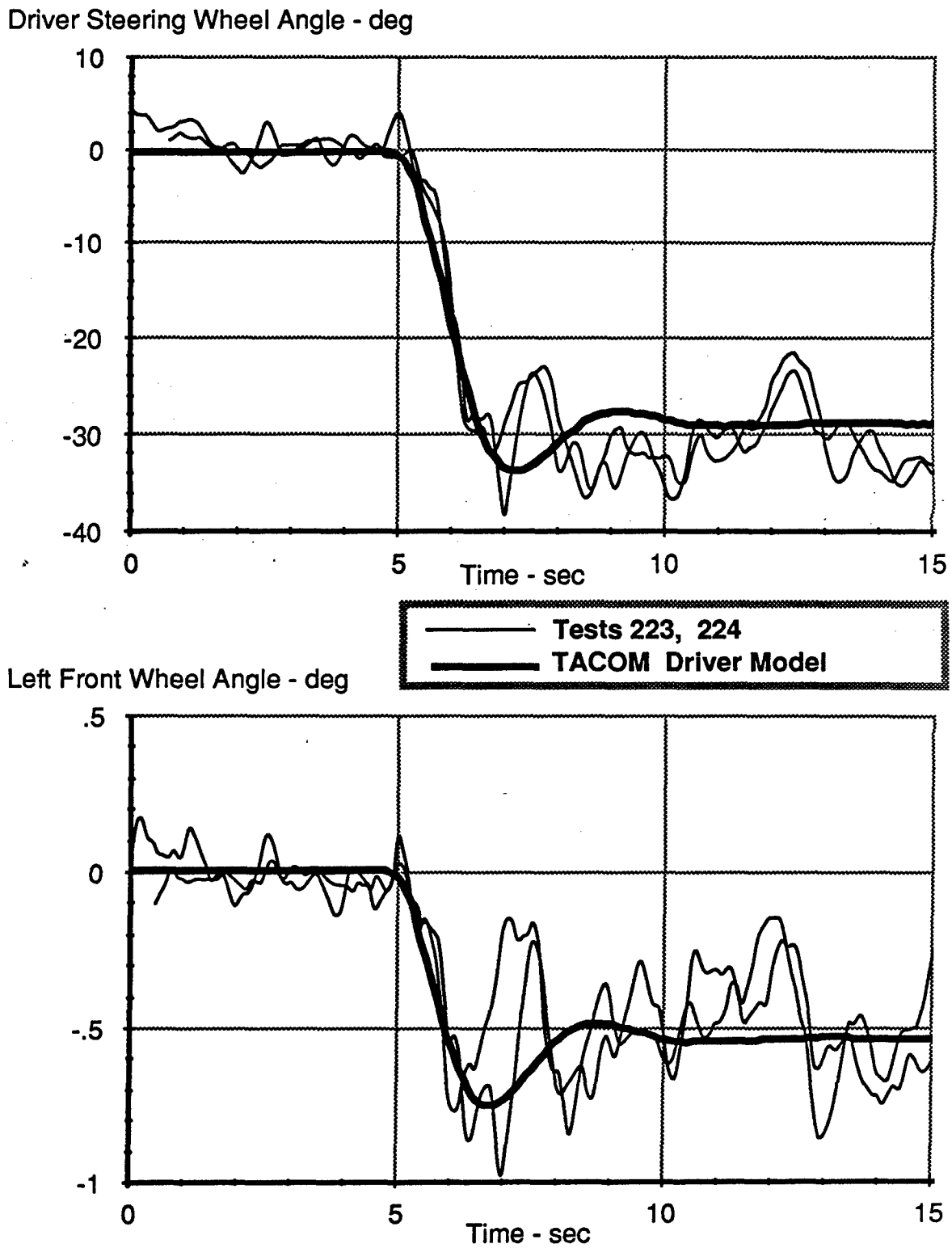

Figure 5-42. Driver Model Validation, 500' Radius, 49 mph

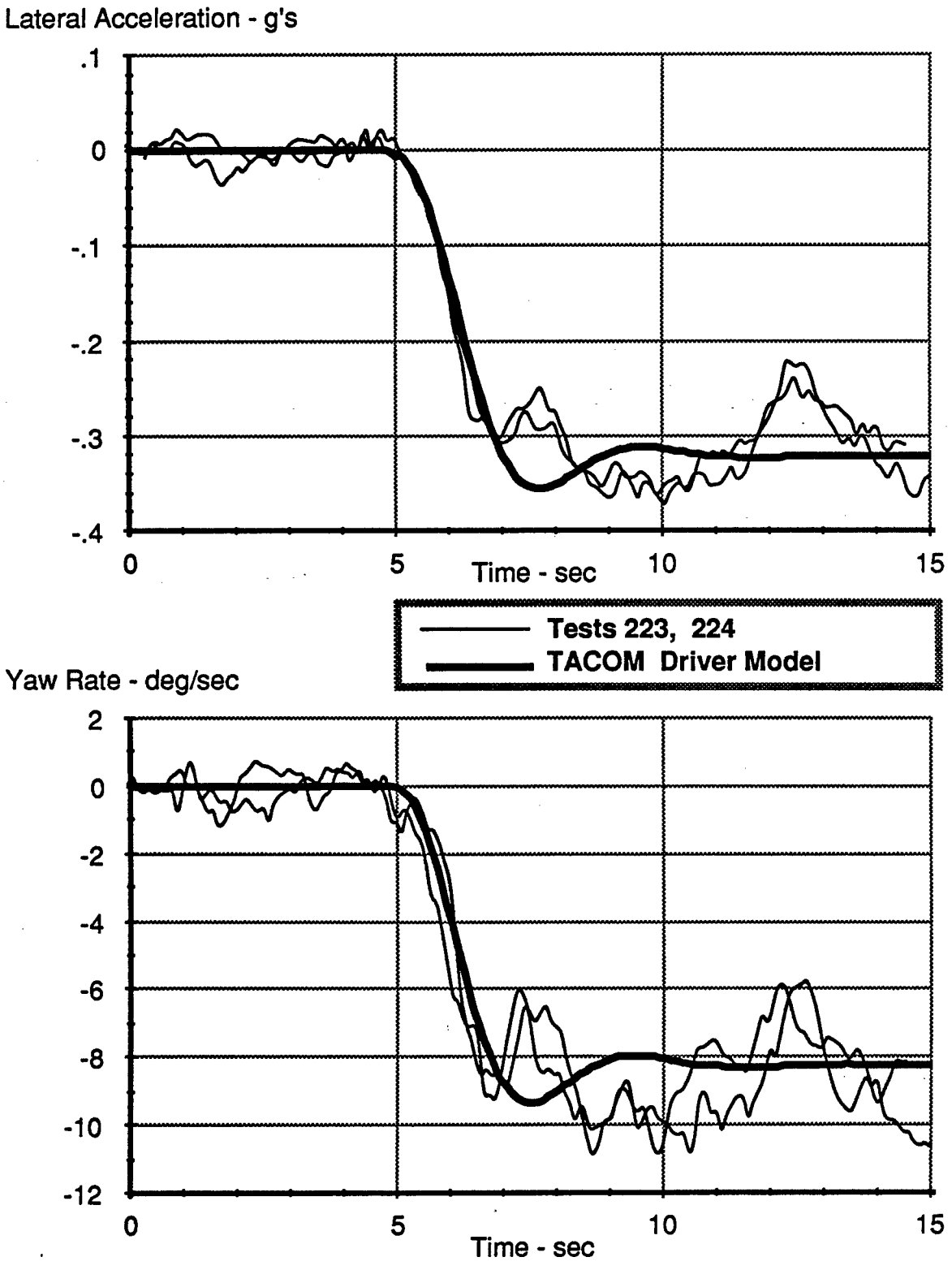

Figure 5-43. Driver Model Validation, 500' Radius, 49 mph

degrees when going from 0.08 g's of lateral acceleration to 0.32 g's of lateral acceleration along the same turn radius, the observed oversteer level of the vehicle is 0.5 / (0.32 - 0.08) or about 2 deg/g with respect to the road wheels.

A final set of steady turn tests were conducted with reduced tire inflation pressures and at elevated speeds in order to produce an unstable set of directional vehicle dynamics for the driver to contend with during the steady turning maneuver. The idea was to introduce an increased level of oversteer into the directional dynamics through controlled reductions in tire inflation pressures. The vehicle would then be steered along the same circular turn at incremented speeds and corresponding lateral acceleration conditions. Provided that 3 to 4 degrees of oversteer could be introduced by appropriate selection of front and rear tire inflation pressures, a critical velocity in the vicinity of 50 mph could be obtained at which point the directional dynamics of the vehicle become unstable. This would then produce a requirement on the part of the test driver to stabilize the vehicle by appropriate steering control actions which would be measured and recorded for subsequent analysis. The next two sets of figures show example results from this experimental approach.

Based upon the tire data shown in Figure 5-23, reduced tire pressures will affect the relative front and rear tire cornering stiffnesses, thereby altering the directional dynamics of the vehicle through a change in understeer level. Referring to Figures 5-44 and 5-45, simulated and measured responses are shown for the condition of reduced tire pressures and an average test speed of 47 mph. When compared with the previous 28 psi, 49 mph, steady turn maneuver, the results do not look extremely different. This is apparently a result of nearly proportional reductions occurring in the front and rear tire cornering stiffnesses, thereby causing little net change in the oversteer condition of the vehicle. Tire heating was also occurring during this sequence of tests causing the tire inflation pressures to rise to approximately 24-26 psi, offsetting somewhat the anticipated increase in oversteer. Further alteration of tire inflation pressures were made at this point in the testing to provide a stronger front/rear bias in tire properties, and in turn, a correspondingly increased oversteer condition of the vehicle.

As speeds were increased to nearly 60 mph with additional side-to-side load transfer also contributing to a greater oversteer condition, unusual driver steering control waveforms characterized by long period oscillations were recorded in several of the tests. At the same time, the tire inflation pressures were gradually increasing again due to further heating of the tires. In test 253, the rear tire pressures were set back to 22 psi in order to maintain an elevated oversteer condition of the vehicle and the nominal 60 mph test was repeated. The result from this test, similar to some of the previous 60 mph tests, is shown in Figures 5-46 and 5-47. The unusual long period steering waveform produced by the driver is a result of controlling the vehicle above its critical velocity and during which the directional

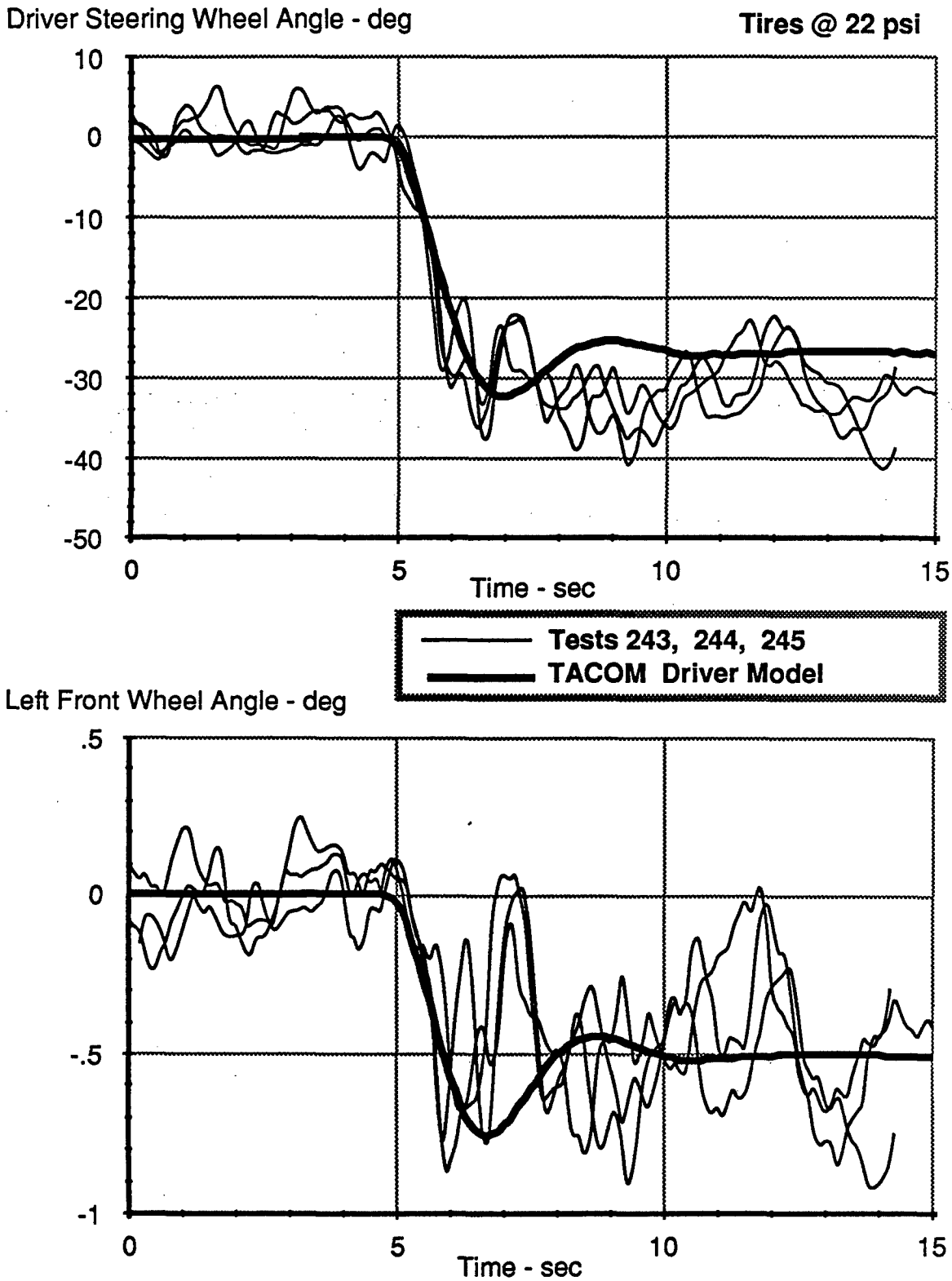

Figure 5-44. Driver Model Validation, 500' Radius, 47 mph

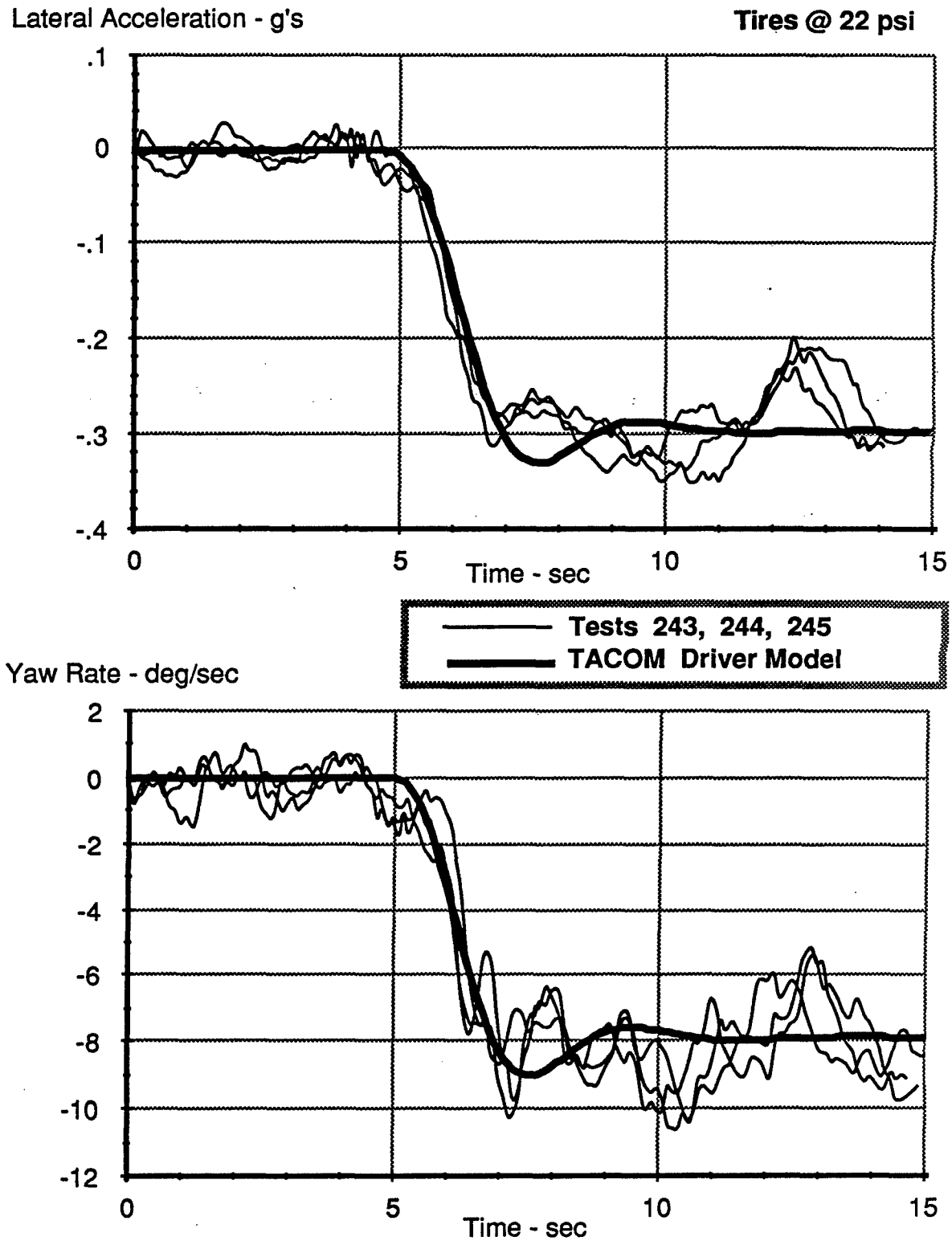

Figure 5-45. Driver Model Validation, 500' Radius, 47 mph

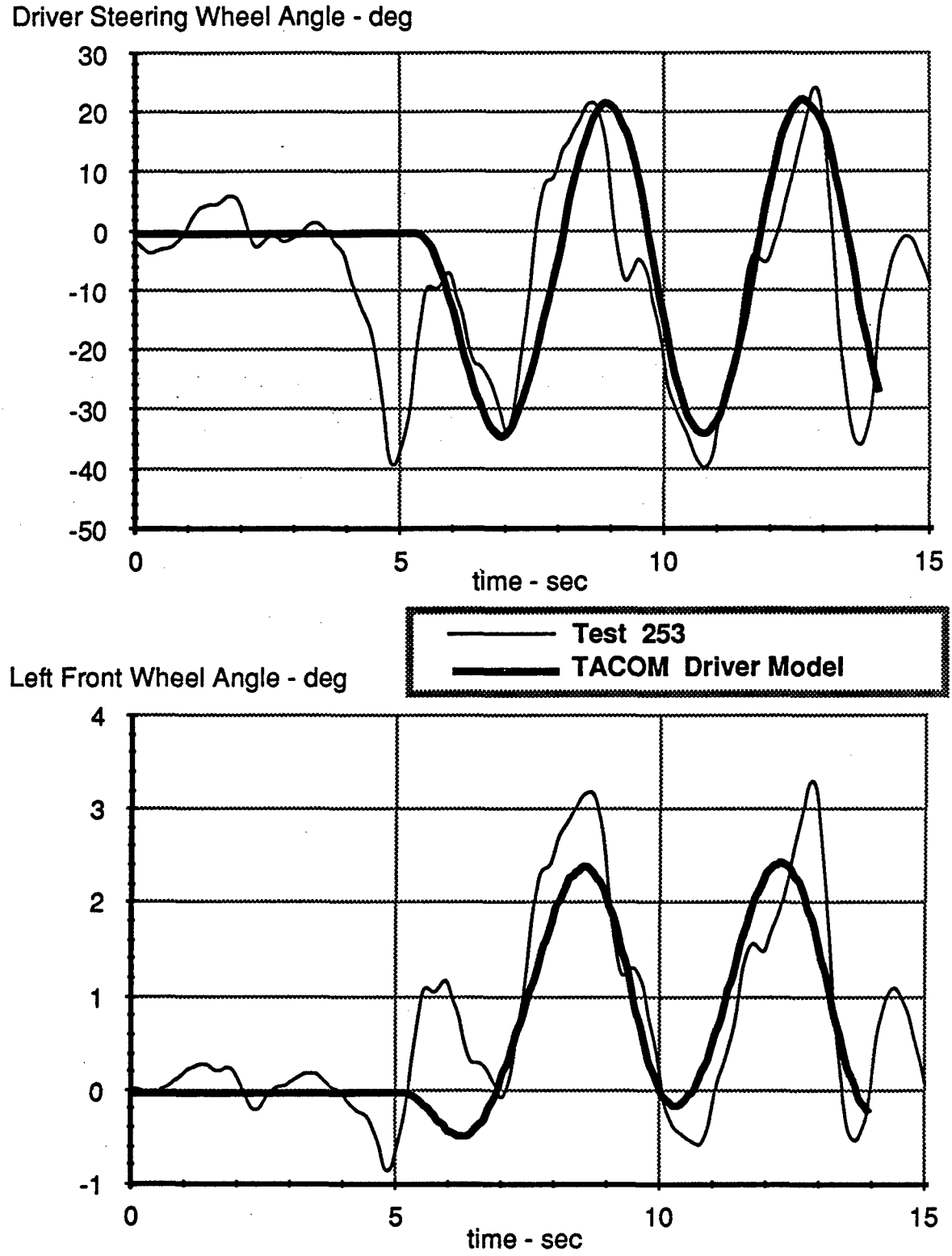

Figure 5-46. Driver Model Validation, 500' Radius, 57 mph

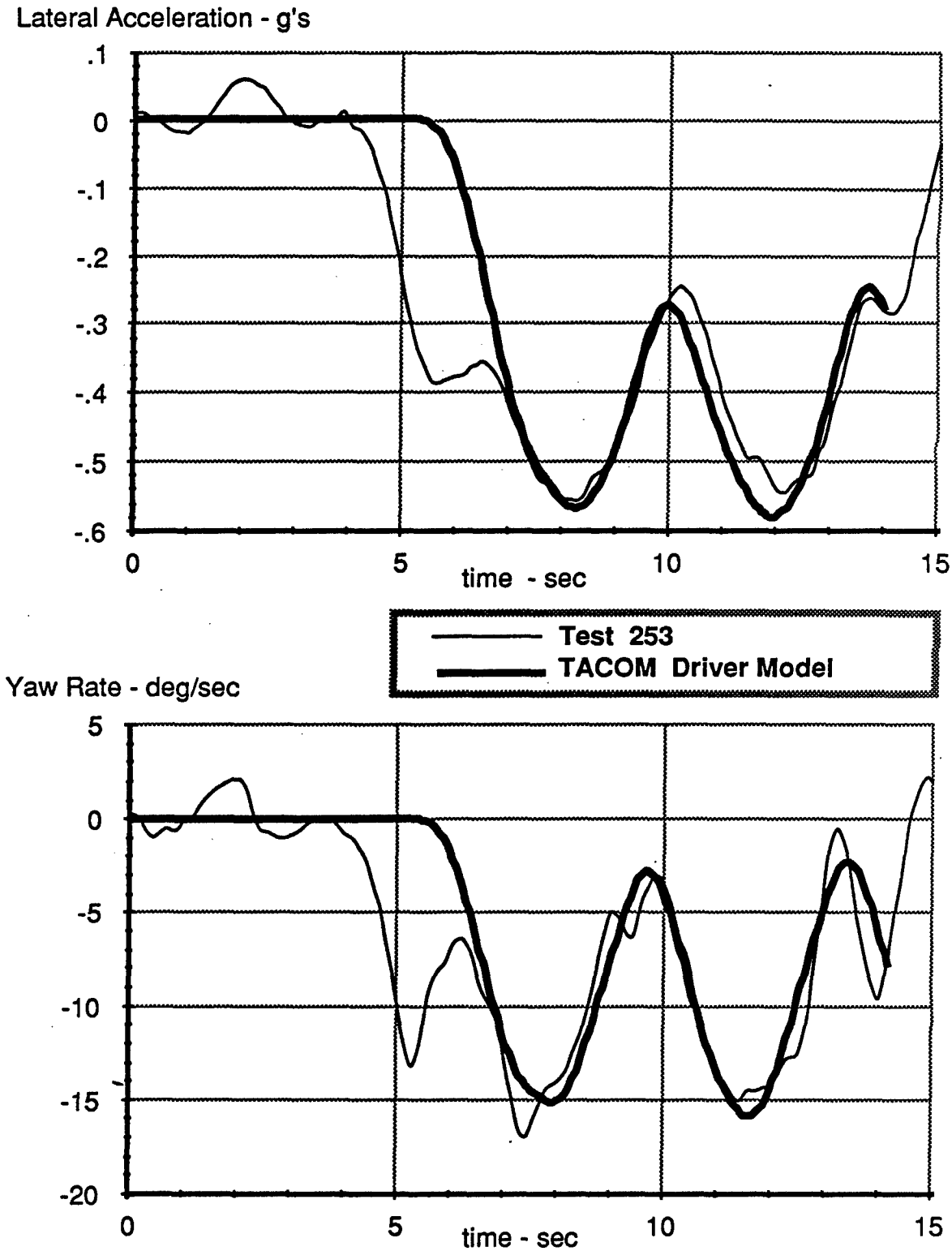

Figure 5-47. Driver Model Validation, 500' Radius, 57 mph

dynamics are unstable. Obvious counter-steering at the front wheels can be seen in the lower portion Figure 5-46, where the left-turning vehicle is being steered by means of an average front wheel angle which is positive, or, steered to the right. The average driver input at the steering wheel is slightly negative, or to the left, due to the compliance in the steering system. The actual average speed recorded during this test was 57 mph.

Also seen in Figures 5-46 and 5-47 is a prediction from the TACOM driver model. In order to obtain the degree of matching seen here between the driver model predictions and the measured test data seen in Figures 5-46 and 5-47, the driver model time delay parameter had to be increased significantly from 0.1 seconds, used during previous validation comparisons, to 0.30 seconds. Also, because of the elevated lateral acceleration condition being experienced during this test maneuver and the likelihood of nonlinear tire properties playing a more significant role, a nonlinear vehicle model [7] was used with the TACOM driver model for this validation comparison. Aside from an initial steering wheel fluctuation not produced in the model result, a reasonably good match occurs between the test results and the model prediction for both amplitude and oscillatory period of each of the responses. Several simulation runs were performed initially with smaller values of driver time delay, all resulting in more well damped and less oscillatory behavior. It was not until the driver time delay was increased beyond 0.25 seconds that the level of agreement seen here was established. As the driver time delay is increased to even larger values, such as 0.35 sec, the basic response of the driver/vehicle system tends to become unstable with each of the successive oscillations growing slowly in magnitude.

The test and model results seen here for the driver-controlled steady turning maneuver and a directionally unstable vehicle, seem to suggest that the driver workload is significantly increased under such circumstances. Not only is the level of steering activity increased markedly for the driver, but the response time of the driver is also increased (as indicated by the larger driver model time delay parameter required to suitably match the test result). Ordinarily, increases in either one of these performance indices would be a sign of increased task difficulty for a human operator.[5] Prior to even conducting any such tests, it would seem that the anticipated change in directional dynamics would present a greater prediction problem for the driver in terms of being able to judge how and to what degree the vehicle would respond to the driver's steering control input. This indeed appeared to be the case based upon the actual test results and the model predictions.

This discussion also raises the question as to how closed-loop tests involving random disturbance inputs may be related to, or interpreted in terms of, these test results — if at all. Since most disturbance testing is normally conducted during straight-line running, or along mild circular curves, the predictability of the path input is very high. However, the response of the vehicle, because it is being disturbed in a random-like manner by the

excitation input, is clearly less predictable during such tests than if no disturbance input is present. This type of test would then seem to fall into a category of test procedures that introduces uncertainty into the vehicle response, and may be viewed as a form of closed-loop testing which tasks the ability of human operators to predict and control the response of an "uncertain" vehicle. In this sense then, the last sequence of high oversteer tests conducted during this study may be more closely related to random disturbance tests than initially thought. In fact, the unstable directional dynamics encountered during such tests can be viewed as the disturbing mechanism to the vehicle motion, causing the driver to continuously counteract it with corrective steering throughout the duration of the test maneuver.

Recalling the earlier results from the lane-change and obstacle avoidance maneuvers, questions also arise regarding the mechanism by which drivers may adjust preview and time delay characteristics according to task difficulty associated with the predictability of a desired path. Previously, the same driver preview and time delay parameters were required for the obstacle course maneuver and the lane-change maneuvers in order to *match* the corresponding test results. Since the obstacle course geometry was expected to be less predictable during each test than the static geometry of the lane-change maneuver, it seemed reasonable that the driver would require additional "processing time" for the obstacle course tests. However, this did not seem to occur. One possibility may be that additional time was in fact available to the driver during the obstacle course tests since they were conducted at a slower speed. Another possibility may be that the obstacle course geometry was still highly predictable because of the known left-right required movements as well as their required sequence. Without additional testing to carefully sort out various alternative explanations, the actual mechanism by which drivers may possibly be affected by different path geometry is not clear. However, from the limited data collected here, it appears that modest changes in path geometry and its corresponding degree of predictability, does not have a primary influence on driver steering behavior.

Finally, the matter of how parameters for the TACOM driver model should be selected is an important issue, particularly if test data is not readily available to directly guide the parameter selection process. Based upon the above discussion, it appears that the TACOM driver model *time delay parameter* should be selected primarily on the basis of task difficulty, as defined by how well behaved and responsive, the controlled vehicle directional dynamics are expected to be. On the one hand, we have experimental evidence from this study that a driver time lag value of 0.1 seconds is reasonable for the HMMWV and, presumably, a similar class of vehicles having relatively sluggish but predictable directional dynamics. On the other hand, previous experimental studies using passenger cars (differentiated from the HMMWV primarily by considerably faster directional dynamics) have identified appropriate values of the same driver model time lag in the range

of 0.2 to 0.3 seconds. These previous results have been obtained using both random disturbance tests and lane-change maneuvers similar to those used in this project. Based upon these observations for vehicles having predictable directional response characteristics, but differing in their relative responsiveness, the following recommendations can be made regarding the selection of reasonable driver model time lag and preview time parameters:

- For maneuvers primarily involving straight-line driving or mild turning with no obstacles in the immediate path, a value for the driver model time delay parameter of approximately 0.25 seconds is reasonable. Values for the driver model preview time parameter ranging from about 1.50 seconds to 3.0 seconds is likewise reasonable for this class of maneuvers and most vehicles, depending upon the level of desired damping and path error control. Larger values of preview time add more damping, but sacrifice path tracking accuracy and system responsiveness.

- For transient type maneuvers involving lane-changes or maneuvering around obstacles in tight quarters, a value for the driver model time delay parameter of approximately 0.10 seconds is recommended for vehicles having sluggish directional dynamics, such as the HMMWV. For vehicles having quicker directional dynamics, such as conventional passenger cars, values in the range of 0.15 to 0.3 seconds for this parameter are recommended. Appropriate values for the driver model preview time parameter here typically would range from about 0.8 seconds to 1.5 seconds, again, depending upon the level of desired damping, path error control, and the geometry of the course.

For vehicles having poor or unconventional handling qualities (e.g., heavily oversteer vehicles, or vehicles having directional control properties not well understood by a driver):

- A value of 0.25 seconds or greater is estimated for the driver model time delay parameter under these conditions to represent likely difficulties human operators may have in controlling such vehicles . A reasonable range of preview times would be 1.0 to 3.0 seconds, depending upon system damping and path control considerations.

Summarizing the primary conclusions from the validation testing and model predictions, it does appear from the validation exercise results that:

1) The drivers used in this test program did react more quickly than what has been traditionally reported in the technical literature as typical of "average" drivers of passenger cars evaluated with "random disturbance" tests and

similar lane-change test procedures. The conclusion here is that such differences in driver response characteristics are attributable to differences in the directional response qualities of the controlled vehicles (i.e. a HMMWV versus most passenger cars). The observed change in driver time delay property is assumed to represent typical human operator adaptation/compensation behavior frequently observed in most man/machine systems.

2) A two degree-of-freedom vehicle model was generally sufficient for representing the directional dynamics of the controlled vehicle within the driver model itself for the types of maneuvers examined in this validation exercise.

and,

3) Regardless of the observed variations exhibited in driver steering behavior during this test program, or in what has been reported previously by others in the technical literature, the TACOM model appears to be quite capable of replicating most of these observed driver steering control behavior patterns through simple adjustment of two basic parameters.

5.8. Implementation of the Driver Model in DADS

The material presented in this section of the report describes how the TACOM driver model was implemented in a recent version of the DADS (Dynamic Analysis and Design System) [40] computer software developed by CADSI (Computer Aided Design Software, Inc.) of Oakdale, Iowa. Reference will be made during this discussion to a number of FORTRAN code subroutines which are part of either the DADS program or the code developed as part of this project. Most of this code appears in Appendices D and E.

Figure 5-48 provides an overview of the interaction between the DADS program, which would normally be used in this context to represent the dynamics of a particular vehicle, and the TACOM driver model. The driver model software (represented here in part by subroutines DRIVER, TRANS, and TRAJ) and most other user-defined programs, interface with the DADS software through a subroutine entitled USER49 seen in the center of the figure. (Depending upon the installation, "USER49" may have a different name.) USER49 is used to place FORTRAN "CALLS" to the driver model subroutines and to update DADS with results from the driver model calculations during the course of a simulation run. The USER49 subroutine therefore acts as communication interface between DADS and other external programs not inherently part of the DADS package.

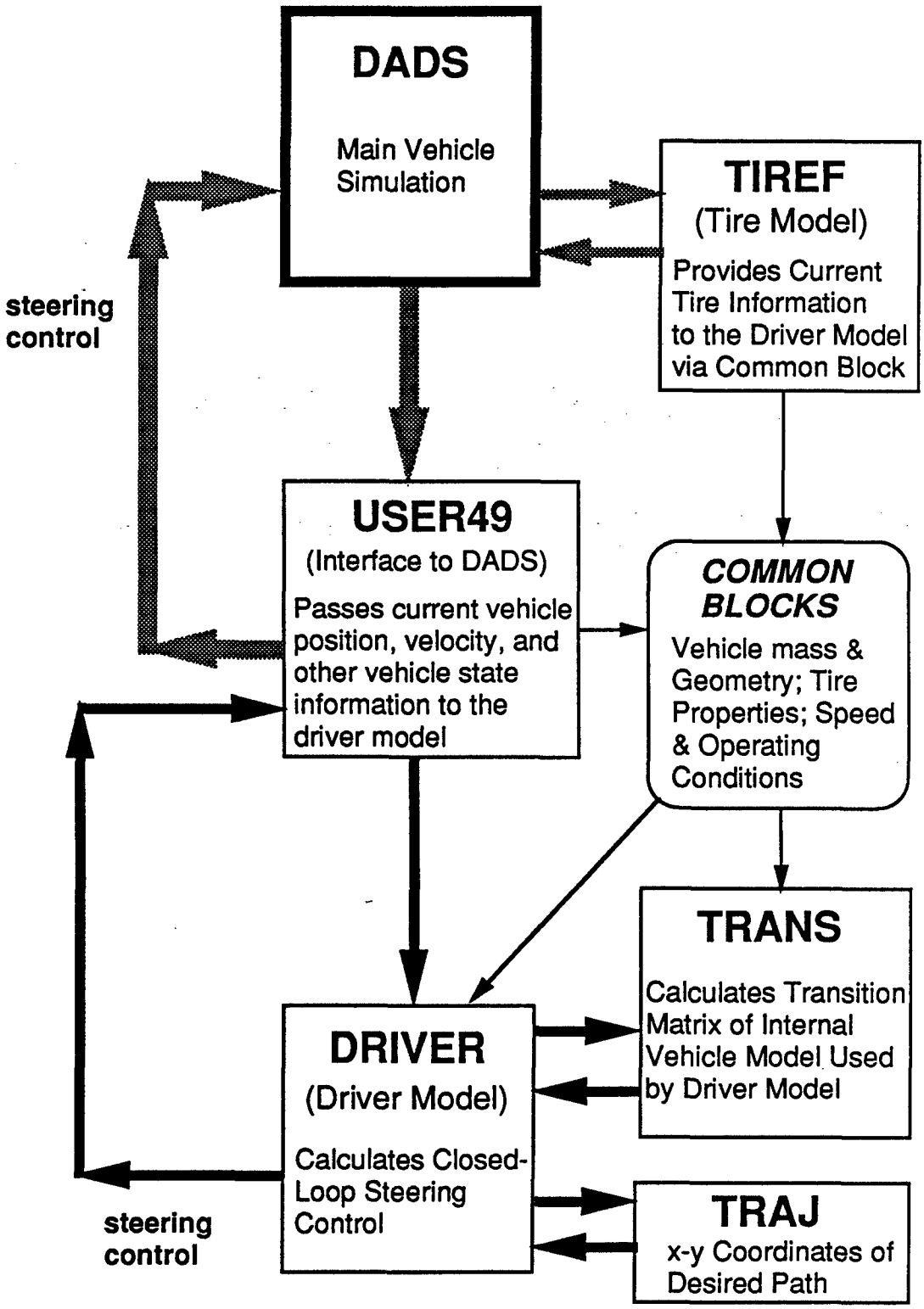

Figure 5-48. Block Diagram of the DADS / Driver Model Interface

A typical sequence of events related to the driver model calculations during an integration time step would be as follows:

- DADS updates its tire forces through calls to the tire model in subroutine TIREF
- DADS calls USER49 to handle any external user-defined *calculations* (such as the driver model)
- USER49 calls the primary driver model subroutine DRIVER to calculate a new steering control. Information such as current vehicle position, velocity, and steering angle are passed to DRIVER.
- DRIVER updates its information on vehicle speed and tire properties available in the COMMON BLOCKS
- DRIVER calls driver model subroutine TRANS to update the transition matrix of the internal linear vehicle model used by DRIVER to predict future positions within the preview interval
- DRIVER then calls subroutine TRAJ to obtain "desired path" information and compares it with its own predicted position calculations to obtain an estimate of previewed path error
- DRIVER then calculates the time lagged optimal preview steering control and returns it to subroutine USER49

Prior to the start of the simulation, a number of initializations have to first occur in the driver model software. Parameters describing the basic features of the vehicle being simulated by the DADS program must be passed to the driver model or read in from external files. These parameters include such items as the vehicle weight, its yaw moment of inertia, vehicle speed, front and rear tire cornering stiffnesses, and the vehicle c.g. location with respect to the front and rear suspensions. The vehicle parameters passed to the driver model at this point are used to define its own internal simplified representation of the complete vehicle being represented by the DADS code. Each of these parameters appeared earlier as part of the section 5.5 discussion and a sample list appears in Figure 5-12. In addition to these basic vehicle parameters, the driver model time delay and preview time parameters must also be made available to the driver model either through USER49 or from an external file. The only remaining item to enter is the set of x-y coordinates

defining the desired path for the driver model to follow. Figure 5-49 outlines this initialization process for the start of a simulation run.

Once the DADS simulation begins, USER49 is called at each integration time step and in turn calls the driver model software. Figure 5-50 shows the sequence of driver model calculations occurring during each integration time step. For most nonlinear vehicle calculations for which large programs such as DADS would ordinarily be used, speed changes due to cornering or braking are kept track of in the driver model by communication with the DRIVER MODEL COMMON BLOCKS. Similarly, front and rear tire cornering stiffness alterations are communicated to the driver model from DADS through these same common blocks. Updating of the transition matrix of the internal vehicle model can then be performed continuously or in an intermittent fashion by the driver model to maintain a "current" representation of the controlled vehicle under changing operating conditions.

The driver model common blocks must be updated periodically by an appropriate DADS subroutine, depending upon the particular parameter in question. For example, tire cornering stiffness values can most easily be updated by the DADS tire model subroutine. In this application, the DADS tire model subroutine is called TIREF, as seen in Figure 5-48, and cornering stiffness calculations for each of the HMMWV tires is performed within this subroutine at each time step of the simulation. A routine was written by TACOM to obtain a local slope from the nonlinear tire data tables ordinarily entered as part of the DADS input. Under low lateral acceleration operating conditions, where a tire experiences only a small range of sideslip and the cornering stiffness remains approximately constant, the effect of updating the tire cornering stiffness obviously has little effect. However, under higher lateral acceleration conditions where the tire properties are normally changing significantly, such updating can be important in terms of keeping the driver model "informed" about current operating conditions and enabling it to better predict future vehicle states.

Example calculations from the DADS / TACOM driver model implementation are seen in Figures 5-51 and 5-52 for a simulated HMMWV performing a 12-ft by 100-ft lane-change maneuver at a speed of 50 mph. The plots seen here were produced by the DADS post processor software. Figure 5-51 shows the average front wheel steer angle (radians) versus time (sec) calculated by the TACOM driver model during the DADS run. The corresponding vehicle trajectory, in units of inches of lateral and longitudinal displacement of the vehicle c.g., is seen in the lower portion of the same figure. Figure 5-52 shows time histories of lateral acceleration (inches/sec/sec) and yaw rate (radians/sec) for the same maneuver. As seen, the predicted responses are quite similar to previous examples and test data for comparable lane-change maneuvers. Continuous updating of the driver model transition matrix (for changes in speed and tire cornering stiffnesses) was occurring

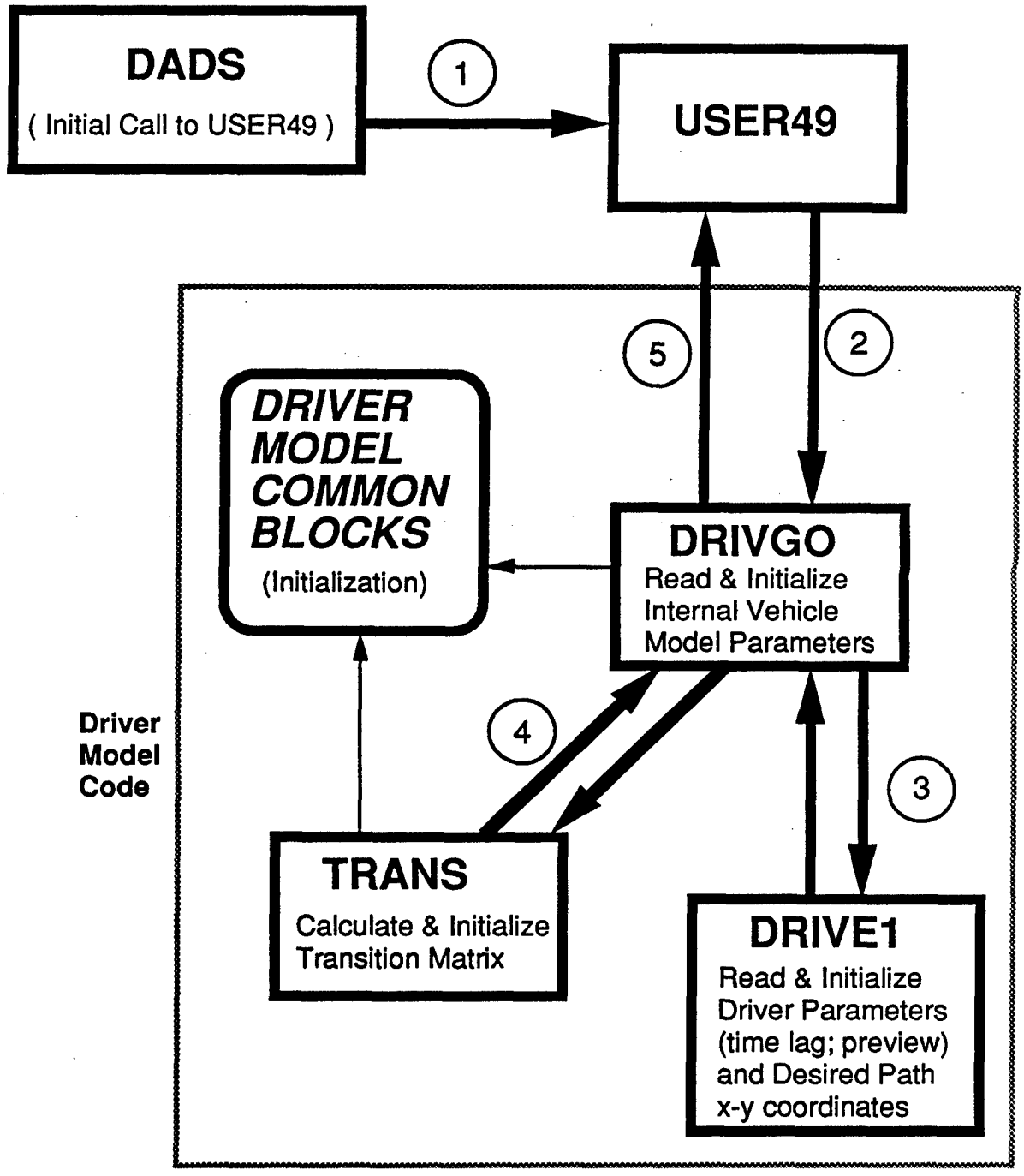

Figure 5-49. Initialization Sequence of Driver Model at Time = 0

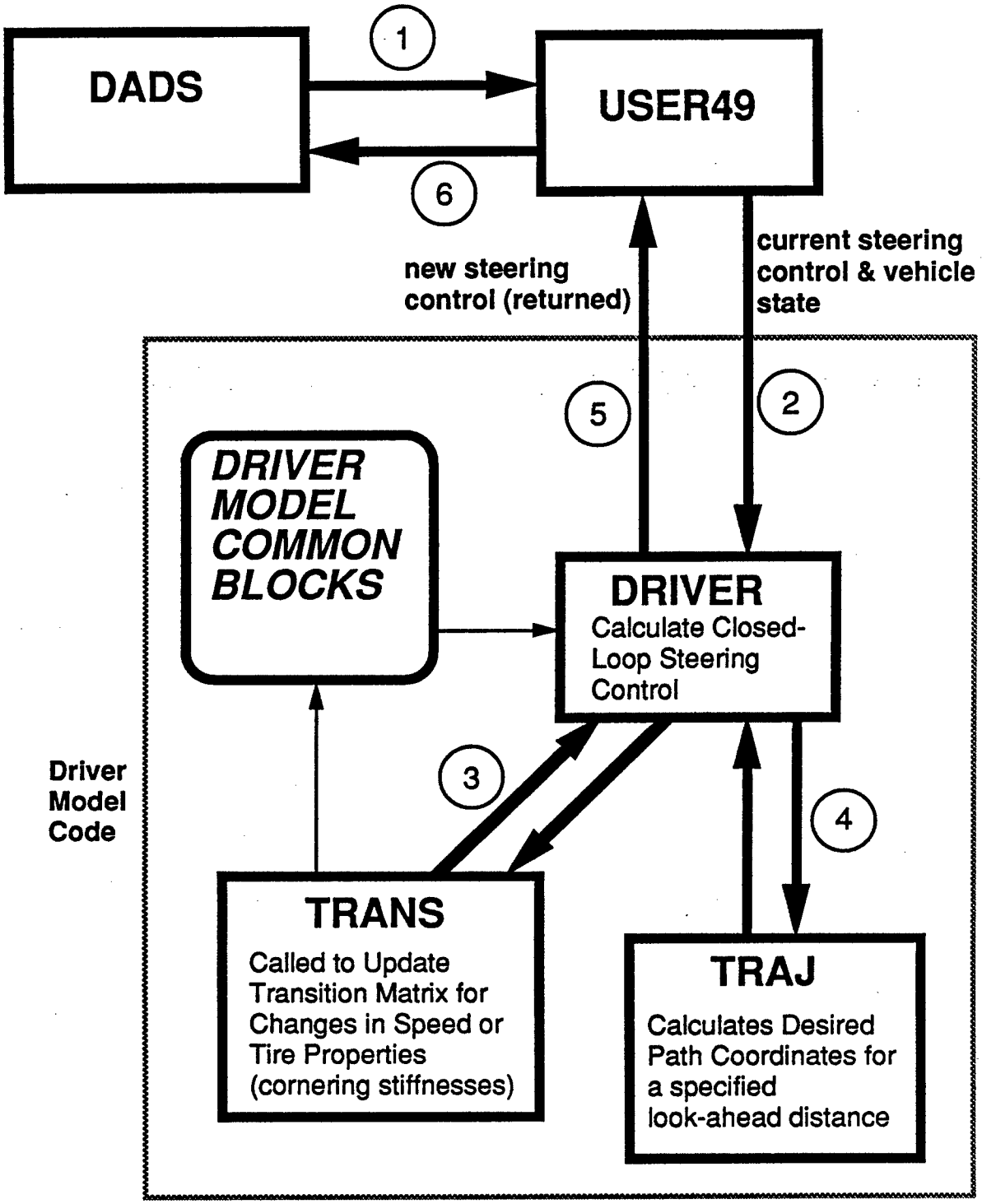

Figure 5-50. Driver Model Calculations During Integration Loop

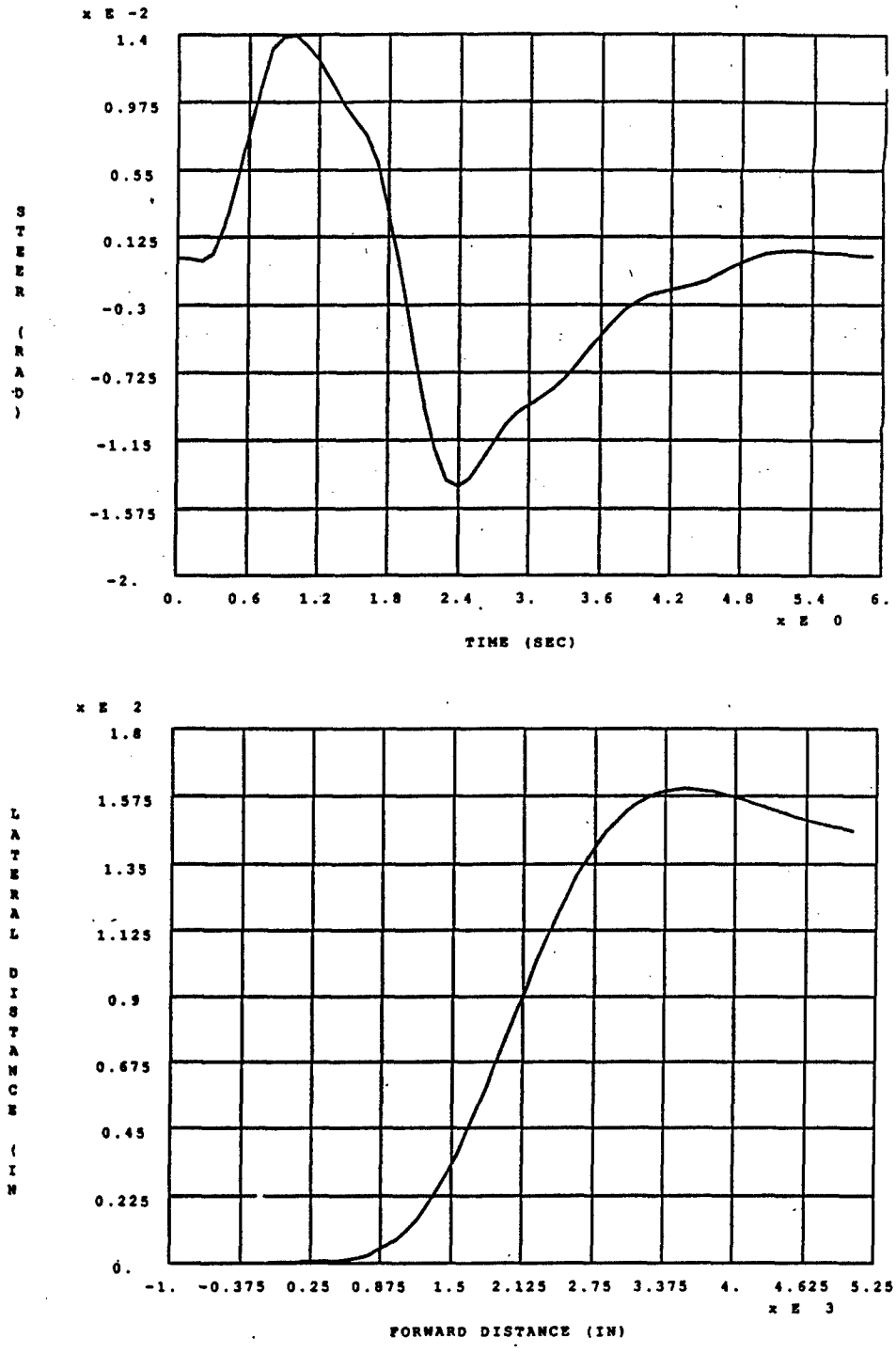

Figure 5-51. Example Lane-Change from DADS Simulation using the TACOM Driver Model

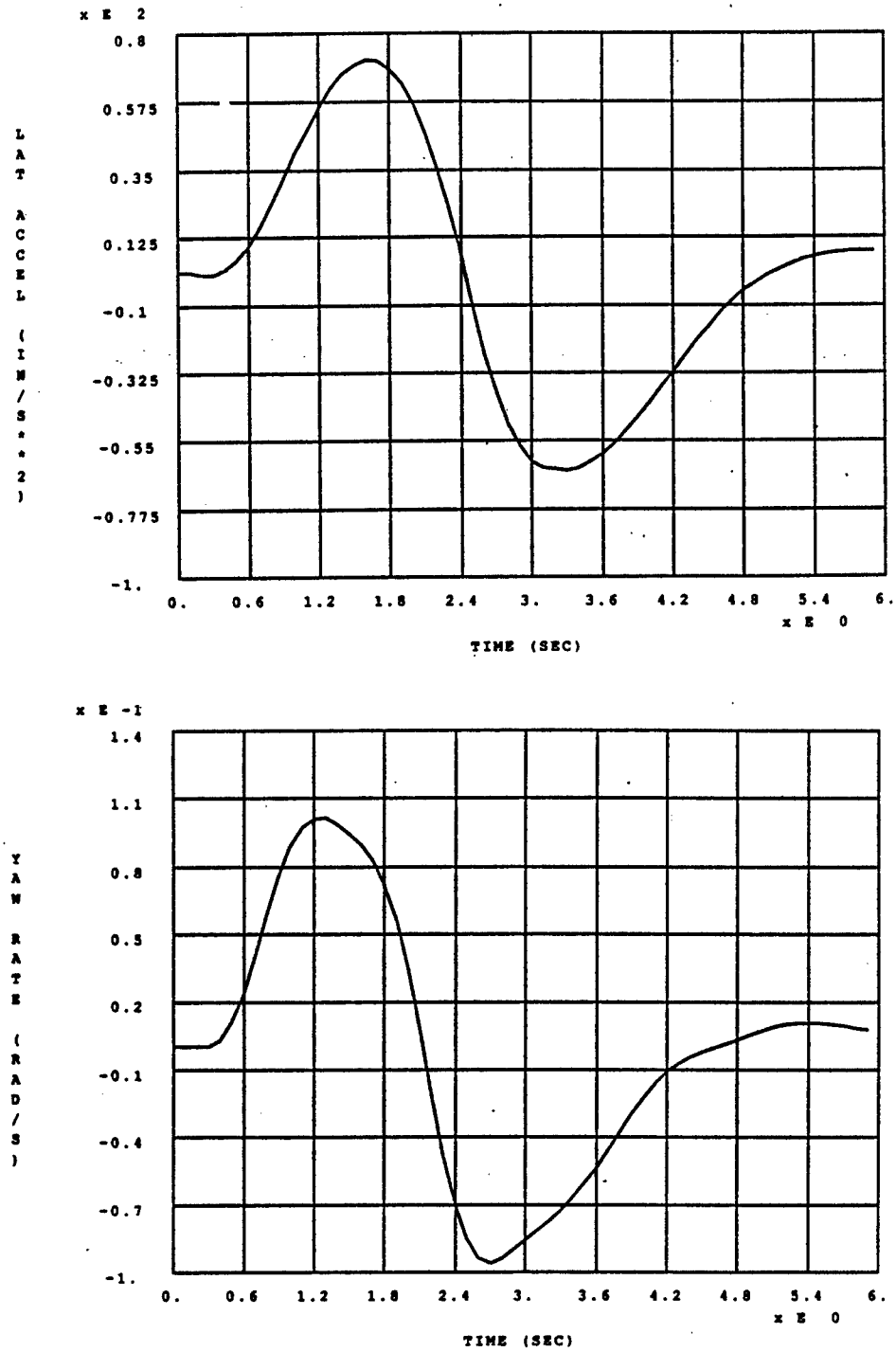

Figure 5-52. Example Lane-Change from DADS Simulation using the TACOM Driver Model

throughout this run. However, because the peak lateral accelerations of approximately 70 in/sec/sec or, 0.18 g's, seen here would categorize this run as a relatively low lateral acceleration maneuver, such updating of the driver model transition matrix would have little beneficial effect in this particular example.

Another example from the DADS / TACOM driver model simulation is seen in Figure 5-53 for a circular turning maneuver along a 500-ft radius path at a speed of 35 mph. Time histories of the average front wheel steering angle (radians) and the corresponding lateral acceleration (g's) are shown. A slight amount of overshoot is seen at about the 4-second point in the run as the vehicle "transitions" from the 100-ft straight approach tangent in to the circular curve.

Lastly, a sequence of animation frames are shown in Figures 5-54 and 5-55, illustrating the same DADS maneuver performed at a higher speed of 50 mph. During this run, the simulated HMMWV is experiencing a significant amount of sideslip and diminished directional stability because of reduced tire traction capabilities and a large rearward-positioned payload. The tires are operating under highly variable sideslip conditions during this maneuver and continuous updating of the localized tire cornering stiffnesses assists the driver model in better maintaining the desired path and directional stability in this example case.

If the transition matrix is not updated, unlike the previous example run, the driver model would use the initial values of tire cornering stiffness and vehicle speed prevailing at the start of the simulation to calculate the transition matrix. As the simulation progresses and significant side-to-side load transfer and vehicle sideslip occurs, the tire properties and localized cornering stiffness values would depart from their initial values prevailing at the start of the maneuver. The change in directional dynamics in this case would not be sensed by the driver model and the vehicle would be steered differently. A preliminary test run performed with no transition matrix updating (for the same 50 mph case) produced a directionally stable result, but large path errors showing the vehicle off-tracking several feet to the outside of the lane during the cornering maneuver.

In most nonlinear simulations, the driver model can still be used effectively without use of transition matrix updating provided that large changes in tire properties or speed do not occur for extended periods of time during the maneuver. Examples of this might be lane-change maneuvers which may have large peak levels of lateral acceleration (e.g. above 0.4 g's) but which are relatively short in duration. The driver model may be temporarily less accurate during these peak acceleration periods in predicting the future position of the vehicle, but the net effect will generally be small when compared to an identical run having continuous transition matrix updating. For some users, the additional execution time and

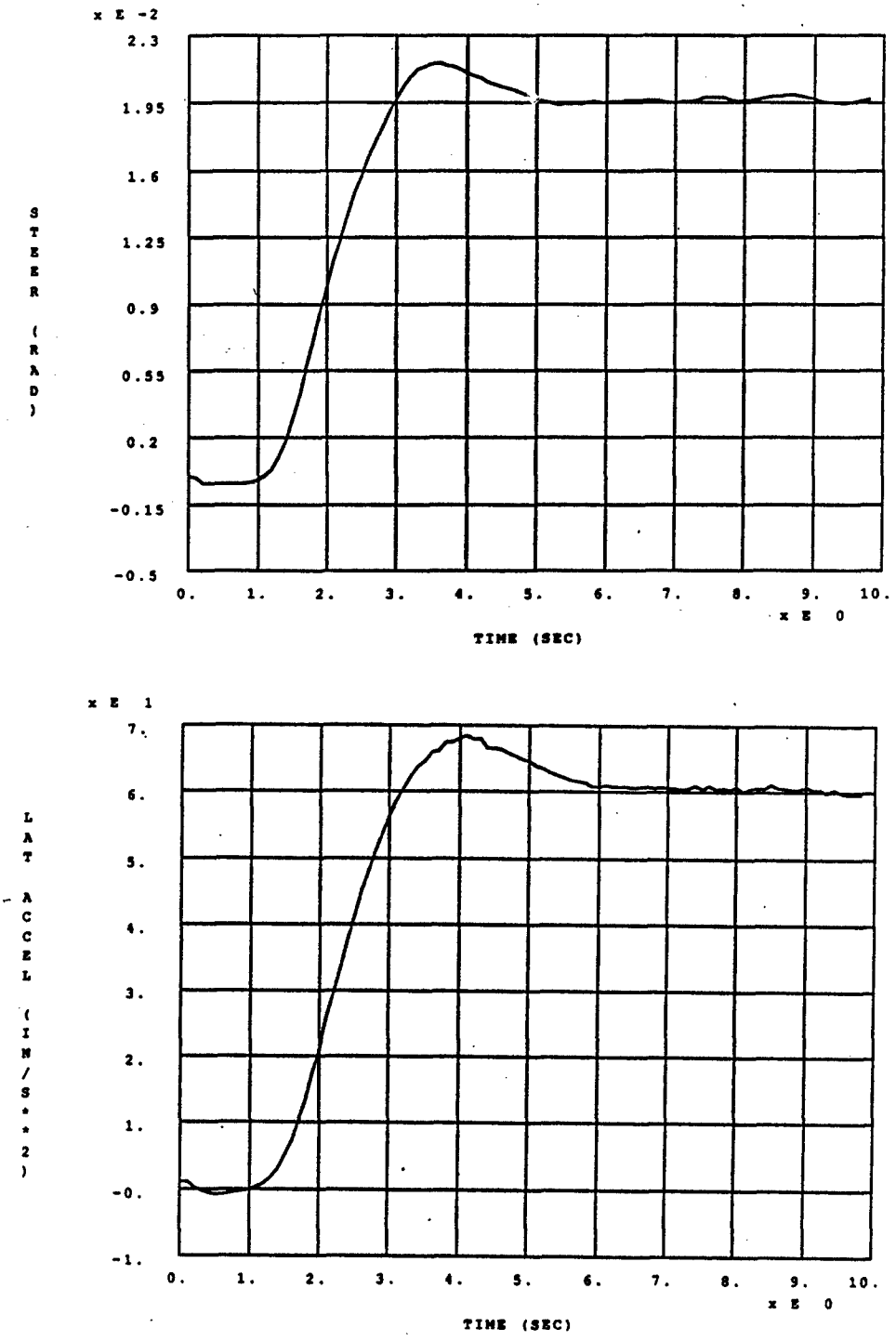

Figure 5-53. Example Circular Turn from DADS Simulation using the TACOM Driver Model

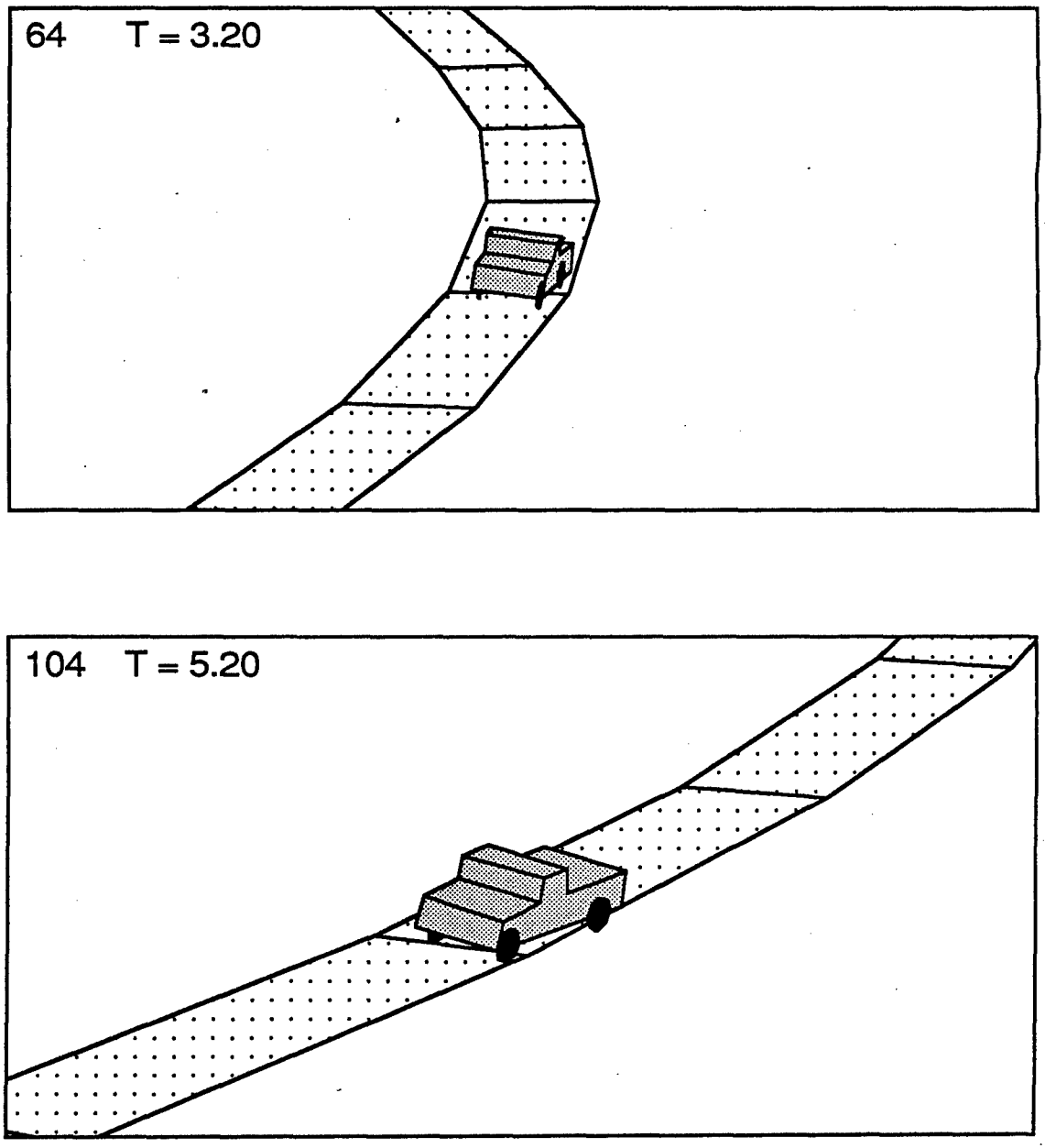

Figure 5-54. DADS / TACOM Driver Model for HMMWV Along Circular Turn at 50 mph

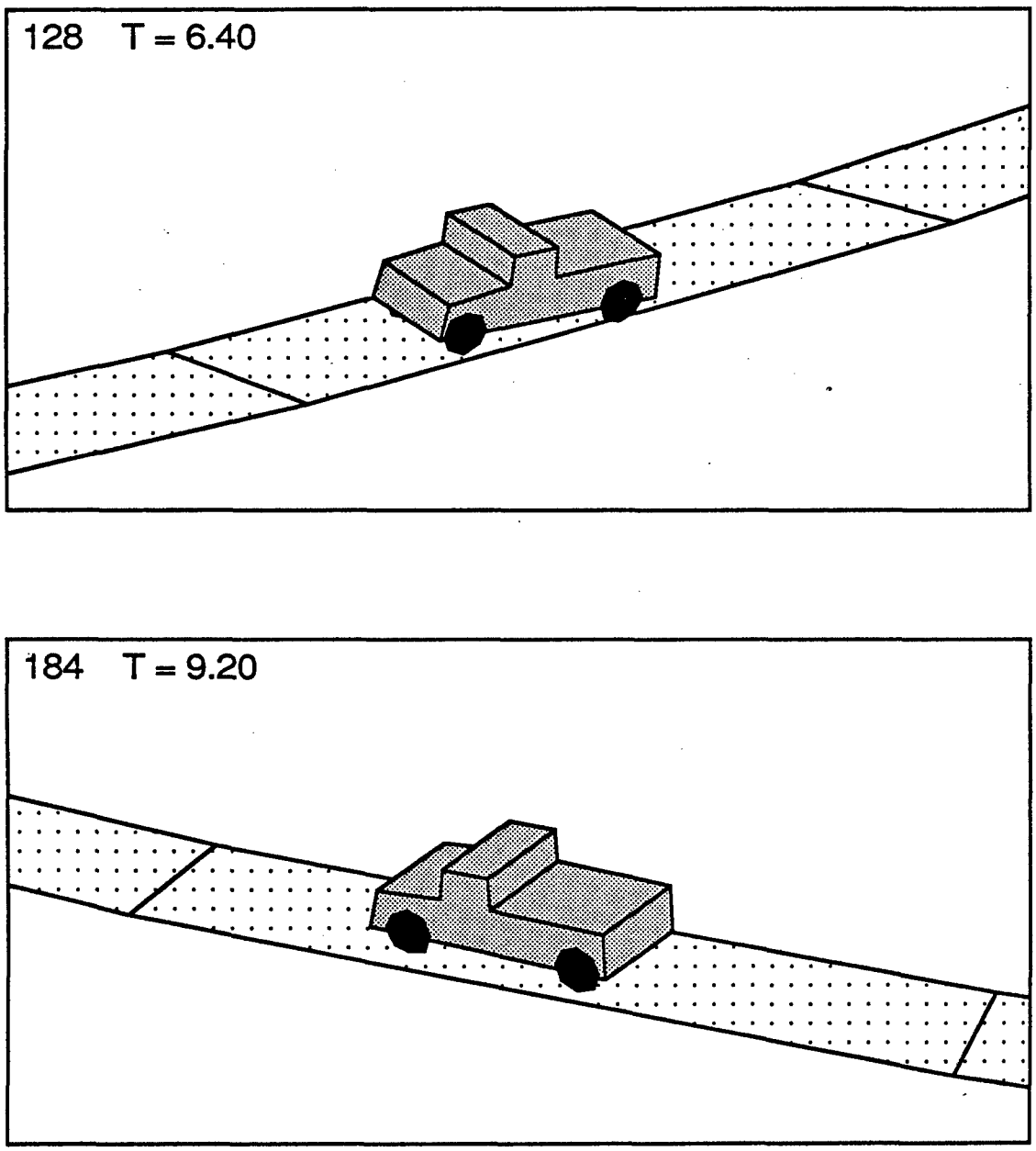

Figure 5-55. DADS / TACOM Driver Model for HMMWV Along Circular Turn at 50 mph

computational requirements of continuously updating the driver model transition matrix may be of concern and not actually needed for most of their maneuvers. In this case, the call to the TRANS subroutine from within the DRIVER subroutine may be removed or temporarily commented out.

It should also be remarked here that the "notion" of updating the transition matrix is in a sense analogous to human operator adaptation behavior observed during experimental tests of man/machine systems during which the dynamics of the controlled element is being altered. Previous research [3, 22, 28, 29, 30, 31, 32] has shown that human operators can adapt quite quickly to large changes in the dynamics of the controlled plant during the course of a tracking task experiment. Very often this adaptation or "re-identification" process by the human subject can occur within less than a second of time. Consequently, including or removing this call to the TRANS subroutine can be a way of representing (or not) the ability of drivers to adapt to changing vehicle dynamics properties during the course of a maneuver. The code that appears in Appendix D for the driver model shows the call from within the DRIVER subroutine to the TRANS subroutine enabled as the default.

5.9. Path Planning and Obstacle Detection Algorithm

This and the next section of the report describe two secondary tasks undertaken during the project which were intended to supplement the basic driver steering model described in earlier sections of the report. The first option, discussed in this section, describes a path planning algorithm which could be used to generate a "desired path" input for the basic steering control model. Instead of the program user specifying a set of x-y coordinates for the vehicle to follow (such as the center-line of a road), the program user would instead provide a more general scene description of the road geometry and any obstacles. The path planning algorithm would then select the specific desired path input for the steering control model to follow based upon an analysis of the scene data.

Initially, several approaches were considered for implementing a "path planning" capability within the driver model. The method described here is based upon compromises between computational efficiency and assumed capabilities of human operators in visually detecting obstacles and selecting paths. The basic outline of the algorithm used to represent a possible path planning capability for the driver model is seen in Figures 5-56 and 5-57. The basic idea of the algorithm is to sweep a forward radial area ahead of the vehicle with radial lines (or rays) originating at the vehicle. A radial profile of any obstacles or left/right boundary lines detected during a sweep is then constructed. A "centroid-like" point from

1. Transform specified left and right boundary lines from (x-y) cartesian inertial coordinates to (r-theta) polar coordinates (centered in the vehicle body axes).

2. Transform circular obstacle definitions, similarly, from cartesian to polar coordinates.

3. Obstacle detection and path selection:

   a. generate radial rays from - to +$theta_{max}$ in increments of delth
      i. step along ray until impact with boundary or obstacle or r_{max} exceeded
      ii. record r and theta values at impact & store as part of r(theta) profile

   b. from stored r(theta) profile:
      i. calculate r* {e.g. sum[r(i)] / i }
      ii. calculate theta* {e.g. [r(i) • theta(i)] / sum[r(i)] }

   c. check to see if r* lies within r(theta) profile
      i. if yes, proceed to step d.
      ii. if no, (left-right choice possible), then perform steps a. and b. twice:
         A. once from -$theta_{max}$ to 0
         B. once from 0 to +$theta_{max}$
         C. compare r* and theta* from A. and B.
         D. select r* having largest value

   d. transform r*(theta*) point to cartesian point and pass to steering model as input

   e. if r* is less than a defined r_{min}, activate closed-loop driver braking control model to stop in distance r*.

4. End of integration loop. Increment position and repeat.

Figure 5-56. Example Path Planning Algorithm for the Driver Model (during integration loop)

this profile is calculated which acts as the target point for the steering control model to then follow.

Figures 5-57 and 5-58 show a hypothetical driver/vehicle system approaching a field of obstacles. The first figure shows the vehicle just entering the field and detecting the first obstacle. The second figure shows the vehicle at an advanced position now detecting all obstacles and moved somewhat to the right of the first obstacle. The r^* and θ^* quantities appearing in these figures represent "centroid-like" coordinates of the driver field of view. At any point in time, the (r^*,θ^*) coordinate (or some variation of it) *would be used* as a point located on and, over time, defining the desired path to be followed by the driver steering control model. The $r(\theta)$ vs θ graph simply represents unobstructed sight distance in the driver's field of view out to some finite maximum distance. The (r^*,θ^*) point moves to the left or right based upon the particular $r(\theta)$ profiles generated in the field of view.

As the scene becomes more crowded or the maneuvering field limited, the centroid-like quantity $r^*(\theta^*)$ will move closer to the driver thereby resulting in a shortening of the preview distance used in the steering control strategy. This is a desirable effect since most drivers will reflect this same basic behavior pattern under similar circumstances.

The same preview distance "shortening mechanism" can be used to trigger the start of a closed-loop braking model such as the one described in the next section 5.10. For example, if $r^*(\theta^*)$ becomes less than some r_{min} level needed for moderate braking under the prevailing tire/surface friction conditions, the brakes would be applied in a closed-loop manner so as to bring the vehicle to a stop in a distance of r_{min}. During the course of the braking maneuver, the obstacle detection/path planning algorithm would still be active, so that, if an "opening" in the obstacle field was detected prior to the stop, the braking could be abandoned and the vehicle steered out through the "opening." Acceleration and speed control of the vehicle could be controlled by a counter-strategy.

A simple computer program (shown listed in Appendix F) was written to implement and test the basic path planning algorithm outlined here. The algorithm provides for a set of left and right boundaries in addition to a number of obstacles in the driver field of view. The left and right boundaries are represented as arbitrary x-y tabular data (with respect to an inertial frame of reference) and the obstacles as *circular* objects of arbitrary radii centered at designated x-y (inertial frame) locations. The computer code that was written to test the described algorithm requires input of those basic items, in addition to such things as driver location, orientation, field of view, and maximum sight distance. At each position, the program then calculates the $r(\theta)$ profile and the centroid-like location, $r^*(\theta^*)$, for that particular scene. By performing these calculations in a sequential fashion with the driver moving forward toward the desired centroid-like location, a path is generated (as defined

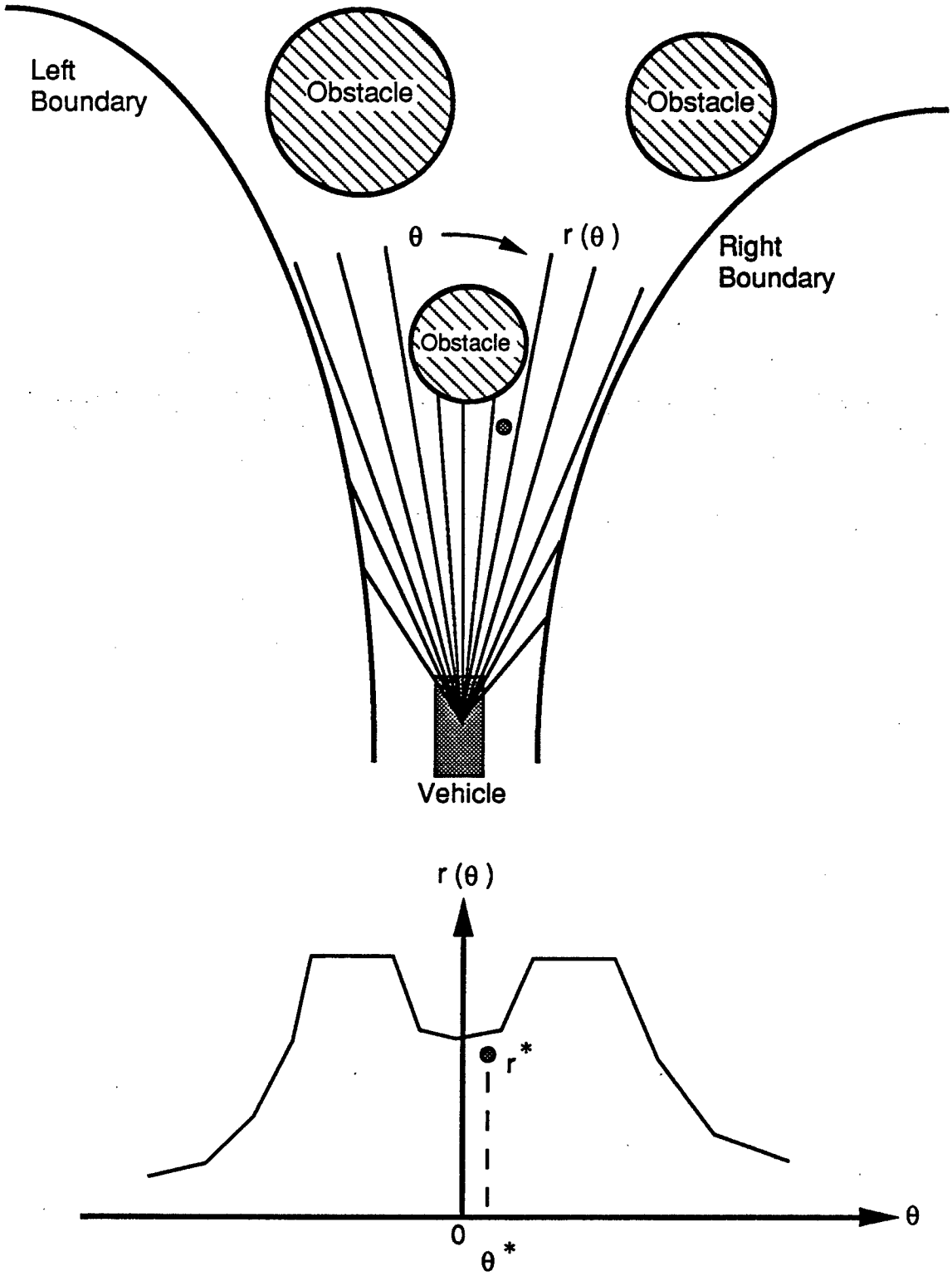

Figure 5-57. Vehicle Entering Field of Obstacles and Corresponding Profile

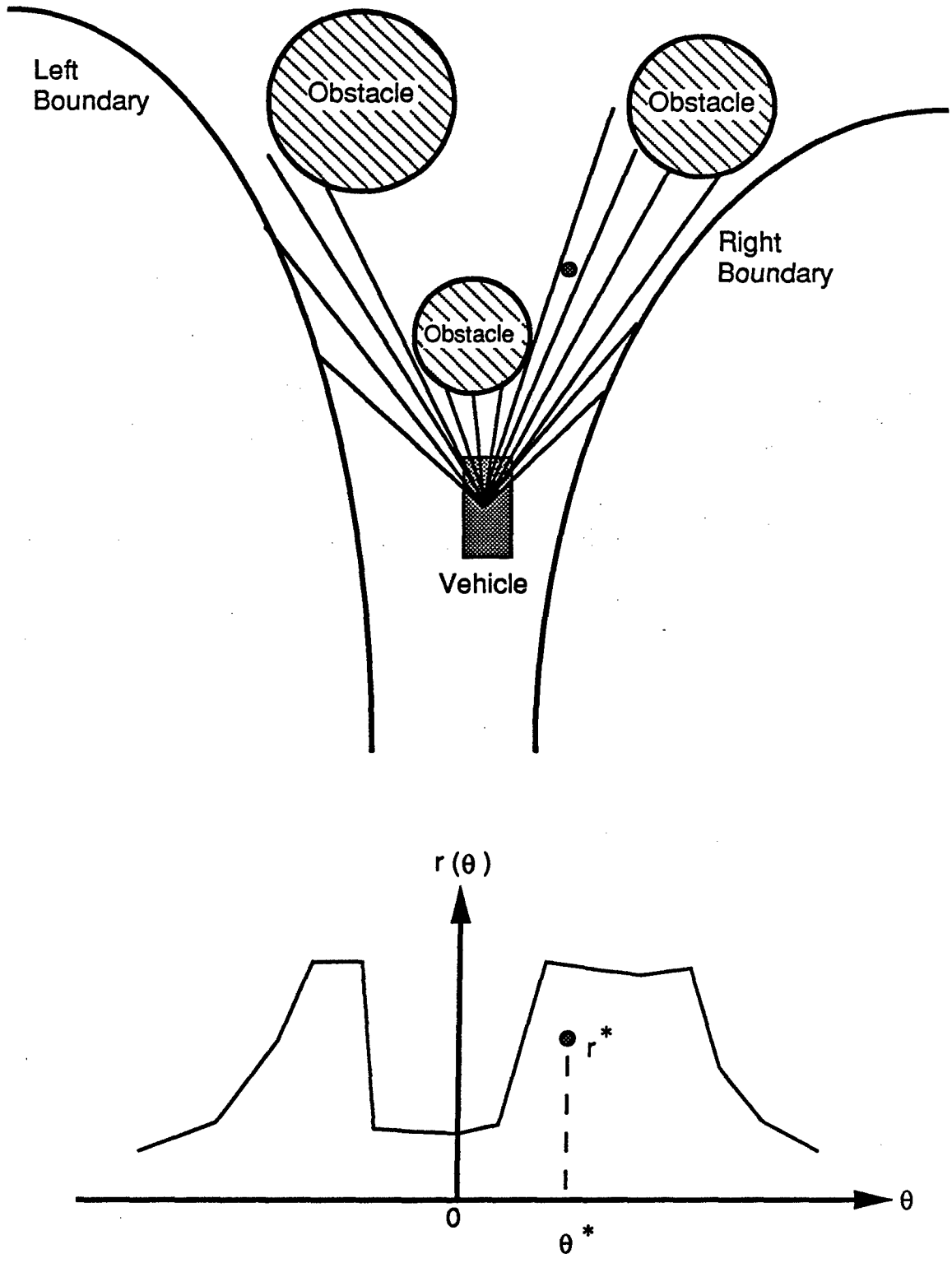

Figure 5-58. Vehicle at Advanced Position and Corresponding Profile

by the sequential locations of that quantity). This path then represents the output of the path planning module and acts as an input to the driver steering control module.

Two examples are presented next which illustrate the operation of the path planning algorithm used in conjunction with the steering control model. Figure 5-59 shows a lane-change course using left and right boundaries (instead of a desired x-y path) to guide the driver/vehicle system during the path-following maneuver. No obstacles are present in this run. Results in the form of time histories are shown in Figures 5-60 and 5-61. The simulated vehicle is a loaded HMMWV travelling at 60 mph. The specified field of view is +/- 0.3 radians. The maximum look-ahead distance, r_{max}, is 150 ft.

As a second example, Figure 5-62 shows a course layout in which the left and right boundaries are straight line segments defining the left and right road boundaries of an obstacle course similar to that used during the test program. Centered in the left-hand lane and directly in front of the vehicle at the start of the run is a circular obstacle with a diameter of 12 ft. An identical second obstacle is located centered in the right-hand lane 112 ft beyond the first obstacle. Results from this run are also seen as a sequence of time histories in Figures 5-63 and 5-64. After the start of the run, the vehicle is steered to the right away from and around the first obstacle. As the vehicle moves forward beyond the first obstacle, it is steered back to the left around the second obstacle. The vehicle then encounters the left/right road boundaries which guide it out the exit in the right-hand lane.

Note that the only information provided to the path planning algorithm are the left and right boundaries (located with respect to an inertial reference frame) and location and size of any obstacles. The model thus decides "where to go" (by means of the path planning module) as well as "how to get there" (by means of the steering control model). The algorithm *continuously* adjusts the driver preview parameter and its "transition matrix" based upon the obstacles or boundary constraints present in the field-of-view. For example, in the obstacle course run seen in Figure 5-62, the preview distance was shortened by the model to a value of about 25 feet when the vehicle was nearing an obstacle/gap, and was lengthened to approximately 100 ft (up to the maximum sight-distance specified) at the start and end of the course where no obstacles were immediately present. This version of the the path planning model uses a *single point* in the preview interval to guide and steer the vehicle in order to minimize the computational requirements of the algorithm. Consequently, the steering responses seen with this type of model will be somewhat more variable than one in which an average of several points over the preview interval are used in the computation (as, for example, the type of calculation performed by the basic version of the TACOM steering control model presented earlier).

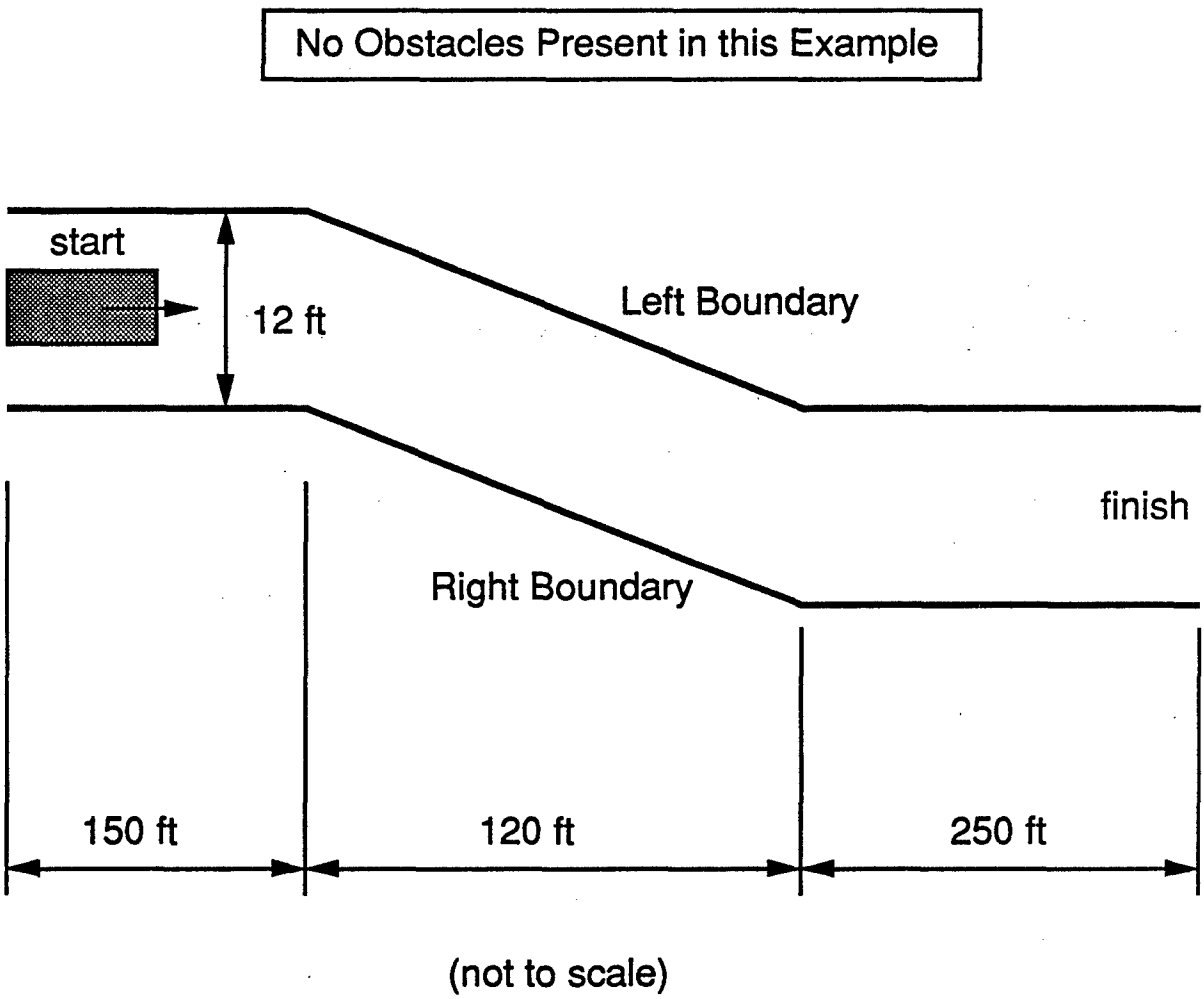

Figure 5-59. Lane-Change Geometry for the Example Calculation using the Path Planning Algorithm

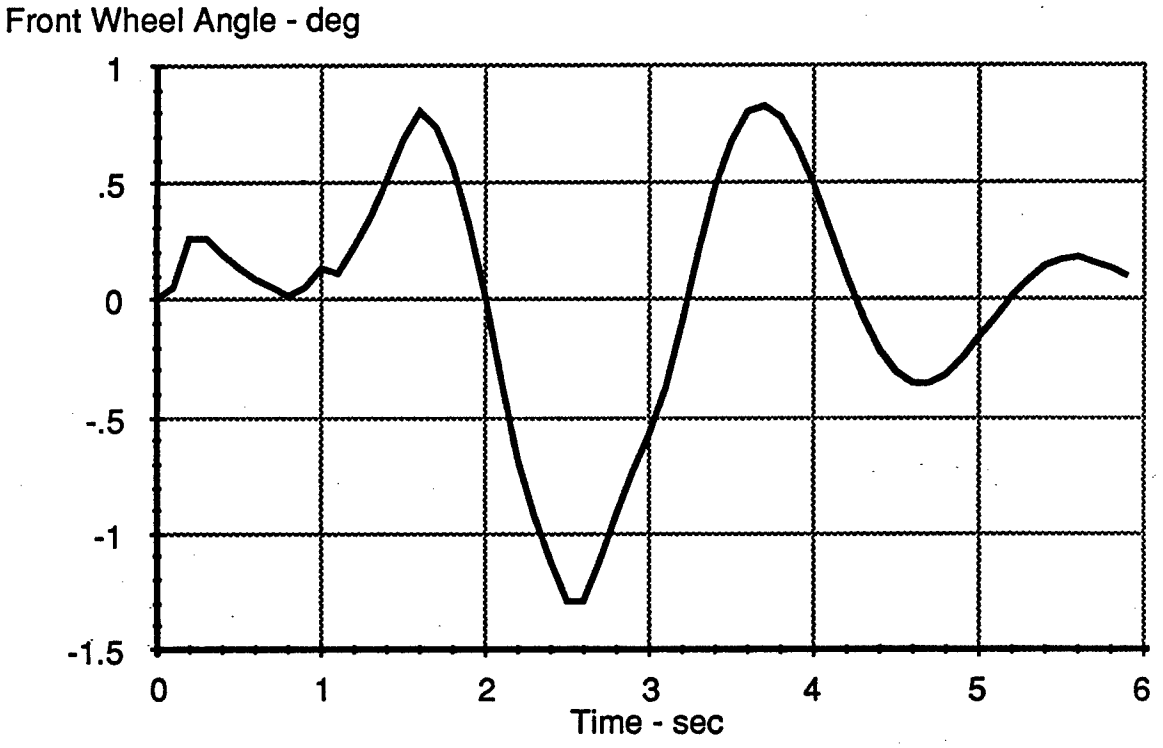

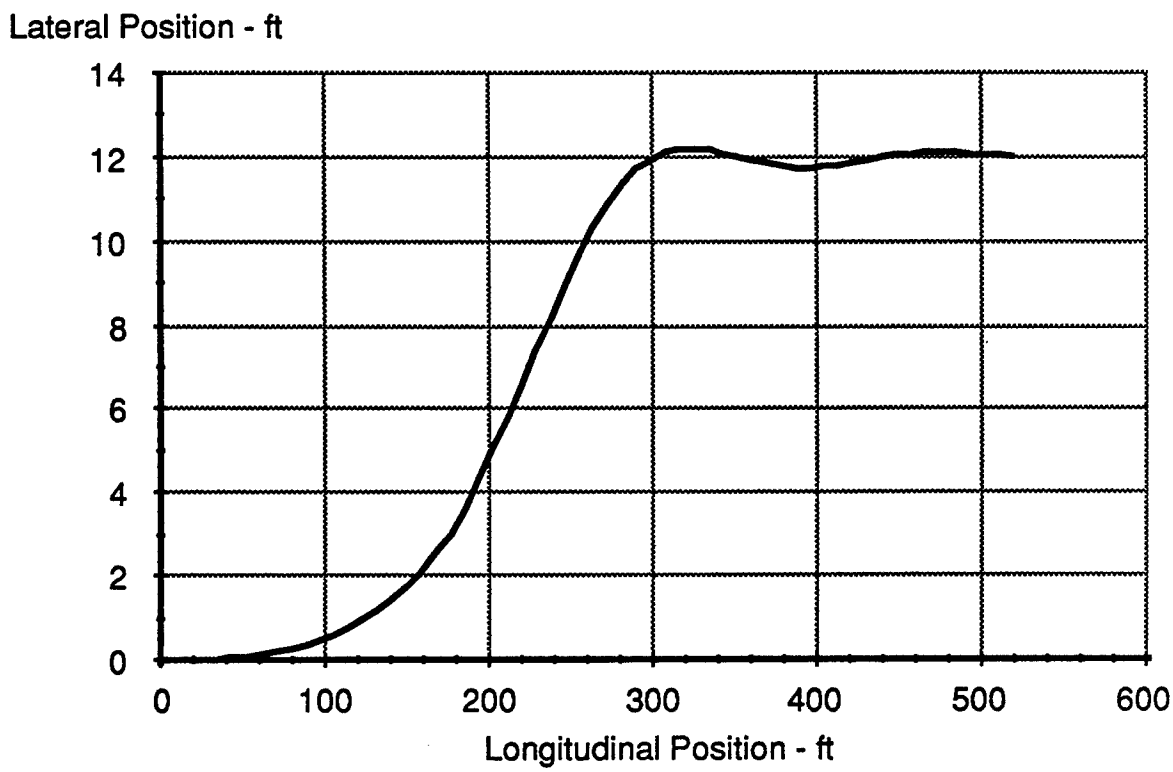

Figure 5-60. Example Calculation using the Path Planning Algorithm - Lane Change Maneuver

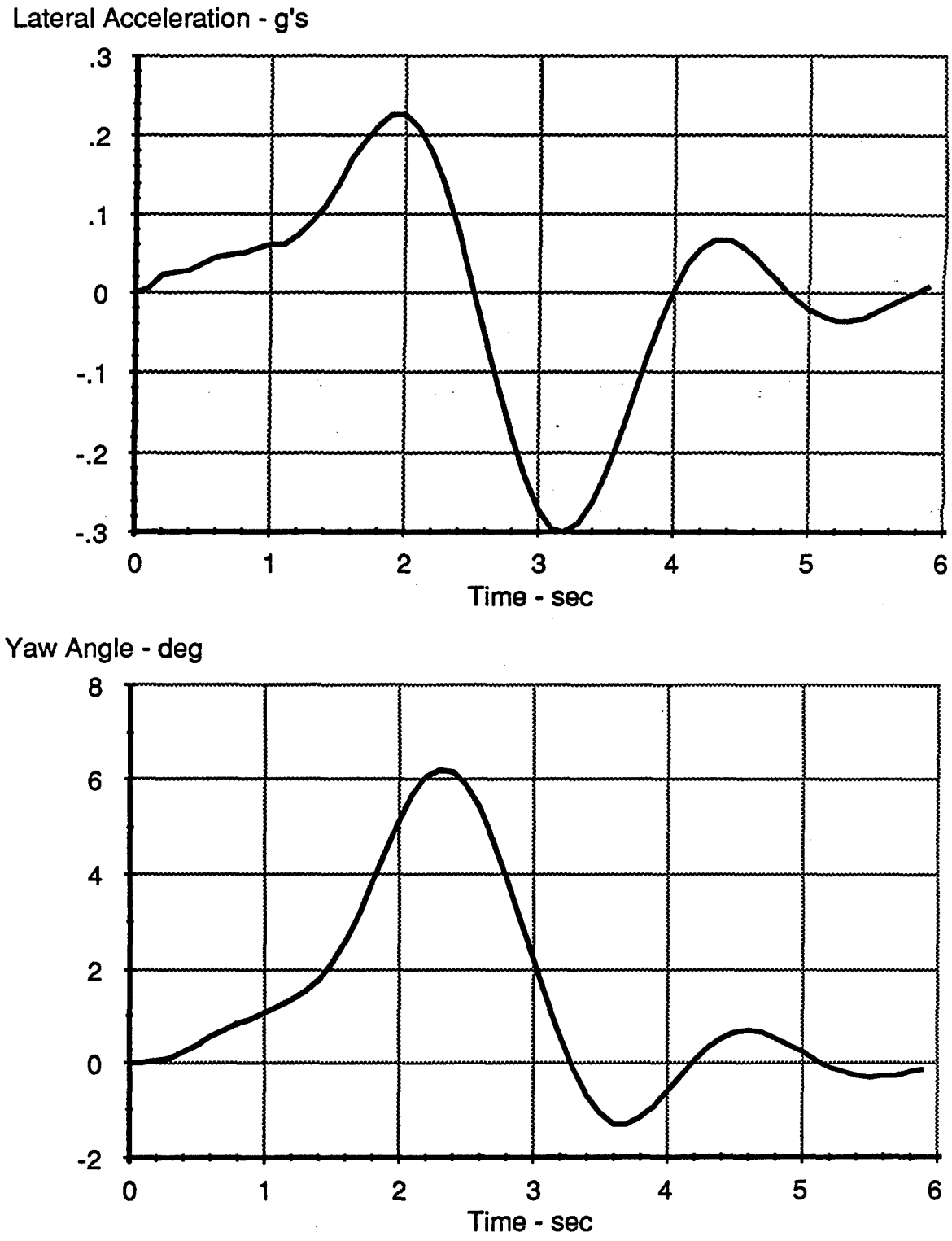

Figure 5-61. Example Calculation using the Path Planning Algorithm - Lane Change Maneuver

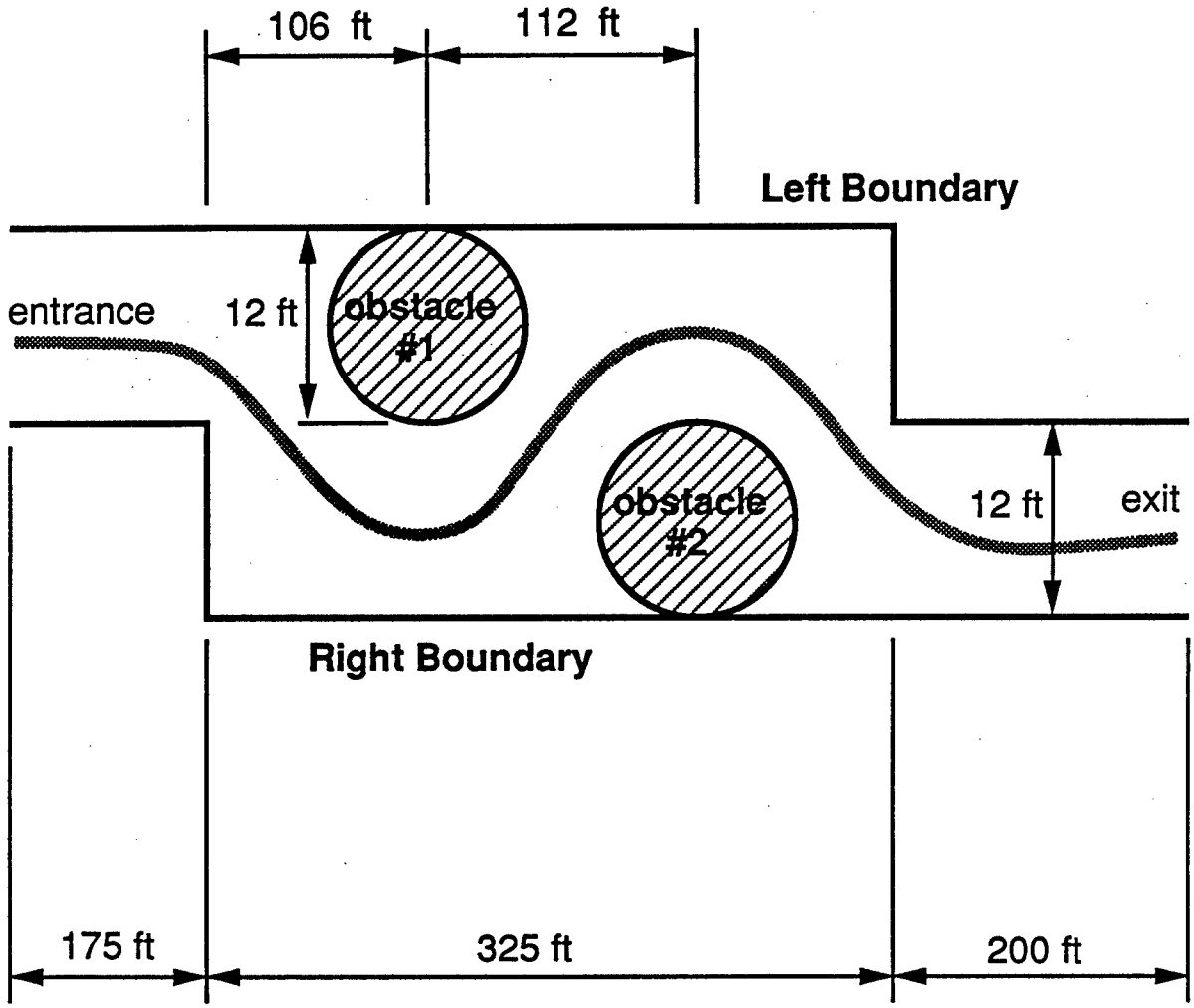

(not to scale)

Figure 5-62. Obstacle Course Geometry for the Example Calculation using the Path Planning Algorithm

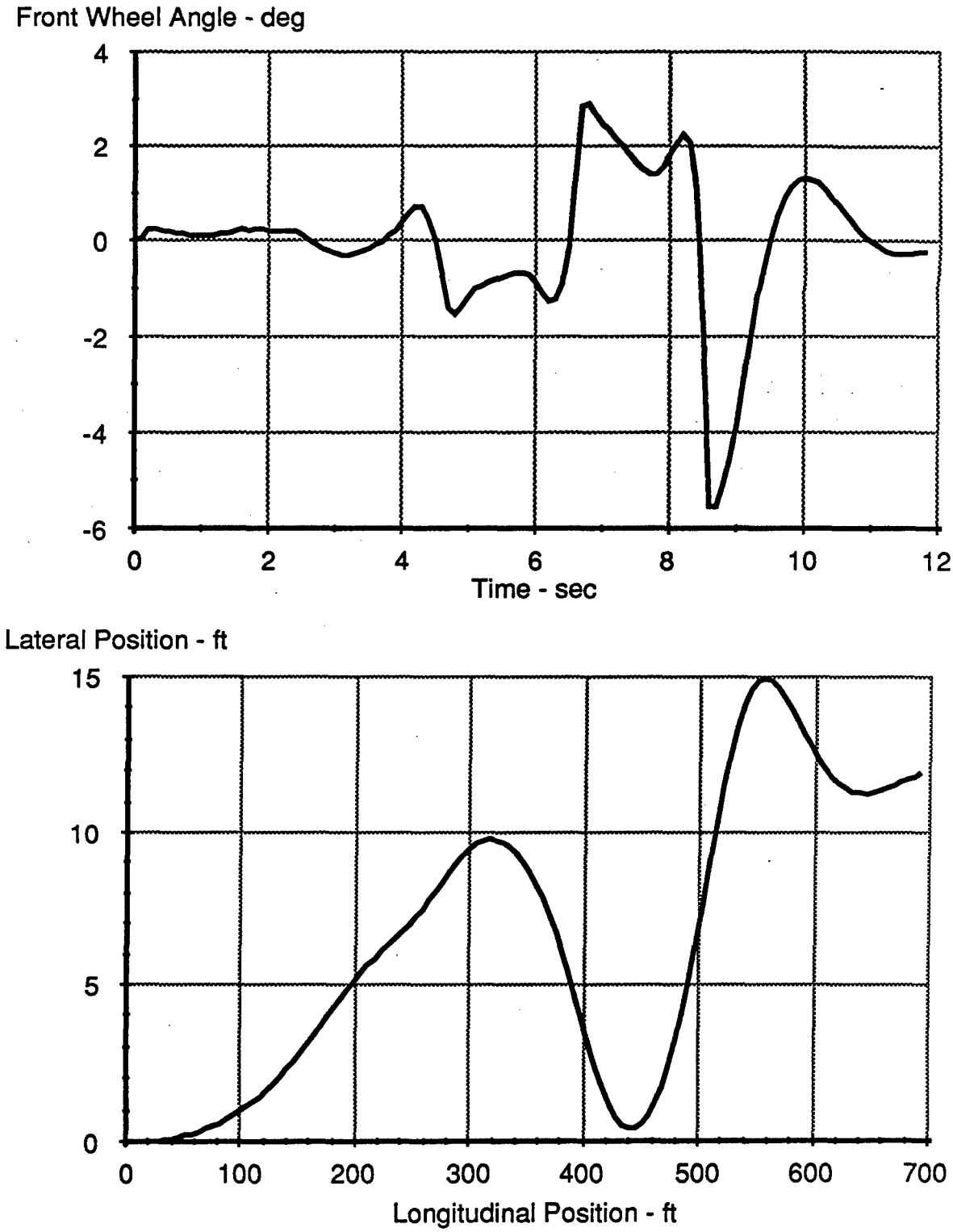

Figure 5-63. Example Calculation using the Path Planning Algorithm - Obstacle Course Maneuver

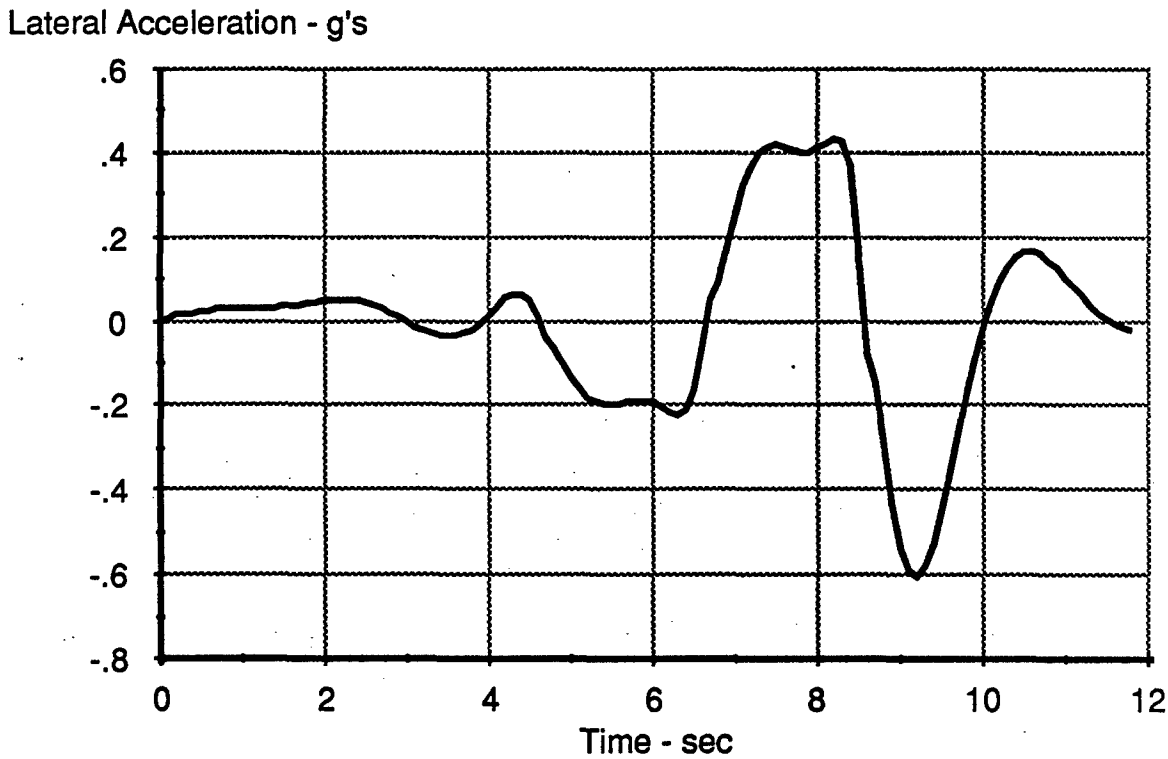

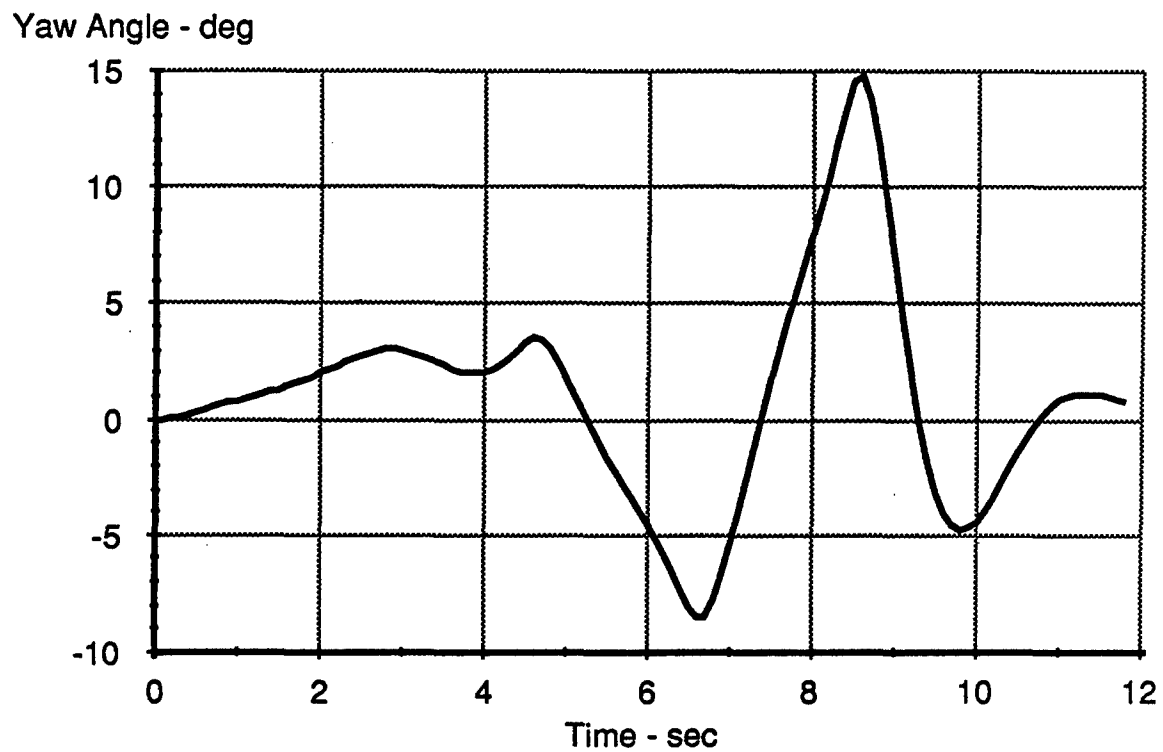

Figure 5-64. Example Calculation using the Path Planning Algorithm - Obstacle Course Maneuver

The advantages of using a path planning feature in combination with the driver steering control model are: 1) geometric descriptions of the roadway or obstacle course can often be supplied in a simple manner, and 2) the path planning module automatically determines the path to be followed based upon the boundary and obstacle data. The chief disadvantage is the large increase in computational effort used by such algorithms in determining the path. More efficient computational schemes could no doubt be offered to improve upon the basic concept described in this report. In general, use of a path planning model is probably best suited to driving scenarios involving arbitrary obstacle courses for which tracking of a particular pre-determined path is not required, or, a likely path is not obvious from simple examination of the course geometry.

5.10. Driver Model Option for Closed-Loop Braking

The TACOM driver model discussed in the previous sections of the report is obviously aimed at simulating the closed-loop *steering* behavior of drivers. No consideration of how drivers might also control or modulate brake pressure during braking maneuvers was initially included in that model. However, in order to study the effects of active driver modulation of brake pressure during vehicle deceleration maneuvers, it will ultimately be necessary to augment and extend the capabilities of the driver steering control model in future studies. This section describes, in general terms, one possible method by which closed-loop braking behavior of drivers could be modelled. Much of the proposed closed-loop *braking* model discussion that follows was initially suggested in a small study performed by UMTRI for the Rockwell International Corporation.[45]

The test data collected under this project for the HMMWV was intended, in part, to support future development and validation of closed-loop braking models by TACOM. Those braking tests, as discussed previously in section 5.6, were all conducted intentionally as *closed-loop* braking tasks during which the driver applied braking so as to bring the vehicle to a uniform stop at a specified point on the test track. Recall that the requested stopping distances were varied in a random-like manner from test to test to prevent the test drivers from "automating" their brake pressure control strategy. Data was collected for braking-in-a-turn as well as for straight-line braking maneuvers.

5.10.1. **Closed-Loop Brake Application Strategy.** The basic idea underlying the proposed model of driver braking behavior is for the model to apply appropriate levels of brake pressure to bring the vehicle to rest at a future position in space. The driver is assumed to be equipped with a simple "understanding" of the longitudinal dynamics of the vehicle in response to command pressure inputs. In addition, the driver is presumed to act in a time-delayed fashion so that the command pressure calculated by the model is applied

to the brake system after some inherent driver delay. In the model, the simple "understanding" is represented by the longitudinal dynamics of a point-mass subject to a braking or retardation force. In essence, the driver model has a simplified "internal model" of the longitudinal dynamics of the vehicle being operated, and can, therefore, predict or estimate future vehicle position in response to command pressure inputs. (This is essentially an extension of the same basic optimal control approach applied successfully during this project for the lateral steering control of vehicles.)

Without presenting the mathematical derivation here, the equation that results from this model is one that relates an ideal driver command pressure, $P^*(t)$, to current longitudinal vehicle position, speed, and desired stopping point:

$$P^*(t) = m\,[V(t)]^2 / \{\, 2\,K\,[xd - x(t)]\,\} \qquad (5.10\text{-}1)$$

where,

- t is time from the start of the braking maneuver
- $P^*(t)$ is the calculated ideal driver command pressure (brake pedal) at each point in time during the braking stop (the calculated "control variable" here)
- m is the total mass of the vehicle
- V(t) is the forward speed of the vehicle at each point in time during the braking stop
- K is a linear gain factor relating driver command pressure to total retardation force (lbs / psi)
- xd is the desired stopping distance from the point of brake application

and,

- x(t) is the vehicle longitudinal position at each point in time during the braking stop

The ideal command pressure, $P^*(t)$, is then delayed an amount t_d seconds (driver time delay for braking), resulting in the final equation for the driver modulated command pressure, P(t), which is the actual pressure applied to the brake system:

$$P(t) = P^*(t - td) \qquad (5.10\text{-}2)$$

As seen, the closed-loop equation (5.10-1) is quite simple and, in fact, is a rearrangement of the well known physics formula (applied on a point-in-time by point-in-time basis) relating stopping distance, x, to initial speed, V, and subject to a constant deceleration, D. [$x = V^2 / (2\ D)$] The driver model, in effect, selects deceleration at each point in time using this formula, translates it to a command pressure equivalent, based upon brake gains and vehicle weight, and then delays it in time to account for an assumed driver lag. Although equation (5.10-1) was not derived from this particular viewpoint, it is helpful to see an analogy between it and a simple explanation in basic physics.

Figure 5-65 shows an example time history for the closed-loop driver command pressure predicted by the model for a braking stop from 30 mph and a desired stopping distance of 150 feet. The calculation is for a 5-axle tractor-semitrailer and was simulated using a modified version of the UMTRI Phase 4 commercial vehicle model.[7] Since the driver braking model approximates the deceleration gain of the braking system by a simple gain constant, K, noted above, differences can exist between the driver "understanding" of the pressure-retardation force relationship and that of the actual brake system. This would be particularly true for vehicles having highly nonlinear torque-pressure relationships and significant levels of hysteresis, or, for cases of low road surface friction where the available retardation torque is limited by the surface friction. Since the vehicle used in this example possessed fairly linear-like brakes (aside from the usual push-out pressure characteristic) and only modest levels of brake hysteresis, reasonable predictions of command pressure would be expected by the model when sufficient tire-road friction is available. Figure 5-65 seems to suggest this. The continued "drooping" of treadle (command) pressure at the end of the stop is attributable to brake hysteresis, which causes a lagging of brake torque requested by the model during the pressure reduction phase. As indicated in the next section, 5.10.2 Closed-Loop Brake Release Strategy, this basic form of brake application will normally be interrupted in the model by front-axle wheel locks and/or vehicle instabilities with more demanding stops attempted for shorter distances.

Figure 5-66 illustrates the differences between the simple linear retardation function expected by the driver model and that experienced by an actual vehicle. For the high friction surface (top diagram) where the retardation forces primarily derive from the torque limitation of the brake (summed over the vehicle), the primary differences lie in the nonlinearities present in the brake system itself. For the case of the low friction surface (bottom diagram), additional saturation-type nonlinearities are introduced because of the tire-surface friction limitations. Consequently, mild over- or under-estimations of total brake retardation forces by the driver model under conditions of high surface friction, can become exaggerated under low friction conditions. This would especially be true for a loaded vehicle and low friction surface combination since the command pressure "expectation" requested by the driver model will be scaled up by the weight of the vehicle

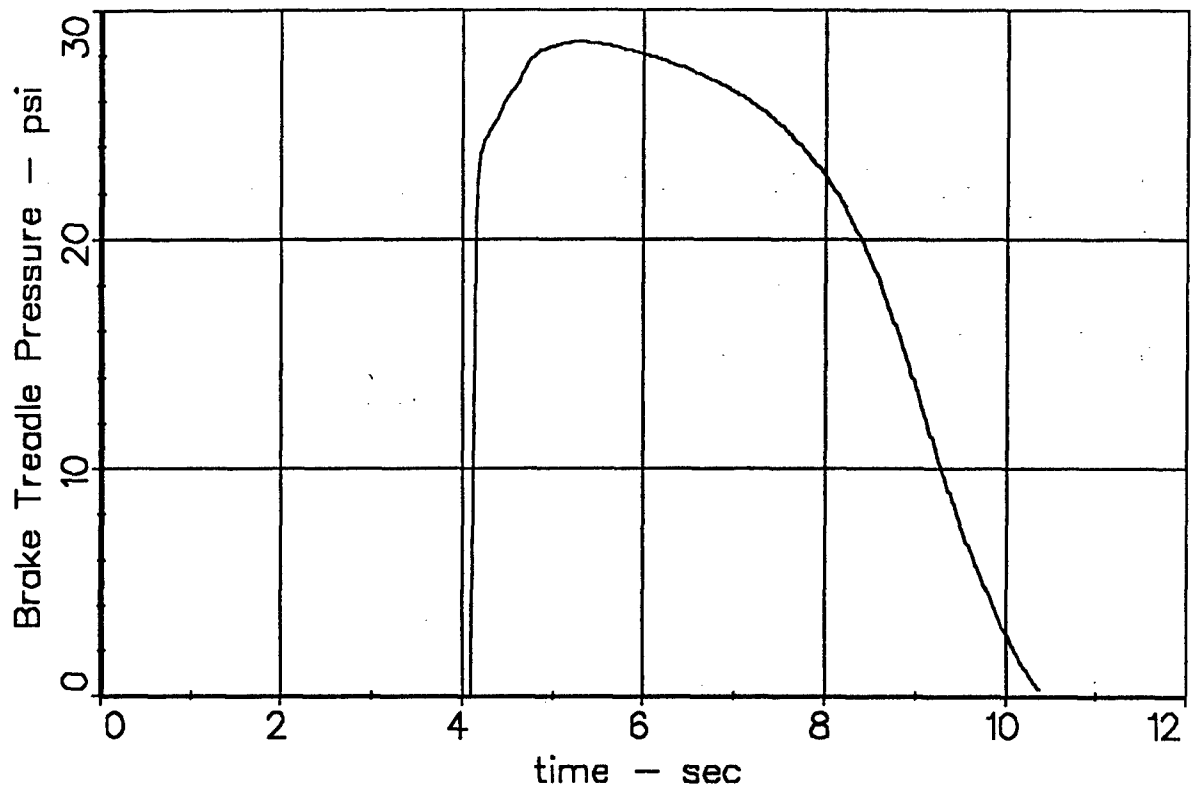

5–axle Tr–Semi; 30 mph; Braking–in–a–Turn; Driver Control;

Figure 5-65. Example Prediction of Command Pressure from the Closed-Loop Driver Braking Model during a Controlled Stop

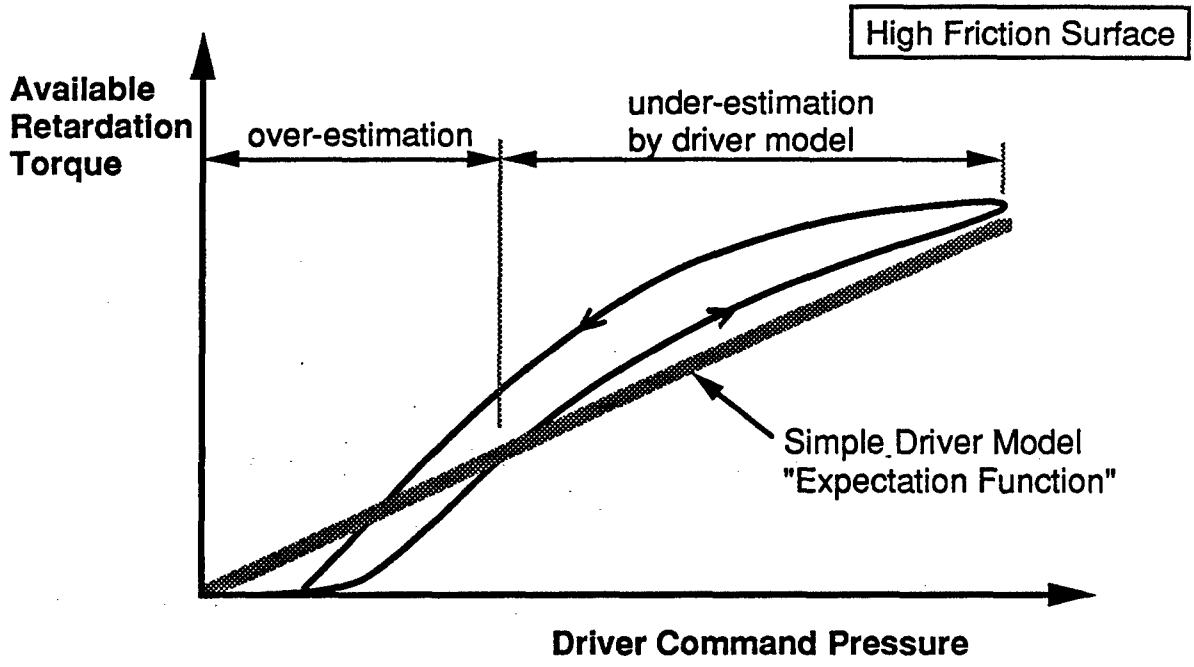

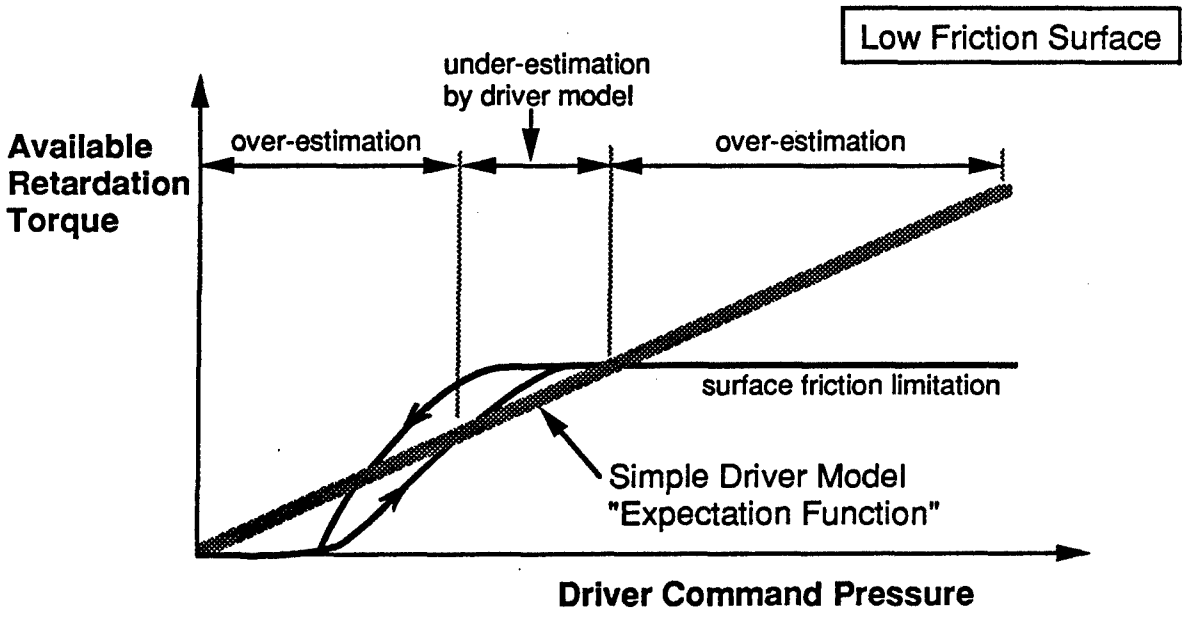

Figure 5-66. Comparison of Simple Driver Model Braking Expectation with Actual Retardation Properties

from the empty vehicle condition on the same surface. This will, in turn, result in a significant over-estimation of the available retardation torque on the part of the model as indicated in Figure 5-66 (lower diagram).

In spite of this, even in cases of significant over-estimation of the available retardation torque by the model, reasonable predictions of command pressure demand can still be obtained from the model. Much of this "success" can be attributed to the other half of the driver model behavior, discussed in the next section, which models how brake pressure is released under various conditions, thereby preventing the model from operating for extended periods of time in modes of mismatch or over-estimation. Further refinement or improvements to the driver "expectation function" of retardation torque are of course possible, such as accounting for the brake system push-out pressure (dead-zone), or, introducing nonlinearities into the expectation function.

5.10.2. **Closed-Loop Brake Release Strategy.** In order to represent a basic response to loss of steering due to front axle lock-up and/or various forms of vehicle directional instability that can occur during heavy braking, the closed-loop braking model may have a number of programmable "rules" for temporarily releasing driver commanded pressure during a braking maneuver. The following "rules" define conditions for possible pressure release by the driver model:

A) left and right axle wheel slip values both exceed value of Smax,
(front -axle lock)

or,

B) absolute value of path error exceeds value of Ymax,
(vehicle 12-foot lane exceedance)

or,

C) absolute value of vehicle sideslip angle exceeds value of Bmax,
(yaw instability)

or,

D) absolute value of tractor-semi articulation angle exceeds value of Gmax,
(jackknife and/or trailer swing for an articulated vehicle)

and,

E) forward speed greater than Vmin.
(ignore brake release "rules" at very low speeds)

Example values for these parameters for a tractor-semitrailer might be:

Smax = 0.5
Bmax = 10 degrees

Ymax = 4.0 feet
Gmax = 10 degrees.
Vmin = 10 ft/sec

Figure 5-67 shows a time history of driver command pressure from the closed-loop driver model for a braking stop on a low friction surface in which front-axle lock-up is occurring and causing interruption of the applied command pressure based upon "rule" A) above. A by-product of this "brake pumping" activity by the driver model is that following each interruption, the next application by the model is successively higher in order to meet the increased stopping demand caused by the previous brake releases. The increasing command pressure, or upward ramping, seen during the first two application cycles by the driver model also reflects "over-estimation" behavior of the model as discussed in the previous section and Figure 5-66. The "over estimation" is caused by insufficient tire-surface friction (semitrailer and tractor rear lock-ups are occurring prior to a tractor front-axle lock-up during these two application cycles).

Overall, the basic command pressure modulation by the closed-loop driver model seems to behave reasonably given the simplicity of the model. Refinements of this model are certainly possible based upon some of the braking data collected under this project. Additional driver-vehicle experiments could also be designed and conducted to extract information useful to a more comprehensive modelling effort.

In summary, it is assumed that the closed-loop braking model outlined above possesses certain capabilities and inherent properties. First, the ability to select, in at least a simple manner, an appropriate value of command pressure to bring the vehicle to a stopping point. This suggests an ability of drivers to "calibrate" themselves to the vehicle being controlled and to, therefore, account for changes in basic vehicle dynamics or operating conditions (estimation of retardation as a function of command pressure; prediction of future vehicle position; adaptation to gross vehicle weight changes). Secondly, it is assumed that the simulated driver does not react in an instantaneous manner to an elected brake control strategy. Consequently, a simple transport time delay property can be assigned to the driver to represent this basic limitation. The value used for this delay was 0.1 second in the calculations seen above (for a very responsive driver), but a value more representative of "average" drivers would probably be somewhat greater [46, 47, 48]. Simulations performed in reference 45 with varying values of this driver model time delay parameter suggested a strong sensitivity between closed-loop stopping performance and this basic driver lag property.

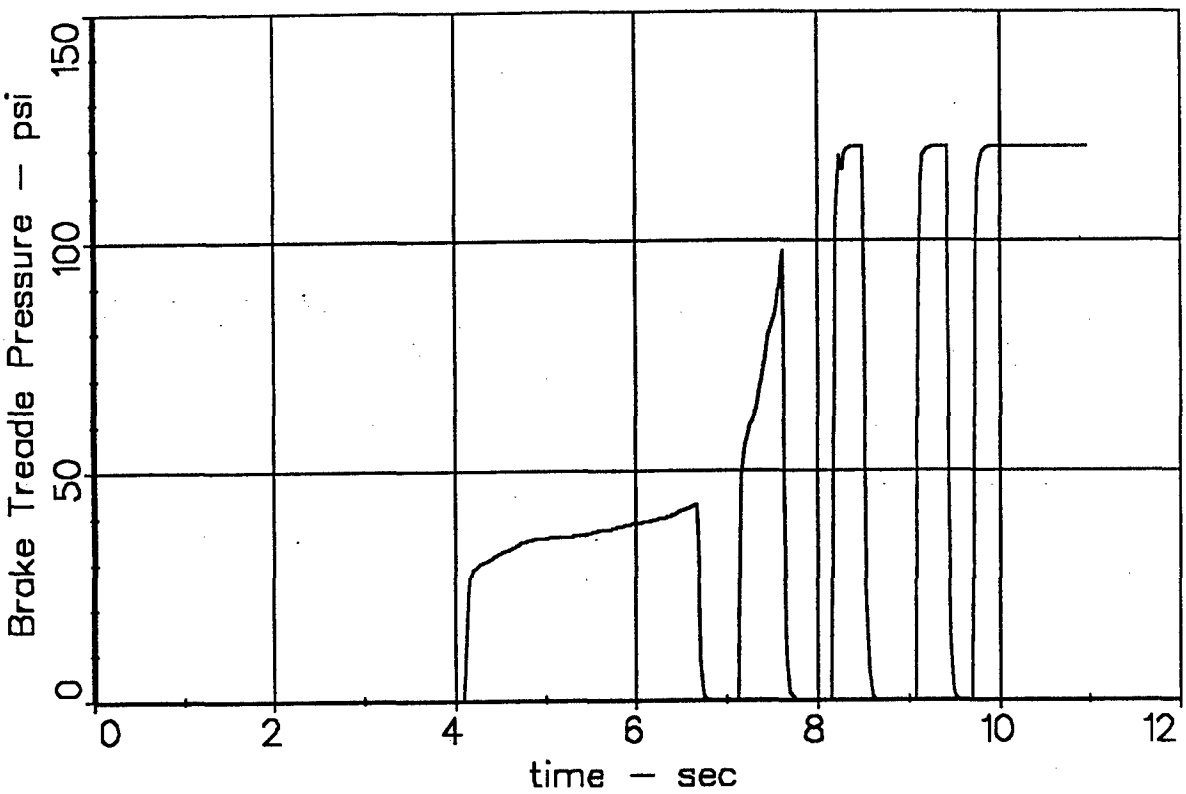

5–axle Tr–Semi; 30 mph; Braking–in–a–Turn; Driver Control;

Figure 5-67. Command Pressure Modulation by the Driver Braking Model in Response to Front Axle Lock-ups

LIST OF REFERENCES

[1] MacAdam, C. C. "Application of an Optimal Preview Control for Simulation of Closed-Loop Automobile Driving." *IEEE Transactions on Systems, Man, and Cybernetics,* SMC-11, June (1981). 393-399.

[2] MacAdam, C.C. "An Optimal Preview Control for Linear Systems." *Journal of Dynamic Systems, Measurement, and Control,* 102, September (1980). 188-190.

[3] Elkind, J. I. "A Survey of the Development of Models for the Human Controller." *Progress in Astronautics and Aeronautics.* (1964). 13: 623-643.

[4] McRuer, D. T., et al. "New Approaches to Human-Pilot/Vehicle Dynamic Analysis." Tech. Report AFFDL-TR-67-150, WPAFB. (1968).

[5] Henderson, R. L. (Editor). "Driver Performance Data Book." Final Report DOT HS 807 126, NHTSA. (1987).

[6] Johannsen, G. "Man-Machine Systems — Introduction and Background." *Proceedings of IFAC Man-Machine Systems,* Baden-Baden, Federal Republic of Germany, (1982).

[7] MacAdam, C. C., et al. "A Computerized Model for Simulating the Braking and Steering Dynamics of Trucks, Tractor-Semitrailers, Doubles, and Triples Combinations." User's Manual - Phase 4, UM-HSRI-80-58. (1980).

[8] Gillespie, T., and MacAdam, C. C. "Constant Velocity Yaw/Roll Program - User's Manual." UMTRI-82-39. (1982).

[9] MacAdam, C. C. "A Microcomputer-Based Model for Studying Open- and Closed-Loop Steering Response of Automobile/Driver Systems." *Proceedings of the Society for Computer Simulation Conference on Modeling and Simulation on Microcomputers: 1983,* Ed. R. Martinez. San Diego, California, SCS, (1983).

[10] MacAdam, C. C. "A Computer-Based Study of the Yaw/Roll Stability of Heavy Trucks Characterized by High Centers of Gravity." *SAE Transactions,* SAE, paper no. 821260, (1982).

[11] MacAdam, C. C. "Frequency Domain Methods for Analyzing the Closed-Loop Directional Stability and Maneuverability of Driver/Vehicle Systems." *Proceedings of the Conference on Modern Vehicle Design Analysis,* Ed. M. Dorgham. London, U.K., (1983).

[12] MacAdam, C. C. "A Computer Simulation Study of the Closed-Loop Stability and Maneuverability of Articulated Coach/Driver Systems." *Proceedings of the 8th IAVSD Symposium of the Dynamics of Vehicles on Roads and Tracks,* Ed. K. Hedrick. Cambridge, Massachussetts, Swets & Zeitlinger B.V. - Lisse, (1983).

[13] MacAdam, C. C. "Computer Model Predictions of the Directional Response and Stability of Driver Vehicle Systems During Anti-Skid Braking." *Proceedings of the IMech E Conference on Antilock Braking Systems for Road Vehicles,* Ed. P. Newcomb. London, U.K., IMech E, (1985).

[14] MacAdam, C. C., and Fancher, P. S. "A Study of the Closed-Loop Directional Stability of Various Commercial Vehicle Configurations." *Proceedings of the 9th IAVSD Symposium of the Dynamics of Vehicles on Roads and Tracks,* Ed. O. Nordstrom. Linkoping, Sweden, Swets & Zeitlinger B.V. - Lisse, (1985).

[15] Fancher, P. S. "Integrating Anti-Lock Braking Systems with the Directional Control Properties of Heavy Trucks." *Proceedings of the IMech E Conference on Antilock Braking Systems for Road Vehicles,* Ed. P. Newcomb. London, U.K., IMech E, (1985).

[16] Rashevsky, N. "Mathematical Biology of Automobile Driving." *Bull. Mathematical Biophysics,* 30, (1968). p 153.

[17] Sheridan, T. B., et al. "Control Models of Creatures Which Look Ahead." *Proceedings of the 5th National Symposium on Human Factors in Electronics,* (1964).

[18] Kondo, M., and Ajimine, A. "Driver's Sight Point and Dynamics of the Driver-Vehicle System Related to It." SAE Automotive Engineering Congress. Detroit, Michigan, SAE, paper no. 680104, (1968).

[19] Mortimer, R. G., and Jorgeson, C. M. "Eye Fixations of Drivers as Affected by Highway and Traffic Characteristics and Moderate Doses of Alcohol." *Proceedings of the Sixteenth Annual Meeting, Human Factors Society,* (1972).

[20] Baron, S. "A Model for Human Control and Monitoring Based on Modern Control Theory." *Journal of Cybernetics and Information Science,* 1, January (1976).

[21] Hatwal, A., and Mikulcik, E. C. "An Optimal Control Approach to the Path Tracking Problem for an Automobile." *Transactions of the Canadian Society for Mechanical Engineering,* 10, 4 (1986). 233-241.

[22] Nagai, M., and Mitschke, M. "Adaptive Behavior of Driver-Car Systems in Critical Situations: Analysis by Adaptive Model." *JSAE Review,* December (1985). 82-89.

[23] Tomizuka, M. "The Optimal Finite Preview Problem and Its Application to Man-Machine Systems." PhD Dissertation. MIT, (1973).

[24] McRuer, D. T., and Klein, R. "Comparison of Human Driver Dynamics in Simulators with Complex and Simple Visual Displays and in an Automobile on the Road." 11th Annual Conference on Manual Control. (1975).

[25] McRuer, D. T., Allen, R. W., and Klein, R. H. "New Results in Driver Steering Control Models." *Human Factors,* 19, 4 (1977). 381-397.

[26] Weir, D., DiMarco, R. J., and McRuer, D. T. "Evaluation and Correlation of Driver/Vehicle Data, Vol II." Final Technical Report, NHTSA, DOT-HS-803-246. (1977).

[27] Hosman, R. J. A. W. and van der Vaart, J. C. "Laboratory and Moving-Base Simulator Experiments on Speed and Accuracy of Visual and Whole-Body Motion Perception." *Proceedings of IFAC Man-Machine Systems,* Varese, Italy, (1985).

[28] Young, L. R. and Stark, L. "Biological Control Systems — A Critical Review and Evaluation." NASA Contractor Report, NASA CR-190. (1965).

[29] Weir, D. and Phatak, A. V. "Model of Human Response to Step Transitions in Controlled Element Dynamics." Technical Report NASA CR-671. (1968).

[30] Phatak, A. V., Bekey, G. A. "Model of the Adaptive Behavior." *IEEE Tansactions on Man-Machine Systems,* MMS-10, September (1969). 72-80.

[31] Miller, D. C. and Elkind, J. I. "The Adaptive Response of the Human Controller to Sudden Changes in Controlled Process Dynamics." *IEEE Transactions on Hman Factors in Electronics,* HFE-8, 3 (1967).

[32] Li, Y.T., Young, L.R., and Meiry, J.L. "Adaptive Functions of Man in Vehicle Control Systems." *Proceedings of the International Federation of Automatic Control Symposium,* Paddington, England, (1965).

[33] Wehage, R. A. "Application of Matrix Partioning and Recursive Projection to O(n) Solution of Constrained Equations of Motion." *ASME Journal,* (in review).

[34] Riede, P. M., Leffert, R. L., and Cobb, W. A. "Typical Vehicle Parameters for Dynamics Studies Revised for the 1980's." SAE Automotive Engineering Congress. Detroit, Michigan, SAE, paper no. 840561, (1984).

[35] MacAdam, C. C. "Development of Driver/Vehicle Steering Interaction Models for Dynamic Analysis." Interim Technical Report, UMTRI-86-41. TACOM Contract DAAE07-85-C-R069. (1986).

[36] Fukunaga, Y. et al. "Improved Handling and Stability Using Four-Wheel Steering." *Proceedings of the 11th International Conference on Experimental Technical Safety Vehicles,* Washington, D. C., (1987).

[37] Sano, S., Furukawa, Y., and Shiraishi, S. "Four Wheel Steering System with Rear Wheel Steer Angle Controlled as a Function of Steering Angle." SAE International Congress and Exposition. Detroit, Michigan, SAE, paper no. 860625, (1986).

[38] Takiguchi, T. et al. "Improvement of Vehicle Dynamics by Vehicle-Speed-Sensing Four Wheel Steering System." SAE International Congress and Exposition. Detroit, Michigan, SAE, paper no. 860624, (1986).

[39] Hayashi, Y. "Optimum Control of a Driver/Four-Wheel Steered-Vehicle System." *Proceedings of the 10th IAVSD Symposium of the Dynamics of Vehicles on Roads and Tracks,* Prague, Cz, (1987).

[40] "DADS User's Manual - Rev 4.0." Computer Aided Design Software, Inc. (1986).

[41] Mousseau, R. "An Investigation Into the Lateral Stability of the M1037 Truck Pulling the M101 Trailer." U.S. Army Tank Automotive Command, Systems Simulation and Technology Division, Final Report. (1988).

[42] Stribersky, A., and MacAdam, C. C. "Lateral Stability of a Controlled Articulated Vehicle — An Application of Bifurcation Theory in Vehicle Dynamics." *Proceedings of the 12th Canadian Congress of Applied Mechanics,* Ottawa, Canada, (1989).

[43] Sayers, M., MacAdam, C. C., and Guy, Y. "Chrysler Wind-Steer Vehicle Simulation." User's Manual. (1988).

[44] "Comparison of Vehicle Test Procedures." Contract DRDA 781433, Highway Safety Research Institute, University of Michigan. (1978).

[45] MacAdam, C. C. et al. "Computer Study of the Braking Performance of a Tractor-Semitrailer." Technical Report for the Rockwell International Corporation. (1987).

[46] Newcomb, T. P. "Driver Behavior During Braking." SAE / I. Mech. E. Exchange Lecture. SAE, paper no. 810832, (1981).

[47] Rompe, K., Schindler, A., and Wallrich, M. "Comparison of the Braking Performance Achieved by Average Drivers in Vehicles with Standard and Anti Wheel Lock Brake Systems." SAE International Congress and Exposition. Detroit, Michigan, SAE, paper no. 870335, (1987).

[48] McLean, D., Newcomb, T. P., and Spurr, R. T. "Simulation of Driver Behavior During Braking." *I. Mech. E. Conference on Braking of Road Vehicles,* IME, paper no. C41/176, (1976).

[49] Sheridan, T. B. "Three Models of Preview Control." *IEEE Transactions on Human Factors in Electronics,* HFE-7, June (1966).

Appendix A

Articulated Vehicle Equations

As noted in section 5.5 of the report, the internal single-unit model used throughout much of this report as the "reference" vehicle used by the driver model, can also be used for steering many articulated vehicles, provided the lead-unit vehicle parameters reflect the presence of the hitch load as described in that section. The alternate approach for steering an articulated vehicle is to apply a more complete set of articulated vehicle equations, such as those appearing in this appendix, as a substitute for the single-unit equations presented earlier.

The equations in this appendix apply to the articulated vehicle model shown in Figure A-1 and Table A-1. This basic model is intended to serve as a "simplified" articulated vehicle with front wheel steering and a provision for an articulation control torque, patterned after the LVS vehicle. These equations would be used to represent the internal vehicle model employed by the driver control algorithm when steering an articulated vehicle, if a fuller treatment of possible driver/vehicle interactions is required. The controlled system dynamics, now represented by an articulated vehicle having one additional degree of freedom in its simplest form, is extended beyond that of the single-unit vehicle assumed by the baseline driver model of section 5.5.

A diagram of the proposed articulated vehicle used by the driver model is seen in Figure A-1. A list of corresponding variable and parameter definitions appears in Table A-1. The model has two control inputs: the front wheel steer angle, δ, and the articulation torque, M_c. (A later simplification slaves the articulation control torque to the front wheel steer angle by a proportional gain factor, thereby resulting in essentially one control input and a gain parameter for controlling the front-wheel-steer / articulation-torque "mixture.") The linearized equations representing the articulated vehicle model now follow.

The sum of lateral forces and sum of yaw torques acting on each of the two articulated masses produces the following four dynamical equations (primes denoting differentiation with respect to time):

$$m_1 v_1' = Fy_1 + Fy_2 - m_1 U r_1 + f_y \qquad \text{(A-1)}$$

(f_y is the lateral hitch constraint force)

$$I_1 r_1' = a_1 Fy_1 - b_1 Fy_2 - c_1 f_y + M_c \qquad \text{(A-2)}$$

$$m_2 v_2' = Fy_2 - m_2 U r_2 - f_y \qquad \text{(A-3)}$$

$$I_2 r_2' = - b_2 Fy_3 - c_2 f_y - M_c \qquad \text{(A-4)}$$

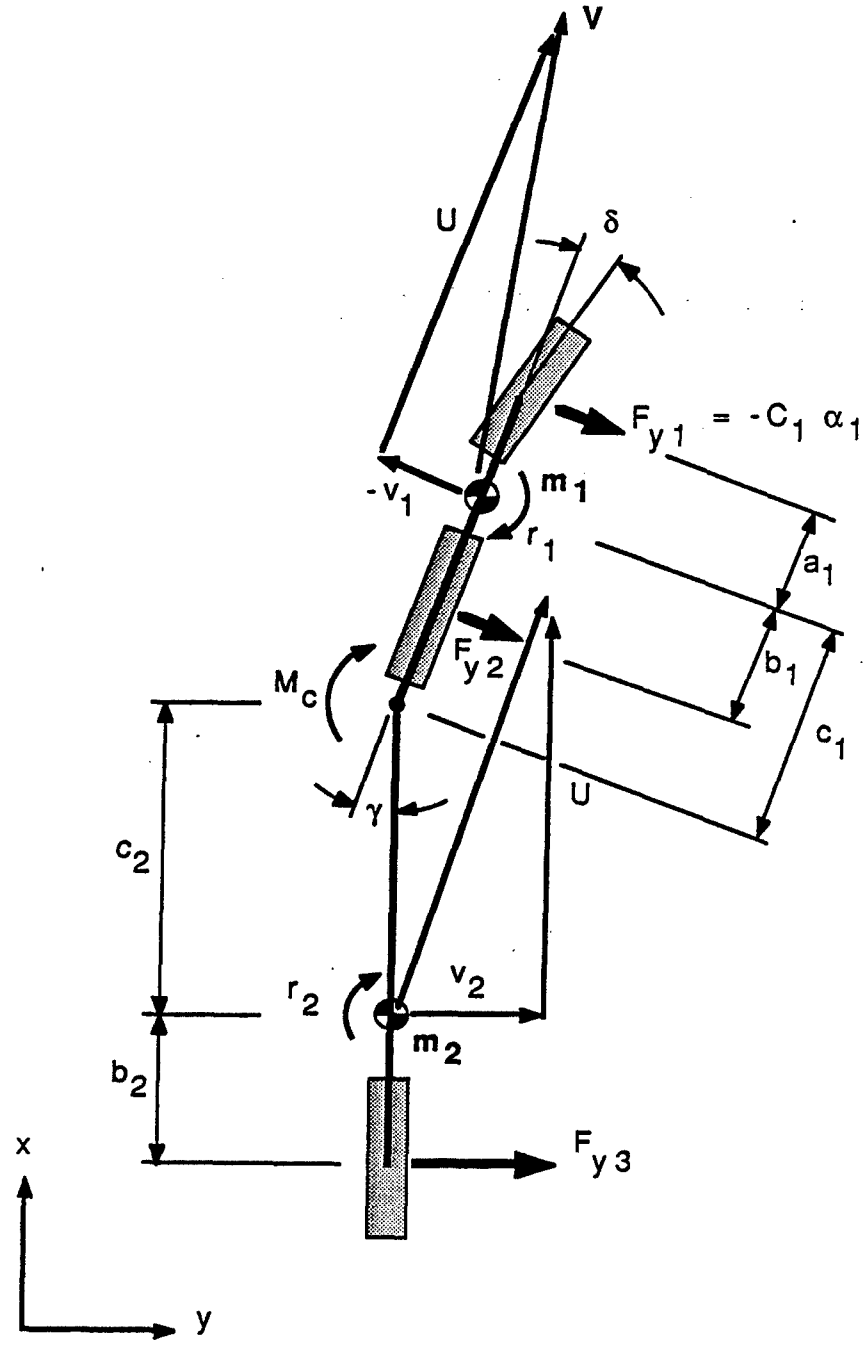

Figure A-1. Articulated Vehicle Model

Table A-1. Articulated Vehicle Model - Parameter Definitions

(Internal Driver Model Representation)

Parameter	Description
m1	mass of front unit
m2	mass of rear unit
v1	lateral sideslip velocity of unit 1
v2	lateral sideslip velocity of unit 2
r1	yaw rate of unit 1
r2	yaw rate of unit 2
a1	distance form c.g. of unit 1 to axle 1
b1	distance form c.g. of unit 1 to axle 2
b2	distance form c.g. of unit 2 to axle 3
c1	distance form c.g. of unit 1 to hitch
c2	distance form c.g. of unit 2 to hitch
U	forward velocity component in x-body axis
δ	front axle steer angle - control variable
γ	articulation angle
α_i	tire sideslip angle (axle i)
C_i	tire cornering stiffness (axle i)
M_c	articulation torque - control variable
F_{yi}	lateral tire force (axle i)

The kinematic constraint for the articulation joint produces the following algebraic relationship between the lateral displacement, y_i, and heading angle variables, ψ_i :

$$y_1 - c_1 \sin\psi_1 = y_2 + c_2 \sin\psi_2 \qquad \text{(A-5)}$$

Differentiating twice and assuming small angles for the heading angles results in the equivalent constraint equation expressed in terms of the associated accelerations:

$$v_1' + U r_1 - c_1 r_1' = v_2' + U r_2 + c_2 r_2' \qquad \text{(A-6)}$$

The tire forces Fy_i can be expressed in terms of the tire cornering stiffnesses and tire sideslip angles as:

$$Fy_i = - C_{\alpha i} \alpha_i \qquad \text{(A-7)}$$

where,

$$\alpha_1 = \tan^{-1}[(v_1 + a_1 r_1) / U] - \delta \qquad \text{(A–8)}$$

$$\alpha_2 = \tan^{-1}[(v_1 - b_1 r_1) / U] \qquad \text{(A–9)}$$

$$\alpha_3 = \tan^{-1}[(v_2 - b_2 r_2) / U] \qquad \text{(A–10)}$$

Assuming small tire sideslip angles for the α_i (replacing the arctan by the angle), Equations (A-1) -> (A-4) become after these substitutions:

$$m_1 v_1' = - C_{\alpha 1} (v_1+a_1 r_1) / U - C_{\alpha 2} (v_1-b_1 r_1) / U + C_{\alpha 1} \delta - m_1 U r_1 + f_y \qquad \text{(A-11)}$$

$$I_1 r_1' = -a_1 C_{\alpha 1} (v_1+a_1 r_1) / U + b_1 C_{\alpha 2} (v_1-b_1 r_1) / U - c_1 f_y + a_1 C_{\alpha 1} \delta + M_c \qquad \text{(A-12)}$$

$$m_2 v_2' = - C_{\alpha 3} (v_2-b_2 r_2) / U - m_2 U r_2 - f_y \qquad \text{(A-13)}$$

$$I_2 r_2' = b_2 C_{\alpha 3} (v_2-b_2 r_2) / U - c_2 f_y - M_c \qquad \text{(A-14)}$$

Expressed in matrix algebra terminology, the equations of motion (A-11) -> (A-14) become:

$$\mathbf{M v'} = \mathbf{A v} + \mathbf{G} \delta + \mathbf{N} f_y + \mathbf{E} M_c \qquad \text{(A-15)}$$

and the kinematic constraint equation (A-6) becomes:

$$\mathbf{C}\,\mathbf{v}' = \mathbf{D}\,\mathbf{v} \qquad \text{(A-16)}$$

where, $\mathbf{v} = \{ v_1, r_1, v_2, r_2 \}^T$.

Solving (A-15) and (A-16) for the constraint force, f_y, and upon back substitution, results in the following set of dynamical equations free of the constraint force:

$$\mathbf{v}' = \mathbf{F}^*\,\mathbf{v} + \mathbf{g}^*\,\delta + \mathbf{h}\,M_c \qquad \text{(A-17)}$$

For a powered articulation scheme with $M_c = K [\delta - \eta (\psi_1 - \psi_2)]$, where the parameter K controls the degree to which the articulation torque is slaved to the front wheel steer angle, δ, and η provides an optional torsional spring effect about the articulation joint, equations (A-17) become:

$$\mathbf{v}' = \mathbf{F}^*\,\mathbf{v} + (\mathbf{g}^* + K\,\mathbf{h})\,\delta + \psi_i \text{ terms} \qquad \text{(A-18)}$$

Addition of the lead unit lateral displacement, y_1, and heading angle state variable, ψ_i, equations, results in the final set of seven linear dynamical equations:

$$\begin{bmatrix} y_1' \\ \psi_1' \\ v_1' \\ r_1' \\ v_2' \\ r_2' \\ \psi_2' \end{bmatrix} = \begin{bmatrix} 0 & U & 1 & 0 & 0 & 0 & 0 \\ 0 & 0 & 0 & 1 & 0 & 0 & 0 \\ 0 & & & & & & \\ 0 & \{-\eta K h\} & & & \mathbf{F}^*_{4x4} & & \{\eta K h\} \\ 0 & & & & & & \\ 0 & & & & & & \\ 0 & 0 & 0 & 1 & 0 & 0 & 0 \end{bmatrix} \begin{bmatrix} y_1 \\ \psi_1 \\ v_1 \\ r_1 \\ v_2 \\ r_2 \\ \psi_2 \end{bmatrix}$$

$$+ \begin{bmatrix} 0 \\ 0 \\ \mathbf{g}^* + K\,\mathbf{h} \\ \\ 0 \end{bmatrix} \delta \qquad \text{(A-19)}$$

or in matrix algebra notation:

$$\{X'\}_{7x1} = [F]_{7x7}\ \{X\}_{7x1} + \{g\}_{7x1}\ \delta_{1x1} \qquad \text{(A-20)}$$

where,

$$M = \begin{bmatrix} m_1 & & 0 & \\ & I_1 & & \\ & & m_2 & \\ & 0 & & I_2 \end{bmatrix}$$

$$A = \begin{bmatrix} -(C_{a1}+C_{a2})/U & (-C_{a1}a_1+C_{a2}b_1)/U-m_1U & 0 & 0 \\ (-a_1C_{a1}+b_1C_{a2})/U & -(C_{a1}a_1{}^2+C_{a2}b_1{}^2)/U & 0 & 0 \\ 0 & 0 & -C_{a3}/U & b_2C_{a3}/U-m_2U \\ 0 & 0 & b_2C_{a3}/U & -C_{a3}b_2{}^2/U \end{bmatrix}$$

$$G = \begin{bmatrix} C_{a1} \\ a_1C_{a1} \\ 0 \\ 0 \end{bmatrix} \qquad N = \begin{bmatrix} 1 \\ -C_1 \\ -1 \\ -C_2 \end{bmatrix} \qquad E = \begin{bmatrix} 0 \\ 1 \\ 0 \\ -1 \end{bmatrix}$$

$$C = \{\ 1,\ -C_1,\ -1,\ -C_2\ \}$$

$$\mathbf{D} = \{ \quad 0, \quad -U, \quad 0, \quad U \quad \}$$

and,

$$\mathbf{F^*} = \mathbf{M^{-1}} (\mathbf{A} + \mathbf{N} [\mathbf{C} \mathbf{M^{-1}} \mathbf{N}]^{-1} (\mathbf{D} - \mathbf{C} \mathbf{M^{-1}} \mathbf{A})) \qquad \text{(A-21)}$$

$$\mathbf{g^*} = \mathbf{M^{-1}} (\mathbf{G} - \mathbf{N} [\mathbf{C} \mathbf{M^{-1}} \mathbf{N}]^{-1} \mathbf{C} \mathbf{M^{-1}} \mathbf{G}) \qquad \text{(A-22)}$$

$$\mathbf{h} = \mathbf{M^{-1}} (\mathbf{E} - \mathbf{N} [\mathbf{C} \mathbf{M^{-1}} \mathbf{N}]^{-1} \mathbf{C} \mathbf{M^{-1}} \mathbf{E}) \qquad \text{(A-23)}$$

To use these equations in the driver model, the **F** and **g** matrices appearing in Equation (A-20) would replace the corresponding **F** and **g** matrices presented earlier in section 5.4, to now represent the internal vehicle dynamics within the driver model.

As indicated above, the LVS vehicle was used as a guide for defining the characteristics of the articulated model. General estimates of the LVS mass and geometric parameters are listed in Table A-2. These parameters were used in an example calculation demonstrating the operation of the equations just presented for steering an LVS-like articulated vehicle.

Example time histories are seen in Figure A-2 for the simulated LVS articulated vehicle, controlled by the extended driver model, performing a 12-foot lane-change maneuver at 60 mph. The input path was a standard 12-ft by 100-ft lane-change. The first four plots correspond to the lead unit. The second four plots apply to the trailing unit. The last group of time histories show lateral acceleration traces for the lead and trailing units, the control variable (degrees of front wheel angle), and the calculated mean squared path error within the preview interval "MSE Preview Path Error." In this particular example, the articulation control torque was active and was slaved to the front wheel steer angle (10,000 ft-lb of articulation control torque / degree of front steer angle). The results seen here were calculated with a modified UMTRI vehicle model (to incorporate the articulation control torque) and used the extended driver model equations from this Appendix.

Table A-2. LVS Parameter Estimates

Parameter	Value
m1	750 slugs
m2	515 slugs
I1	9,000 ft^2-slug (lead unit yaw inertia)
I2	20,000 (rear unit " ")
a1	2.5 ft
b1	2.5 ft
c1	5.3 ft
b2	2.0 ft
c2	14.25 ft
U	88 ft/sec
C_1	42,000 lb/rad/suspension-side (tire cornering stiffness)
C_2	68,000 "
C_3	62,000 "
TF	1.5 sec (driver preview time)
Tau	0.25 sec (driver transport lag)
RKMOM	570,000 ft-lb/rad (articulation control moment-front steer gain)

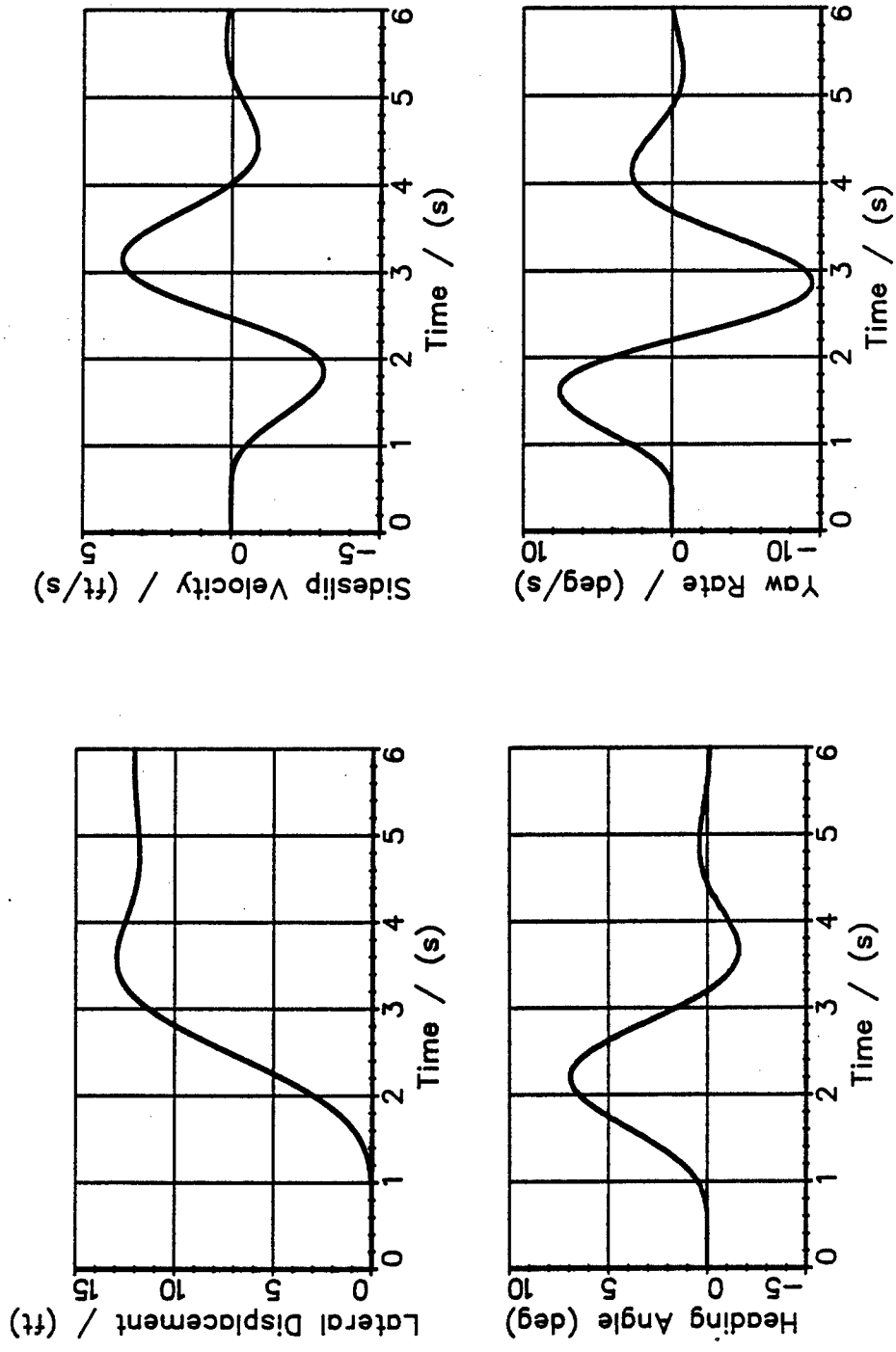

Figure A-2. Example Calculations for a Simulated LVS

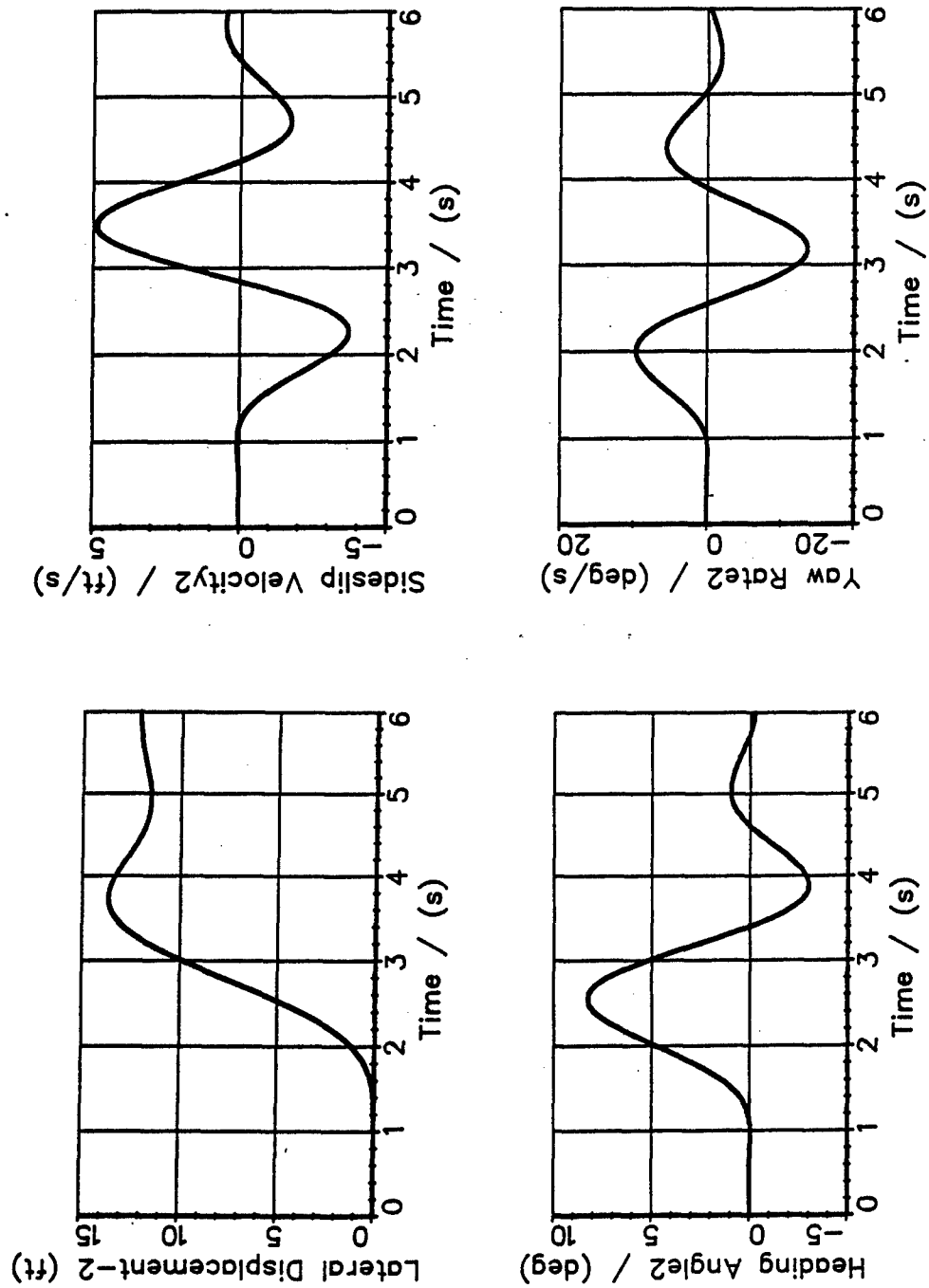

Figure A-2. Example Calculations for a Simulated LVS

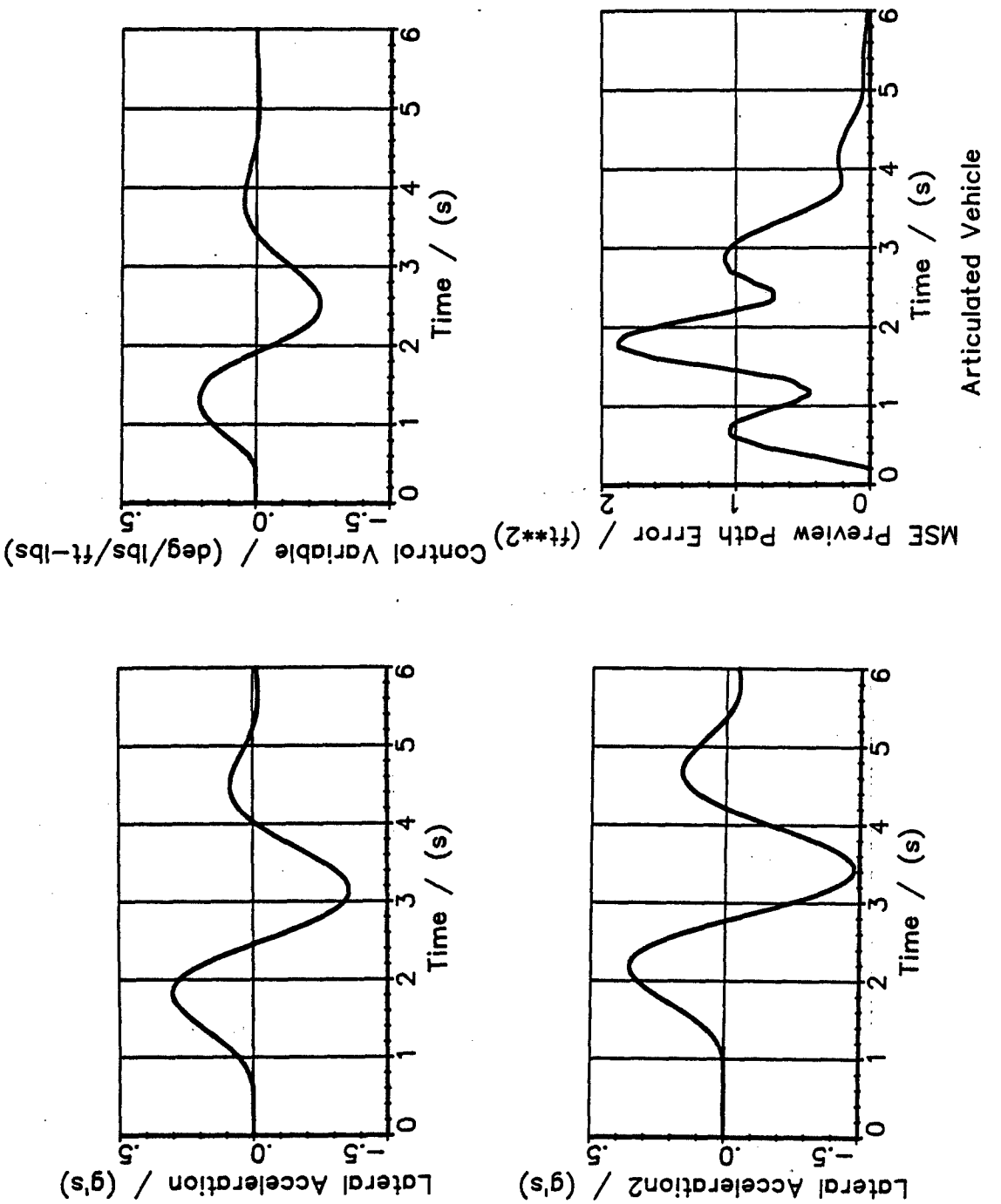

Figure A-2. Example Calculations for a Simulated LVS

Appendix B

HMMWV Test Data

The material contained in this Appendix supplements the test data appearing in earlier sections of the report and helps document the types of test maneuvers performed. Example time histories are provided here for each test maneuver conducted during the test program. The complete set of data collected during the project are being supplied to TACOM on floppy disks with corresponding UMTRI software used to graphically view the time history data. Log sheets for all of the test data collected during the test program appear in Table 5-2 of section 5.6.

The first set of Figures B-1 to B-4 apply to the steady turning maneuver performed at 50 and 25 mph respectively (tests 105 and 110 from Table 5-2). Measurements of forward speed, driver steering wheel angle, and lateral acceleration are seen in Figures B-1 and B-3. Figures B-2 and B-4 show corresponding measurements of roll angle, yaw rate, and left front wheel angle. The "spikes" seen in the roll angle measurement data are due to faulty contacts occuring within the roll angle transducer wiper assembly. Irregular drifting of the roll angle measurement was also encountered with this same transducer. For most of the tests performed in this study, this particular measurement was of secondary importance and is only shown here to provide a "ballpark" estimate of the vehicle roll response.

Figures B-5 to B-8 show example test results from the braking-in-a-turn maneuver from an initial speed of 50 mph and along a curve of 500-ft radius. Figures B-5 and B-6 correspond to a short stopping distance of 132 ft (test 118); Figures B-7 and B-8 show comparable results for a longer stopping distance of 195 ft (test 120). Driver brake pressure, longitudinal acceleration, and forward speed are seen in Figures B-5 and B-7. Figure B-6 and B-8 show the corresponding driver steering wheel angle and lateral acceleration measurements.

Example results from the constrained lane-change maneuver at 60 and 30 mph are seen in Figures B-9 through B-12. The 60 mph results are from test 127; the 30 mph results are from test 137.

Two example runs from the obstacle course tests are seen in Figure B-13 to B-16. The first example, seen in Figures B-13 and B-14, are from test 184 and correspond to a "short/short" obstacle placement (L=80 ft; L2=100; L3=120 ft) as discussed in section 5.6. Figures B-15 and B-16 are from run 185 and correspond to a "long/long" obstacle placement (L1=120 ft; L2=100; L3=80 ft). The previous results seen for the obstacle course in section 5.7 were for a "center/center" setting of the two obstacles.

Figures B-17 to B-19 correspond to three different straight-line braking tests (213, 215, and 214). Figure B-17 is for a relatively long stopping distance showing the driver clearly modulating the brake pressure about an approximate value of 350 psi. Figure B-18 is for a

realtively short stopping distance of 145 ft. The driver brake pressure application is considerably larger and noticeably different. In fact, this particular trace closely resembles the shape of the time history prediction from the closed-loop braking model seen in Figure 5-65. The last straight-line braking test result seen in Figure B-19 is for a stopping distance of 125 ft but included wheel lock occurences at both the front and rear axles. Midway through this stop, the driver is seen releasing the brake pressure temporarily to regain directional control of the vehicle. Sharp steering to the right by the driver is also seen at the 7-second mark in response to the directional disturbance to the vehicle motion caused by the wheel locks.

Lastly, Figure B-20 shows a sample result from a "Random Steer Test" initially conducted to obtain open-loop frequency response characteristics on the HMMWV directional dynamics. These were subsequently not needed but are available for future studies as part of the HMMWV test data library being delivered to TACOM. A typical random steer test would last from 45 to 75 seconds depending upon the test speed. Shown in Figure B-20 are the first 20 seconds from test 202 conducted at 60 mph. The driver is simply applying a "random-like" steering input to the vehicle while travelling along a straight-line course. The intent of this test is to excite the directional dynamics with a wide variety of steering frequencies, thereby allowing a subsequent Fourier analysis to be applied to the recorded data. The Fourier analysis then produces the frequency response of the vehicle directional dynamics due to the steering input.

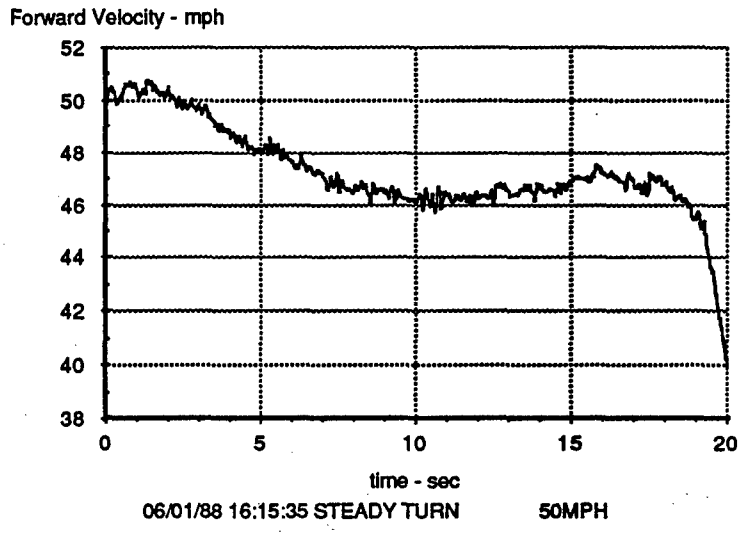

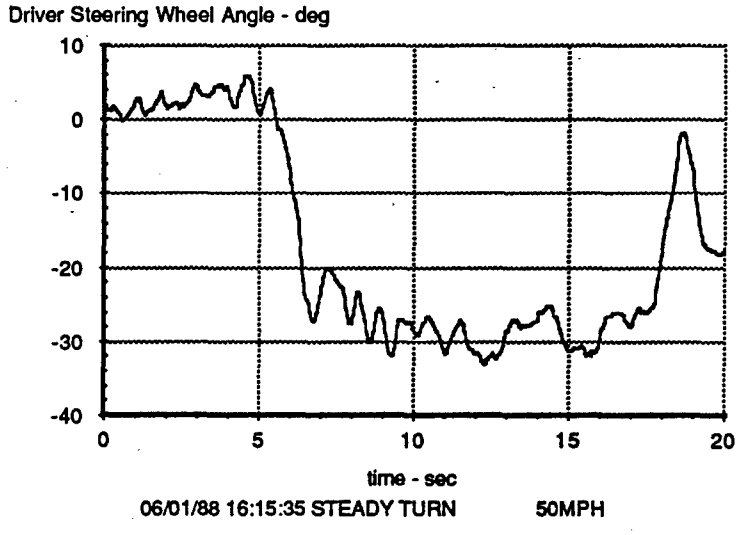

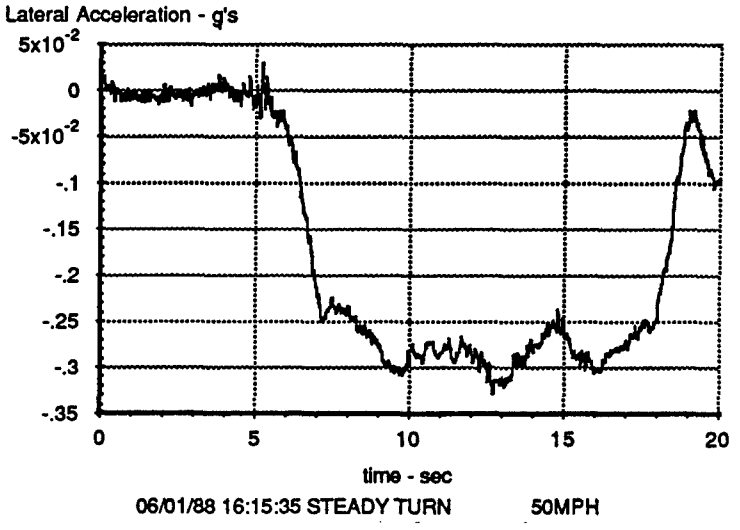

Figure B-1. HMMWV Test: 50 mph Steady Turn

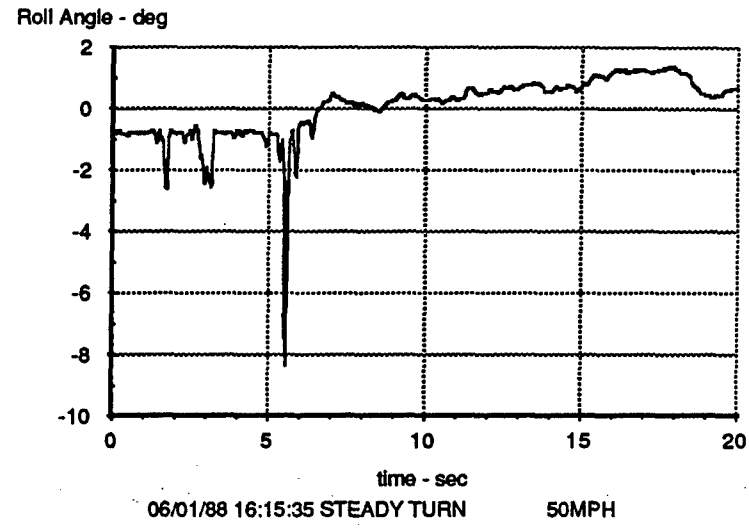

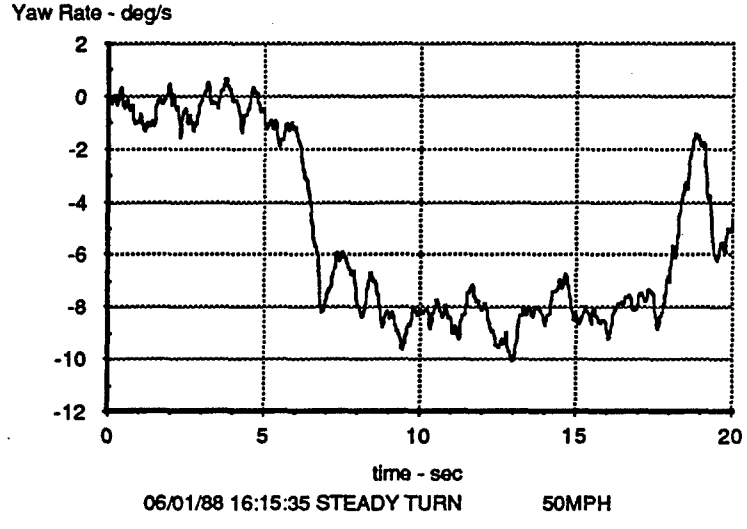

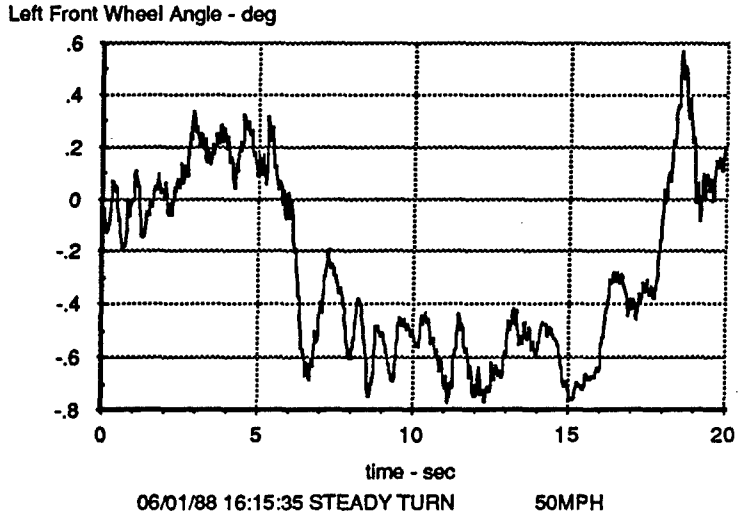

Figure B-2. HMMWV Test: 50 mph Steady Turn

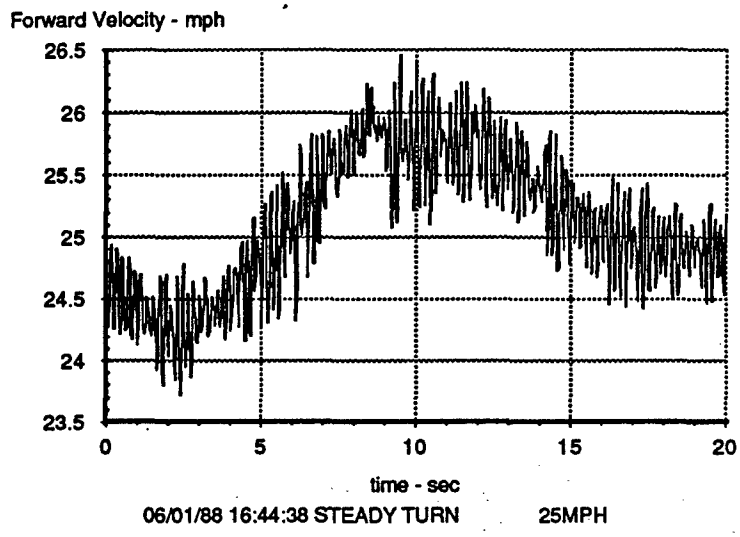

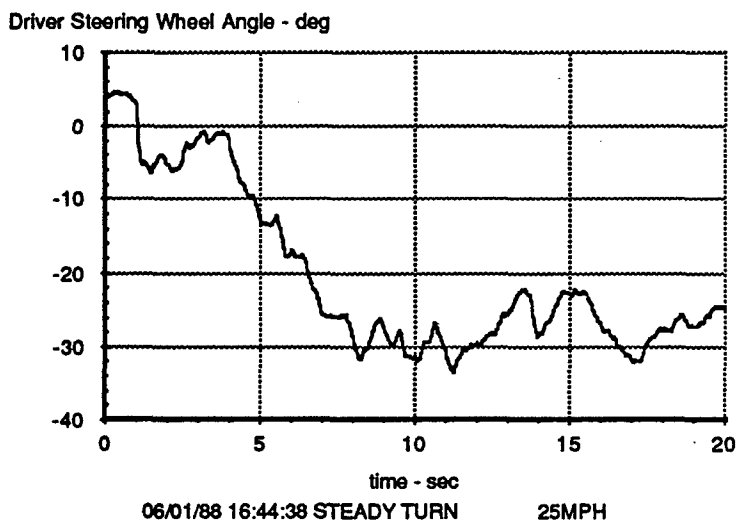

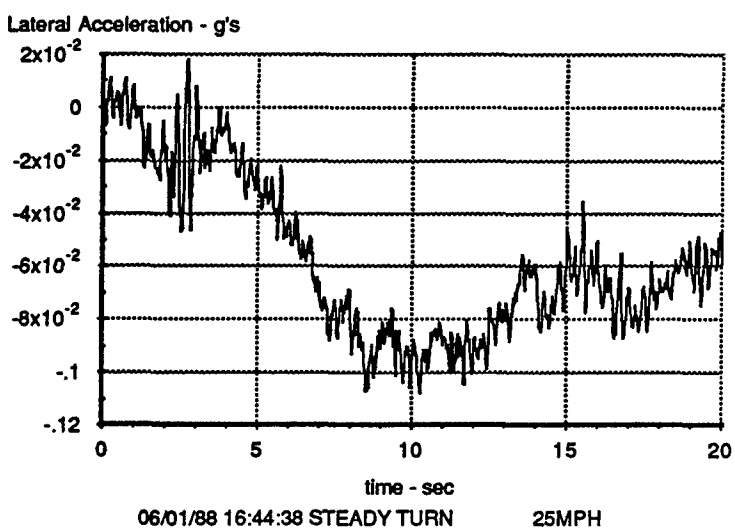

Figure B-3. HMMWV Test: 25 mph Steady Turn

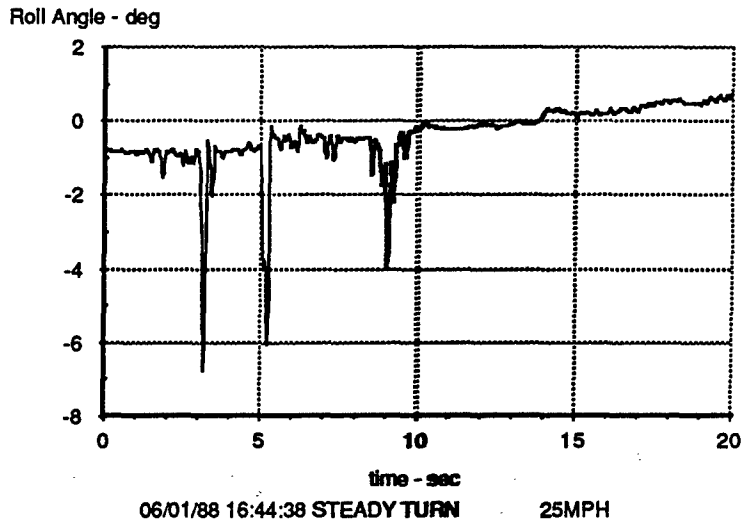

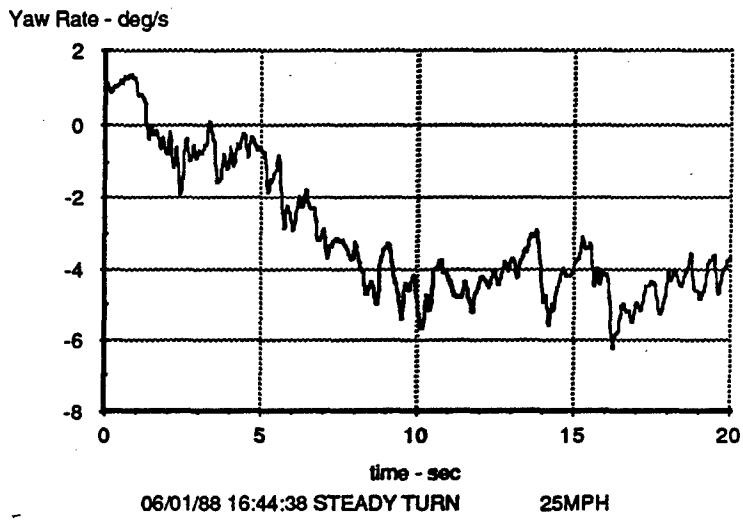

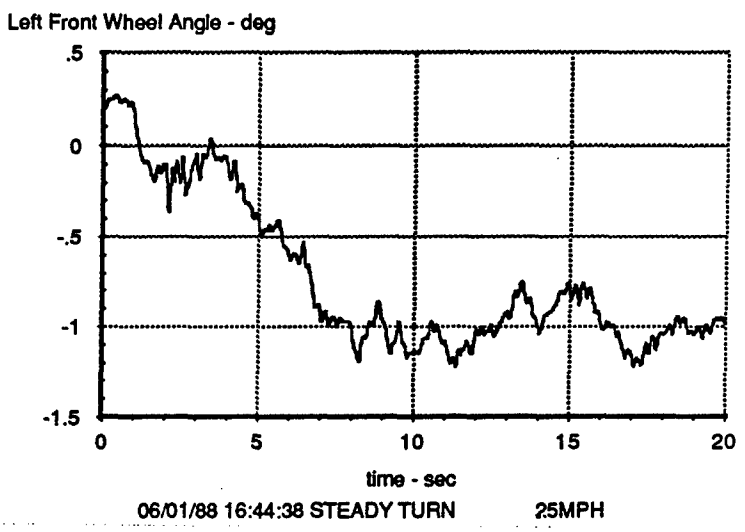

Figure B-4. HMMWV Test: 25 mph Steady Turn

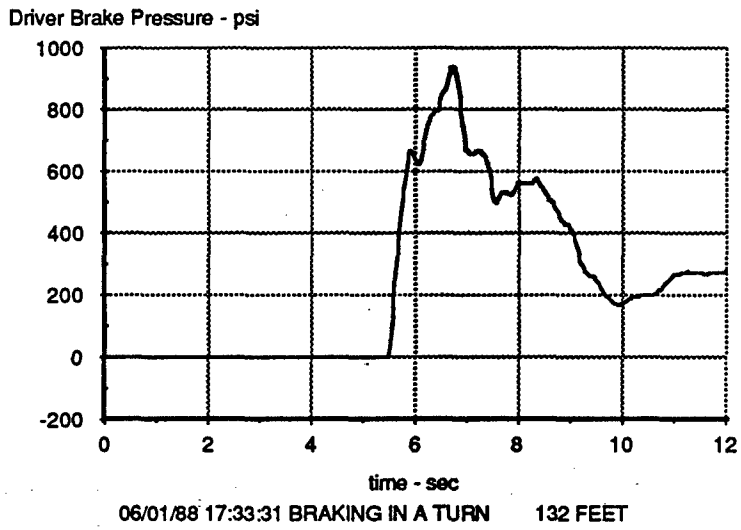

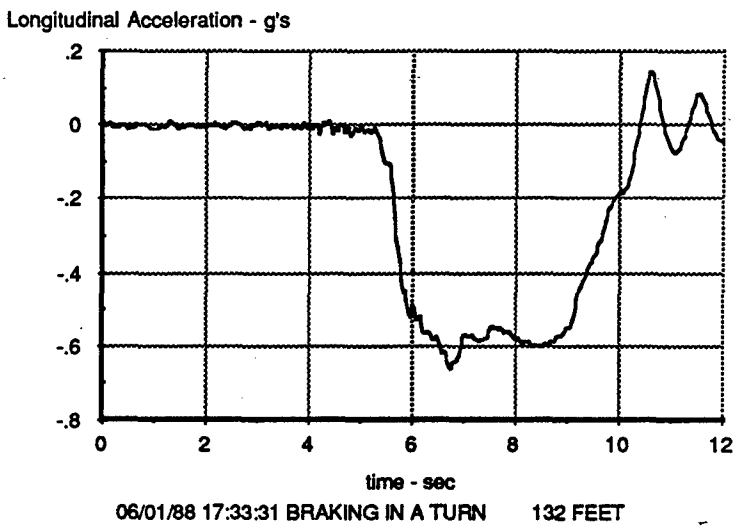

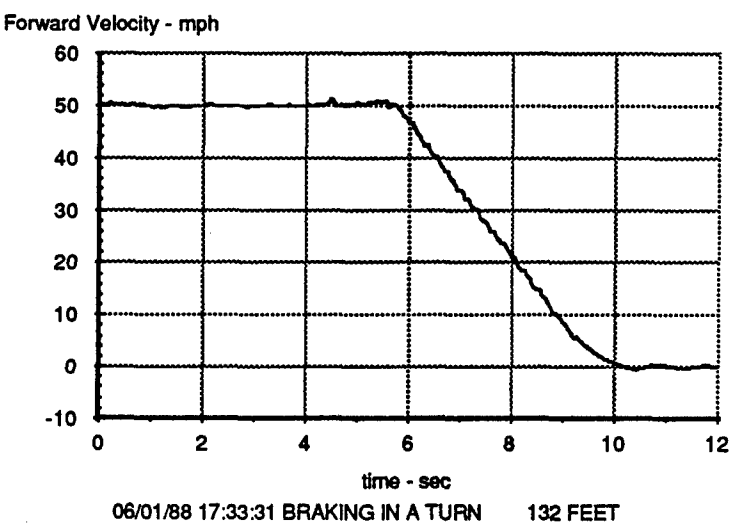

Figure B-5. HMMWV Test: Braking-in-a-Turn, 132 ft

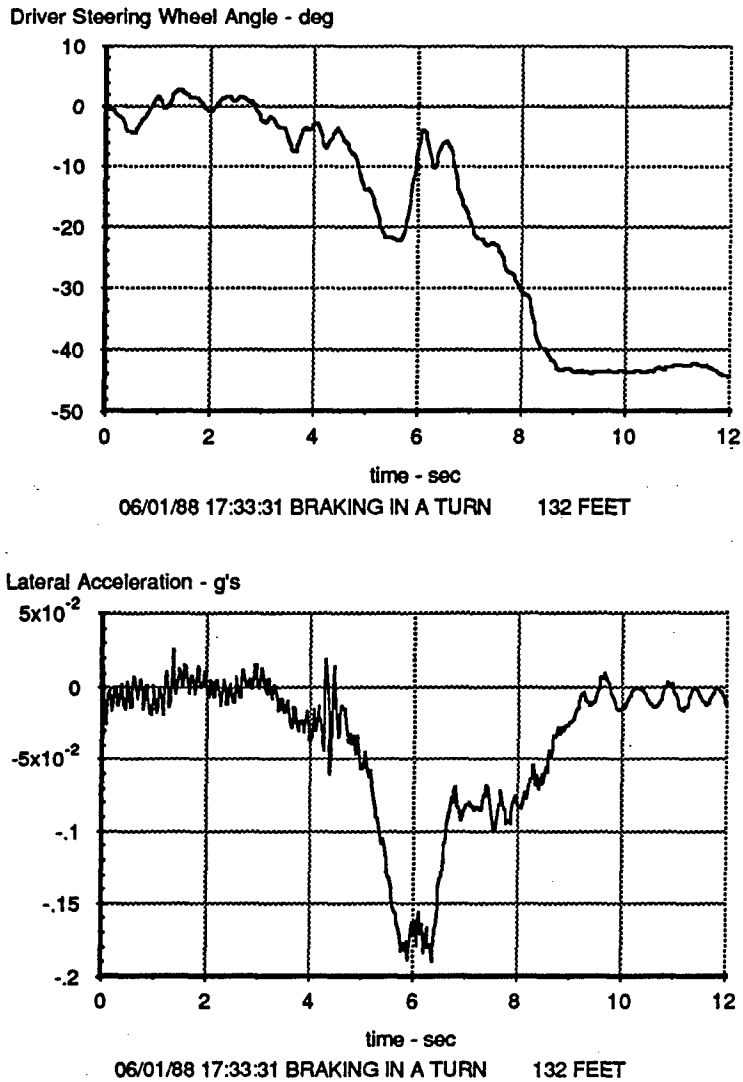

Figure B-6. HMMWV Test: Braking-in-a-Turn, 132 ft

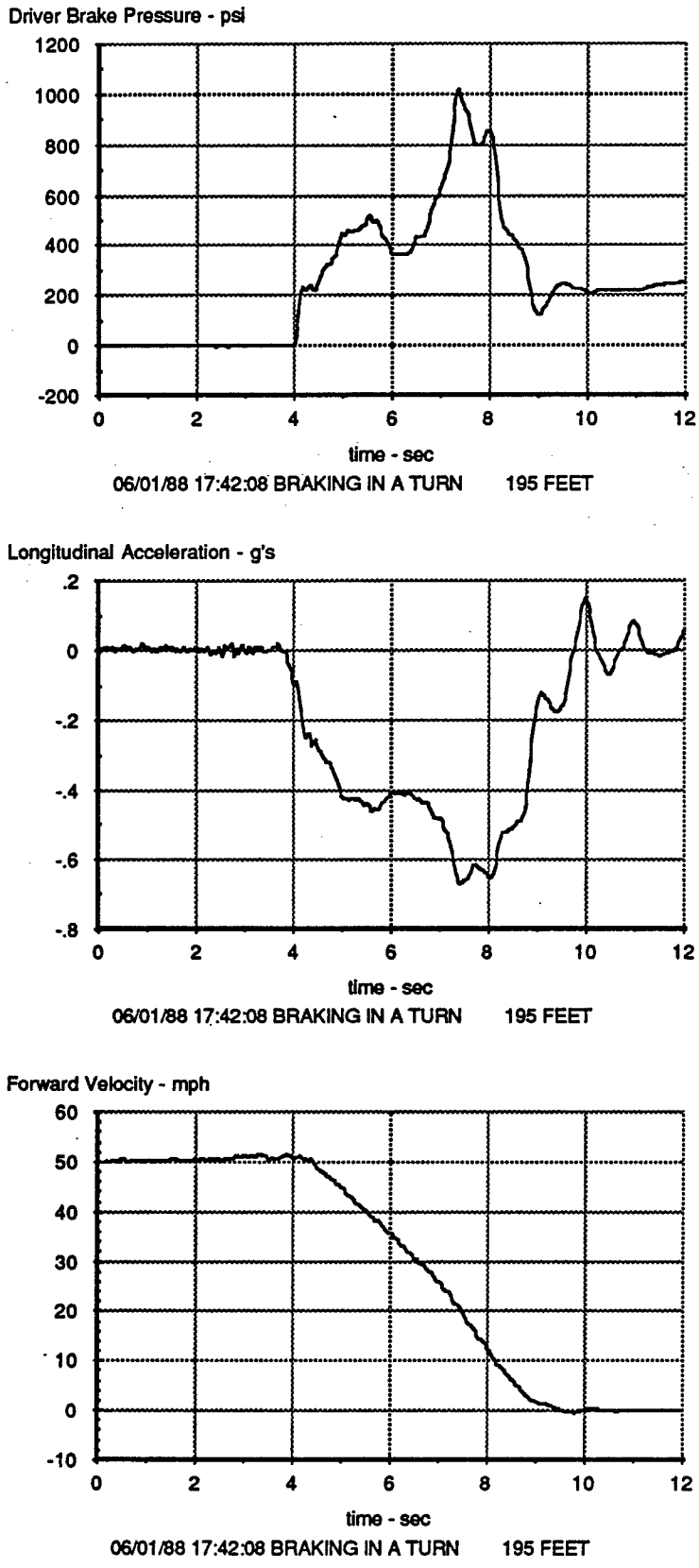

Figure B-7. HMMWV Test: Braking-in-a-Turn, 195 ft

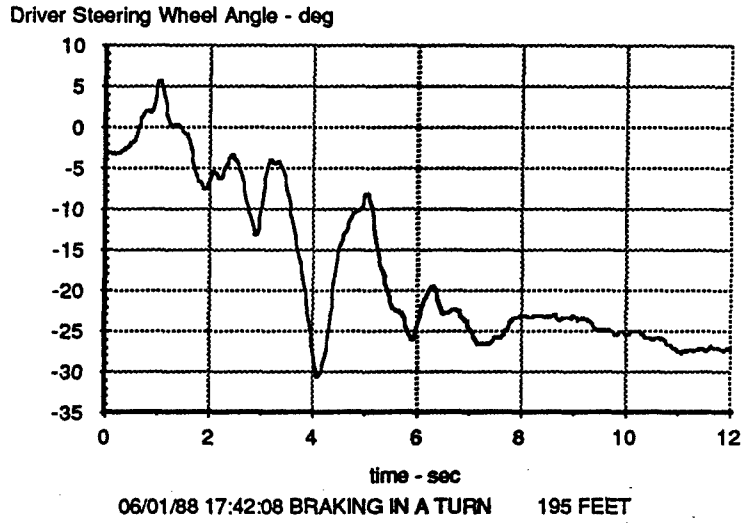

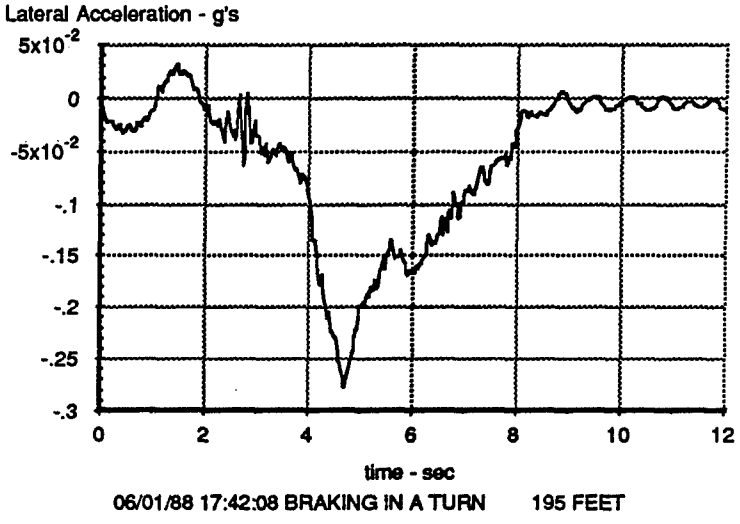

Figure B-8. HMMWV Test: Braking-in-a-Turn, 195 ft

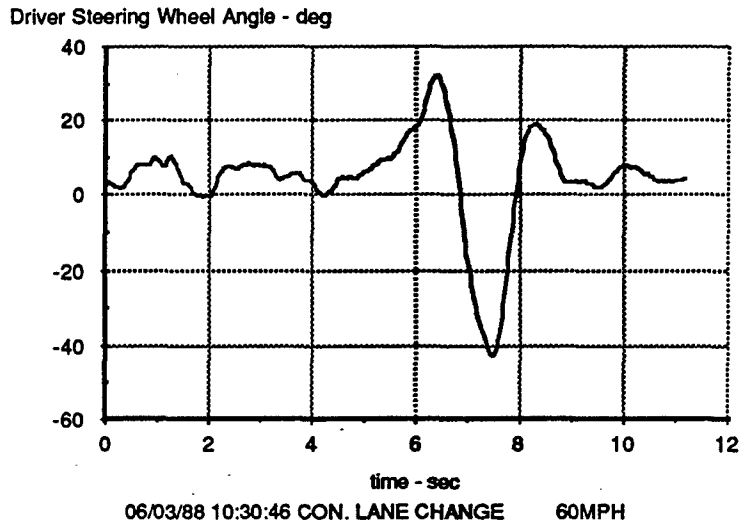

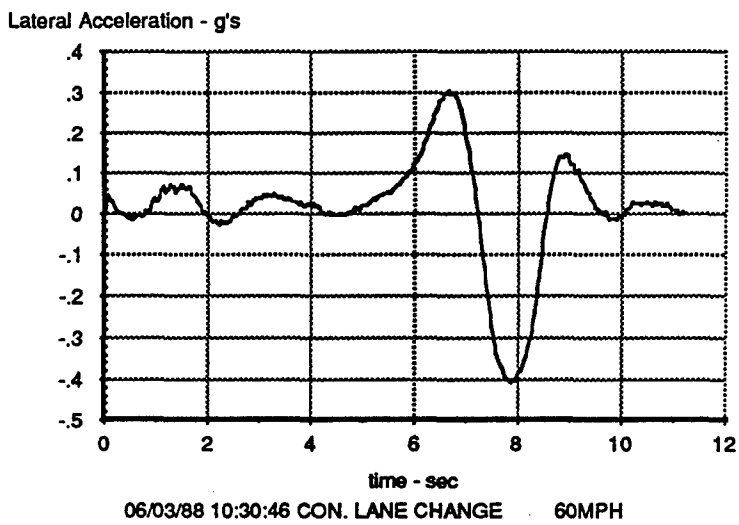

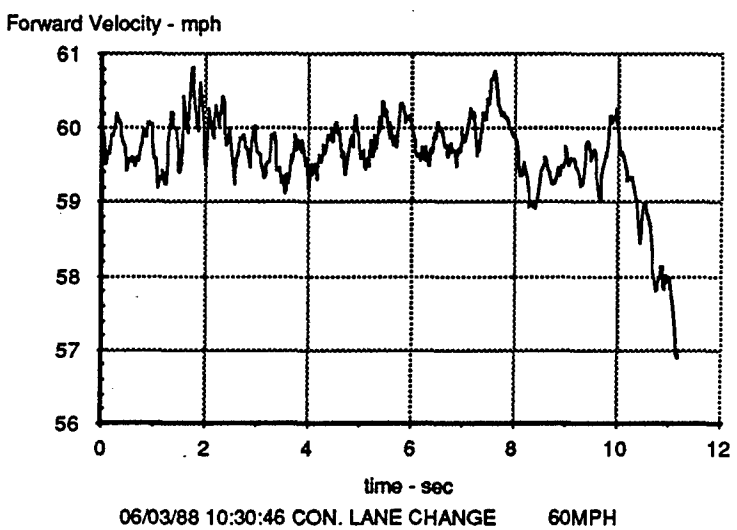

Figure B-9. HMMWV Test: Lane-Change, 60 mph

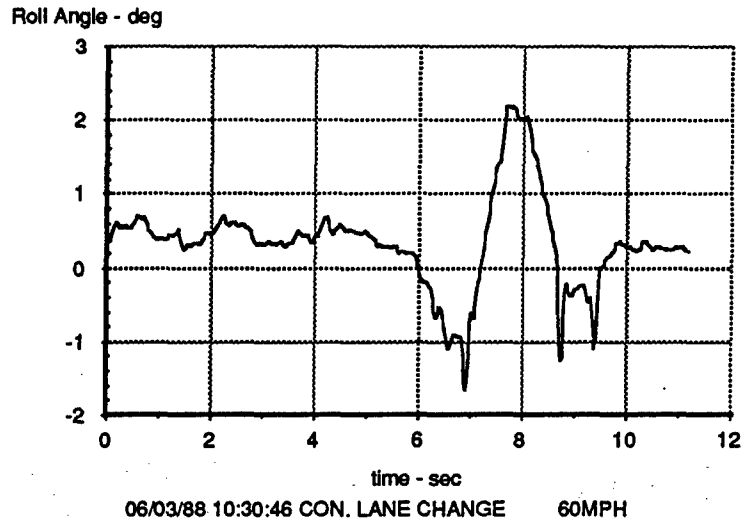

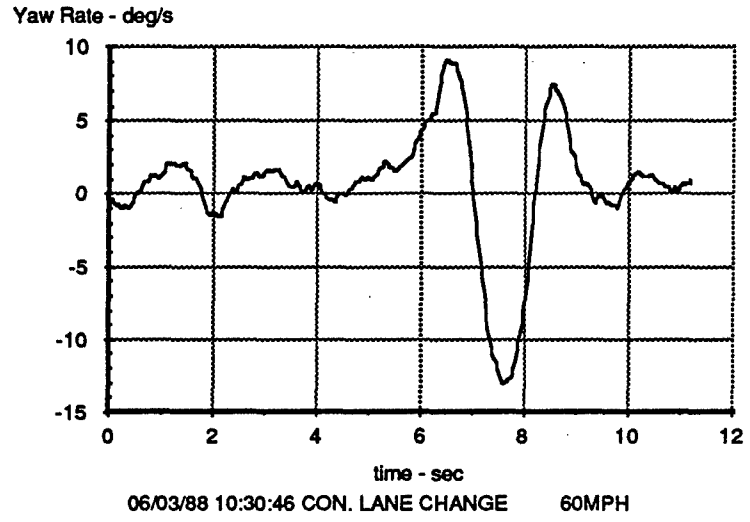

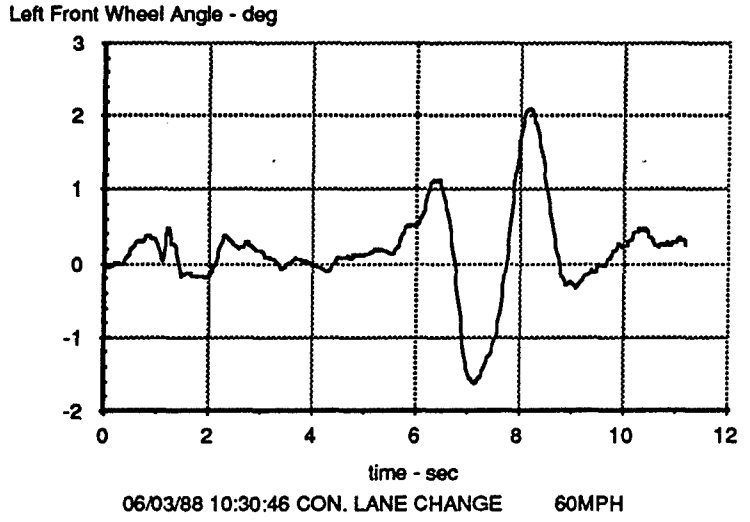

Figure B-10. HMMWV Test: Lane-Change, 60 mph

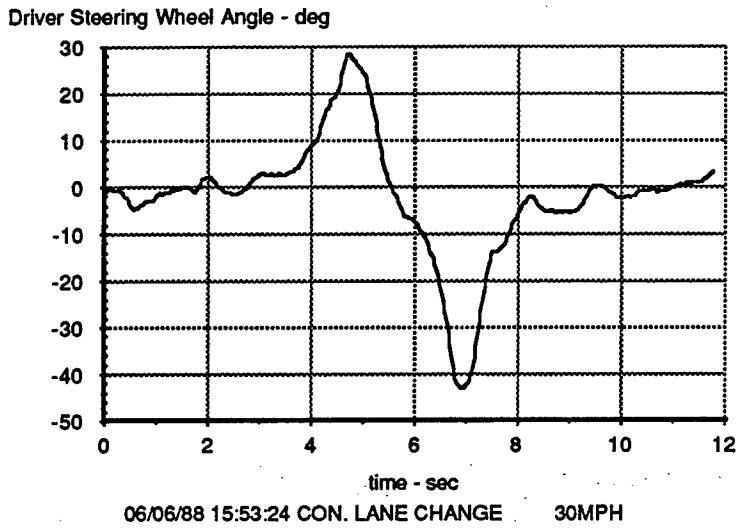

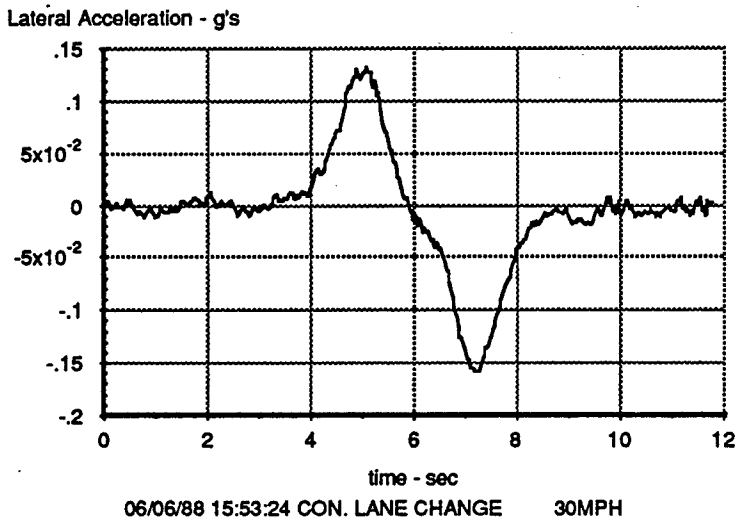

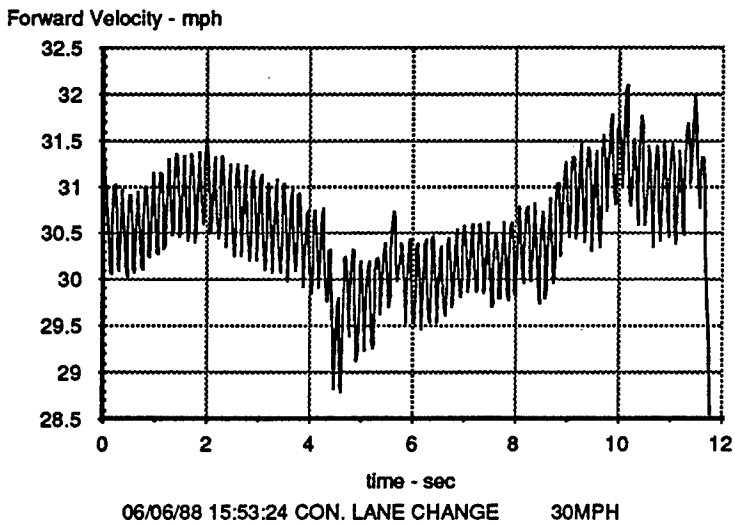

Figure B-11. HMMWV Test: Lane-Change, 30 mph

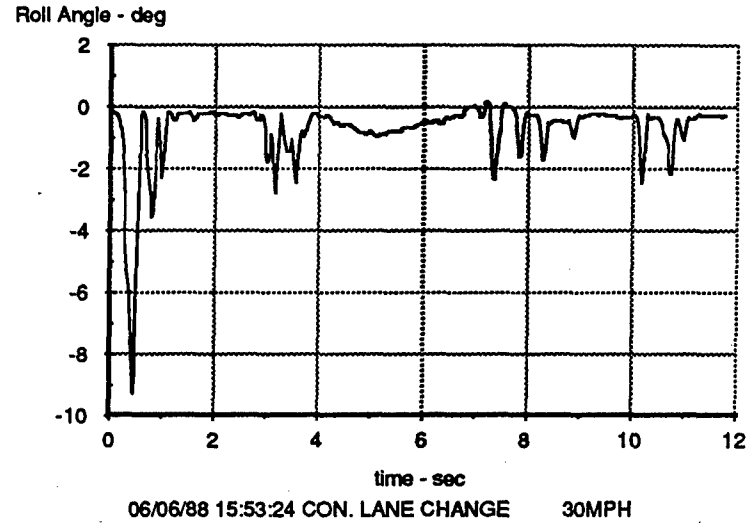

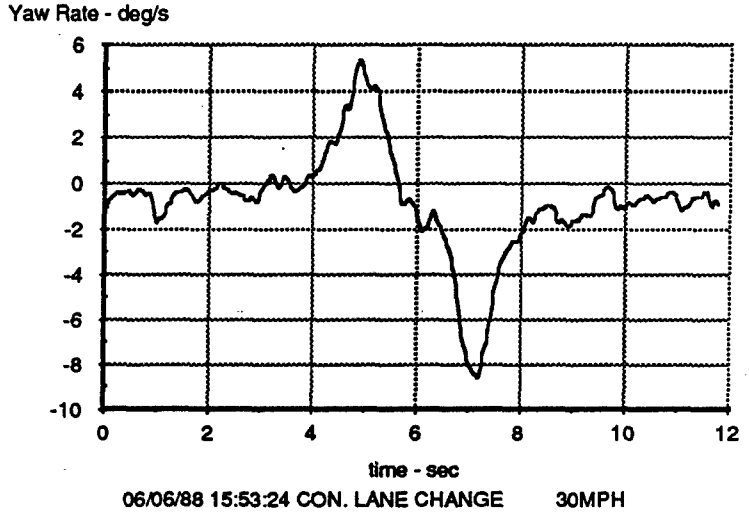

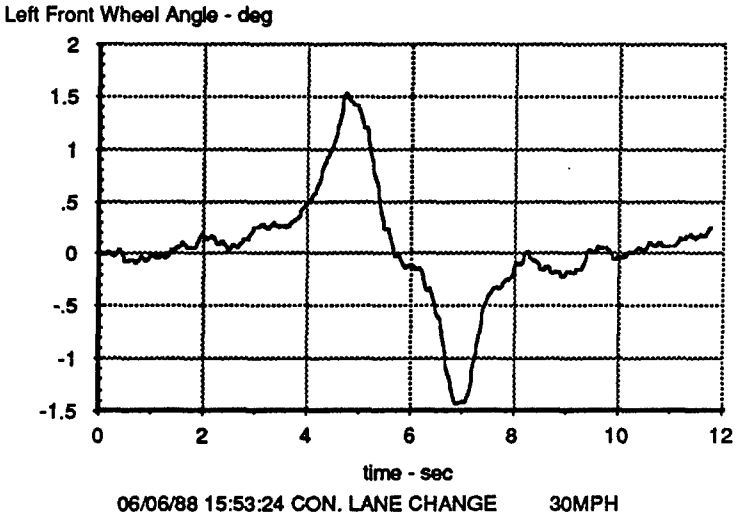

Figure B-12. HMMWV Test: Lane-Change, 30 mph

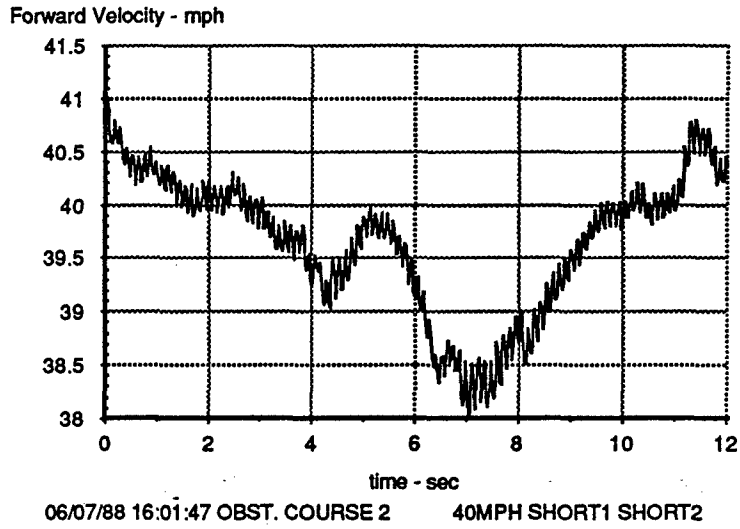

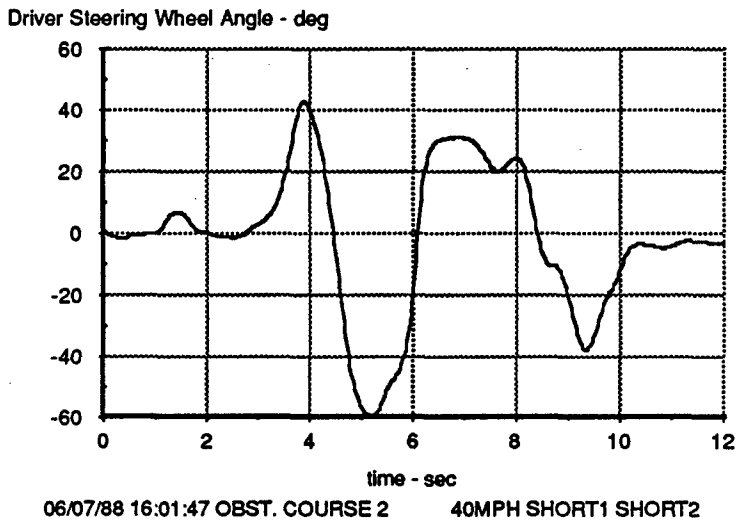

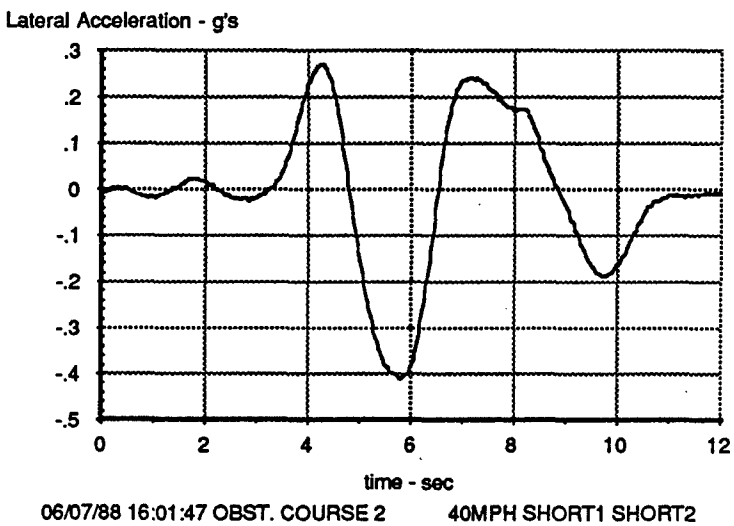

Figure B-13. HMMWV Test: Obstacle Course, short/short

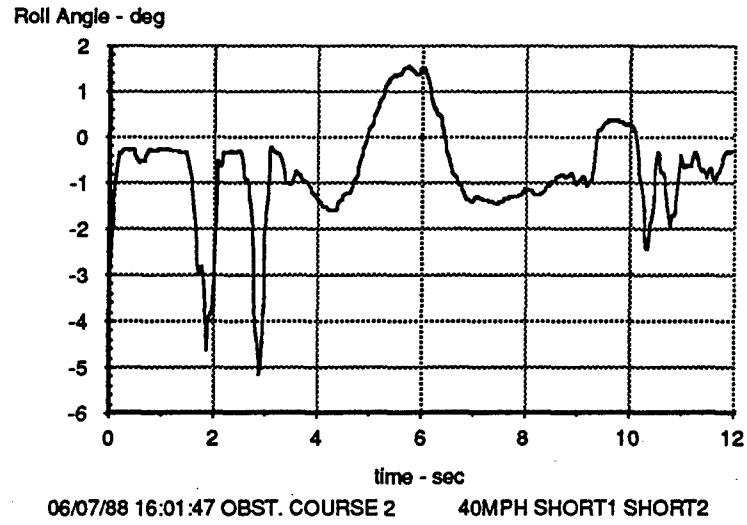

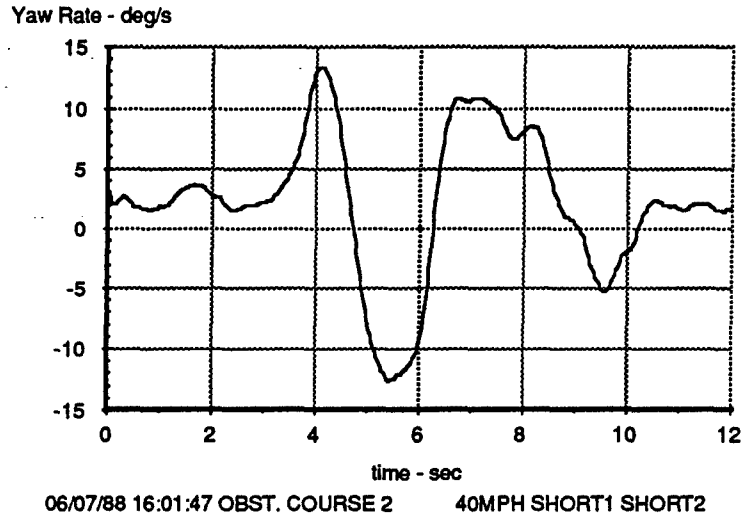

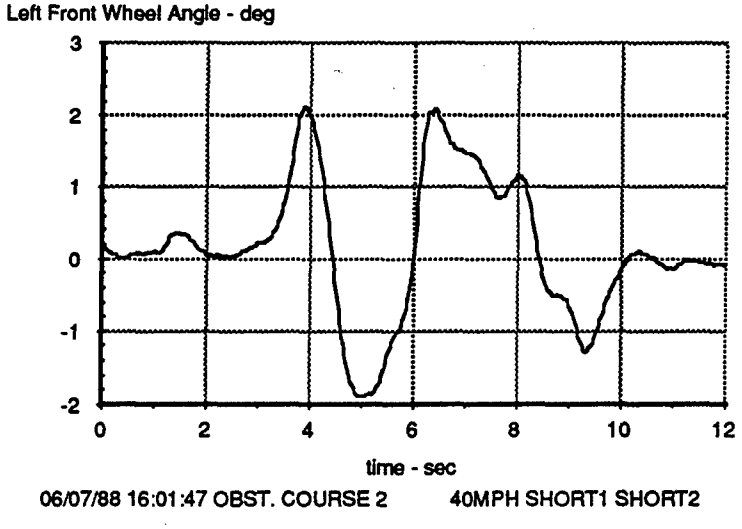

Figure B-14. HMMWV Test: Obstacle Course, short/short

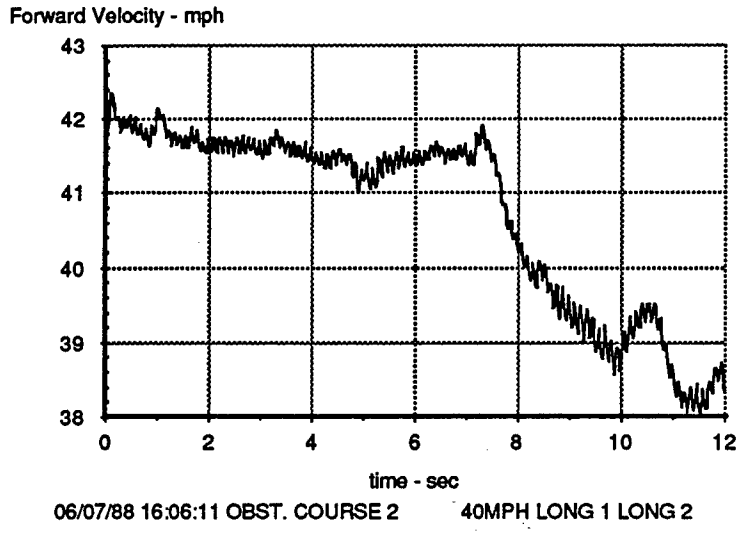

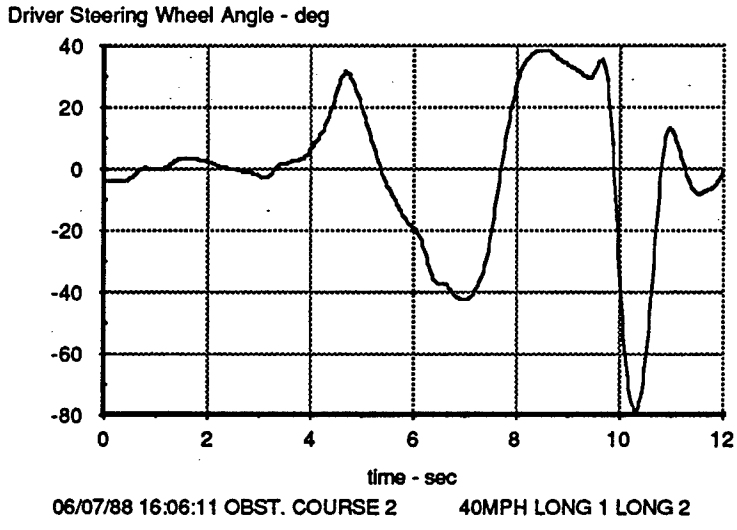

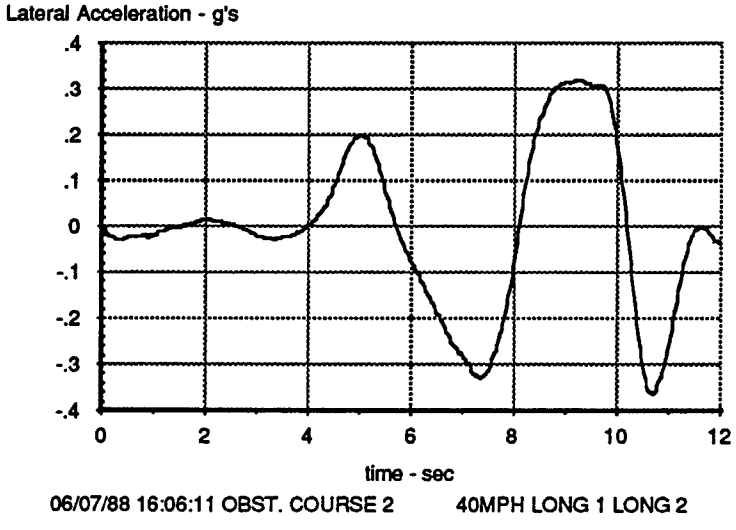

Figure B-15. HMMWV Test: Obstacle Course, long/long

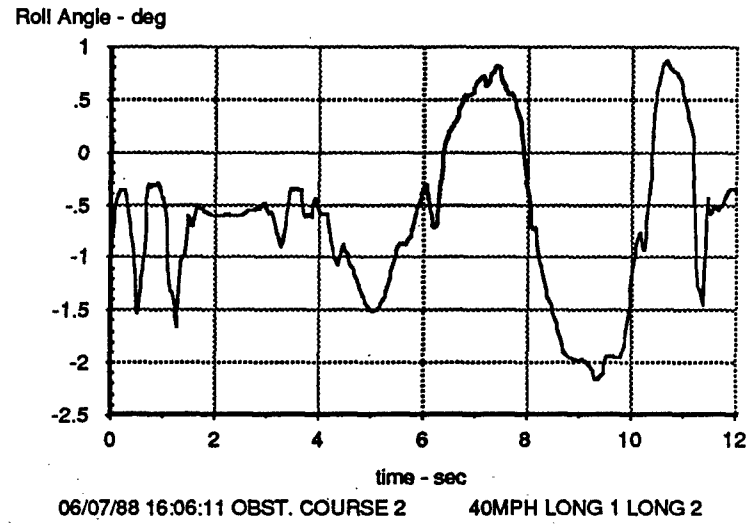

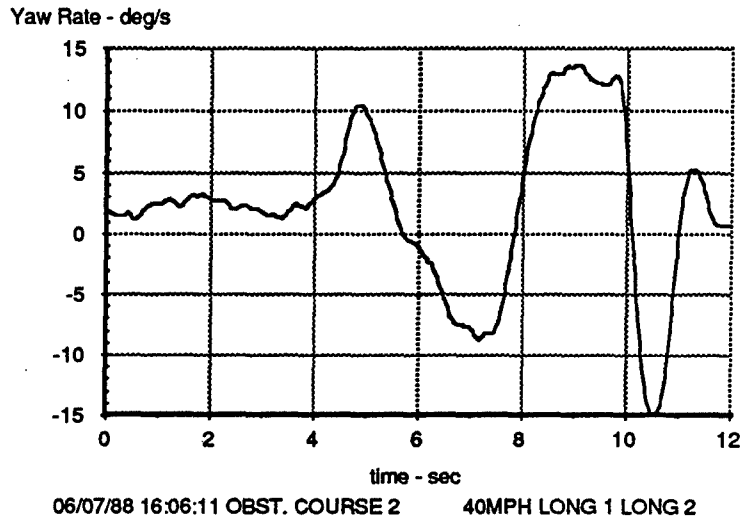

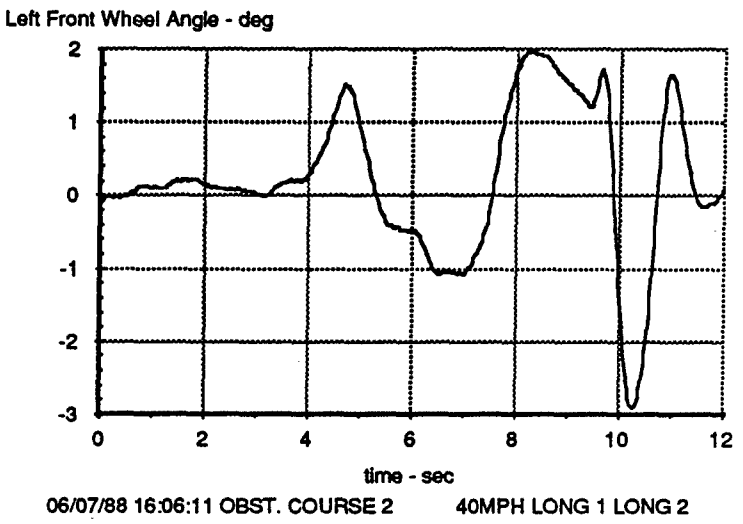

Figure B-16. HMMWV Test: Obstacle Course, long/long

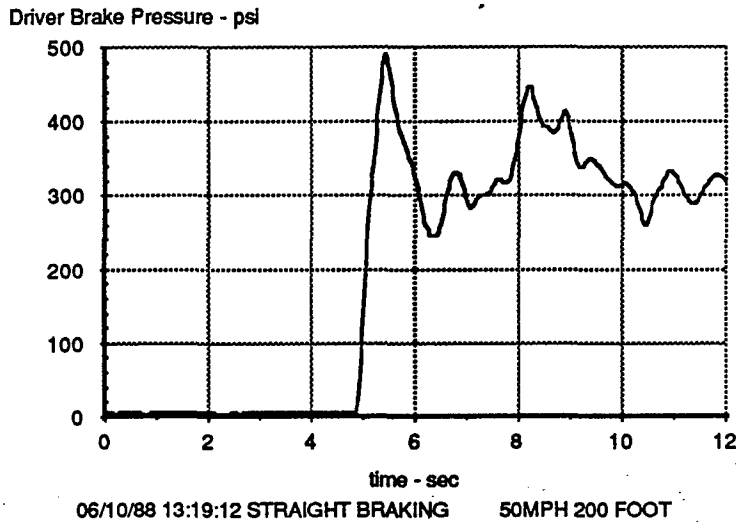

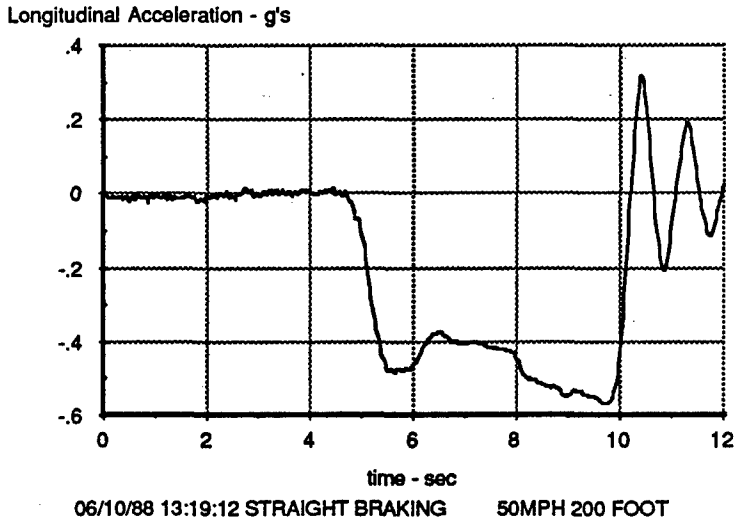

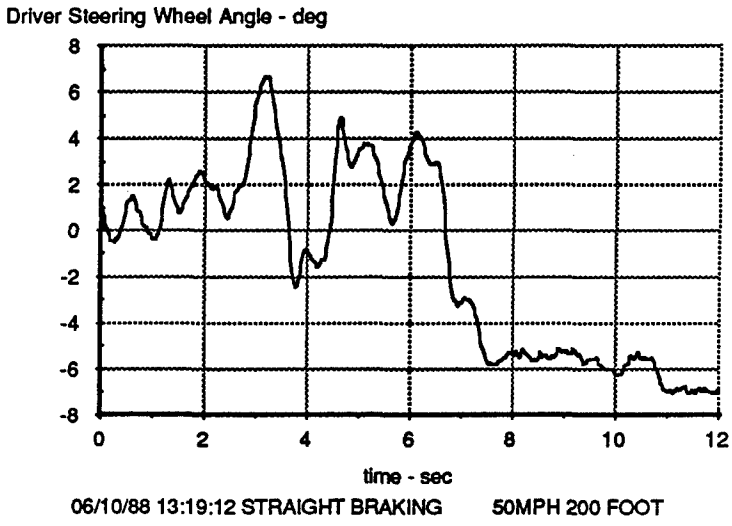

Figure B-17. HMMWV Test: Straight-Line Braking, 200 ft

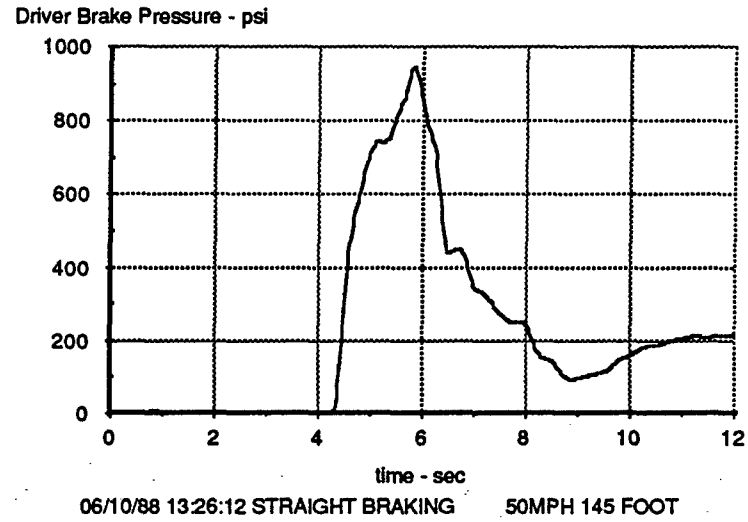

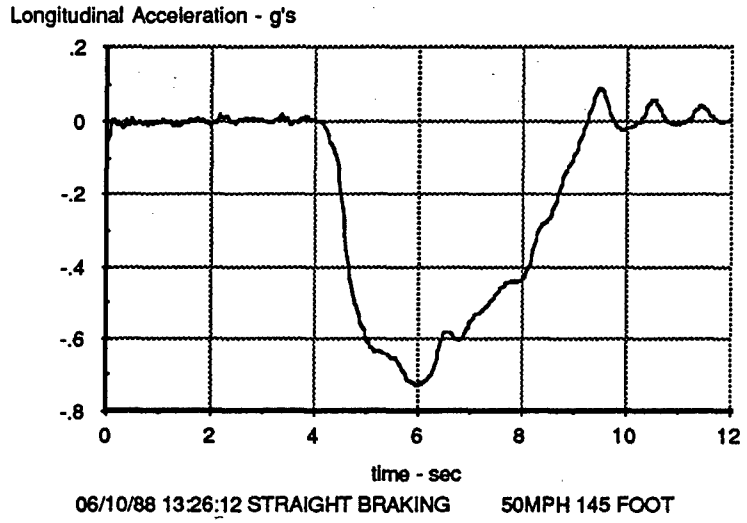

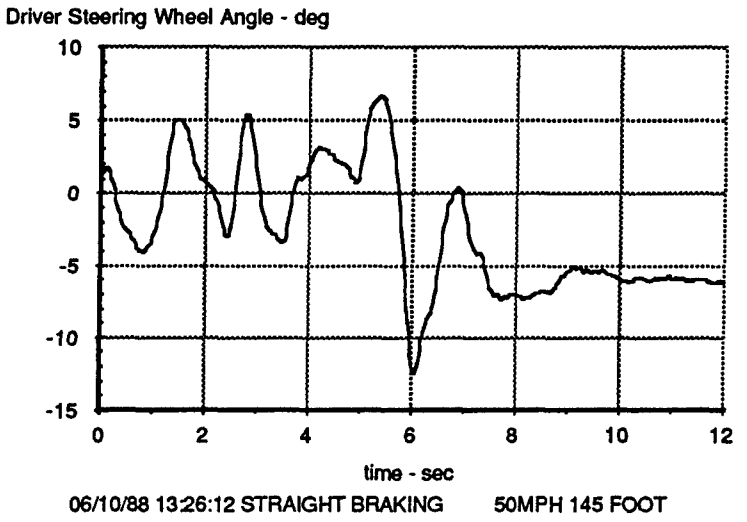

Figure B-18. HMMWV Test: Straight-Line Braking, 145 ft

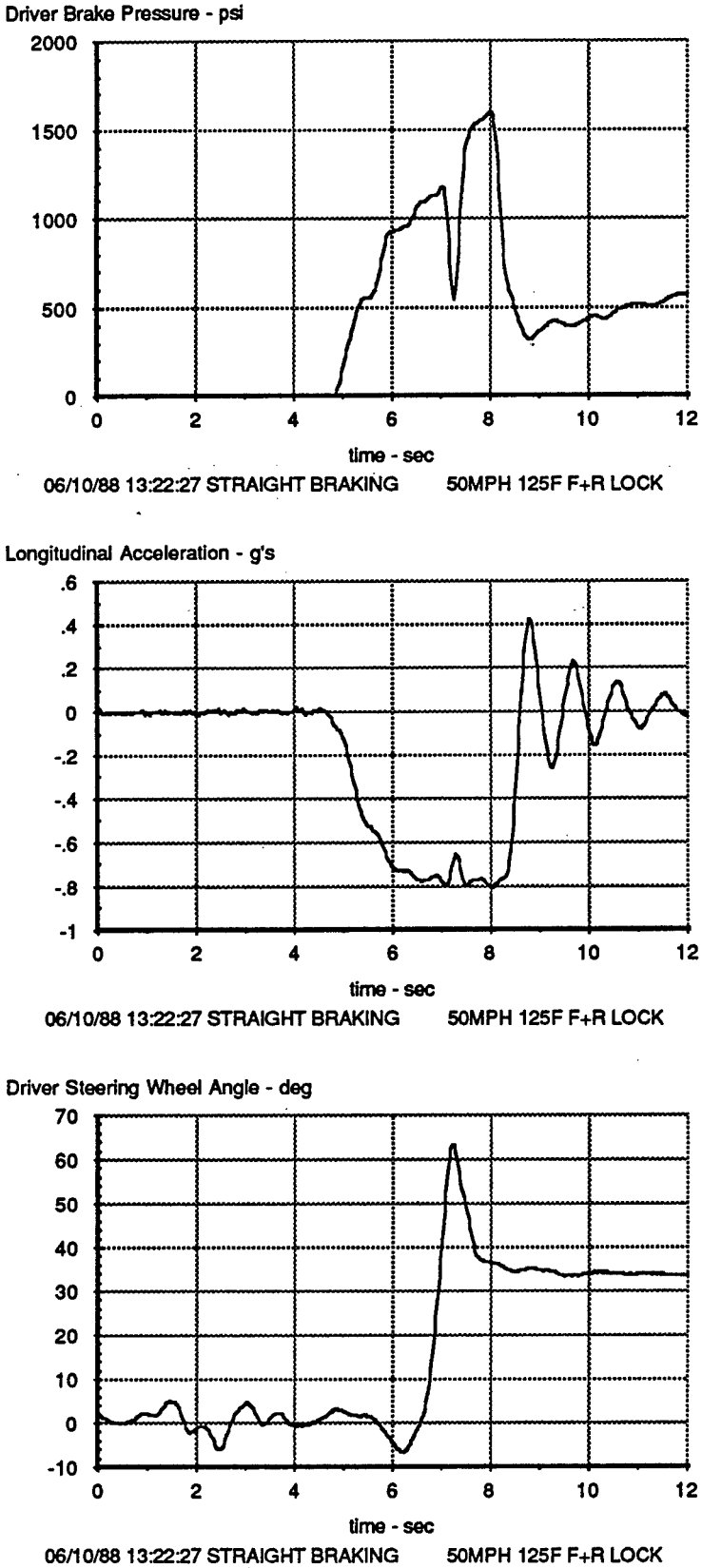

Figure B-19. HMMWV Test: Straight-Line Braking, 125 ft

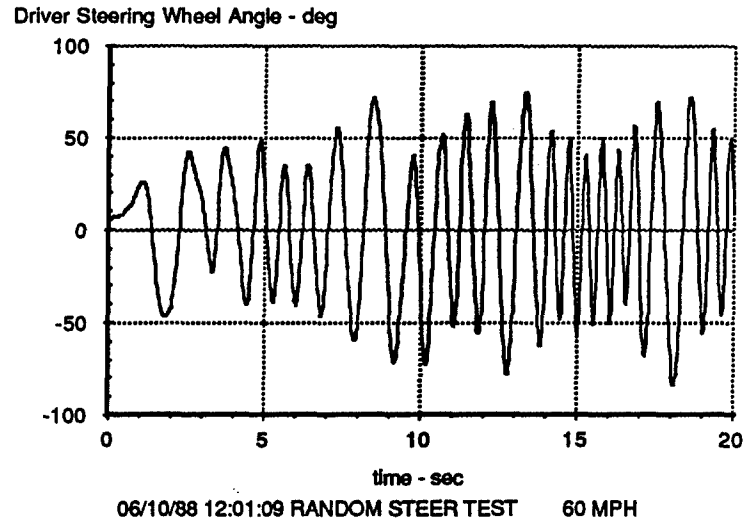

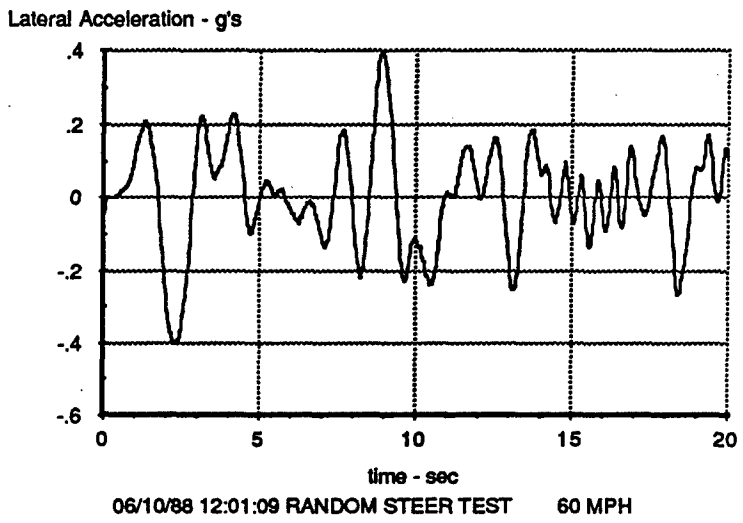

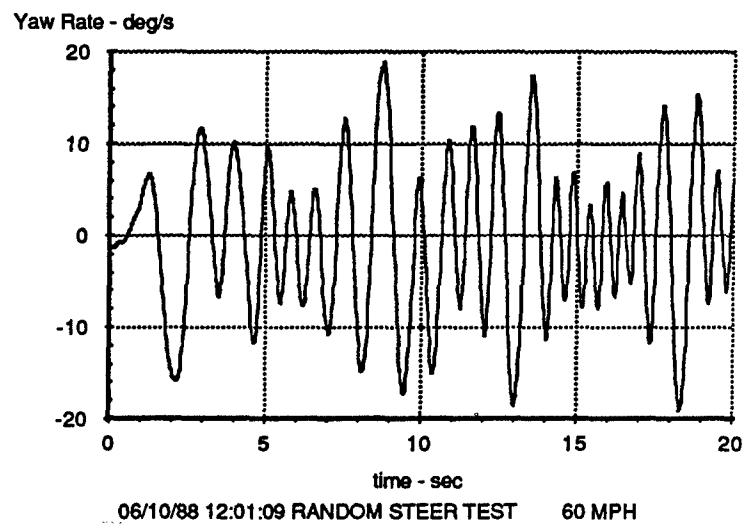

Figure B-20. HMMWV Test: Random Steer Application

Appendix C

HMMWV-Trailer Test Data

The test data appearing in this appendix are for the combined HMMWV-Trailer vehicle tests. Mousseau, in reference 41, utilized these data in validating a DADS computer model of the HMMWV-Trailer combination and in further studying the dynamic response of that system. The log sheets appearing as Table 5-2 in section 5.6 list these data as tests 271-310. During this sequence of tests, the trailer payload of approximately 1600 lb was located directly over the trailer axle. This loading resulted in a vertical hitch load of 176 lb on the HMMWV. Three different types of handling tests were conducted for the combination vehicle and an example of each appears in Figures C-1 through C-8.

Figures C-1 to C-3 correspond to a nominal 50 mph lane-change maneuver (test 281). The first two figures, C-1 and C-2, apply to the lead unit (HMMWV). Figure C-3 shows the HMMWV-trailer articulation angle and the lateral acceleration experienced by the trailer. The trailer lateral accelerometer was body-mounted (as opposed to the stable platform mounting in the HMMWV). Consequently, its measurement includes a small component of gravity due to trailer roll angle which should be accounted for in any subsequent analyses.

Figures C-4 and C-5 show measured results from steady turning test 296.

The data seen in Figures C-6 through C-8 are from the braking-in-a-turn test 308.

A sequence of additional HMMWV-Trailer tests having unusual (fore/aft) trailer loadings are listed as tests 320-348 in Table 5-2. During these tests, the same 1600 lb trailer payload as used in the previous test series was moved either (a) all the way forward in the trailer ("Divergence Tests" 320-335), or, (b) all the way rearward (Oscillation Tests" 336-348). These tests were part of a special trailer stability study reported on in reference 42 by Stribersky, and were intended to help validate the application of "bifurcation" theory to non-linear vehicle systems. That reference is included as part of Appendix G.

An example divergence test is seen in Figure C-9. In general, these tests proved to be largely uneventful, with the test driver having no dificulty in maintaining directional stablity of the vehicle.

Two examples of the trailer oscillation tests are seen in Figures C-10 through C-13. Figures C-10 and C-11 correspond to test 342 showing the response of the combination vehicle to a sinusoidal-like steering wheel disturbance applied by the driver in order to excite the system. Following this initial steering input, the driver only attempted to stabilize the lead HMMWV unit along a straight-line path. The resulting vehicle oscillations that build up due to the adverse rearward loading of the trailer are clearly seen in the accompanying figures. Figures C-12 and C-13 correspond to test 343 in which the same test was repeated but with a larger initial steering wheel input. In both of these tests, the loss of forward speed during the tests helps to eventually damp out the limit cycle oscillations that are initially excited by the steering inputs.

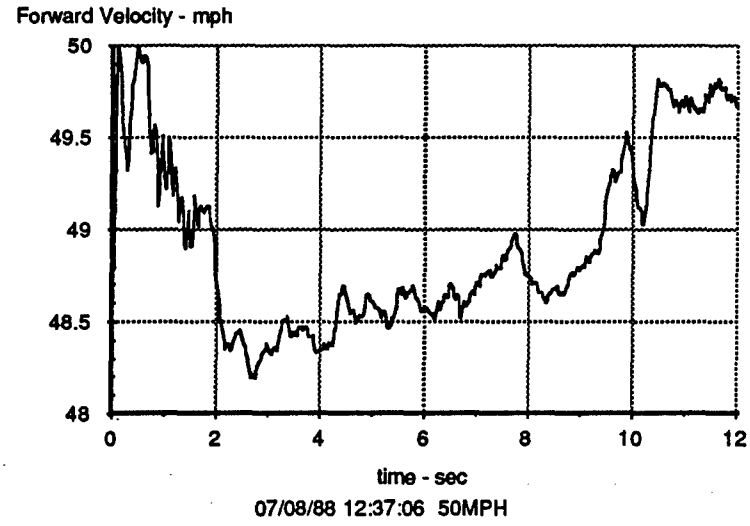

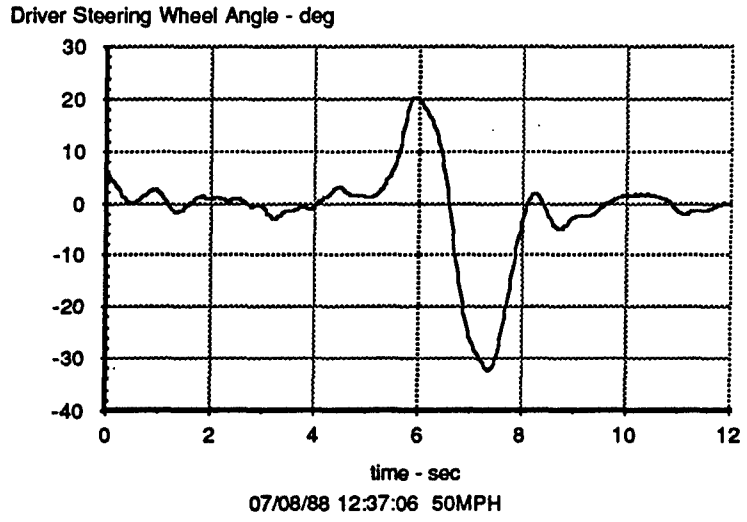

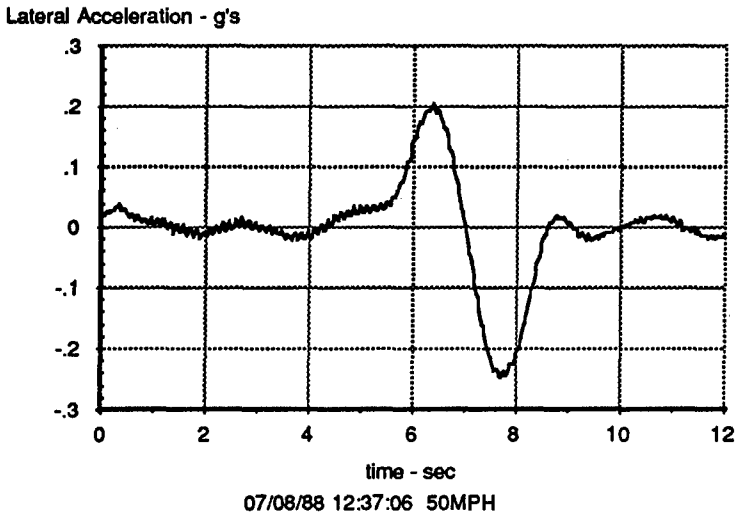

Figure C-1. HMMWV / Trailer Lane-Change Test

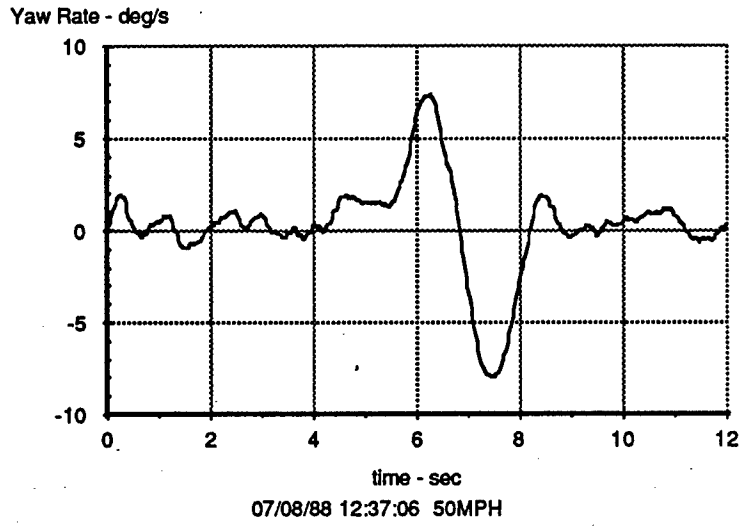

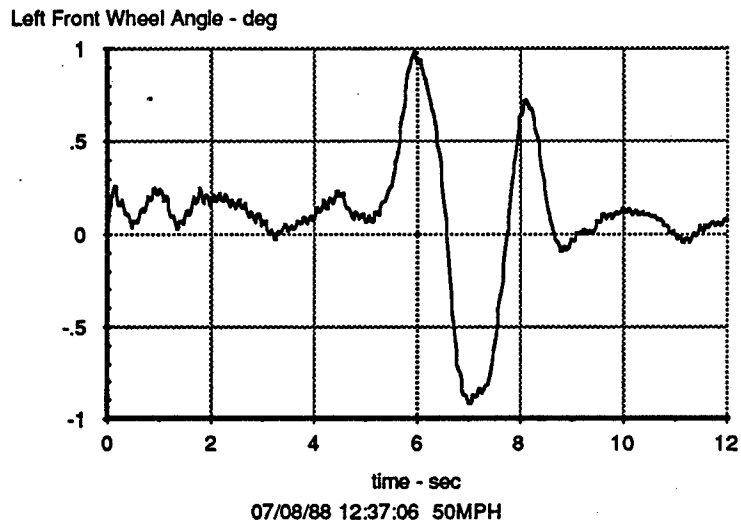

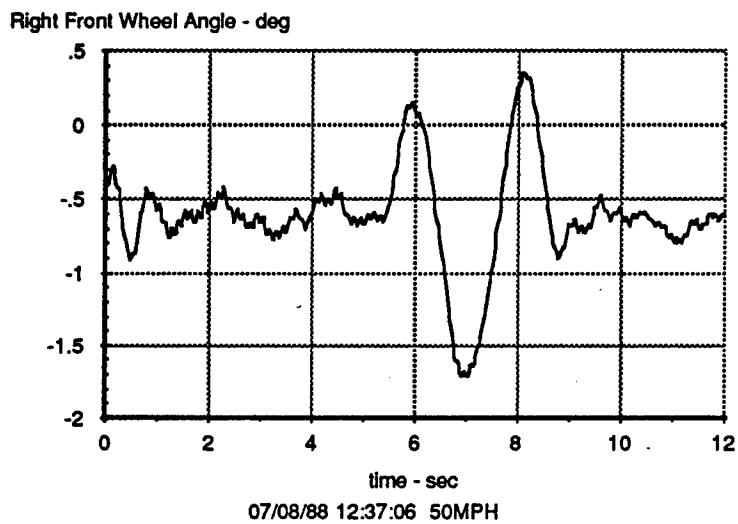

Figure C-2. HMMWV / Trailer Lane-Change Test

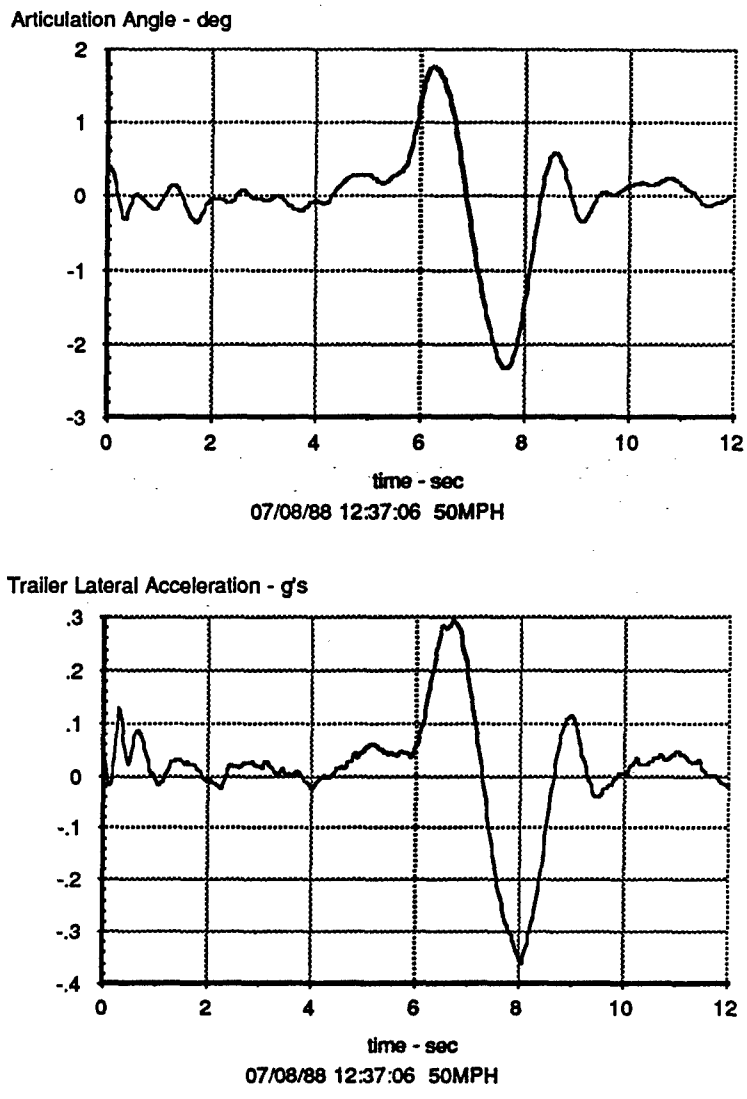

Figure C-3. HMMWV / Trailer Lane-Change Test

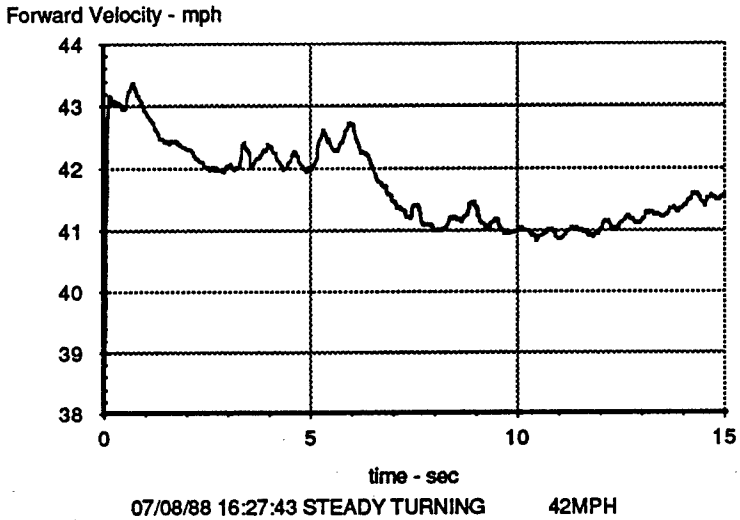

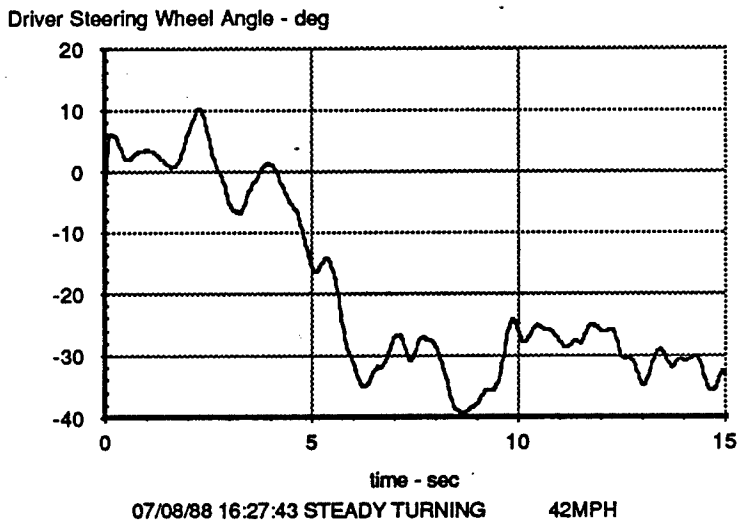

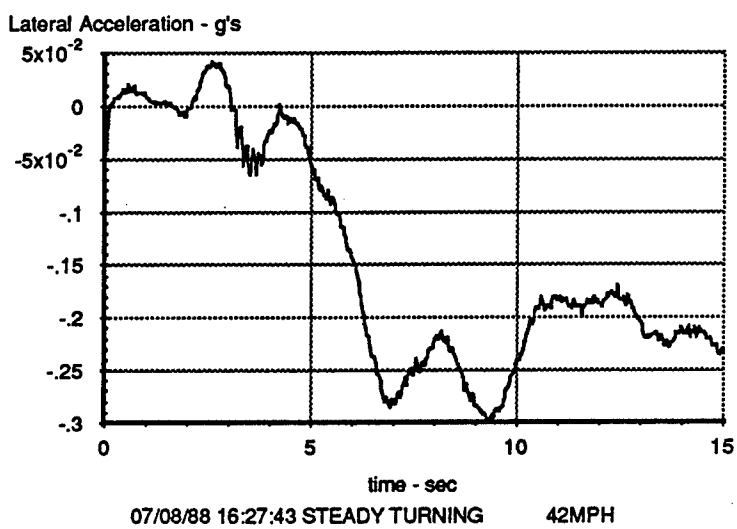

Figure C-4. HMMWV / Trailer Steady Turning Test

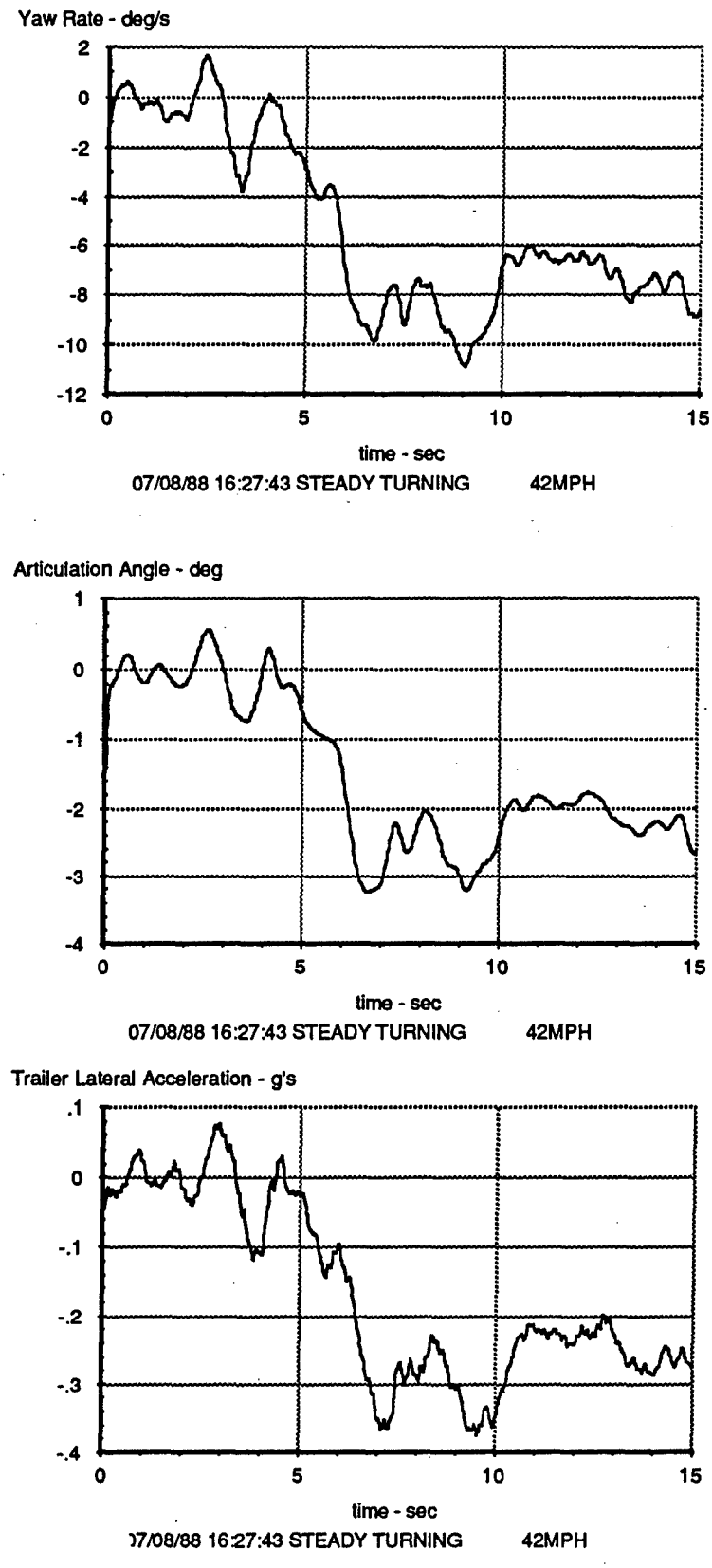

Figure C-5. HMMWV / Trailer Steady Turning Test

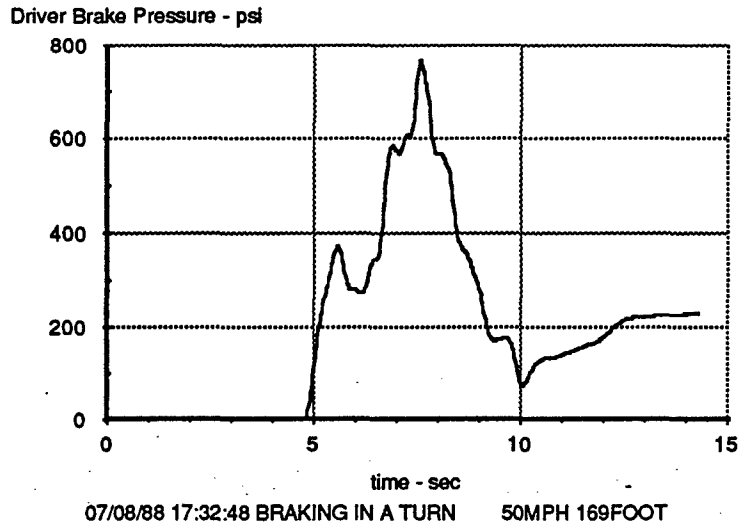

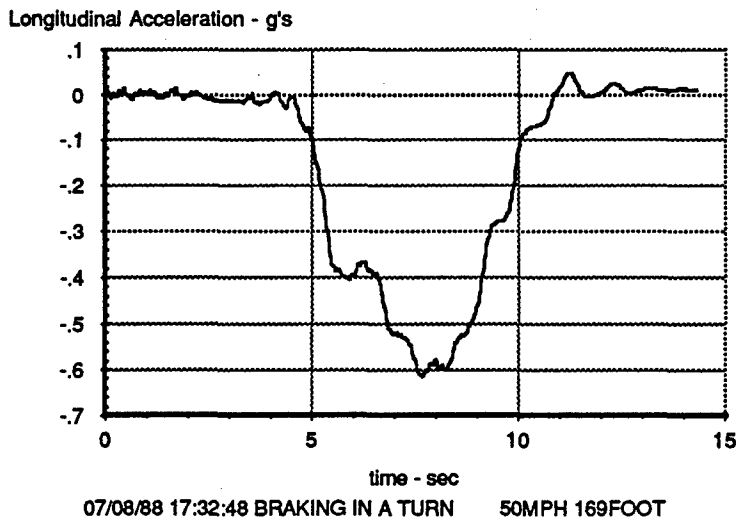

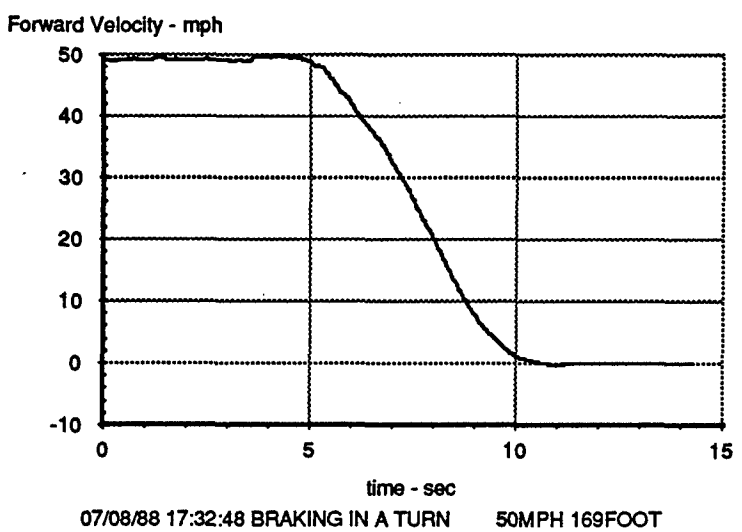

Figure C-6. HMMWV / Trailer Braking-in-a-Turn Test

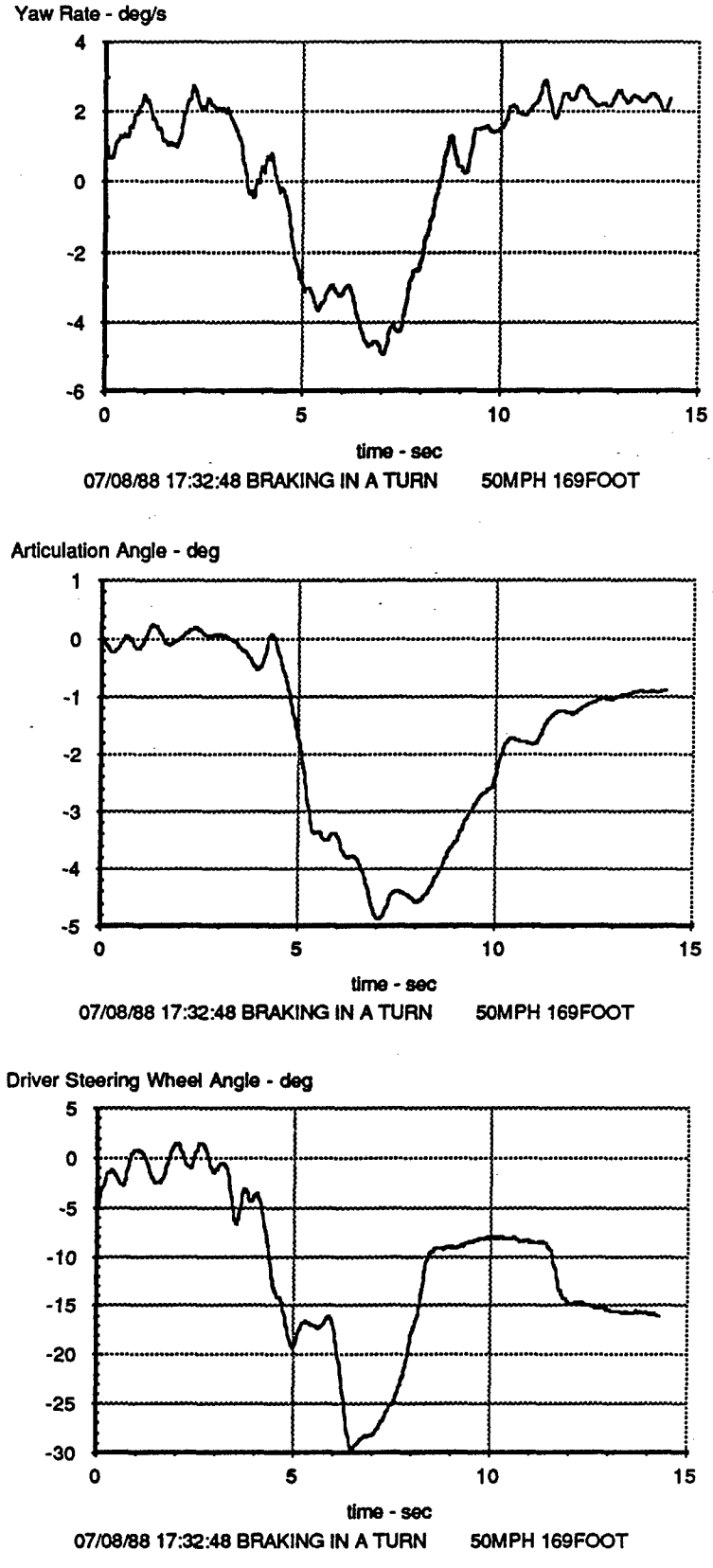

Figure C-7. HMMWV / Trailer Braking-in-a-Turn Test

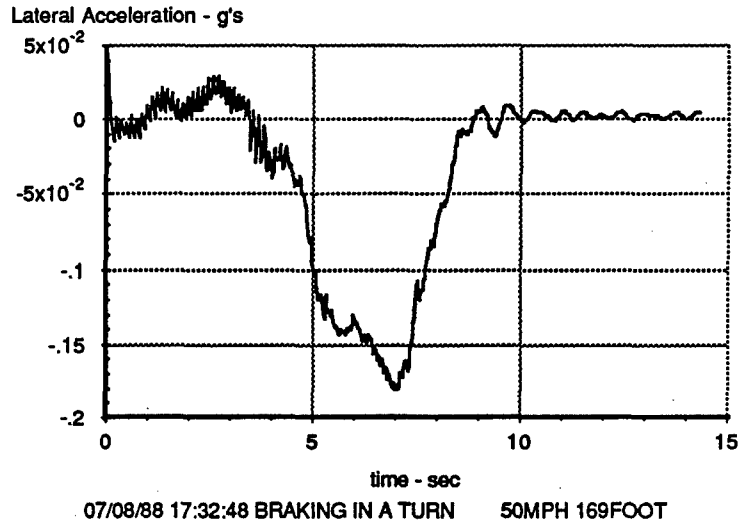

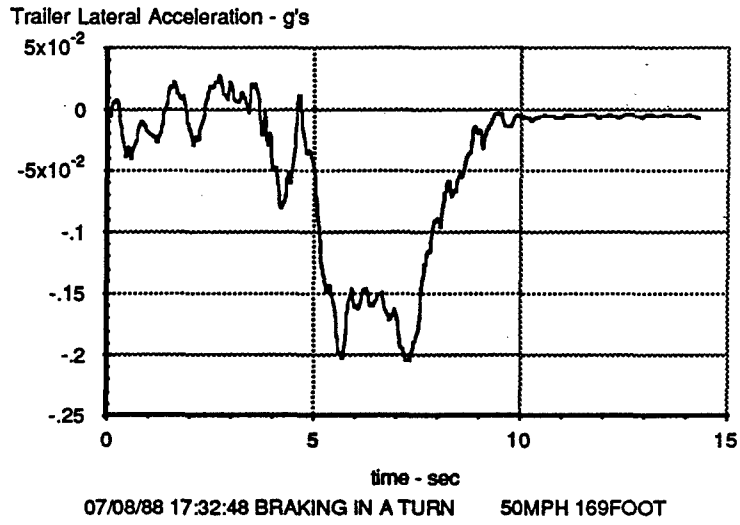

Figure C-8. HMMWV / Trailer Braking-in-a-Turn Test

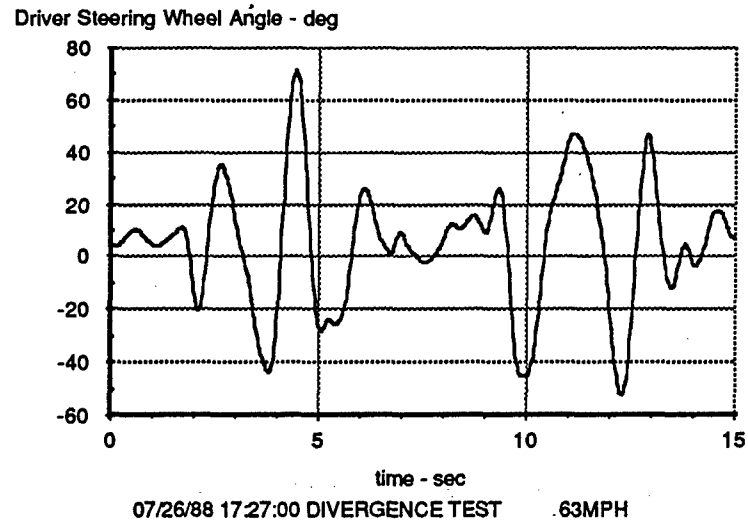

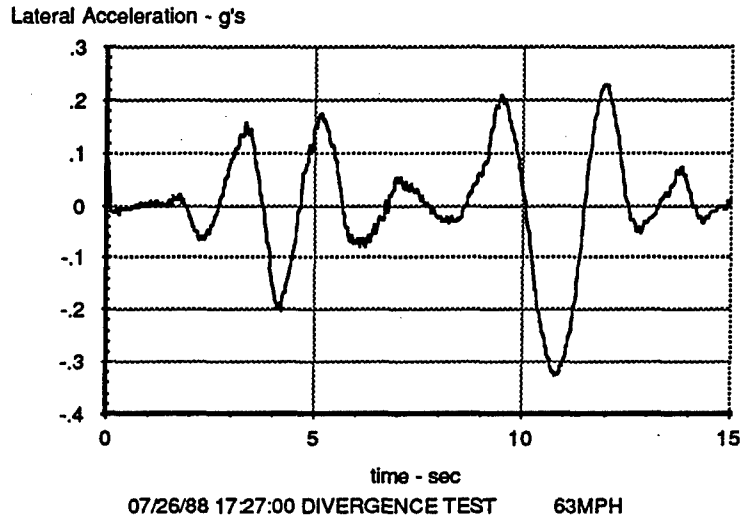

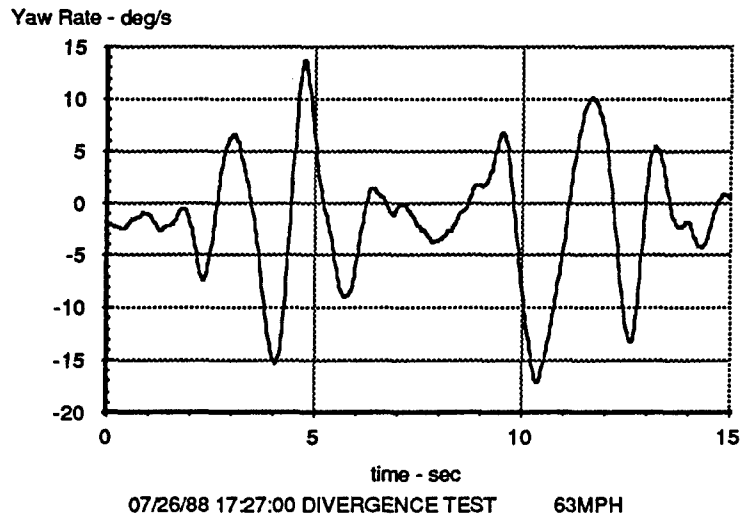

Figure C-9. HMMWV / Trailer "Divergence" Test

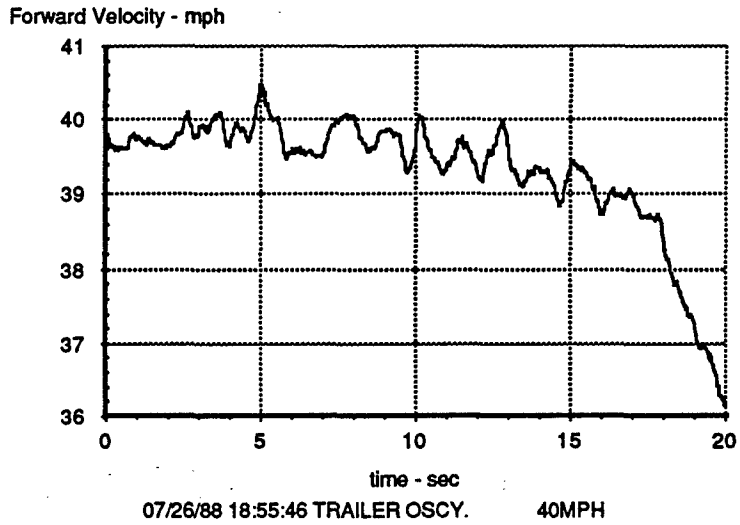

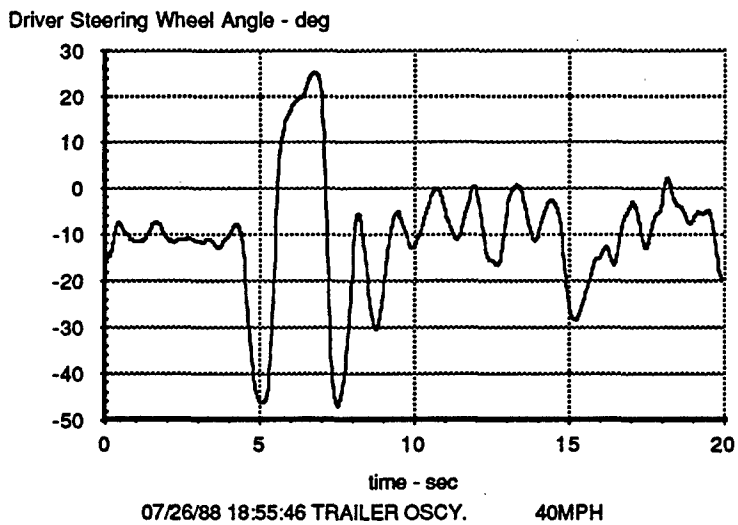

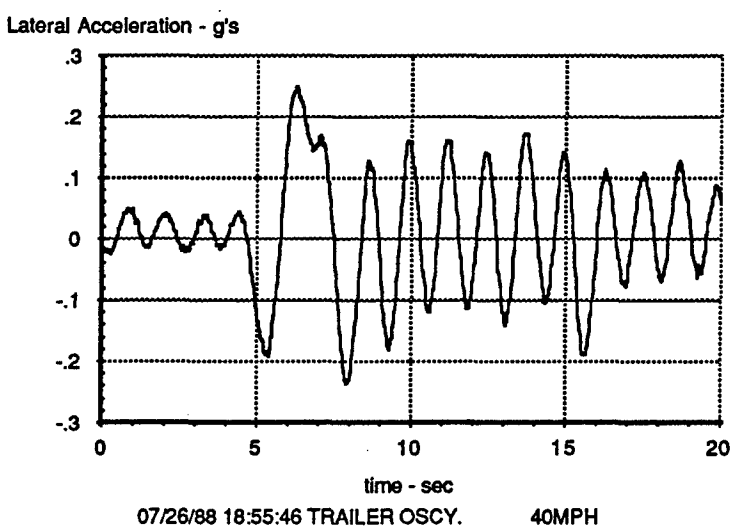

Figure C-10. HMMWV / Trailer "Oscillation" Test

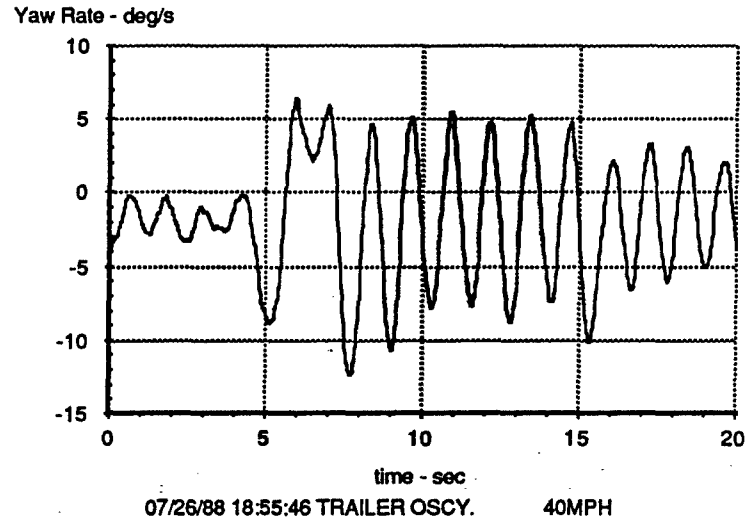

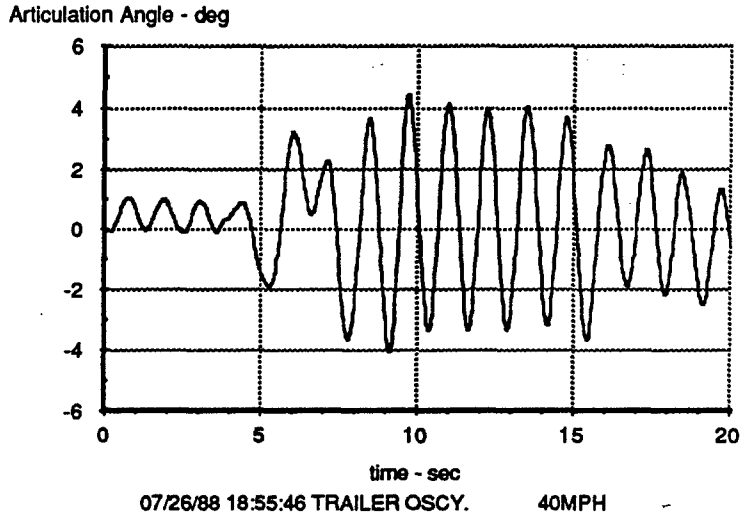

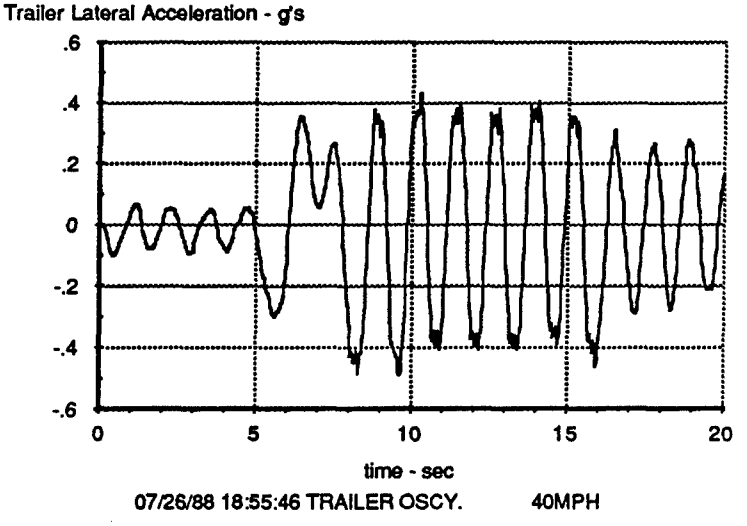

Figure C-11. HMMWV / Trailer "Oscillation" Test

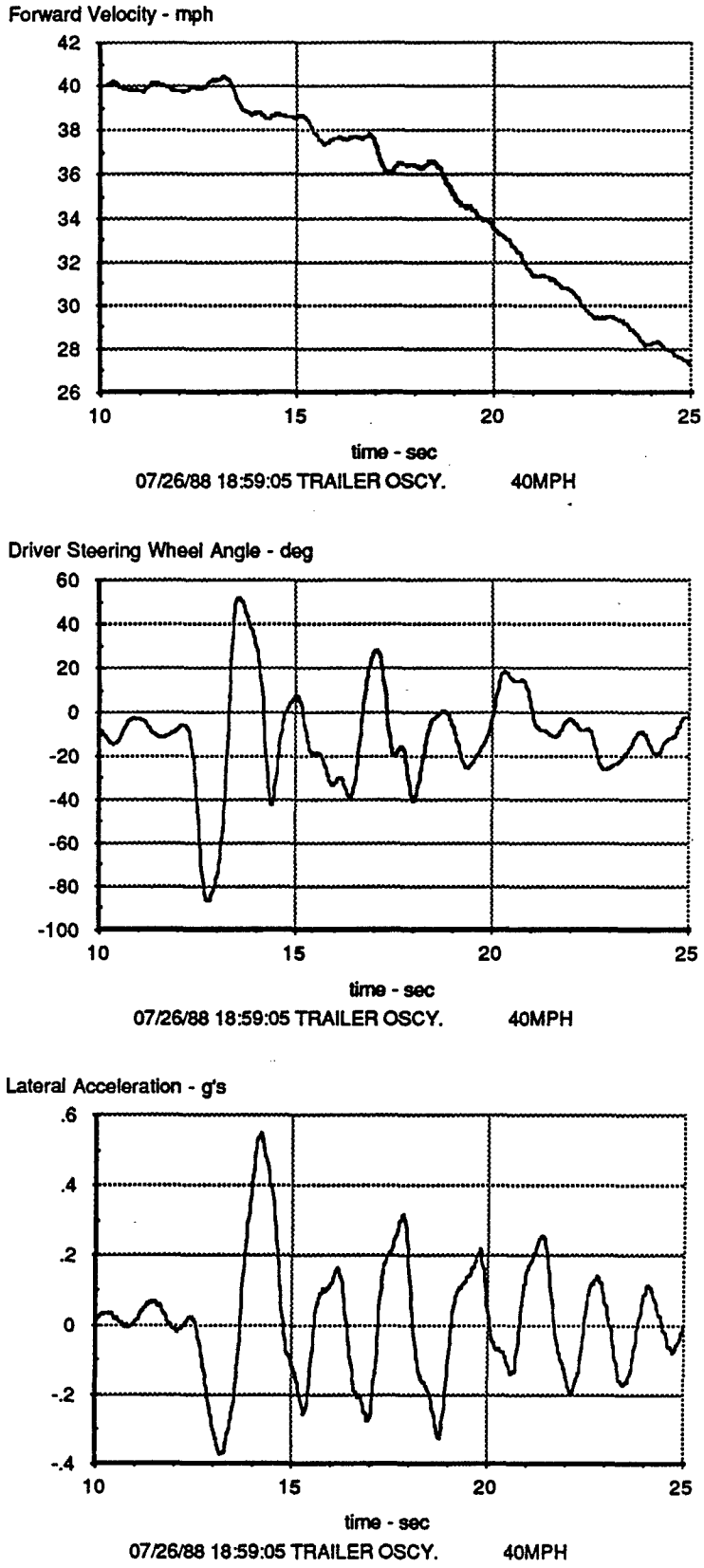

Figure C-12. HMMWV / Trailer "Oscillation" Test

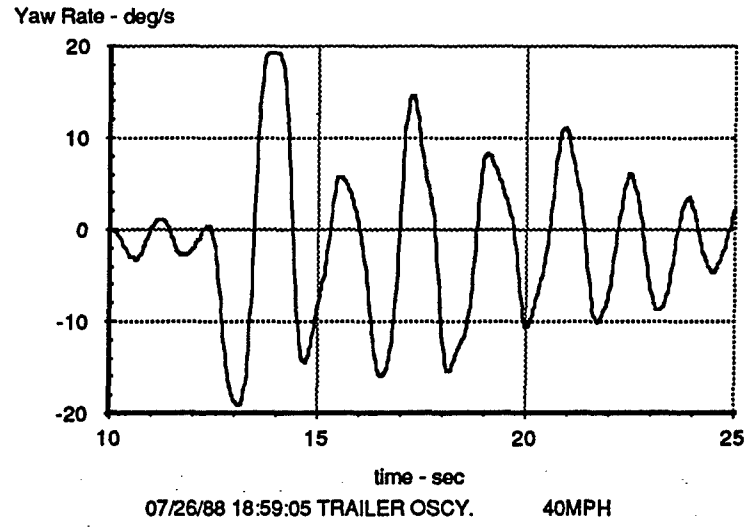

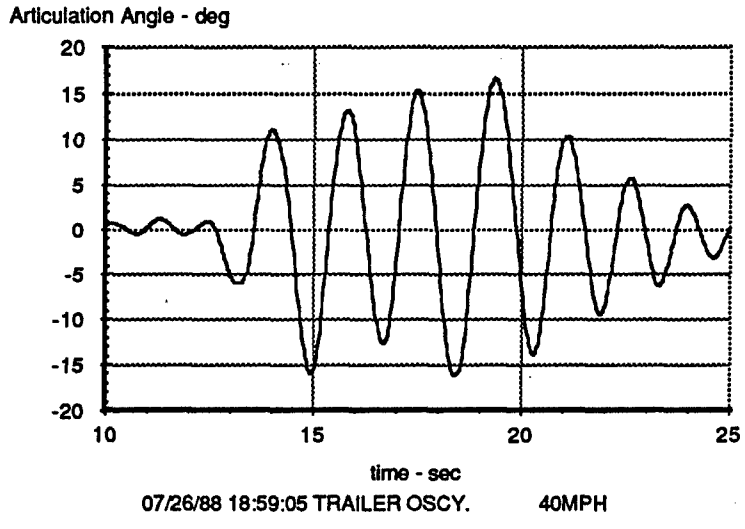

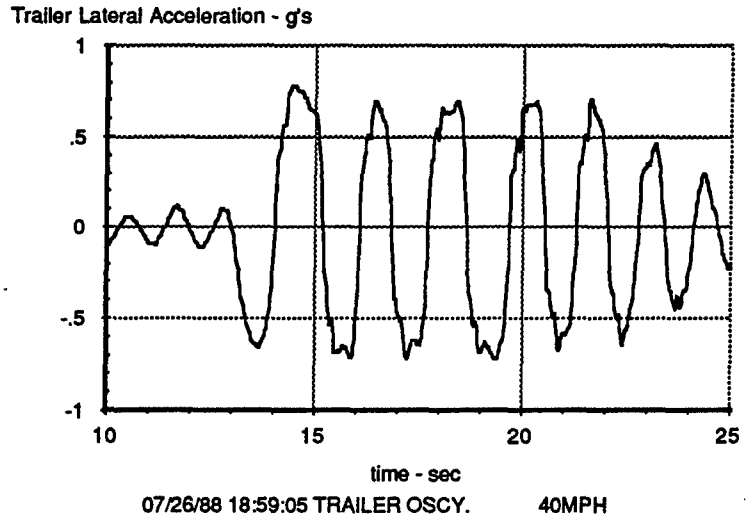

Figure C-13. HMMWV / Trailer "Oscillation" Test

Appendix D

FORTRAN Driver Model Code

This appendix contains FORTRAN code defining the basic single-unit driver steering control model interfaced to the CADSI / DADS program used at TACOM. Other DADS subroutines such as USER49, TIREF, and FILTER that were used to call the driver model or calculate information for the model are contained in Appendix E.

The following subroutine are listed in this appendix:

- **DRIVGO** called once by DADS at time zero
- **OUT** (optional) called by DADS for reporting out
- **DRIVE1** called by DRIVGO
- **TRANS** called by DRIVGO & DRIVER
- **DRIVER** called by USER49 (DADS) each time step
- **TRAJ** called by DRIVER
- **GMPRD** called by DRIVER

```
C  The following FORTRAN code documents the basic driver model
C  subroutines used with the DADS program to simulate a closed-loop
C  vehicle-driver system.  Most portions of this code, not specific to
C  DADS, may be used to represent the driver model within other vehicle
C  simulation programs.  The code listed here utilizes a 2-DOF vehicle
C  model for the driver's internal vehicle representation.
C
C
C*************************************************************************
C*************************************************************************
C
C    ***  DADS3D Initialization Entry for the Driver Model  ***
C
C DRIVGO: Intializes driver model variables and opens driver model
C          files
C
C============Author and Modification Section============================
C
C  Author:       C. C. MacAdam
C
C  Date written: 01/01/88
C
C  Written on:
C
C  Modifications:
C
C=======================================================================
C
C============Algorithm Description======================================
C
C  Purpose and use:
C
C  Error conditions:
C
C  References:
C
C     [1]       MacAdam, C.C.  "Development of Driver/Vehicle Steering
C                     Interaction Models for Dynamic Analysis," Final
C                     Technical Report, U.S. Army Tank Automotive Command
C                     Contract No. DAAE07-85-C-R069, The University of
C                     Michigan Transportat'n Research Inst, December 1988
C
C     [2]       MacAdam, C.C.  "Application of an Optimal Preview Control
C                     for Simulation of Closed-Loop Automobile Driving,"
C                     IEEE Transactions on Systems, Man, and Cybernetics,
C                     Vol. 11, June 1981.
C
C     [3]       MacAdam, C.C.  "An Optimal Preview Control for Linear
C                     Systems," Journal of Dynamic Systems, Measurement,
C                     and Control, ASME, Vol. 102, No. 3, September 1980.
C
C
C  Machine dependencies: none
C
C  Called By: USER49.F77
```

```
C
C=============================================================================
C
      SUBROUTINE DRIVGO
C
C============Variable Descriptions============================================
C
C---Arguments passed:  None
C
      INTEGER R, W
C
C---COMMON blocks-----------------------------------------------------------
C
      COMMON /DRIV/ CAF, CAR, WHBS, WF, WR, U
      SAVE/DRIV/
      COMMON /INOUT/ R, W
      SAVE/INOUT/
C
C---COMMON Variables--------------------------------------------------------
C    R.....Driver Model Input I/O unit ("DMINPUT.INP")  - optional
C    W.....Driver Model Output I/O unit ("DMOUTPUT.OUT")  - optional
C
C---DRIV.BLK common block variables----------------------------------------
C
C  CAF...total cornering stiffness of tires on left front susp (lb/rad)
C  CAR...total cornering stiffness of tires on left rear susp (lb/rad)
C  WHBS..wheelbase of vehicle (center-line of front & rear susp) (ft)
C  WF....static load on front suspension (lb)
C  WR....static load on rear suspension (lb)
C  U.....initial velocity (ft/sec)
C
C---Local variables--------------------------------------------------------
C
C  A.....distance from c.g. to front suspension center-line (ft)
C  B.....distance from c.g. to rear suspension center-line (ft)
C  WGHT..total static weight on front and rear suspsensions (lb)
C  RM....total static mass (slug)
C  DFW...steer angle of front tires [or average] (rad)
C
C---Functions and subroutines----------------------------------------------
C
      EXTERNAL DRIVE1, TRANS
C
C=============================================================================
C
C============Process Block====================================================
C
C
      R=33
      W=34
      GRAV = 32.16666
      OPEN (R,FILE='DMINPUT.INP',STATUS='UNKNOWN')
      OPEN ( W, FILE='DMOUTPUT.OUT',STATUS='UNKNOWN')
C
C  Driver model internal vehicle model parameters can be read in from
```

```
C  external files, as here, or passed from DADS through common blocks
C
      READ (R,10) CAF, CAR, WGHT, U, A, B, RI
  10  FORMAT (7F10.3)
  11  FORMAT(3F10.3)
C
      RM = WGHT / GRAV
      WHBS = A + B
      WF = WGHT * B / WHBS
      WR = WGHT * A / WHBS
C
C  Call DRIVE1 to read driver model parameters & initialize
C
      CALL DRIVE1(DFW)
C
C  Call TRANS to Calculate Transition Matrix at time zero
C
      CALL TRANS
C
      RETURN
      END
C*******************************************************************************
C*******************************************************************************
C
C  ***  Out Subroutine  ***              *** OPTIONAL  SUBROUTINE ***
C
C OUT: Writes driver model calculations on unit W
C
C==========Author and Modification Section==============================
C
C  Author:       C. C. MacAdam
C
C  Date written: 01/01/88
C
C  Written on:
C
C  Modifications:
C
C=======================================================================
C
C==========Algorithm Description=======================================
C
C  Purpose and use:
C
C  Error conditions:
C
C  Machine dependencies: none
C
C  Called By: DRIVGO
C
C=======================================================================
C
      SUBROUTINE OUT(T, Y, YD, DFW)
C
C==========Variable Descriptions=======================================
```

```
C
C---Arguments passed:
C  T.....current time in simulation (sec)
C  Y.....driver model state vector of dimension 5 comprised of the
C        following physical quantities: [1] inertial lateral
C        displacement (ft), [2] lateral veloc in body frame (ft/s),
C        [3] yaw rate global (rad/s), [4] SAE global yaw angle (rad),
C        [5] global forward displacent (ft).
C  YD....rates of change of Y
C  DFW...steer angle of front tires [or average] (rad)
C
      INTEGER R, W
      DIMENSION Y(5), YD(5), YOUT(5), YDOUT(5)
C
C---COMMON blocks-------------------------------------------------------
C
      COMMON /DRIV/ CAF, CAR, WHBS, WF, WR, U
      SAVE/DRIV/
      COMMON /INOUT/ R, W
      SAVE/INOUT/
C
C---COMMON Variables---------------------------------------------------
C
C    R.....Driver Model Input I/O unit ("DMINPUT.INP")
C    W.....Driver Model Output I/O unit ("DMOUTPUT.OUT")
C
C---DRIV.BLK common block variables------------------------------------
--
C
C  CAF...total cornering stiffness of tires on left front susp (lb/rad)
C  CAR...total cornering stiffness of tires on left rear susp (lb/rad)
C  WHBS..wheelbase of vehicle (center-line of front & rear susp) (ft)
C  WF....static load on front suspension (lb)
C  WR....static load on rear suspension (lb)
C  U.....initial velocity (ft/sec)
C
C---Local variables----------------------------------------------------
C
C  YOUT....output buffer in engineering / english units for Y vector
C  YDOUT...  "      "                                YD  "
C  DFWPRT..steer angle in degrees
C  RADIAN..radian to degree conversion factor (deg/rad)
C
C---Functions and subroutines------------------------------------------
C
C      None
C
C================================================================
C
C==========Process Block=========================================
C
C
      DATA RADIAN /57.3/
C
      DO 10 I = 1, 5
```

```
        YOUT(I) = Y(I)
        YDOUT(I) = YD(I)
   10 CONTINUE
      YOUT(2) = Y(2) / U * RADIAN
      YOUT(3) = Y(3) * RADIAN
      YOUT(4) = Y(4) * RADIAN
      YDOUT(2) = YD(2) / U * RADIAN
      YDOUT(3) = YD(3) * 57.3
      YDOUT(4) = YD(4) * RADIAN
      DFWPRT = DFW * RADIAN
      WRITE (W,20) T, DFWPRT, (YOUT(I),I=1,5), (YDOUT(I),I=1,5)
   20 FORMAT (12F8.2)
      RETURN
      END
C*************************************************************************
C*************************************************************************
C
C  ***  Initialization Subroutine  ***
C
C DRIVE1: Intializes variables and echoes driver model parameters on W
C
C============Author and Modification Section==============================
C
C  Author:       C. C. MacAdam
C
C  Date written: 01/01/88
C
C  Written on:
C
C  Modifications:
C
C=========================================================================
C
C============Algorithm Description=======================================
C
C  Purpose and use:
C
C  Error conditions:
C
C  Machine dependencies: none
C
C  Called By: DRIVGO
C
C=========================================================================
C
      SUBROUTINE  DRIVE1(DFW)
C
C============Variable Descriptions=======================================
C
C---Arguments passed:
C
C  DFW...steer angle of front tires [or average] (rad)
C
      INTEGER R, W
C
```

```
C---COMMON blocks-------------------------------------------------------
C
      COMMON /DRVST1/ GRAV, TICYCL, TSS, DMAX, XP(100), YP(100), TAUMEM,
     1       TFF, RM, A, B, RI, PSI0, NTF, NP, TLAST, DFWLST, TILAST,
     2       DMEM(1000,2), XT(100), YT(100)
      SAVE/DRVST1/
      COMMON /DRIV/ CAF, CAR, WHBS, WF, WR, U
      SAVE/DRIV/
      COMMON /INOUT/ R, W
      SAVE/INOUT/
C
C---COMMON Variables---------------------------------------------------
C    R.....Driver Model Input I/O unit ("DMINPUT.INP")
C    W.....Driver Model Output I/O unit ("DMOUTPUT.OUT")
C
C---DRIV.BLK common block variables------------------------------------
--
C
C  CAF...total cornering stiffness of tires on left front susp (lb/rad)
C  CAR...total cornering stiffness of tires on left rear susp (lb/rad)
C  WHBS..wheelbase of vehicle (center-line of front & rear susp) (ft)
C  WF....static load on front suspension (lb)
C  WR....static load on rear suspension (lb)
C  U.....initial velocity (ft/sec)
C
C---DRVST1.BLK common block variables
C
C   GRAV.....gravitational constant
C   TICYCL...driver model sample time (sec)
C   TSS......minimum preview time (sec)
C   DMAX.....upper bound on front wheel angle steer (rad)
C   XP,YP....x-y path coords(SAE) wrt inertial coords [input] (ft)
C   TAUMEM...driver transport time dealy [input parameter] (sec)
C   TFF......driver model preview time [input parameter] (sec)
C   RM.......vehicle mass (slug)
C   A........distance from c.g. to front suspension center-line (ft)
C   B........distance from c.g. to rear suspension center-line (ft)
C   RI.......total vehicle yaw inertia (slug-ft)
C   PSIO.....current yaw angle reference value (rad)
C   NTF......number of points in the preview time interval
C   NP.......number of points in the x-y trajectory table
C   TLAST....last time driver model calulated a steer value (sec)
C   DFWLST...last value of steer calculated by driver model (rad)
C   TILAST...last sample time driver model calulated a steer value (sec)
C   DMEM.....2-dim array (time & steer history) used in delay calculat'n
C   XT,YT....transformation of XP,YP in vehicle body axes (ft)
C
C---Local variables----------------------------------------------------
C
C  WGHT..total static weight on front and rear suspsensions (lb)
C  DFW...steer angle of front tires [or average] (rad)
C
C---Functions and subroutines------------------------------------------
C
C      None
```

```
C
C=================================================================
C
C==========Process Block==========================================
C
C
C
      GRAV = 32.16666
      TICYCL = 0.000001
      TSS = 0.0
      DMAX = 0.2
C
C  Read & Echo Driver Model Path, Time Delay, and Preview Parameters
C  - OPTIONAL.  May be passed instead from DADS through common blocks
C  and echoed as part of DADS standard I/O
C
      WRITE (W,10)
   10 FORMAT ('0', T20, 'CLOSED-LOOP PATH FOLLOWING MODE', /, '0', T20,
     1       'X-Y ', 'PATH', ' COORDINATES :', /, '0', T50, 'X', T60,
     2       'Y', /, /'0', T47, '(FEET)', T57, '(FEET)')
C
      READ (R,20) NP
   20 FORMAT (I3)
      DO 40 J = 1, NP
        READ (R,30) XP(J), YP(J)
   30   FORMAT (2F10.2)
        WRITE (W,50) XP(J), YP(J)
   40 CONTINUE
   50 FORMAT (' ', T43, 2F10.2)
      READ (R,60) TAUMEM, TFF
   60 FORMAT (F10.4)
      WRITE (W,70) TAUMEM, TFF
   70 FORMAT (' ', /, ' ', T20, 'DRIVER TRANSPORT LAG (SEC) :', T60,
     1       F4.2, /, ' ', T20, 'END OF PREVIEW INTERVAL (SEC) :', T60,
     2       F4.2/)
      RM = (WF + WR) / GRAV
      B = WHBS * WF / (WF + WR)
      A = WHBS - B
      RI = A * B * RM
      PSI0 = 0.0
      NTF = 10
      DO 80 J = 1, NP
        XT(J) = XP(J) * COS(PSI0) + YP(J) * SIN(PSI0)
        YT(J) = -XP(J) * SIN(PSI0) + YP(J) * COS(PSI0)
   80 CONTINUE
      TLAST = 0.
      DFWLST = 0.
      TILAST = 0.
      DFW = 0.
      DO 90 I = 1, 1000
        DMEM(I,1) = 0.
   90 DMEM(I,2) = -1.
      RETURN
      END
C*****************************************************************************
```

```
C*************************************************************************
C
C  ***  Transition Matrix Calculation Subroutine  ***
C
C
C TRANS: Computes transition matrix (and integral) of the linearized
C        system, F, described in references.  Result stored in common
C        arrays TTT and TTT1 repectively.  10 pts per preview interval.
C
C============Author and Modification Section============================
C
C  Author:       C. C. MacAdam
C
C  Date written: 01/01/88
C
C  Written on:
C
C  Modifications:
C
C=======================================================================
C
C============Algorithm Description=====================================
C
C  Purpose and use: Used by the driver model in predicting future states
C
C  Error conditions:
C
C  Machine dependencies: none
C
C  Called By: DRIVGO
C
C=======================================================================
C
      SUBROUTINE TRANS
C
C============Variable Descriptions=====================================
C
C---Arguments passed:  None
C
      INTEGER R, W
      DIMENSION SV(4), SD(4), SVI(4)
C
C---COMMON blocks-----------------------------------------------------
C
      COMMON /DRVST1/ GRAV, TICYCL, TSS, DMAX, XP(100), YP(100), TAUMEM,
     1       TFF, RM, A, B, RI, PSI0, NTF, NP, TLAST, DFWLST, TILAST,
     2       DMEM(1000,2), XT(100), YT(100)
      SAVE/DRVST1/
      COMMON /DRIV/ CAF, CAR, WHBS, WF, WR, U
      SAVE/DRIV/
      COMMON /INOUT/ R, W
      SAVE/INOUT/
      COMMON /TRSSTR/ TTT(4,4,10), TTT1(4,4,10), G(4)
      SAVE/TRSSTR/
C
```

```
C  Control Coefficients A, B, C, D  defined in section 5.5 of
C  reference [1] and passed from DADS through common block VEHTYP
C  ( A = 1, C=1; B = D = k = 0 defines a conventional front steer
C  vehicle, etc. )
C
      COMMON /VEHTYP/ AAA, BBB, CCC, DDD, RATIO
      SAVE/VEHTYP/
C
C---COMMON Variables--------------------------------------------------
C    R.....Driver Model Input I/O unit ("DMINPUT.INP")
C    W.....Driver Model Output I/O unit ("DMOUTPUT.OUT")
C
C---DRIV.BLK common block variables-----------------------------------
C
C  CAF...total cornering stiffness of tires on left front susp (lb/rad)
C  CAR...total cornering stiffness of tires on left rear susp (lb/rad)
C  WHBS..wheelbase of vehicle (center-line of front & rear susp) (ft)
C  WF....static load on front suspension (lb)
C  WR....static load on rear suspension (lb)
C  U.....initial velocity (ft/sec)
C
C---DRVST1.BLK common block variables
C
C   GRAV.....gravitational constant
C   TICYCL...driver model sample time (sec)
C   TSS......minimum preview time (sec)
C   DMAX.....upper bound on front wheel angle steer (rad)
C   XP,YP....x-y path coords(SAE) wrt inertial coords [input] (ft)
C   TAUMEM...driver transport time dealy [input parameter] (sec)
C   TFF......driver model preview time [input parameter] (sec)
C   RM.......vehicle mass (slug)
C   A........distance from c.g. to front suspension center-line (ft)
C   B........distance from c.g. to rear suspension center-line (ft)
C   RI.......total vehicle yaw inertia (slug-ft)
C   PSIO.....current yaw angle reference value (rad)
C   NTF......number of points in the preview time interval
C   NP.......number of points in the x-y trajectory table
C   TLAST....last time driver model calulated a steer value (sec)
C   DFWLST...last value of steer calculated by driver model (rad)
C   TILAST...last sample time driver model calulated a steer value (sec)
C   DMEM.....2-dim array (time & steer history) used in delay calculat'n
C   XT,YT....transformation of XP,YP in vehicle body axes (ft)
C
C---TRSSTR.BLK common block variables---------------------------------
C
C  TTT.......transition matrix at 10 discrete points in preview interval
C  TTT1......integral of trans matrix wrt preview time
C  G.........vector of control gain coefficients
C
C---VEHTYP common block variables-------------------------------------
C
C  AAA....Control coefficient A defined in section 5.5 of ref [1]
C  BBB....Control coefficient B defined in section 5.5 of ref [1]
C  CCC....Control coefficient C defined in section 5.5 of ref [1]
C  DDD....Control coefficient D defined in section 5.5 of ref [1]
```

```
C  RATIO..rear steer / front steer ratio, k, defined in section 5.5
C
C---Local variables---------------------------------------------------
C
C   DELT.....time step in local Euler integration (sec)
C   A1.......lat accel coefficient of sideslip veloc in linearizd system
C   B1.......    "            yaw rate            "
C   A2.......yaw accel    "        sideslip vel        "
C   B2.......    "            yaw rate            "
C   C1.......steer control gain coefficient for lateral accel
C   C2.......steer control gain coefficient for yaw moment
C   ULAST....last value of forward velocity (ft/sec)
C   NBEG.....integer startin counter value
C   NEND1....integer ending counter value
C   NENDV....integer ending counter value
C   J........integer counter
C   SV.......state vector: y,v,r,yaw,x  [SAE]
C   SV1......integral of state vector
C   SD.......state vector derivative
C
C---Functions and subroutines-----------------------------------------
C
C      None
C
C=======================================================================
C
C============Process Block=============================================
C
C
C
C
      DELT = 0.01
      A1 = -2. * (CAF + CAR) / RM / U
      B1 = 2. * (CAR * B - CAF * A) / RM / U  -  U
      A2 = 2. * (CAR * B - CAF * A) / RI / U
      B2 = -2. * (CAR * B * B + CAF * A * A) / RI / U
      C1 = 2. * (CAF + RATIO * CAR) / RM * AAA  +  BBB / RM
      C2 = 2. * (A * CAF - RATIO * B * CAR) / RI * CCC  +  DDD / RI
      ULAST = U
      G(1) = 0.
      G(2) = C1
      G(3) = C2
      G(4) = 0.
      DO 70 J = 1, 4
        NBEG = TSS / DELT + 1
        NEND1 = (TFF + .001 - TSS) / NTF / DELT
        NENDV = NEND1
        DO 10 L = 1, 4
          SV(L) = 0.0
          SVI(L) = 0.0
   10   CONTINUE
        TIME = 0.
C
C  Initialize each state in turn to 1.0 and integrate.
C
```

```
          SV(J) = 1.0
          DO 60 I = 1, NTF
            DO 40 K = NBEG, NENDV
              SD(1) = SV(2) + U * SV(4)
              SD(2) = A1 * SV(2) + B1 * SV(3)
              SD(3) = A2 * SV(2) + B2 * SV(3)
              SD(4) = SV(3)
              DO 20 L = 1, 4
                SV(L) = SV(L) + SD(L) * DELT
    20        CONTINUE
              TIME = TIME + DELT
              DO 30 L = 1, 4
                SVI(L) = SVI(L) + SV(L) * DELT
    30        CONTINUE
    40      CONTINUE
C
C   Store "impulse" responses in TTT columns, integral in TTT1.
C   TTT is a NPT-point tabular transition matrix,  TTT1 is its integral.
C   (See References 2 & 3.)
C
            DO 50 L = 1, 4
              TTT(L,J,I) = SV(L)
              TTT1(L,J,I) = SVI(L)
    50      CONTINUE
            NBEG = NBEG + NEND1
            NENDV = NENDV + NEND1
    60    CONTINUE
    70  CONTINUE
        RETURN
        END
C*******************************************************************************
C*******************************************************************************
C
C   *** Closed-Loop Steer Calculation Subroutine  ***
C
C DRIVER: Computes closed-loop steering control during the simulation
C
C============Author and Modification Section==================================
C
C  Author:        C. C. MacAdam
C
C  Date written: 01/01/88
C
C  Written on:
C
C  Modifications:
C
C===============================================================================
C
C============Algorithm Description============================================
C
C  Purpose and use:
C
C  Error conditions:
C
```

```
C  References:
C
C     [1]       MacAdam, C.C.  "Development of Driver/Vehicle Steering
C                     Interaction Models for Dynamic Analysis," Final
C                     Technical Report, U.S. Army Tank Automotive Command
C                     Contract No. DAAE07-85-C-R069, The University of
C                     Michigan Transportat'n Research Inst, December 1988
C
C     [2]       MacAdam, C.C.  "Application of an Optimal Preview Control
C                     for Simulation of Closed-Loop Automobile Driving,"
C                     IEEE Transactions on Systems, Man, and Cybernetics,
C                     Vol. 11, June 1981.
C
C     [3]       MacAdam, C.C.  "An Optimal Preview Control for Linear
C                     Systems," Journal of Dynamic Systems, Measurement,
C                     and Control, ASME, Vol. 102, No. 3, September 1980.
C
C
C  Machine dependencies: none
C
C  Called By: USER49.F77
C
C=======================================================================
C
      SUBROUTINE DRIVER(X, Y, DFW, DFWNOW)
C
C==========Variable Descriptions=======================================
C
C---Arguments passed:
C
C  ->  X.....time in the simulation (sec)
C  ->  Y.....current driver model state vector obtained from DADS.
C        Driver model state vector of dimension 5 comprised of the
C        following physical quantities: [1] inertial lateral
C        displacement (ft), [2] lateral veloc in body frame (ft/s),
C        [3] yaw rate global (rad/s), [4] SAE global yaw angle (rad),
C        [5] global forward displacement (ft).
C
C  <-  DFW......closed-loop steering control returned to DADS (returned)
C  ->  DFWNOW...current steering angle [average] of front wheels, passed
C      in after effects of roll-steer, compliance, etc.
C
      INTEGER R, W
      DIMENSION Y(5), YC(5)
      DIMENSION DUMV11(4)
      DIMENSION DUMV1(4), VECM(4)
      DIMENSION DUMM1(4,4), DUMM2(4,4)
C
C---COMMON blocks-----------------------------------------------------
C
      COMMON /DRVST1/ GRAV, TICYCL, TSS, DMAX, XP(100), YP(100), TAUMEM,
     1       TFF, RM, A, B, RI, PSI0, NTF, NP, TLAST, DFWLST, TILAST,
     2       DMEM(1000,2), XT(100), YT(100)
      SAVE/DRVST1/
      COMMON /DRIV/ CAF, CAR, WHBS, WF, WR, U
```

```
      SAVE/DRIV/
      COMMON /INOUT/ R, W
      SAVE/INOUT/
      COMMON /TRSSTR/ TTT(4,4,10), TTT1(4,4,10), G(4)
      SAVE/TRSSTR/
C
C  Get Tire Cornering Stiffnesses, Vertical Tire Loads, and Speed
C  from DADS Through Common Block DMTIR
C
      COMMON/DMTIR/CCAF1,CCAF2,CCAR1,CCAR2,FFZL1,FFZL2,FFZL3,FFZL4,
     + DMVELC
C
C---COMMON Variables--------------------------------------------------
C    R.....Driver Model Input I/O unit ("DMINPUT.INP")
C    W.....Driver Model Output I/O unit ("DMOUTPUT.OUT")
C
C---DRIV.BLK common block variables-----------------------------------
C
C  Initial Values from Time Zero:
C
C  CAF...total cornering stiffness of tires on left front susp (lb/rad)
C  CAR...total cornering stiffness of tires on left rear susp (lb/rad)
C  WHBS..wheelbase of vehicle (center-line of front & rear susp) (ft)
C  WF....static load on front suspension (lb)
C  WR....static load on rear suspension (lb)
C  U.....initial velocity (ft/sec)
C
C--- DMTIR.BLK common block variables ------------------------------
C
C  Updates during simulation run:
C
C  CCAF1...Left front tire cornering stiffness from DADS during run
C  CCAF2...Right front tire cornering stiffness from DADS during run
C  CCAR1...Left rear tire cornering stiffness from DADS during run
C  CCAR2...Right rear tire cornering stiffness from DADS during run
C  FFZL1...Left front tire vertical load from DADS during run
C  FFZL2...Right front tire vertical load from DADS during run
C  FFZL3...Left rear tire vertical load from DADS during run
C  FFZL4...Right rear tire vertical load from DADS during run
C  DMVELC...Forward speed from DADS
C
C---DRVST1.BLK common block variables -------------------------------
C
C   GRAV.....gravitational constant
C   TICYCL...driver model sample time (sec)
C   TSS......minimum preview time (sec)
C   DMAX.....upper bound on front wheel angle steer (rad)
C   XP,YP....x-y path coords(SAE) wrt inertial coords [input] (ft)
C   TAUMEM...driver transport time dealy [input parameter] (sec)
C   TFF......driver model preview time [input parameter] (sec)
C   RM.......vehicle mass (slug)
C   A........distance from c.g. to front suspension center-line (ft)
C   B........distance from c.g. to rear suspension center-line (ft)
C   RI.......total vehicle yaw inertia (slug-ft)
C   PSIO.....current yaw angle reference value (rad)
```

```
C   NTF......number of points in the preview time interval
C   NP.......number of points in the x-y trajectory table
C   TLAST....last time driver model calulated a steer value (sec)
C   DFWLST...last value of steer calculated by driver model (rad)
C   TILAST...last sample time driver model calulated a steer value (sec)
C   DMEM.....2-dim array (time & steer history) used in delay calculat'n
C   XT,YT....transformation of XP,YP in vehicle body axes (ft)
C
C---TRSSTR.BLK common block variables --------------------------------
C
C  TTT.......transition matrix at 10 discrete points in preview interval
C  TTT1......integral of trans matrix wrt preview time
C  G.........vector of control gain coefficients
C
C---Local variables--------------------------------------------------
C
C   YC.......local (body-axis based) copy of state vector Y
C   VECM.....observer vector - lateral displacement from state vector
C   DUMV1....work vector
C   DUMV11...   "
C   DUMM1....work matrix
C   DUMM2....   "
C   T........time in the simulation (sec)
C   EPSI.....yaw angle between body axis and current index value, PSI0
C   PSIO.....current nominal value of yaw angle used for linearization
C   NP.......number of points in x-y path table
C   XP,YP....x-y inertial path table [input] (ft)
C   XT,YT....x-y path table transformed to body axis [PSIO] system (ft)
C   EPSY2....cumulative preview path error squared
C   EPSY.....mean squared value of cumulative preview path error
C   TSUM.....scalar work quantity
C   SSUM.....scalar work quantity
C   DFWLST...steering control from last calculation (rad)
C   TJI......preview time ahead from present time value (sec)
C   I,J,K....integer counters
C   XCAR.....preview distance ahead in feet (ft)
C   X0.......present forward postion of vehicle c.g. (ft)
C   TTAB.....current time less the driver delay, TAUMEM. Used to access
C         the delayed driver response stored in DMEM array. (sec)
C   S1.......scalar work quantity
C   T1.......scalar work quantity
C   EP.......previewed path error (ft)
C
C---Functions and subroutines----------------------------------------
C
       EXTERNAL TRAJ, GMPRD
C
C=====================================================================
C
C============Process Block============================================
C
C
      DATA VECM /1.0, 3*0.0/
C
   1  T = X
```

```
      EPSI = ABS(Y(4) - PSI0)
      DO 10 I = 1, 5
   10 YC(I) = Y(I)
      IF (EPSI .LE. .0002) GO TO 30
C
C  Update Coordinate Transformation
C
      PSI0 = Y(4)
      DO 20 J = 1, NP
        XT(J) = XP(J) * COS(PSI0) + YP(J) * SIN(PSI0)
   20 YT(J) = -XP(J) * SIN(PSI0) + YP(J) * COS(PSI0)
C
   30 Y0 = -Y(5) * SIN(PSI0) + Y(1) * COS(PSI0)
      X0 = Y(5) * COS(PSI0) + Y(1) * SIN(PSI0)
      YC(1) = Y0
      YC(4) = Y(4) - PSI0
      EPSY2 = 0.
      TSUM = 0.
      SSUM = 0.
      DFW = DFWLST
C
C  Return if time from last calculation less than sample interval
C
      IF (T - TILAST .LE. TICYCL) RETURN
C
C  The next 6 lines of executable code may be commented out to
C  bypass continuous updating of the transition matrices, if not
C  required.  See section 5.8 of reference 1.
C
C  Update tire cornering stiffnesses and vehicle velocity
C  and recalculate transition matrix:
C
      CAFTEM = (CCAF1*FFZL1+CCAF2*FFZL2) / (FFZL1+FFZL2)
      CARTEM = (CCAR1*FFZL3+CCAR2*FFZL4) / (FFZL3+FFZL4)
      CAF = CAFTEM
      CAR = CARTEM
      U = DMVELC
C
C  Update Transition Matrices
C
      CALL TRANS
C
C  Loop to calculate optimal preview control per References 2 & 3:
C   (NTF points within the preview interval)
C
      DO 50 I = 1, NTF
        TJI = (TFF - TSS) / NTF * I + TSS
        DO 40 J = 1, 4
          DO 40 K = 1, 4
            DUMM1(J,K) = TTT1(J,K,I)
   40   DUMM2(J,K) = TTT(J,K,I)
        CALL GMPRD(VECM, DUMM1, DUMV11, 1, 4, 4)
        CALL GMPRD(VECM, DUMM2, DUMV1, 1, 4, 4)
        CALL GMPRD(DUMV1, YC, T1, 1, 4, 1)
C
```

```
C  Get observed path input, YPATH, within preview interval at XCAR ft:
C
      XCAR = X0 + U * TJI
      CALL TRAJ(XCAR, XT, YT, YPATH)
C
      CALL GMPRD(DUMV11, G, S1, 1, 4, 1)
C
C  EP is the previewed path error at this preview point.
C
      EP = T1 + S1 * DFWNOW - YPATH
      TSUM = TSUM + EP * S1
      SSUM = SSUM + S1 * S1
C
C  Cumulative preview error calculation (unrelated to control)
C
      EPSY2 = EPSY2 + EP * EP * (TFF - TSS) / NTF
C
   50 CONTINUE
C
C  Cumulative preview error calculation (unrelated to control)
C
      EPSY = SQRT(EPSY2) / (TFF - TSS)
C
C  Optimal value - no delay yet.
C
      DFW = -TSUM / SSUM + DFWNOW
C
C  Maximum steer bound set at DMAX (arbitrary)
C
      IF (ABS(DFW) .GT. DMAX) DFW = DMAX * SIGN(1.,DFW)
C
C  Store steer history and corresponding times in DMEM.
C  Retrieve steer delayed by TAUMEM sec and return as
C  delayed driver steer control, DFW.
C
      DO 60 J = 1, 2
        DO 60 I = 1, 999
   60 DMEM(1001 - I,J) = DMEM(1000 - I,J)
      DMEM(1,1) = DFW
      DMEM(1,2) = T
      TTAB = T - TAUMEM
      DO 70 I = 1, 999
        IF (DMEM(I + 1,2) .LE. TTAB .AND. DMEM(I,2) .GE. TTAB)
     1     GO TO 90
   70 CONTINUE
      WRITE (W,80)TAUMEM,DFW,X
   80 FORMAT ('0', '***** TAUMEM PROBABLY TOO LARGE *****',
     &        /,3(1X,G12.6))
      CALL EXIT
   90 DFW = DMEM(I,1)
C
C  Save steer and time values for next calulation.
C
      DFWLST = DFW
      TLAST = X
```

```
      TILAST = X
      RETURN
      END
C*******************************************************************************
C*******************************************************************************
C
C    *** Trajectory Subroutine ***
C
C TRAJ: Computes lateral displacement of previewed path as a table
C       look-up
C
C============Author and Modification Section==============================
C
C  Author:       C. C. MacAdam
C
C  Date written: 01/01/88
C
C  Written on:
C
C  Modifications:
C
C=======================================================================
C
C============Algorithm Description=======================================
C
C  Purpose and use:
C
C  Error conditions:
C
C  Machine dependencies: none
C
C  Called By: DRIVER
C
C=======================================================================
C
      SUBROUTINE TRAJ(X, XT, YT, YPATH)
C
C============Variable Descriptions=======================================
C
C---Arguments passed:
C
C  ->X.......forward displacement (ft)
C  ->XT......longitudinal path coordinates (ft)
C  ->YT......lateral path coordinated corresponding to XT values (ft)
C  <-YPATH...lateral displacement of path corresponding to X, (ft)
C
C
      INTEGER R, W
      DIMENSION XT(*), YT(*)
C
C---COMMON blocks-----------------------------------------------------
C
      COMMON /INOUT/ R, W
      SAVE/INOUT/
C
```

```
C---COMMON Variables--------------------------------------------------
C    R.....Driver Model Input I/O unit ("DMINPUT.INP")
C    W.....Driver Model Output I/O unit ("DMOUTPUT.OUT")
C
C---Local variables---------------------------------------------------
C
C  J.......integer counter
C  SLOPE...dYT/dXT of path at X
C
C---Functions and subroutines-----------------------------------------
C
C      None
C
C=================================================================
C
C============Process Block=======================================
C
C  SEARCH FOR XI,XI+1:
      DO 10 J = 1, 99
        IF (X .GE. XT(J) .AND. X .LT. XT(J + 1)) GO TO 30
   10 CONTINUE
      WRITE (W,20)
   20 FORMAT ('0', 'X-SEARCH IN SUB. TRAJ FAILED.')
      CALL EXIT
   30 SLOPE = (YT(J + 1) - YT(J)) / (XT(J + 1) - XT(J))
      YPATH = YT(J) + SLOPE * (X - XT(J))
      RETURN
      END
C*****************************************************************
C*****************************************************************
C
C  *** Matrix Product  Subroutine ***
C
C GMPRD: Computes matrix product
C
C============Author and Modification Section=====================
C
C  Author:       IBM Scientific Subroutine
C
C  Date written:
C
C  Written on:
C
C  Modifications:  C. MacAdam
C
C=================================================================
C
C============Algorithm Description===============================
C
C  Purpose and use:  R = A B
C
C  Error conditions:
C
C  Machine dependencies: none
C
```

```
C  Called By: DRIVER
C
C=============================================================================
C
      SUBROUTINE GMPRD(A, B, R, N, M, L)
C
C============Variable Descriptions============================================
C
C---Arguments passed:
C
C   A.....N x M matrix
C   B.....M x L matrix
C   R.....N x L resultant matrix = A B product
C   N.....integer row dimension of A
C   M.....integer column dimension of A (or row dimension of B)
C   L.....integer column dimension of B
C
      DIMENSION A(N*M), B(M*L), R(N*L)
C
C---COMMON blocks-----------------------------------------------------------
C
C     None
C
C---COMMON Variables--------------------------------------------------------
C
C     None
C
C---Local variables---------------------------------------------------------
C
C  IR, IK, M, K, L, IR, JI, J, N, IB, IK, etc ......integer counters
C
C---Functions and subroutines-----------------------------------------------
C
C      None
C
C=============================================================================
C
C============Process Block=====================================================
C
      IR = 0
      IK = -M
      DO 10 K = 1, L
        IK = IK + M
        DO 10 J = 1, N
          IR = IR + 1
          JI = J - N
          IB = IK
          R(IR) = 0.
          DO 10 I = 1, M
            JI = JI + N
            IB = IB + 1
   10 R(IR) = R(IR) + A(JI) * B(IB)
      RETURN
      END
C*****************************************************************************
```

Appendix E

FORTRAN DADS / Driver Model Interface Code

This appendix contains FORTRAN code that was used by the CADSI / DADS program at TACOM to call the driver model code appearing in Appendix D or to calculate information for its use with DADS. Most of this code was developed by TACOM personnel and is included here to illustrate the calling mechanisms used to interface the DADS code to the driver model of Appendix D.

The following subroutines are listed in this appendix:

- **USER49** called by DADS; USER49 calls DRIVER of Appendix D
- **TIREF** called by DADS for tire forces / cornering stiffnesses
- **FILTER** called by USER49
- **EULANG** called by USER49

USER49 is the primary interface between DADS and the driver model and is used to control external calls to user-defined functions. TIREF is included to show how the tire cornering stiffnesses are calculated and stored in a common block for use by the driver model routine DRIVER.

The subroutine FILTER is a second order filter called by USER49 to obtain first and second order derivatives of the driver steering control returned by DRIVER. These derivatives were required by DADS for the constraint calculations associated with the pitman arm steering mechanism. An additional FILTER call was used to further smooth the derivative time histories. Small delays introduced by the filtering were compensated by reducing the driver model time delay parameter.

EULANG is an auxilliary subroutine used to calcuate and write out to an external file Euler angle and position information for subsequent animation processing at UMTRI. (optional)

```
C
C  USER49: Calculates User supplied values for the driving function
C
C============Author and Modification Section==============================
C
C  Author:        James A. Aardema, C. MacAdam
C
C  Date written: 07/01/87, 02/01/88
C
C  Written on:
C
C  Modifications:
C
C=======================================================================

C============Algorithm Description=======================================
C
C  Purpose and use:
C
C  Error conditions:
C
C  Machine dependencies: none
C
C  Called By: FUN49.FOR
C
C=======================================================================

      SUBROUTINE USER49 ( IRE, FN, AJ, ND, DRV, IDRV, Q, QD, A, IA,
     &                    MPTRS, NPTRS, RB, NPRB, QDR, QDDR, NB, RVLT,
     &                    TRAN, CYL, NPRT, NPTRN, NPCYL, QDD,
     &                    CST, CSTD, CSTDD, IDRIVER )

C============Variable Descriptions=======================================
C
C---Arguments passed--------------------------------------------------
C
C   ND    ................ number of driving constraint
C   IA    ................ total integer array
C   A     ................ total real array
C   IDRV  ...IA(MP(12))... integer array for the driving constraint
C   NPTRS ................ real data item per constraint
C   TRAN ................. Real data for the translational joint.
C   CYL .................. Real data for the cylindrical joint.
C   RVLT ................. Real data for the revolute joint.
C   NPTRN ................ Number of real data per translational joint.
C   NPCYL ................ Number of real data per cylindrical joint.
C   NPRT ................. Number of real data per revolute joint.
C   DRV   ....A(NP(12))... real data for driving constraint
C   Q     ....A( N1  )..... position
C   QD    ....A( N2  )..... velocity
C   QDD   ....A( N3  )..... acceleration
C   QDR   ....Q(IQ(MM))... position
C   QDDR  ....QD(IQ(MM)).. velocity
```

```
C   AJ    ....A( N5  )....  Jacobian matrix
C   FN    ....A( N8  )....  temporary array for the constraint equation
C                           r.h.s. of velocity or acceleration equation
C   IRE   ...IA( M7  )....  flag for redundant constraint
C   NB    ..............    number of rigid bodies in the model
C   CST    ... driving function
C   CSTD   ... first derivative of driving function
C   CSTDD  ... second derivative of driving function
C   IDRIVER...Current driver being analyzed

      INTEGER  MPTRS, NPTRS, ND, IDRV(MPTRS,ND), IA(0:1),
     &         IRE(1),NPRB, NB, NPTRN, NPCYL, NPRT, IDRIVER

      DOUBLE PRECISION  FN(1), AJ(1), DRV(NPTRS,ND), Q(7,1), QD(7,1),
     &                  RB(NPRB,NB), QDR(1), QDDR(1), A(0:1),
     &                  TRAN(NPTRN,1), CYL(NPCYL,1), RVLT(NPRT,1),
     &                  QDD(7,1), CST, CSTD, CSTDD
C
C---COMMON blocks-----------------------------------------------------

$INSERT CADSI>DADS4.DIR>COMMON>STEPHT

$INSERT CADSI>HMMWV>STEER>COMMON>UPLOT.BLK

C---COMMON Variables--------------------------------------------------
C
C---STEPHT common block variables-------------------------------------
C
C  H........Integration predictor step size.
C  HMAX.....Maximum integration predictor step size.
C  TSTART...Time at the start of the simulation.
C  TEND.....Time when simulation is to stop.
C  TSTEP....Integration step size.
C  T........Current time during the simulation.
C  HSTLEN...Length of the history arrays.
C  HSTPTR...Pointer to the last used location in the history arrays.
C  HSTCNT...Count of the number of time steps for which integration
C           history was saved.
C  HSTH.....Past history of the integration time step.
C  HSTK.....Past history of the integration order.
C  HSTERR...Past history of the integration error estimate.
C
C---UPLOT.BLK Common Variables----------------------------------------
C
C   UPLOT....Array for storing user variables
C   NPLOT....Number of plot variables used
C
C---Local variables---------------------------------------------------
C
C    K11.... EQ.0 : do not evaluate Jacobian matrix
C            EQ.1 : evaluate Jacobian matrix
C    K22.... EQ.1 : evaluate Jacobian matrix
C            EQ.2 : evaluate constraint equation
C            EQ.3 : evaluate r.h.s. of the velocity equation
C            EQ.4 : evaluate r.h.s. of the acceleration equation
```

```
C   JB1    ... first body number of driving constraint is imposed
C   JB2    ... second body number of driving constraint is imposed
C   JTYPE .. type of driving constraint joint.
C            =1 Revolute joint
C            =2 Cylindrical joint
C            =3 Translational joint
C   FTYPE .. Driving function.
C             EQ.1 : polynomial driving function
C                    coeff1 + coeff2*T + coeff3*T**2 + coeff4*T**3
C             EQ.2 : harmonic driving function
C                    coeff1 + coeff2 * SIN ( coeff3*T - coeff4 )
C             EQ.3 : general driving function
C
C             coefficients of the driving functions
C             polynomial          harmonic          general
C
C    coeff1:  constant term       constant term     not used
C    coeff2:  1st order coef.     amplitude         not used
C    coeff3:  2nd order coef.     frequency         not used
C    coeff4:  3rd order coef.     phase shift       not used
C
C   DTYPE ...Type of constraint defined:
C             EQ.1 : constrain Xpi
C             EQ.2 : constrain Ypi
C             EQ.3 : constrain Zpi
C             EQ.4 : constrain Xpj - Xpi
C             EQ.5 : constrain Ypj - Ypi
C             EQ.6 : constrain Zpj - Zpi
C             EQ.7 : constrain distance between two position
C             EQ.8 : relative angle constraint on revolute or cylin-
C                    drical joint
C             EQ.9 : constrain relative position on translational or
C                    cylindrical joint
C   FT     ... value of general curve
C   NZHS   ... pointer for Jacobian array
C   ITEMP  ... temporary value
C   PNTR   ... pointer into the input data array
C   DNAME  ... name of a distance driver
C   JN ... joint number.
C   ICHS...Body number of the chassis

      INTEGER  JB1, JB2, DTYPE, JTYPE, K11, K22, NZHS, ITEMP,
     &         PNTR, FTYPE, JN, ICHS

      DOUBLE PRECISION  ACHS(3,3), PHI, STEER, DSTEER, DDSTEER

      REAL*4 Y(5), DFWOUT, DFWOLD, DF, DFVEL, DFACC, DFF
      REAL TDRIV
      REAL*4 A1LST,B1LST,C1LST,D1LST,E1LST,A2LST,B2LST,
     1 C2LST,D2LST,E2LST

      CHARACTER*20  DNAME

C
C---Functions and subroutines----------------------------------------
```

```
C
      EXTERNAL  FSPLIN, SIMDR, ELMDR, DISTDR, TRANDR, SINE, COSINE,
     &          TRULEN, DRIVER, FILTER
      EXTERNAL EULANG

      INTEGER   TRULEN

      DOUBLE PRECISION  FSPLIN
      DOUBLE PRECISION YANIM(3)

      INTRINSIC  DCOS, MOD, DSIN, DABS, DATAN, DSIGN, DATAN2,
     &           SNGL, DBLE
      SAVE DFWOLD
      SAVE  A1LST,B1LST,C1LST,D1LST,E1LST,A2LST,B2LST,
     1 C2LST,D2LST,E2LST
C
C=======================================================================


C============Process Block=============================================
C
C  Initalize filter varaibles to zero at start.
C
      IF(T .LE. 0.001) THEN
        DFWOUT = 0.0
        STEER = 0.0
        A1LST=0.0
        B1LST=0.0
        C1LST=0.0
        D1LST=0.0
        E1LST=0.0
        A2LST=0.0
        B2LST=0.0
        C2LST=0.0
        D2LST=0.0
        E2LST=0.0
      ENDIF

C---Get the chassis body number

      ICHS = IDRV(1,IDRIVER)    /* IDRIVER is the current driver being
analyzed

C---Get the chassis transformation matrix

      ACHS(1,1) = RB(38,ICHS)
      ACHS(2,1) = RB(39,ICHS)
      ACHS(3,1) = RB(40,ICHS)
      ACHS(1,2) = RB(41,ICHS)
      ACHS(2,2) = RB(42,ICHS)
      ACHS(3,2) = RB(43,ICHS)
      ACHS(1,3) = RB(44,ICHS)
      ACHS(2,3) = RB(45,ICHS)
      ACHS(3,3) = RB(46,ICHS)
C
```

```
C  Call to EulAng for Animation Output
C
       YANIM(1) = Q(2,ICHS) / 12.
       YANIM(2) = Q(1,ICHS) / 12.
       YANIM(3) = -(Q(3,ICHS) - RB(20,ICHS)) / 12.
       CALL EULANG(T, YANIM, ACHS)
C

       Y(2) = SNGL( ACHS(1,1)*QD(1,ICHS) +
      &             ACHS(2,1)*QD(2,ICHS) +
      &             ACHS(3,1)*QD(3,ICHS))/12.0   /* lateral velocity in
body cs

C---Get the current vehicle global position
C
C  SAE conventions used to define position and orientation for driver
C  model arguments passed in:
C
C  Y(1)  lateral SAE global position (DADS global X)
C  Y(2)  SAE body sideslip velocity component (see above)
C  Y(3)  SAE yaw rate (DADS:  minus "PHIDOT")
C  Y(4)  SAE Yaw angle (DADS:  minus "PHI")
C  Y(5)  forward SAE global position (DADS global Y)

       Y(1) = SNGL(Q(1,ICHS))/12.0     /* LATERAL DISPLACEMENT - SAE
       Y(5) = SNGL(Q(2,ICHS))/12.0     /* FORWARD DISPLACEMENT - SAE

       Y(3)  = -SNGL(RB(34,ICHS))       /* SAE YAW RATE - GLOBAL
       PHI = DATAN2(ACHS(1,2), ACHS(2,2) )  /*  SAE YAW ANGLE
       Y(4) =  SNGL(PHI)
C
C  Plot variables:
C
        UPLOT(NPLOT+1) = DBLE(Y(1))
        UPLOT(NPLOT+2) = DBLE(Y(2))
        UPLOT(NPLOT+3) = DBLE(Y(3))
        UPLOT(NPLOT+4) = DBLE(Y(4))
        UPLOT(NPLOT+5) = DBLE(Y(5))

C---Calculate the steering control from the steering model
C   If STEER > 0.0 Turn Right
C   If STEER < 0.0 Turn Left

      TDRIV = SNGL(T)
C
C  Call to Driver Model:
C
       CALL DRIVER ( TDRIV, Y, DFWOUT, DFWOLD )
C
C  Filter DFWOUT steering control from DRIVER for derivatives DFVEL
C  and DFACC:
C
       CALL FILTER(TDRIV,DFWOUT,DF,DFVEL,DFACC,A1LST,B1LST,C1LST,
     1 D1LST,E1LST)
C
```

```
C  Plot variables:
C
        UPLOT(NPLOT+6) = DBLE(DFWOUT)
        UPLOT(NPLOT+7) = DBLE(DFWOLD)
        UPLOT(NPLOT+8) = DBLE(0.0)

       UPLOT(NPLOT+9) = DBLE(DF)
       UPLOT(NPLOT+10) = DBLE(DFVEL)
       UPLOT(NPLOT+11) = DBLE(DFACC)
C
C  Further smoothing (optional):
C
        CALL FILTER(TDRIV,DF,DFF,DFVEL,DFACC,A2LST,B2LST,C2LST,
     1 D2LST,E2LST)
        DFWOLD = DFF
C
        STEER   = DBLE(DFF)
        DSTEER  = DBLE(DFVEL)
        DDSTEER = DBLE(DFACC)
C
C  Plot variables:
C
        UPLOT(NPLOT+12) = STEER
        UPLOT(NPLOT+13) = DSTEER
        UPLOT(NPLOT+14) = DDSTEER

C---Calculate the pitman arm angle from the tire steering angle
C   The ratio between steering angle and pitman arm angle is 1.166D0

       CST   = 1.166D0 * STEER
       CSTD  = 1.166D0 * DSTEER
       CSTDD = 1.166D0 * DDSTEER


C       CST = FSPLIN(T, 0.0, IDRV(5,IDRIVER), 1, A, IA, 0, 0)
C       IF ( ERRCOD .NE. 0 ) RETURN
C       CSTD = FSPLIN(T, 0.0, IDRV(5,IDRIVER), 1, A, IA, 1, 0)
C       IF ( ERRCOD .NE. 0 ) RETURN
C       CSTDD = FSPLIN(T, 0.0, IDRV(5,IDRIVER), 1, A, IA, 2, 0)
C       IF ( ERRCOD .NE. 0 ) RETURN

C---Pitman arm travel is limited to 38.25 degrees or 0.668 radians

       IF ( DABS(CST) .GE. 0.668D0 ) THEN
          CST   = DSIGN(0.668D0,CST)
          CSTD  = 0.0D0
          CSTDD = 0.0D0
       ENDIF

C       PRINT*, ' '
C       PRINT*, 'H...Integration predictor step size', H

       RETURN
       END
C
```

```
C
C---TIREF: Calculates the forces exerted on the tire through the road.

C============Author and Modification Section==============================
C
C  Author:        James A. Aardema, Rick Mousseau, Roger Weahage
C
C  Date written: Unknown
C
C  Written on:
C
C  Modifications:
C
C=======================================================================

C============Algorithm Description=======================================
C
C  Purpose and use:      Calculates the slip angle, lateral,
C                        longitudinal, and normal tire forces for a
C                        point follower tire model.
C
C=======================================================================

      SUBROUTINE TIREF ( I, Q, QD, QDD, FRC, ITIR, TIR, RB, A, IA,
     &                   NB, NTR, MPTRS, NPTRS, NPRB, UDE, DUDE, NWHDE )


      IMPLICIT DOUBLE PRECISION (A-H,P-Z)

C============Variable Descriptions=======================================
C
C---Arguments passed--------------------------------------------------
C
C  I......Current tire being calculated
C  Q......Array of generalized coordinates.
C  QD.....Array of velocities.
C  QDD....Array of acceleration values.
C  FRC....Array of generalized forces.
C  ITIR...Array of integer data from this module.
C  TIR....Array of real data from this module.
C  RB.....Array of rigid body real data.
C  A......Vector of all real data.
C  IA.....Vector of all integer data.
C  NB.....Number of rigid bodies.
C  NTR....Number of tire elements.
C  NPTRS..Number of real data per element.
C  MPTRS..Number of integer data per element.
C  NPRB...Number of real data per rigid body.
C  UDE....Array of user differential equations, Position terms
C  DUDE...Array of user differential equations, Velocity terms

      INTEGER NTR, MPTRS, NPTRS, NPRB, NWHDE,
```

```
     &        NB, IA(0:1), ITIR(MPTRS,NTR), I

      DOUBLE PRECISION A(0:1), Q(7,1), QD(7,1), QDD(7,I), FRC(7,1),
     &                 TIR(NPTRS,NTR), RB(NPRB,NB),
     &                 UDE(NWHDE), DUDE(NWHDE)

C
C---COMMON blocks-----------------------------------------------------------
C
$INSERT CADSI>DADS4.DIR>COMMON>STEPHT
$INSERT CADSI>DADS4.DIR>COMMON>PARAM
$INSERT CADSI>DADS4.DIR>COMMON>POTEN

$INSERT CADSI>HMMWV>STEER>COMMON>ALTOR1.BLK
$INSERT CADSI>HMMWV>STEER>COMMON>ALTOR2.BLK
$INSERT CADSI>HMMWV>STEER>COMMON>RUNFLAT.BLK
$INSERT CADSI>HMMWV>STEER>COMMON>SDFRC1.BLK
$INSERT CADSI>HMMWV>STEER>COMMON>SDFRC2.BLK
C
C  Used to pass tire cornering stiffnesses and loads to driver model:
C
$INSERT CADSI>HMMWV>STEER>COMMON>DMTIR.BLK

C---STEPHT common Variables-------------------------------------------------
C
C  H........Integration predictor step size.
C  HMAX.....Maximum integration predictor step size.
C  TSTART...Time at the start of the simulation.
C  TEND.....Time when simulation is to stop.
C  TSTEP....Integration step size.
C  T........Current time during the simulation.
C  HSTLEN...Length of the history arrays.
C  HSTPTR...Pointer to the last used location in the history arrays.
C  HSTCNT...Count of the number of time steps for which integration
C           history was saved.
C  HSTH.....Past history of the integration time step.
C  HSTK.....Past history of the integration order.
C  HSTERR...Past history of the integration error estimate.
C
C
C----PARAM.BLK Common Variables---------------------------------------------
C
C  This file contains a number of constants which are used in various
C  subroutines throughout the code and are stored here to insure
C  accuracy and make any changes easier.
C
C    PI.......pi
C    TWOPI....two times pi
C    DEGRAD...degrees per radian
C    MCHEPS...machine epsilon
C    BODMOD...number of the rigid body module
C    CRVMOD...number of the curve module
C    INPEPS...epsilon value used to check error in normalized input
C             values
C
```

```
C---POTEN Common Variables-----------------------------------------
C
C    MSTAT.....Flag controling whether total energy is to be calculated.
C    V.........Scalar of potential energies.
C    VBGN......Working vector.
C    F.........Function value working vector.
C
C---ALTOR1.BLK Common Variables-------------------------------------
--
C
C     NSA1......Number of slip angle points
C     NFZ1......Number of vertical force points
C     SANGLE1...Array containing the slip angle points
C     FZ1.......Array containing the vertical points
C     ALTOR1....Grid array containing the aligning torque values
C     IPSA1.....Array containg slip angle pointers
C     IPFZ1.....Array containg vertical force pointers
C
C---ALTOR2.BLK Common Variables-------------------------------------
--
C
C     NSA2......Number of slip angle points
C     NFZ2......Number of vertical force points
C     SANGLE2...Array containing the slip angle points
C     FZ2.......Array containing the vertical points
C     ALTOR2....Grid array containing the aligning torque values
C     IPSA2.....Array containg slip angle pointers
C     IPFZ2.....Array containg vertical force pointers
C
C---RUNFLAT.BLK Common Variables------------------------------------
C
C     RFRAD....Run Flat Radius
C     RFSTIF...Run Flat Stiffness
C     RFDAMP...Run Flat Damping
C
C---SDFRC1 Common Variables-----------------------------------------
C
C     SFRC1(20,20).
C     ALREF1(20)...
C     FZREF1(20)...
C     IPA1(20).....
C     IPF1(20).....
C     NAPNT1.......
C     NFPNT1.......
C
C---SDFRC1 Common Variables-----------------------------------------
C
C     SFRC2(20,20).
C     ALREF2(20)...
C     FZREF2(20)...
C     IPA2(20).....
C     IPF2(20).....
C     NAPNT2.......
C     NFPNT2.......
C
```

```
C---Local variables-----------------------------------------------------
C
C     IBDY.....ITIR(1,I)...Body number wheel is attached to
C     ICHS.....ITIR(2,I)...Body number defined as the chassis
C     IUTIL....ITIR(3,I)...Utility curve number
C     ITK......ITIR(4,1)...Vertical Spring rate Curve number
C     ILNG.....ITIR(5,1)...Torque Curve number
C     ISTR.....ITIR(6,I)...Steer Curve number
C     TYPE.....ITIR(7,I)...Model type
C     RC(1)....TIR(1,I)....Wheel center postion in local coordinates
C     RC(2)....TIR(2,I)
C     RC(3)....TIR(3,I)
C     RAD......TIR(4,I)....Tire Radius
C     RR.......TIR(5,I)....Rolling Resistance
C     TD.......TIR(6,I)....Tire Damping constant
C     TK.......TIR(7,I)....Tire Vertical Spring Stiffness
C     CALP.....TIR(8,I)....Lateral Stiffness of the tire
C     STRAG....TIR(9,I)....Steer angle
C     MU.......TIR(10,I)...Friction Coefficient
C     YAW......TIR(11,I)...Yaw angle of the wheel body
C     VX.......TIR(12,I)...Velocity of wheel center in road system
C     VY.......TIR(13,I)
C     VZ.......TIR(14,I)
C     TIRE1....TIR(15,I)...Global position of the tire center
C     TIRE2....TIR(16,I)
C     TIRE3....TIR(17,I)
C     TIREX....TIR(18,I)...Global postion of the tire bottom
C     TIREY....TIR(19,I)
C     TIREZ....TIR(20,I)
C     ZROAD....TIR(21,I)...Ground Elevation
C     DEFL.....TIR(22,I)...Tire Deflection - Ground Penetration
C     FSPR.....TIR(23,I)...Spring Force
C     FDAMP....TIR(24,I)...Damping Force
C     FNORM....TIR(25,I)...Normal Force
C     SLIP.....TIR(26,I)...Tire Slip
C     FLAT.....TIR(27,I)...Lateral force
C     S........TIR(28,I)...Longitudinal slip
C     FLONG....TIR(29,I)...Longitudinal force
C     GFRC.....TIR(30,I)...Wheel torque
C     PENRF....TIR(31.I)...Penetration into the run flat assembly
C     FRF......TIR(32,I)...Run flat force due to penetration onto run
flat
C     ALGNTQ...TIR(33,I)...Aligning Torque due to lateral slip
C     FNTEMP...............Tempary Variable to hold normal force
C     ANGV.................Angular Velocity of the wheel
C     SCO..................Absoulute value of the longitudinal slip
C     FCOEF................Coefficient relating long force and normal
force
C     FMAX.................Maximum force on tire allowed by friction
C     FTOT.................Magniutude of the force on the tire
C     RATIO................Ratio between Maximum and total force
C     CSTIFF...............Conering Stiffness at the given point in the
carpet p
lot
C                          (Currently not used for anything )
```

```
      INTEGER   IBDY, ICHS, IUTIL, ITK, ILNG, ISTR, TYPE

      DOUBLE PRECISION RC(3), RAD, RR, TD, TK, CALP, STRAGL, MU,
     &                 YAW, VX, VY, VZ, TIRE1, TIRE2, TIRE3,
     &                 TIREX, TIREY, TIREZ, ZROAD,
     &                 DEFL, FSPR, FDAMP, FNORM, SLIP, FLAT,
     &                 S, FLONG, GFRC, FRF, PENRF,
     &                 FNTEMP, ANGV, SCO, FCOEF, FMAX, FTOT,
     &                 RATIO, ALGNTQ, CSTIFF

C---Functions and subroutines-----------------------------------------

      DOUBLE PRECISION FSPLIN,  CUBIC, CUBIC1, CARPET

      EXTERNAL         FSPLIN,  CUBIC, CUBIC1, CARPET

      INTRINSIC        DABS, DSIGN, DCOS, DSIN, DATAN2,
     &                 DSQRT, DMAX1

C==========Process Block=================================================

C---Initialize the output quanities to zero in case wheel is off ground

      FLONG  = 0.0D0                    /* Tire Longitudinal force
      GFRC   = 0.0D0                    /* turning wheel torque
      FLAT   = 0.0D0                    /* Tire Lateral force
      ALGNTQ = 0.0D0                    /* Aligning Torque

      FSPR   = 0.0D0                    /* Tire Spring Force
      FDAMP  = 0.0D0                    /* Tire Damping Force
      FNORM  = 0.0D0                    /* Total Normal Force
      FRF    = 0.0D0                    /* Run Flat Force
      PENRF  = 0.0D0                    /* Penetration into run flat
      SLIP   = 0.0D0                    /* Lateral Slip
      S      = 0.0D0                    /* Longintudinal Slip

C---Calculate the tire-spring deflection.
C   Difference between road elevation and tire bottom elevation
C   Ground  penetration  if DEFL >  0.0
C   Wheel off the ground if DEFL <= 0.0

      TIREZ = TIR(20,I)
      ZROAD = TIR(21,I)
      DEFL  = ZROAD - TIREZ

C---Calculate the normal force from ground if the wheel has deflected
C   into the ground.  If the tire is not deflected there are no
C   forces on the tire, skip to the end

      IF ( DEFL .LE. 0.0D0 ) THEN
        DEFL = 0.0D0
        GOTO 1000
      ENDIF
```

```
C---The wheel has penetrated the ground so we must calculate tire forces

C---Get variables from ITIR and TIR arrays

C     IBDY  = ITIR(1,I)          /* Body number wheel is attached to
      ICHS  = ITIR(2,I)          /* Body number defined as the chassis
      IUTIL = ITIR(3,I)          /* Utility curve number
      ITK   = ITIR(4,1)          /* Vertical Spring rate Curve number
      ILNG  = ITIR(5,1)          /* Torque Curve number
      ISTR  = ITIR(6,I)          /* Steer Curve number
C     TYPE  = ITIR(7,I)          /* Model type

C     RC(1) = TIR(1,I)           /* Wheel center postion in local
coordinates
C     RC(2) = TIR(2,I)
C     RC(3) = TIR(3,I)
      RAD   = TIR(4,I)           /* Tire Radius
      RR    = TIR(5,I)           /* Rolling Resistance
      TD    = TIR(6,I)           /* Tire Damping constant
      TK    = TIR(7,I)           /* Tire Vertical Spring Stiffness
      CALP  = TIR(8,I)           /* Lateral Stiffness of the tire
C     STRAGL= TIR(9,I)           /* Steer angle
      MU    = TIR(10,I)          /* Friction Coefficient

C     YAW   = TIR(11,I)          /* Yaw angle of the wheel body
      VX    = TIR(12,I)          /* Velocity of wheel center in road
system
      VY    = TIR(13,I)
      VZ    = TIR(14,I)
C     TIRE1 = TIR(15,I)          /* Global position of the tire center
C     TIRE2 = TIR(16,I)
C     TIRE3 = TIR(17,I)
C     TIREX = TIR(18,I)          /* Global postion of the tire bottom
C     TIREY = TIR(19,I)
C     TIREZ = TIR(20,I)
C     ZROAD = TIR(21,I)          /* Ground Elevation

C---Define the normal force, test for a constant spring or curve data

      IF ( ITK .EQ. 0 ) THEN                    /* No Spring Curve
defined
        FSPR  = TK * DEFL                       /* Tire Stiffness
      ELSE
        FSPR = FSPLIN ( DEFL, 0.D0, ITK, 1, A, IA, 0, 0 )
      ENDIF

C---Define potential energy for static analysis

      IF ( MSTAT .LE. 1 ) THEN
        IF ( ITK .EQ. 0 ) THEN
          V = V + TK * DEFL**2 / 2.0D0
        ELSE
          V = V + FSPLIN ( DEFL, 0.D0, ITK, 1, A, IA, -1, 0 )
        ENDIF
      ENDIF
```

```
C---Define the normal force resulting from tire damping

      FDAMP = -VZ * TD * CUBIC1(DEFL)      /* Tire Damping force

C---The radius of the run flat assembly is given by (RFRAD)
C   Add 1 inch to this radius to account for tire carcuss thickness
C   Check to see if the  tire has deflected into the run flat assembly
C   If TRUE, then add additional forces
C   Run flat stiffness is stored in RFSTIF
C   Run flat damping is stored in RFDAMP
C   Use cubic1 with a tolerance of plus on minus 1/16 inch

      PENRF = RFRAD + 1.0D0 + 0.0625D0  - (RAD-DEFL)      /* Run flat
penetration
      IF ( PENRF .GT. 0.0D0 ) THEN
        FRF =   RFSTIF * PENRF * CUBIC1(8.0D0*PENRF)
     &        + RFDAMP * (-VZ) * CUBIC1(8.0D0*PENRF)      /* Run flat
force
        FRF = DMAX1(0.0D0,FRF)
      ELSE
        PENRF = 0.0D0                                     /* Reset for
reporting
        FRF   = 0.0D0
      ENDIF

C---Sum up all the forces that may act on the tire
C   Limit the normal force so that it can not go negative

      FNORM = FSPR + FDAMP + FRF                        /* Normal force on
tire
      FNORM = DMAX1(0.0D0,FNORM)

C---If the tire is off the ground there are no longitudinal forces,
C   lateral forces, or torques turning the wheel.
C   else if the tire has penetrated the ground then calculate the
C   tire slip angle.

      IF ( DSQRT ( VX*VX + VY*VY ) .GT. 1.D-2 ) THEN
        SLIP = -DATAN2 (VX, VY)
      ELSE
        SLIP = 0.D0
      ENDIF
C
C  Velocity in X_Y plane for driver model:
C
      DMVELC = SNGL(DSQRT(QD(1,ICHS)**2 + QD(2,ICHS)**2) / 12.)
C

C---For the Front tires use the Lateral Force Data and Aligning Torque
C   Date from the first data arrays

      IF ( I .EQ. 1 .OR. I .EQ. 2 ) THEN                /* Front Tires

C---Save the normal force in a temporary variable
```

```
C   Calculate lateral force from the carpet plot
C   Carpet plot is a family of normal force Curves versus slip angle

        FNTEMP = FNORM
        FLAT = CARPET( DABS(SLIP), DABS(FNTEMP), I, SFRC1(1,1),
     &                 ALREF1(1), FZREF1(1), IPA1(1), IPF1(1),
     &                 NAPNT1, NFPNT1, NTR, CSTIFF )
        FLAT = DSIGN(FLAT,SLIP)
C
C  Cornering Stiffness and vertical tire load updates (front axle):
C  (for driver model)
C
      IF(I.EQ.1) THEN
        CCAF1 = SNGL(CSTIFF)
        FFZL1 = SNGL(FNORM)
      ELSE
        CCAF2 = SNGL(CSTIFF)
        FFZL2 = SNGL(FNORM)
      ENDIF

C---Calculate alinging torque from carpet plot

        ALGNTQ = CARPET ( DABS(SLIP), DABS(FNTEMP), I, ALTOR1(1,1),
     &                    SANGLE1(1), FZ1(1), IPSA1(1), IPFZ1(1),
     &                    NSA1, NFZ1, NTR, CSTIFF )
        ALGNTQ = DSIGN(ALGNTQ,SLIP)
      END IF

C---For the Rear tires use the Lateral Force Data and Aligning Torque
C   Date from the second data arrays

      IF ( I .EQ. 3 .OR. I .EQ. 4 ) THEN                  /* Rear Tires

C---Save the normal force in a temporary variable
C   Calculate lateral force from the carpet plot
C   Carpet plot is a family of normal force Curves versus slip angle

        FNTEMP = FNORM
        FLAT = CARPET( DABS(SLIP), DABS(FNTEMP), I, SFRC2(1,1),
     &                 ALREF2(1) , FZREF2(1), IPA2(1), IPF2(1),
     &                 NAPNT2, NFPNT2, NTR, CSTIFF )
        FLAT = DSIGN(FLAT,SLIP)
C
C  Cornering Stiffness and vertical tire load updates (rear axle):
C  (for driver model)
C
      IF(I.EQ.3) THEN
        CCAR1 = SNGL(CSTIFF)
        FFZL3 = SNGL(FNORM)
      ELSE
        CCAR2 = SNGL(CSTIFF)
        FFZL4 = SNGL(FNORM)
      ENDIF
C
```

```
C---Calculate alinging torque from carpet plot

         ALGNTQ = CARPET( DABS(SLIP), DABS(FNTEMP), I, ALTOR2(1,1),
     &                    SANGLE2(1), FZ2(1), IPSA2(1), IPFZ2(1),
     &                    NSA2, NFZ2, NTR, CSTIFF )
         ALGNTQ = DSIGN(ALGNTQ,SLIP)
       END IF

C---Define the longitudinal force for the turning wheel model
C    Get local velocity in the steer direction
C    Get the angular velocity of the wheel; Postive velocity is in the
C    the negative Y direction

C    Defn: Long Slip = ( Velocity - R*W ) / Velocity

C    if Vel > R*w  then slip > 0.0   Wheel is turning to slow causing
slip
C    if Vel = R*w  then slip = 0.0
C    if Vel < R*w  then slip < 0.0   Wheel is turning to fast causing
slip

       ANGV = UDE( I+NTR )                          /* Angular velocity of
wheel
       IF ( DABS(VY) .GT. 0.0001D0 ) THEN
         S = ( VY + ANGV*(RAD-DEFL)) / VY           /* Definition of Long.
Slip
       ELSE
         S = 0.D0
       END IF
       SCO = DABS( S )                             /* temporary variable
       IF ( SCO .GT. 1.D0 ) SCO=1.D0               /* Limit slip

C---The Utility spline curve is used for calculating slip.
C    Longitudinal force = Fcoef * Fnorm

       FCOEF =  FSPLIN ( SCO, 0.D0, IUTIL, 1, A, IA, 0, 0 )
       FLONG = -DSIGN  ( FCOEF*FNORM, S )

C---Limit the long. and lateral forces using the friction ellipse
(circle).

       FMAX  = MU*DABS(FNORM)
       FTOT  = DSQRT(FLONG**2 + FLAT**2)
       IF ( FTOT .GT. FMAX ) THEN
         RATIO = FMAX/FTOT
         FLAT  = RATIO*FLAT
         FLONG = RATIO*FLONG
       END IF

C---Calculate the torque due to the longitudinal force causing the wheel
C    to turn

       GFRC = FLONG * ( RAD-DEFL )

 1000 CONTINUE
```

```
C---Save values in ITIR and TIR arrays

      TIR(22,I) = DEFL              /* Tire Deflection - Ground
Penetration
      TIR(23,I) = FSPR              /* Spring Force
      TIR(24,I) = FDAMP             /* Damping Force
      TIR(25,I) = FNORM             /* Normal Force
      TIR(26,I) = SLIP              /* Tire Slip
      TIR(27,I) = FLAT              /* Lateral force
      TIR(28,I) = S                 /* Longitudinal slip
      TIR(29,I) = FLONG             /* Longitudinal force
      TIR(30,I) = GFRC              /* Wheel torque
      TIR(31,I) = PENRF             /* Penetration into run flat
      TIR(32,I) = FRF               /* Force due to run flat
      TIR(33,I) = ALGNTQ            /* Aligning Torque

      RETURN
      END
C
```

```
C
      SUBROUTINE FILTER(TIME, XNOW, YNOW, VNOW, ANOW, YLAST, VLAST,
     1 ALAST, XLAST, TLAST)
*
*  Second Order Filter:
*
*  TIME.....current time (sec)
*  XNOW.....current input signal to be filtered (input)
*  YNOW.....filtered value of XNOW signal (output)
*  VNOW.....first derivative of YNOW (output)
*  ANOW.....second derivative of YNOW (output)
*  YLAST....value of YNOW at last filter computation (input)
*  VLAST....value of VNOW at last filter computation (input)
*  ALAST....value of ANOW at last filter computation (input)
*  XLAST....value of XNOW at last filter computation (input)
*  TLAST....value of TIME at last filter computation (input)
*
*  Set Filter cutoff frequency and damping:
*
      WN = 25.0
      ZETA = 0.707
*
*  UPDATE RETURN VALUES FROM LAST ENTRY IN CASE OF T<=0 RETURN
*
      YNOW = YLAST
      VNOW = VLAST
      ANOW = ALAST
*
*  INITIALIZE FOR TIME ZERO
*
      IF(TIME .LE. 0.0) THEN
              YLAST = XNOW
              VLAST = 0.0
              XLAST = XNOW
              TLAST = 0.0
              YNOW = XNOW
              VNOW = 0.0
              ANOW = 0.0
      END IF
*
      T = TIME - TLAST
*
      IF(T .LE. 0.0) RETURN
*
*
*  COMPUTE CONSTANTS IN RECURSION EXPRESSIONS
*
            C1 = 4.+ 4.*T*ZETA*WN - T*T*WN*WN
            C2 = 4.*T
            C3 = T*T*WN*WN
            DET = 4.*(1+T*ZETA*WN)+WN*WN*T*T
            C4 = -4.*T*WN*WN
            C5 = 4.-4.*T*ZETA*WN-T*T*WN*WN
            C6 = 2.*T*WN*WN
*
```

```
*  CALCULATE FILTERED VALUES OF DISPLACEMENT, VELOCITY, AND ACCEL:
*
            YNOW = ( C1*YLAST + C2*VLAST + C3*(XNOW+XLAST) ) / DET
            VNOW = ( C4*YLAST + C5*VLAST + C6*(XNOW+XLAST) ) / DET
            ANOW = (WN*WN)*(XNOW - YNOW) - (2.0*ZETA*WN)*VNOW
*
*
*  UPDATE VALUES FOR NEXT ENTRY PRIOR TO RETURNING
*
          YLAST = YNOW
          VLAST = VNOW
          XLAST = XNOW
          ALAST = ANOW
          TLAST = TIME
*
          RETURN
*
          END
```

```
C
C  Auxilliary routine used to calculate Euler angles & position
C  information and write results to an external file.  Output used by
C  by post processing software for animation.
C
          SUBROUTINE EULANG(T, Y, A)

        DOUBLE PRECISION A(3,3), Y(3), T, BOT, TLAST
        DOUBLE PRECISION PSI, THETA, PHI
        SAVE IOPEN, TLAST
C
        IF(T .LE. 0.02) THEN
                TLAST = 0.0
                IOPEN = 0
        ENDIF
C
        IF(T-TLAST .LE. 0.0495) RETURN
C
C  Heading Angle
        PSI = DATAN2( A(1,2), A(2,2) )
C  Pitch Angle
        BOT = DSQRT( A(1,2)*A(1,2) + A(2,2)*A(2,2) )
        THETA = DATAN2( A(3,2), BOT)
C  Roll Angle
        BOT = DSQRT( A(1,1)*A(1,1) + A(2,1)*A(2,1) )
        PHI = -DATAN2( A(3,1), BOT)
C
        IF(IOPEN .EQ. 0) OPEN(35, FILE='DADS.ANIM',STATUS='UNKNOWN')
        IOPEN = 1
        WRITE(35,100) Y,PSI,THETA,PHI
  100 FORMAT(6F12.4)
C
        TLAST = T
        RETURN
        END
```

Appendix F

Path Planning / Obstacle Detection Example Code

This appendix contains example FORTRAN code that was used to demonstrate the path planning and obstacle detection algorithm discussed in section 5.9. The code is only minimally documented but may be helpful as an outline and starting point for other studies interested in using and interfacing the driver model code.

The code also contains a linear vehicle model with 3 degrees of freedom which may be instructive, by example, for persons interested in altering or extending the vehicle dynamics portion of the driver model to other types of vehicles or applications.

Below is a brief outline of the code that follows:

- read in vehicle parameters for a 3-DOF vehicle model (yaw, lateral displacement, and roll motion)
- read in left / right boundary tables and obstacle positions
- within the integration loop:
    - calculate r(theta) profiles relative to current vehicle position and orientation
    - calculate r*, theta* & transform to x*, y* inertial coordinates as the "input path" (target point) for the single-point driver model
    - calculate a new preview time based upon r* and forward speed
    - update the transition matrix for the new preview time
    - pass x*,y* to the driver model and obtain a steering command
    - integrate the linear equations of motion and obtain a new state
- end of the integration loop
- stop

```
C    *** Driver Model - Main Calling Program  ***
C    *** Path Planning / Obstacle Detection Example Code  ***
C
      PROGRAM MAIN
      SAVE
      INTEGER R, W
C
      REAL OBST(3,3)
      REAL LB(99,2), RB(99,2)
      REAL RLB(99), THLB(99)
      REAL RRB(99), THRB(99)
      REAL RD(200), TH(200)
      REAL PHICOF(3,3)
C
      CHARACTER*80 TITLE
      COMMON /ERDINF/ TITLE
      SAVE /ERDINF/
      COMMON /DRIV/ CAF, CAR, WHBS, WF, WR, U
      SAVE /DRIV/
      COMMON /ROLL/ HRC, ROLLK, ROLLC, RIROLL
      SAVE /ROLL/
      COMMON /INOUT/ R, W
      SAVE /INOUT/
      COMMON /TIRE/ FY1L,FY1R,FY2L,FY2R
      SAVE /TIRE/
      COMMON /DRVST1/ GRAV, TICYCL, TSS, DMAX, XP(100), YP(100), TAUMEM,
     1       TFF, RM, A, B, RI, PSI0, NTF, NP, TLAST, DFWLST, TILAST,
     2       DMEM(100,2), XT(100), YT(100)
      SAVE /DRVST1/
      DIMENSION Y(7), YD(7)
      DATA IERD/8/
C
      GRAV = 32.16666
      R = 1
      W = 2
      OPEN (R,FILE='DMOBST.IN')
      OPEN (W,FILE='DMOBST.OUT')
C      OPEN (6,FILE='OUT.6')
C      OPEN (7,FILE='OUT.7')
C
      READ(R,3) TITLE
  3   FORMAT(A80)
C
C  Read vehicle & simulation parameters:
C
      READ (R,10) CAF, CAR, WGHT, U, A, B, RI
      READ (R,10) HRC, ROLLK, ROLLC, RIROLL
      READ (R,10) TEND, DT, DTPR
   10 FORMAT (7F10.3)
C
C
      RM = WGHT / GRAV
      WHBS = A + B
      WF = WGHT * B / WHBS
      WR = WGHT * A / WHBS
```

```
C
C  Call DRIVE1 to read driver model parameters & initialize
C
      CALL DRIVE1(DFW)
C
C  Read in left & right boundary tables, obstacle positions,
C  and initial vehicle location
C
       CALL GETBOU(LB, RB, NLB0, NRB0, VEHWID)
       CALL GETOBS(NOBST, OBST, VEHWID)
       CALL GETPAR(THMAX, RMAX, DELTH, DELR, NPOWER)
C
C
C  Call TRANS to Calculate Initial Transition Matrix
C
      CALL TRANS
C
      A1 = -2. * (CAF + CAR) / RM / U
      B1 = 2. * (CAR*B - CAF*A) / RM / U - U
      A2 = 2. * (CAR*B - CAF*A) / RI / U
      B2 = -2. * (CAR*B*B + CAF*A*A) / RI / U
      C1 = 2. * CAF / RM
      C2 = 2. * CAF / RI * A
      A0 = HRC
      D1 = HRC
      B3 = (WF+WR)/GRAV*HRC*U/RIROLL
      B4 = (-(WF+WR)*HRC + ROLLK) / RIROLL
      B5 = ROLLC / RIROLL
C
C  Initialization of state (3-DOF vehicle model: lateral, yaw, roll) ->
C
C  Y(1)  lateral inertial position
C  Y(2)  lateral velocity in body axis system
C  Y(3)  yaw rate
C  Y(4)  yaw angle
C  Y(5)  longitudinal inertial position
C  Y(6)  roll rate
C  Y(7)  roll angle
C
      DO 20 I = 1, 7
        Y(I) = 0.0
        YD(I) = 0.0
   20 CONTINUE
      YD(5) = U
C
      DFWOLD = 0.0
      DFWOUT = 0.0
      IEND = INT(TEND/DT + 0.00001)
C
C  Start of Integration Loop:
C
      DO 30 I = 0, IEND
        T = I * DT
C
C  State Velocity: YD(1)
```

```
C
      YD(1) = Y(2) + U * Y(4) + A0*Y(7)
C
C  Current vehicle position and heading:
C
            XV = Y(5)
            YV = Y(1)
            PSI = Y(4)
C
C  No of pts in left and right boundary tables
C
             NLB = NLB0
             NRB = NRB0
C
C  Transform x,y boundary and obstacle data to polar coords:
C
              CALL TRPOLR(XV, YV, PSI, LB, NLB, RLB, THLB, 0)
              CALL MONO(NLB, THLB, RLB)
              CALL TRPOLR(XV, YV, PSI, RB, NRB, RRB, THRB, 1)
              CALL MONO(NRB, THRB, RRB)
C
              DO 25 J=1,NOBST
              CALL TRANOB(XV, YV, PSI, OBST, PHICOF, J)
 25   CONTINUE
C
C  Ray tracing to calculate boundary/obstacle intersects:
C
              CALL GENRAY(XV, YV, PSI, NLB, RLB, THLB, NRB, RRB, THRB,
     +  NOBST, PHICOF, THMAX, RMAX, DELTH, DELR, RD, TH)
C
C  Calculate r* from r(theta) profile returned by GENRAY:
C
      CALL CALCRS(RD, TH, THMAX, DELTH, RSTAR)
C
C  Calculate theta*:
C
      CALL CALCTH(RD, TH, THMAX, DELTH, NPOWER, THSTAR)
C
C  Transform  polar r*, theta* coords to inertial x*, y* coords:
C  (save x*,y* as single-point target for driver model)
C
      CALL TRANXY(XV, YV, PSI, RSTAR, THSTAR, XSTAR, YSTAR)
C
C  Adjust driver model preview time based upon r* and forward speed:
C
      TFF = RSTAR / U
C
C  Update driver model transition matrix for current preview time:
C
      CALL TRANS
C
C
C  Call to Driver Model: returns calculated steer angle, DFW.
C
      CALL STEER(T, Y, DFWOUT, DFWOLD, XSTAR, YSTAR)
```

```
C
C  Optional screen output:
C
C      WRITE(9,999) T,(Y(JK),JK=1,7),DFWOLD,DFWOUT
C  999 FORMAT(10F8.2)
C
       DFW = DFWOUT
       DFWOLD = DFWOUT
C
C  State Derivatives:
C
       YD(2) = A1 * Y(2) + B1 * Y(3) + C1 * DFW
       YD(3) = A2 * Y(2) + B2 * Y(3) + C2 * DFW
       YD(4) = Y(3)
       YD(5) = U
       YD(6) = Y(7)
       YD(7) = -B3*(Y(3) + YD(2)/U) - B4*Y(6) - B5*Y(7)
C
C  State Position: Y(i)
C
       Y(1) = Y(1) + YD(1) * DT
       Y(2) = Y(2) + YD(2) * DT
       Y(3) = Y(3) + YD(3) * DT
       Y(4) = Y(4) + YD(4) * DT
       Y(5) = Y(5) + YD(5) * DT
       Y(6) = Y(6) + YD(6) * DT
       Y(7) = Y(7) + YD(7) * DT
C
       FY1L = -CAF*( (Y(2)+Y(3)*A)/U - DFW )
       FY1R = -CAF*( (Y(2)+Y(3)*A)/U - DFW )
       FY2L = -CAF*(Y(2)-Y(3)*B)/U
       FY2R = -CAF*(Y(2)-Y(3)*B)/U
C
C  Call Output Subroutine to Print Results (optional)
C
       CALL OUT(T, Y, YD, DFW)
C
C  Call ERD plotter routines:  (optional)
C
        IF(T .EQ. 0.0) THEN
         CALL SETERD(IERD, NBYTES)
         CALL OUTERD(IERD, NBYTES, T, Y, YD, DFWOUT, DFW, DFVEL, DFACC)
        ELSE
         CALL OUTERD(IERD, NBYTES, T, Y, YD, DFWOUT, DFW, DFVEL, DFACC)
        ENDIF
C
C  End of Integration Loop:
C
   30 CONTINUE

      CLOSE (R)
      CLOSE (W)
C       CLOSE (6)
C       CLOSE (7)
      READ (9,40) ISTOP
```

```
   40 FORMAT (I1)
      STOP
      END
C
C  ***    End of Main Calling Program    ***
C
C
C  ***  Output Subroutine  ***
C
      SUBROUTINE OUT(T, Y, YD, DFW)
      SAVE
      INTEGER R, W
      COMMON /INOUT/ R, W
      SAVE /INOUT/
      COMMON /DRIV/ CAF, CAR, WHBS, WF, WR, U
      SAVE /DRIV/
      DIMENSION Y(7), YD(7), YOUT(7), YDOUT(7)
      DATA RADIAN /57.3/
      DO 10 I = 1, 7
        YOUT(I) = Y(I)
        YDOUT(I) = YD(I)
   10 CONTINUE
      YOUT(2) = Y(2) / U * RADIAN
      YOUT(3) = Y(3) * RADIAN
      YOUT(4) = Y(4) * RADIAN
      YOUT(6) = Y(6)*RADIAN
      YOUT(7) = Y(7)*RADIAN
      YDOUT(2) = YD(2) / U * RADIAN
      YDOUT(3) = YD(3) * 57.3
      YDOUT(4) = YD(4) * RADIAN
      DFWPRT = DFW * RADIAN
      WRITE (W,20) T, DFWPRT, (YOUT(I),I=1,7), (YDOUT(I),I=1,5)
   20 FORMAT (14F8.2)
      RETURN
      END
C
C
C  ***    Start of Driver Model Routines    ***
C
C
C   *** Driver Model Subroutine ***
C
C  Initialization
C
      SUBROUTINE DRIVE1(DFW)
      SAVE
      INTEGER R, W
      COMMON /INOUT/ R, W
      SAVE /INOUT/
      COMMON /DRIV/ CAF, CAR, WHBS, WF, WR, U
      SAVE /DRIV/
      COMMON /DRVST1/ GRAV, TICYCL, TSS, DMAX, XP(100), YP(100), TAUMEM,
     1       TFF, RM, A, B, RI, PSI0, NTF, NP, TLAST, DFWLST, TILAST,
     2       DMEM(100,2), XT(100), YT(100)
      SAVE /DRVST1/
```

```
C
      GRAV = 32.16666
      TICYCL = 0.0001
      TSS = 0.0
      DMAX = 0.2
C
      WRITE (W,10)
   10 FORMAT ('0', T20, 'CLOSED-LOOP PATH FOLLOWING MODE', /, '0', T20,
     1       'X-Y ', 'PATH', ' COORDINATES :', /, '0', T50, 'X', T60,
     2       'Y', /, /'0', T47, '(FEET)', T57, '(FEET)')
C
      READ (R,20) NP
   20 FORMAT (I3)
      DO 40 J = 1, NP
        READ (R,30) XP(J), YP(J)
   30   FORMAT (2F10.2)
        WRITE (W,50) XP(J), YP(J)
   40 CONTINUE
   50 FORMAT (' ', T43, 2F10.2)
      READ (R,60) TAUMEM, TFF
   60 FORMAT (F10.4)
      WRITE (W,70) TAUMEM, TFF
   70 FORMAT (' ', /, ' ', T20, 'DRIVER TRANSPORT LAG (SEC) :', T60,
     1       F4.2, /, ' ', T20, 'END OF PREVIEW INTERVAL (SEC) :', T60,
     2       F4.2/)
      RM = (WF + WR) / GRAV
      B = WHBS * WF / (WF + WR)
      A = WHBS - B
      RI = A * B * RM
      PSI0 = 0.0
C
C
      NTF = 1
C
C
      DO 80 J = 1, NP
        XT(J) = XP(J) * COS(PSI0) + YP(J) * SIN(PSI0)
        YT(J) = -XP(J) * SIN(PSI0) + YP(J) * COS(PSI0)
   80 CONTINUE
      TLAST = 0.
      DFWLST = 0.
      TILAST = 0.
      DFW = 0.
      DO 90 I = 1, 100
        DMEM(I,1) = 0.
   90 DMEM(I,2) = -1.
      RETURN
      END
C
C  Transition Matrix Calculation
C
      SUBROUTINE TRANS
      SAVE
      INTEGER R, W
      COMMON /INOUT/ R, W
```

```
      SAVE /INOUT/
      COMMON /DRIV/ CAF, CAR, WHBS, WF, WR, U
      SAVE /DRIV/
      COMMON /ROLL/ HRC, ROLLK, ROLLC, RIROLL
      SAVE /ROLL/
      COMMON /DRVST1/ GRAV, TICYCL, TSS, DMAX, XP(100), YP(100), TAUMEM,
     1       TFF, RM, A, B, RI, PSI0, NTF, NP, TLAST, DFWLST, TILAST,
     2       DMEM(100,2), XT(100), YT(100)
      SAVE /DRVST1/
      COMMON /TRSSTR/ TTT(6,6,10), TTT1(6,6,10), G(6)
      SAVE /TRSSTR/
      DIMENSION SV(6), SD(6), SVI(6)
C
      DELT = 0.01
      GRAV = 32.16666
      A1 = -2. * (CAF + CAR) / RM / U
      B1 = 2. * (CAR*B - CAF*A) / RM / U - U
      A2 = 2. * (CAR*B - CAF*A) / RI / U
      B2 = -2. * (CAR*B*B + CAF*A*A) / RI / U
      C1 = 2. * CAF / RM
      C2 = 2. * CAF / RI * A
      A0 = HRC
      D1 = HRC
      B3 = (WF+WR)/GRAV*HRC*U/RIROLL
      B4 = (-(WF+WR)*HRC + ROLLK) / RIROLL
      B5 = ROLLC / RIROLL
      ULAST = U
      G(1) = 0.
      G(2) = C1
      G(3) = C2
      G(4) = 0.
      G(5) = 0.
      G(6) = 0.
      DO 70 J = 1, 6
        NBEG = TSS / DELT + 1
        NEND1 = (TFF + .001 - TSS) / NTF / DELT
        NENDV = NEND1
        DO 10 L = 1, 6
          SV(L) = 0.0
          SVI(L) = 0.0
   10   CONTINUE
        TIME = 0.
        SV(J) = 1.0
        DO 60 I = 1, NTF
          DO 40 K = NBEG, NENDV
            SD(1) = SV(2) + U * SV(4) + A0*SV(6)
            SD(2) = A1 * SV(2) + B1 * SV(3)
            SD(3) = A2 * SV(2) + B2 * SV(3)
            SD(4) = SV(3)
            SD(5) = SV(6)
            SD(6) = -B3 * (SV(3) + SD(2)/U) - B4*SV(5) - B5*SV(6)
            DO 20 L = 1, 6
              SV(L) = SV(L) + SD(L) * DELT
   20       CONTINUE
            TIME = TIME + DELT
```

```
            DO 30 L = 1, 6
              SVI(L) = SVI(L) + SV(L) * DELT
   30       CONTINUE
   40     CONTINUE
          DO 50 L = 1, 6
            TTT(L,J,I) = SV(L)
            TTT1(L,J,I) = SVI(L)
   50     CONTINUE
          NBEG = NBEG + NEND1
          NENDV = NENDV + NEND1
   60   CONTINUE
   70 CONTINUE
      RETURN
      END
C
C  Closed-Loop Steer Calculation
C
      SUBROUTINE STEER(X, Y, DFW, DFWNOW, XSTAR, YSTAR)
C
C  (Subroutine "DRIVER" in other versions)
C
      SAVE
      INTEGER R, W
      COMMON /INOUT/ R, W
      SAVE /INOUT/
      COMMON /DRIV/ CAF, CAR, WHBS, WF, WR, U
      SAVE /DRIV/
      COMMON /DRVST1/ GRAV, TICYCL, TSS, DMAX, XP(100), YP(100), TAUMEM,
     1       TFF, RM, A, B, RI, PSI0, NTF, NP, TLAST, DFWLST, TILAST,
     2       DMEM(100,2), XT(100), YT(100)
      SAVE /DRVST1/
      COMMON /TRSSTR/ TTT(6,6,10), TTT1(6,6,10), G(6)
      SAVE /TRSSTR/
      DIMENSION Y(7), YC(7)
      DIMENSION DUMV11(6)
      DIMENSION DUMV1(6), VECM(6)
      DIMENSION DUMM1(6,6), DUMM2(6,6)
      DATA VECM /1.0, 5*0.0/
C
        NP = 1
       XP(1) = XSTAR
       YP(1) = YSTAR
      T = X
C     EPSI = ABS(Y(4) - PSI0)
      DO 10 I = 1, 4
   10 YC(I) = Y(I)
        YC(5) = Y(6)
        YC(6) = Y(7)
        YC(7) = Y(5)
C     IF (EPSI .LE. .002) GO TO 30
C
C  Update Coordinate Transformation
C
      PSI0 = YC(4)
      DO 20 J = 1, NP
```

```
      XT(J) = XP(J) * COS(PSI0) + YP(J) * SIN(PSI0)
   20 YT(J) = -XP(J) * SIN(PSI0) + YP(J) * COS(PSI0)
C
   30 Y0 = -YC(7) * SIN(PSI0) + YC(1) * COS(PSI0)
      X0 = YC(7) * COS(PSI0) + YC(1) * SIN(PSI0)
      YC(1) = Y0
      YC(4) = YC(4) - PSI0
      EPSY2 = 0.
      TSUM = 0.
      SSUM = 0.
      IF (T - TILAST .LE. TICYCL) RETURN
      DO 50 I = 1, NTF
        TJI = (TFF - TSS) / NTF * I + TSS
        DO 40 J = 1, 6
          DO 40 K = 1, 6
            DUMM1(J,K) = TTT1(J,K,I)
   40   DUMM2(J,K) = TTT(J,K,I)
        CALL GMPRD(VECM, DUMM1, DUMV11, 1, 6, 6)
        CALL GMPRD(VECM, DUMM2, DUMV1, 1, 6, 6)
        CALL GMPRD(DUMV1, YC, T1, 1, 6, 1)
        XCAR = X0 + U * TJI
C
         CALL TRAJ(XCAR, XT, YT, YPATH)
C
       YPATH = YT(1)
C
        CALL GMPRD(DUMV11, G, S1, 1, 6, 1)
        EP = T1 + S1 * DFWNOW - YPATH
        TSUM = TSUM + EP * S1
        SSUM = SSUM + S1 * S1
        EPSY2 = EPSY2 + EP * EP * (TFF - TSS) / NTF
   50 CONTINUE
      EPSY = SQRT(EPSY2) / (TFF - TSS)
      DFW = -TSUM / SSUM + DFWNOW
      IF (ABS(DFW) .GT. DMAX) DFW = DMAX * SIGN(1.,DFW)
      DO 60 J = 1, 2
        DO 60 I = 1, 99
   60 DMEM(101 - I,J) = DMEM(100 - I,J)
      DMEM(1,1) = DFW
      DMEM(1,2) = T
      TTAB = T - TAUMEM
      DO 70 I = 1, 99
        IF (DMEM(I + 1,2) .LE. TTAB .AND. DMEM(I,2) .GE. TTAB)
     1     GO TO 90
   70 CONTINUE
      WRITE (W,80)
   80 FORMAT ('0', '***** TAUMEM PROBABLY TOO LARGE *****')
      CALL EXIT
C  90 DFW =DMEM(I-2,1)+DMEM(I-1,1)+DMEM(I,1)+DMEM(I+1,1)+DMEM(I+2,1)
C     DFW = DFW/5.
   90 DFW = 0.0
      IF(T .GE. TAUMEM) DFW = DMEM(I,1)
      TLAST = X
      TILAST = X
      RETURN
```

```
      END
C
C   *** Trajectory Subroutine ***
C
      SUBROUTINE TRAJ(X, XT, YT, YPATH)
      SAVE
      INTEGER R, W
      COMMON /INOUT/ R, W
      SAVE /INOUT/
      COMMON /DRIV/ CAF, CAR, WHBS, WF, WR, U
      SAVE /DRIV/
      DIMENSION XT(*), YT(*)
C
C  SEARCH FOR XI,XI+1:
      DO 10 J = 1, 99
        IF (X .GE. XT(J) .AND. X .LT. XT(J + 1)) GO TO 30
   10 CONTINUE
      WRITE (W,20)
   20 FORMAT ('0', 'X-SEARCH IN SUB. TRAJ FAILED.')
      CALL EXIT
   30 SLOPE = (YT(J + 1) - YT(J)) / (XT(J + 1) - XT(J))
      Y2 = YT(J) + SLOPE * (X - XT(J))
      YPATH = Y2
      RETURN
      END
C
C  *** Matrix Product  Subroutine ***
C
      SUBROUTINE GMPRD(A, B, R, N, M, L)
      DIMENSION A(N*M), B(M*L), R(N*L)
      IR = 0
      IK = -M
      DO 10 K = 1, L
        IK = IK + M
        DO 10 J = 1, N
          IR = IR + 1
          JI = J - N
          IB = IK
          R(IR) = 0.
          DO 10 I = 1, M
            JI = JI + N
            IB = IB + 1
   10 R(IR) = R(IR) + A(JI) * B(IB)
      RETURN
      END
C
C   ***  End of Driver Model Code    ***
C
C
C   ***  Start of Path Planning / Obstacle Detection Code   ***
C
C
      SUBROUTINE GETBOU(LB, RB, NLB, NRB, VEHWID)
      SAVE
      INTEGER R, W
```

```
      COMMON /INOUT/ R, W
      SAVE /INOUT/
                REAL LB(99,2), RB(99,2), VEHWID

                READ(R,100) VEHWID
  100   FORMAT(F10.3)
                READ(R,150) NLB
  150   FORMAT(I2)

                DO 200 I=1,NLB
                READ(R,50) LB(I,1),LB(I,2)
   50   FORMAT(2F10.3)
                LB(I,2) = LB(I,2) + VEHWID/2.
  200   CONTINUE

                READ(R,150) NRB
                DO 300 I=1,NRB
                READ(R,50) RB(I,1),RB(I,2)
                RB(I,2) = RB(I,2) - VEHWID/2.
  300   CONTINUE
                RETURN
                END
C
C
C
      SUBROUTINE GETOBS(NOBST, OBST, VEHWID)
      SAVE
      INTEGER R, W
      COMMON /INOUT/ R, W
      SAVE /INOUT/
                REAL OBST(3,3)

                READ(R,100) NOBST
  100   FORMAT(I2)
                DO 200 I=1,NOBST
                READ(R,300) (OBST(I,J), J=1,3)
                OBST(I,3) = OBST(I,3) + VEHWID/2.
  200   CONTINUE
  300   FORMAT(3F10.3)
                RETURN
                END
C
C
      SUBROUTINE GETPAR(THMAX, RMAX, DELTH, DELR, NPOWER)
      SAVE
      INTEGER R, W
      COMMON /INOUT/ R, W
      SAVE /INOUT/

                READ(R,100) THMAX, RMAX, DELTH, DELR, NPOWER
  100   FORMAT(4F10.3,I2)
                RETURN
                END
C
C
```

```
      SUBROUTINE GETPOS(X, Y, PSI)
      SAVE
      INTEGER R, W
      COMMON /INOUT/ R, W
      SAVE /INOUT/
C
            READ(R,100) X, Y, PSI
  100   FORMAT(3F10.3)
            RETURN
            END
C
C
             SUBROUTINE TRPOLR(X, Y, PSI, BOUND, NB, RB, THB, LR)
            SAVE
            REAL X, Y, PSI, BOUND(99,2), RB(*), THB(*)
            REAL RHO(2,99), ATRANS(2,2), DUMV(2)
            DATA PI /3.1416/
C
            ATRANS(1,1) = COS(PSI)
            ATRANS(1,2) = SIN(PSI)
            ATRANS(2,1) = -SIN(PSI)
            ATRANS(2,2) = COS(PSI)
C
            DO 100 I=1,NB
            DUMV(1) = BOUND(I,1) - X
            DUMV(2) = BOUND(I,2) - Y
            CALL GMPRD(ATRANS, DUMV, RHO(1,I), 2, 2, 1)
            RB(I) = SQRT( RHO(1,I)*RHO(1,I) + RHO(2,I)*RHO(2,I) )
         IF(RHO(1,I) .NE. 0.) THEN
            THB(I) = ATAN( RHO(2,I) / RHO(1,I) )
      IF(RHO(2,I).LT.0..AND. RHO(1,I).LT.0.) THB(I) = -PI/2.*(-1)**LR
      IF(RHO(2,I).GT.0..AND. RHO(1,I).LT.0.) THB(I) = PI/2.*(-1)**(LR+1)
         ELSE
            THB(I) = PI/2.
            IF(RHO(2,I).LT.0.)THB(I) = -PI/2.
         ENDIF
  100    CONTINUE
      RETURN
      END
C
      SUBROUTINE TRANOB(X, Y, PSI, OBST, COEFF, I)
      SAVE
      REAL X, Y, PSI, OBST(3,3), COEFF(3,3)
C
      COEFF(I,1) = 2.*(COS(PSI)*(X - OBST(I,1)) + SIN(PSI)*(Y - OBST(I,2
     + )))
      COEFF(I,2) = 2.*(-SIN(PSI)*(X-OBST(I,1)) + COS(PSI)*(Y - OBST(I,2
     + )))
      COEFF(I,3) = (X - OBST(I,1))*(X - OBST(I,1)) + (Y - OBST(I,2))*
     +   (Y - OBST(I,2)) - (OBST(I,3)) * (OBST(I,3))
      RETURN
      END
C
      SUBROUTINE GENRAY(X,Y,PSI,NLB,RLB,THLB,NRB,RRB,THRB,NOBST,
     +  PHICOF, THMAX, RMAX, DELTH, DELR, R, TH)
```

```
      SAVE
      REAL X, Y, PSI, RLB(*), THLB(*), RRB(*), THRB(*), PHICOF(3,3)
     +  ,R(*),TH(*)
      REAL RADLST(200)
      SAVE RADLST
C
      JMAX = 2*THMAX/DELTH+1
      THETA = -THMAX - DELTH
      DO 100 J=1, JMAX
              THETA = THETA + DELTH
              CALL SEARCH(1, NLB, THLB, RLB, THETA, RNOWL, 1)
              CALL SEARCH(1, NRB, THRB, RRB, THETA, RNOWR, 1)
              R(J) = RNOWR
              IF(RNOWL .LT. RNOWR) R(J) = RNOWL
        IF(NOBST .GT. 0) THEN
                    RADIUS = 0.0
                    ISTART = RADIUS/DELR
                    IEND = RMAX/DELR
                DO 90 I=ISTART,IEND
                   RADIUS = RADIUS  + DELR
                   CALL EVALOB(RADIUS, THETA, PHICOF, NOBST, VALUE)
                        IF(VALUE .LT. 0) THEN
                           IF( RADIUS .LT. R(J) ) R(J) = RADIUS
                           GO TO 95
                        ENDIF
   90              CONTINUE
   95 CONTINUE
      ENDIF
C
              IF( RMAX .LT. R(J) ) R(J) = RMAX
              TH(J) = THETA
C
              RADLST(J) = R(J)
C
  100   CONTINUE
C
      RETURN
      END
C
C
      SUBROUTINE CALCRS(R, TH, THMAX, DELTH, RSTAR)
      SAVE
      REAL R(*), TH(*), THMAX, DELTH, RSTAR
C
      SUM = 0.0
C
      IMAX = 2*THMAX/DELTH+1
      DO 100 I=1,IMAX
                SUM = SUM + R(I)
  100   CONTINUE
              RSTAR = SUM / IMAX
C
              RETURN
              END
C
```

```
C
      SUBROUTINE CALCTH(R, TH, THMAX, DELTH, NPOWER, THSTAR)
      SAVE
      REAL R(*), TH(*), THMAX, DELTH, THSTAR
C
      SUM1=0.0
      SUM2=0.0
C
      IMAX = 2*THMAX/DELTH+1
      DO 100 I=1,IMAX
              SUM1 = SUM1 + (R(I)**NPOWER) * TH(I)
              SUM2 = SUM2 + (R(I)**NPOWER)
  100   CONTINUE
C
      THSTAR = SUM1 / SUM2
C
      RETURN
      END
C
C
      SUBROUTINE EVALOB(R, THETA, PHICOF, NOBST, VALUE)
      SAVE
      REAL R, THETA, PHICOF(3,3), VALUE
      DIMENSION VAL(3)
C
      DO 100 I=1, NOBST
      VAL(I)=R*R+( PHICOF(I,1)*COS(THETA) + PHICOF(I,2)*SIN(THETA))
     +           * R + PHICOF(I,3)
  100   CONTINUE
C
      VALUE = VAL(1)
      DO 90 I=1,NOBST
              IF(VAL(I) .LT. VALUE) VALUE = VAL(I)
   90   CONTINUE
C
      RETURN
      END
C
C
      SUBROUTINE TRANXY(X, Y, PSI, RSTAR, THSTAR, XSTAR, YSTAR)
      SAVE
      REAL X, Y, PSI, RSTAR, THSTAR, XSTAR, YSTAR
      XSTAR = X + RSTAR*COS(PSI+THSTAR)
      YSTAR = Y + RSTAR*SIN(PSI+THSTAR)
      RETURN
      END
C
C
       SUBROUTINE SEARCH(M, N, X, Y, A, B, IDIR)
       SAVE
       DIMENSION X(*), Y(*)
C
C  IDIR = 1  => FORWARD SEARCH;  IDIR = -1  => REVERSE SEARCH.
C
      IF(IDIR .EQ. -1) GO TO 800
```

```
  400 CONTINUE
C
      DO 100 I = M, N-1
               B = Y(I)
              IF(A.EQ.X(I)) RETURN
               IF(A .GE. X(I) .AND. A .LT. X(I+1)) THEN
                  B = Y(I) + (Y(I+1)-Y(I))/(X(I+1)-X(I))*(A-X(I))
                  RETURN
               ENDIF
C
               IF(A .LE. X(I) .AND. A .GT. X(I+1)) THEN
                  B = Y(I) + (Y(I+1)-Y(I))/(X(I+1)-X(I))*(A-X(I))
                  RETURN
               ENDIF
  100  CONTINUE
      B = Y(N)
      IF((A .LE. X(M)) .AND. (X(M).LE.X(N))) B = Y(M)
      RETURN
C
C  REVERSE SEARCH:
C
  800 CONTINUE
C
      DO 200 I = N,M+1,-1
               B = Y(I)
              IF(A.EQ.X(I)) RETURN
               IF(A .GE. X(I) .AND. A .LT. X(I-1)) THEN
                  B = Y(I) + (Y(I-1)-Y(I))/(X(I-1)-X(I))*(A-X(I))
                  RETURN
               ENDIF
C
               IF(A .LE. X(I) .AND. A .GT. X(I-1)) THEN
                  B = Y(I) + (Y(I-1)-Y(I))/(X(I-1)-X(I))*(A-X(I))
                  RETURN
               ENDIF
  200  CONTINUE
      B = Y(M)
      IF((A .LE. X(N)) .AND. (X(N).LE.X(M))) B = Y(N)
      RETURN
      END
C
C
               SUBROUTINE MONO(N, X, Y)
              SAVE
              DIMENSION X(*), Y(*)
C
              IF( X(1) .LT. X(N) ) RETURN
C
              M = N/2
C
              DO 100 I=1,M
                     DUM = X(I)
                     X(I) = X(N-I+1)
                     X(N-I+1) = DUM
  100   CONTINUE
```

```
C
                DO 200 I=1,M
                        DUM = Y(I)
                        Y(I) = Y(N-I+1)
                        Y(N-I+1) = DUM
  200   CONTINUE
C
                RETURN
                END
```

Appendix G

Background References

The first two technical papers included in this appendix (references 1 and 2 from the List of References) provide principal background material for much of the work initially undertaken in this project and are included here as a convenience. The third technical paper appearing in this appendix reports on analyses performed by Stribersky (reference 42) using the HMMWV-Trailer combination vehicle test data from this project to confirm findings predicted by the application of bifurcation theory to vehicle dynamic systems.

Application of an Optimal Preview Control for Simulation of Closed-Loop Automobile Driving

CHARLES C. MACADAM

Abstract—An optimal preview control method is applied to the automobile path following problem. The technique is first used to examine the straight-line regulatory driving task and results compared with similar experimental measurements. The method is further demonstrated by closed-loop simulation of an automobile driver/vehicle system during transient lane-change maneuvers. The computer simulation results are compared with equivalent vehicle test measurements.

I. Introduction

THIS PAPER presents example applications (to the automobile path following problem) of a general method of control synthesis presented in [1]. The method is demonstrated here by simulation of a closed-loop automobile/driver system and the results compared with driver/vehicle test measurements. Results for the optimal preview control are also discussed within the context of manual control pursuit tracking task findings.

The control technique demonstrated herein is designed for application to linear time-invariant systems utilizing preview control strategies for regulation or tracking tasks. A common example of this type of control strategy occurs during normal automobile path following in which drivers "look-ahead" to follow a desired path. Human operators, as part of various man–machine systems, typically employ preview control strategies to control and stabilize such systems. It is widely recognized that human operators are capable of controlling and adapting to a wide variety of dynamical systems, many of which are vehicles with preview-oriented control requirements such as automobiles, bicycles, and complex aircraft [2]–[8]. Clearly human control of most vehicles would not be possible without some training by the operator to acquire an understanding of the vehicle response to various control inputs. While a certain portion of this training serves to identify and reinforce learned open-loop responses for repeated and familiar control task scenarios, the remainder frequently serves to identify and reinforce the operator's understanding or "feel" of the vehicle response to control inputs continually in use for closed-loop regulation and/or pursuit needs. It is in this latter control category for general linear system representations capable of preview control strategies, that the method presented in [1] can find particular application. As will be demonstrated in this paper, application to the automobile path following problem produces substantive agreement when compared with driver/vehicle experimental measurements for both straight-line regulatory driving and transient lane-change maneuvers.

Manuscript received October 10, 1980; revised March 2, 1981.
The author is with the Highway Safety Research Institute of the University of Michigan, Ann Arbor, MI 48109.

II. The Optimal Preview Control

Before applying the optimal preview control of [1] to the automobile path following problem, the main results and symbol definitions contained therein are briefly reviewed in this section for later reference. As derived in [1], for the linear system

$$\dot{x} = Fx + gu \tag{1}$$

$$y = m^T x \tag{2}$$

where

x $n \times 1$ state vector,
y scalar output related to the state by the $n \times 1$ constant observer vector transpose,
F constant $n \times n$ system matrix,

and

g constant $n \times 1$ control coefficient vector,

the optimal control $u^0(t)$ which minimizes a special form of the local performance index,

$$J \triangleq \frac{1}{T}\int_t^{t+T}\{[f(\eta) - y(\eta)]W(\eta - t)\}^2\, d\eta \tag{3}$$

over the current preview interval $(t, t+T)$ where

W arbitrary weighting function over the preview interval

and

f previewed input,

is given by

$$u^0(t) = \left[\int_t^{t+T}\left\{f(\eta) - m^T\left[I + \sum_{n=1}^{\infty}\frac{F^n(\eta - t)^n}{n!}\right]x(t)\right\}\cdot\left\{(\eta - t)m^T\left[I + \sum_{n=1}^{\infty}\frac{F^n(\eta - t)^n}{(n+1)!}\right]g\right\}W(\eta - t)\, d\eta\right] \Bigg/ \left[\int_t^{t+T}\left\{(\eta - t)m^T\left[I + \sum_{n=1}^{\infty}\frac{F^n(\eta - t)^n}{(n+1)!}\right]g\right\}^2 \cdot W(\eta - t)\, d\eta\right] \tag{4}$$

0018-9472/81/0600-0393$00.75

where I is the identity matrix. For the special case of $W(\eta - t) = \delta(T^*)$, the Dirac delta function for $0 < T^* \leq T$, (4) simplifies to

$$u^0(t) = \frac{f(t+T^*) - \boldsymbol{m}^T\left[I + \sum_{n=1}^{\infty} \frac{F^n(T^*)^n}{n!}\right]\boldsymbol{x}(t)}{T^*\boldsymbol{m}^T\left[I + \sum_{n=1}^{\infty} \frac{F^n(T^*)^n}{(n+1)!}\right]\boldsymbol{g}} \quad (5)$$

$$= \left[f(t+T^*) - y_0(t+T^*)\right]/(T^*K), \quad (6)$$

the single-point preview control version of (4), where

$$K \triangleq \boldsymbol{m}^T\left[I + \sum_{n=1}^{\infty} \frac{F^n(T^*)^n}{(n+1)!}\right]\boldsymbol{g}.$$

Equation (6) represents a proportional controller with gain inversely related to the preview interval T^* and operating on the error between the previewed input $f(t+T^*)$ and $y_0(t+T^*)$, that portion of the previewed output deriving from the state vector's current initial condition. Likewise (4) can be interpreted as a proportional controller operating on a similar error averaged and weighted over the preview interval $(t, t+T)$ by the additional terms appearing in (4).

It is also shown in [1] that the optimal solution $u^0(t)$ can be expressed in terms of any current nonoptimal $u(t)$ and correspondingly nonzero preview output error $\epsilon(t)$ as

$$u^0(t) = u(t) + \frac{\int_t^{t+T} \epsilon(\eta)A(\eta)W(\eta - t)\,d\eta}{\int_t^{t+T} A^2(\eta)W(\eta - t)\,d\eta} \quad (7)$$

where

$$A(\eta) \triangleq (\eta - t)\boldsymbol{m}^T\left[I + \sum_{n=1}^{\infty} \frac{F^n(\eta - t)^n}{(n+1)!}\right]\boldsymbol{g}$$

$$\epsilon(\eta) \triangleq f(\eta) - \boldsymbol{m}^T\boldsymbol{\phi}(\eta, t)\boldsymbol{x}(t) - u(t)A(\eta)$$

$$\boldsymbol{\phi}(\eta, t) \triangleq I + \sum_{n=1}^{\infty} \frac{F^n(\eta - t)^n}{n!}.$$

For the special case of $W(\eta - t) = \delta(T^*)$, as before, (7) reduces to

$$u^0(t) = u(t) + \frac{\epsilon(t+T^*)}{T^* \cdot K}. \quad (8)$$

The formulation expressed by (7) can be useful in describing systems which do not achieve, though closely approximate, the defined optimal system behavior. Such cases may arise from limitations in achieving the precise optimal control due to time lags or dynamic properties inherent in the controller and not accounted for *a priori* in the optimization. The next two sections adopt this view for the car/driver man–machine system in an attempt to describe and explain actual closed-loop driving behavior.

Finally, it was also shown in [1] that information concerning stability of the closed-loop system utilizing the optimal preview control of (4) or (7) is provided by the characteristic roots of the constant matrix

$$\left[F - \boldsymbol{g}\boldsymbol{c}^T\right] \quad (9)$$

where

$$\boldsymbol{c}^T = \frac{\boldsymbol{m}^T \int_0^T \boldsymbol{\phi}(\eta, 0)\left\{\eta\boldsymbol{m}^T\left[I + \sum_{n=1}^{\infty} \frac{F^n(\eta)^n}{(n+1)!}\right]\boldsymbol{g}\right\}W(\eta)\,d\eta}{\int_0^T \left\{\eta\boldsymbol{m}^T\left[I + \sum_{n=1}^{\infty} \frac{F^n(\eta)^n}{(n+1)!}\right]\boldsymbol{g}\right\}^2 W(\eta)\,d\eta}.$$

For the special case of $W(\eta) = \delta(T^*)$, (9) becomes

$$F - \boldsymbol{g}\boldsymbol{m}^T\left[I - \sum_{n=1}^{\infty} \frac{F^n(T^*)^n}{n!}\right] \Big/ (T^* \cdot K)\Bigg\}. \quad (10)$$

III. Application to Manual Control Pursuit Tracking Tasks as Represented by Straight-Line Automobile Driving

The most well-known and characteristic property exhibited by human operators in tracking tasks is the transport delay deriving from perceptual and neuromuscular mechanisms. By introducing this inherent delay property *a posteriori* in the optimal preview control formulation, excellent agreement can be demonstrated between typical manual control pursuit tracking task results and the resulting optimal preview controller modified to include the inherent transport delay (heretofore referred to as the "modified" optimal preview control).

For reasons of clarity and notational simplicity, the discussion in this section will make use only of (8), the single-point preview control version of (7). Equation (8) can be represented by the block diagram of Fig. 1, where $G(s) = [Is - F]^{-1}\boldsymbol{g}$ represents the controlled element vector transfer function, and $u(t)$, the current control, is related to the optimal control $u^0(t)$ by a transfer function $H(s)$ (previously assumed equal to one in the derivation of the optimal control $u^0(t)$). The introduction of the $H(s)$ transfer function is useful in describing systems which function (or are presumed to do so) in an error minimization fashion, but fail to achieve the precise optimal control due to an inherent limitation within the controller or control process itself, e.g., delays resulting from processor calculations and sample hold operations in digital systems, or perceptual/neuromuscular lags in the case of a human controller. By letting $H(s) = e^{-s\tau}$, those actual delay limitations displayed by human operators during tracking tasks can be approximated by the parameter τ, an effective transport lag. By incorporating this approximation and noting then that the transfer function relating $u(t)$ and $\epsilon(t+T^*)$ is $e^{-s\tau}/(1 - e^{-sT})KT^*$, Fig. 1 reduces to Fig. 2, a single-loop pursuit tracking formulation. The open-loop transfer function $Y_0(s)$ relating $y(t+T^*)$ and $\epsilon(t+T^*)$ is given by

$$Y_0(s) = \frac{e^{-s\tau}}{1 - e^{-sT}}\left[1 + \frac{\boldsymbol{m}^T\boldsymbol{\phi}(t+T^*, t)G(s)}{KT^*}\right]. \quad (11)$$

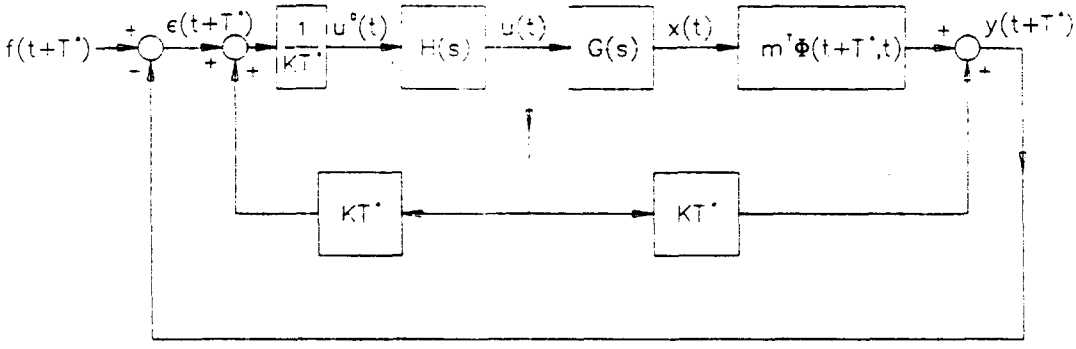

Fig. 1. Block diagram for the single-point preview control.

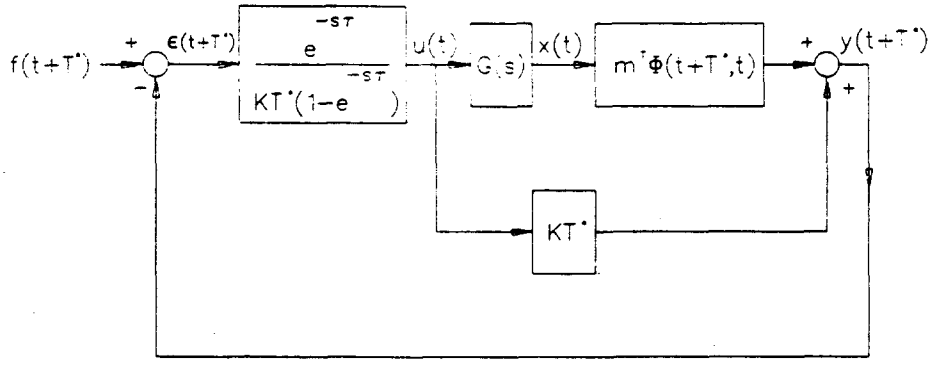

Fig. 2. Equivalent block diagram for the single-point preview control, $H(s) = e^{-s\tau}$.

The stability of this system is determined by the characteristic roots of $1 + Y_0(s)$, or equivalently,

$$1 + e^{-s\tau}\boldsymbol{m}^T\phi(t + T^*, t)G(s)/KT^* = 0. \qquad (12)$$

To test the utility of this model by comparison with experimental findings, open-loop gain/phase frequency response results measured by Weir *et al.* [9, Fig. 12-C] for an automobile straight-line regulatory control task are presented in Figs. 3 and 4. These experimental results represent the open-loop frequency response relating the driver's output (presumably an estimate of future lateral position) to an assumed error, derived by the driver, between the previewed input (straight road ahead) and the driver's output. Since this may be categorized as a form of linear pursuit tracking, the formulation of (11) is accommodated. Also shown in Figs. 3 and 4 is the frequency response calculation for (11) with parameters $T^* = 3.0$ (s) and $\tau = 0.26$ (s). The model output $y(t + T^*)$ is the estimated vehicle lateral position at time $t + T^*$; the input $f(t + T^*) \equiv 0$ is the lateral displacement of the previewed path. The automobile $(F, \boldsymbol{g})$ dynamics used in (11) appear in Appendix I-A and duplicate those identified in [9]. The values of T^* and τ were selected to fit the experimental data as closely as the single-point model would permit. As can be seen, the model and experimental results display excellent agreement. Not only does the preview model reproduce the -6 db/octave slope of the familiar manual control "crossover" model [2], [8] gain characteristic, but also the peaking phase characteristic usually displayed in manual control task experimental data of this kind.

The model parameters T^* and τ appearing in (11) represent the average preview time used by the driver and

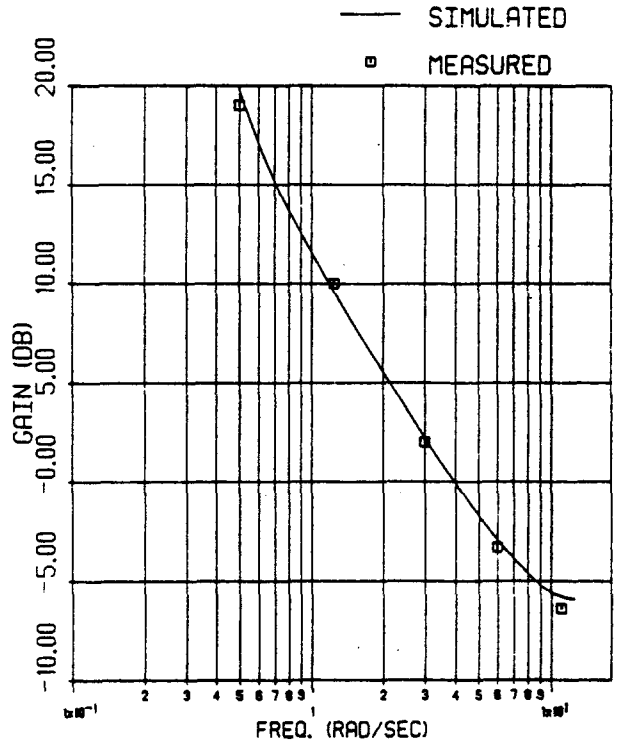

Fig. 3. Frequency response gain comparison.

his/her effective transport lag associated with this particular control task. The values of T^* and τ used here fall well within the range identified by other investigators studying straight-line automobile driving [10]–[12] and human operator tracking performance [2], [4], [9].

Interestingly, for the relatively simple control task of typical straight-line automobile regulation as discussed here,

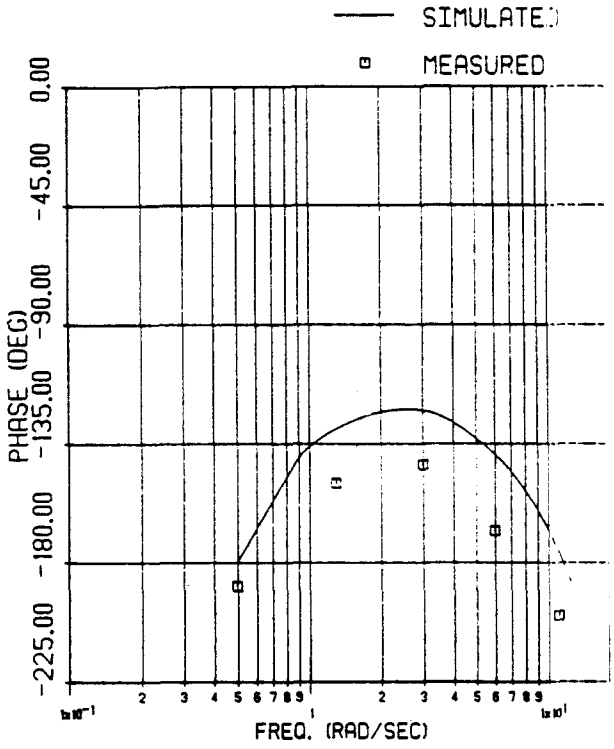

Fig. 4. Frequency response phase comparison.

the vehicle dynamics portion of the total transfer function (11) does not play a dominant role except at very low frequencies. As a result, the open-loop transfer function gain characteristic (11) is closely approximated by the human operator term, $e^{-s\tau}/(1-e^{-s\tau}) \approx e^{-s\tau}/\tau s$. Such a result would support the well-known fact that tracking task test results for simple automobile regulation [8], [9] can generally be approximated by the "cross-over" model form $Ce^{-s\tau}/s$ (C being the "cross-over" gain constant) in the vicinity of the cross-over frequency. Moreover, in such cases where the above approximation does hold, $1/\tau$ becomes C in the "cross-over" model representation.

For the simple manual control pursuit tracking task, as represented here by straight-line automobile regulation, the modified optimal preview controller, even employed in only a single-point form [$W(\eta - t) = \delta(T^*)$], appears to accurately mimic human control behavior. It might, therefore, seem reasonable to conjecture that human operator strategy during simple pursuit tracking (or at least straight-line automobile regulation) is closely akin to an optimal preview error minimization process which ignores or is unaware of transport delay mechanisms inherent in the control processor. A more stringent test of this hypothesis is offered in the following section wherein transient automobile path following is examined using the modified optimal preview control model in its complete form.

Application of the Optimal Preview Control for Simulation of Closed-Loop Transient Automobile Path Following

The previous section addressed the applicability of the optimal preview control to the problem of preview regulation and the effects of an inherent transport delay within the controller. Using straight-line automobile regulation as an example, the single-point preview model was compared with experimental results within the frequency domain. In this section application to the tracking problem is demonstrated using the general preview control model (7), with an inherent transport time delay to simulate a closed-loop automobile/driver path following maneuver. Results from the model are compared with time history measurements from corresponding full-scale vehicle tests.

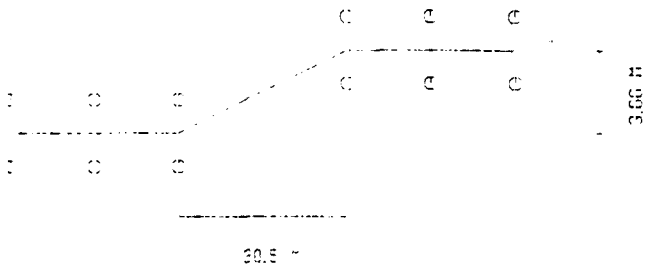

Fig. 5. Lane-change test course.

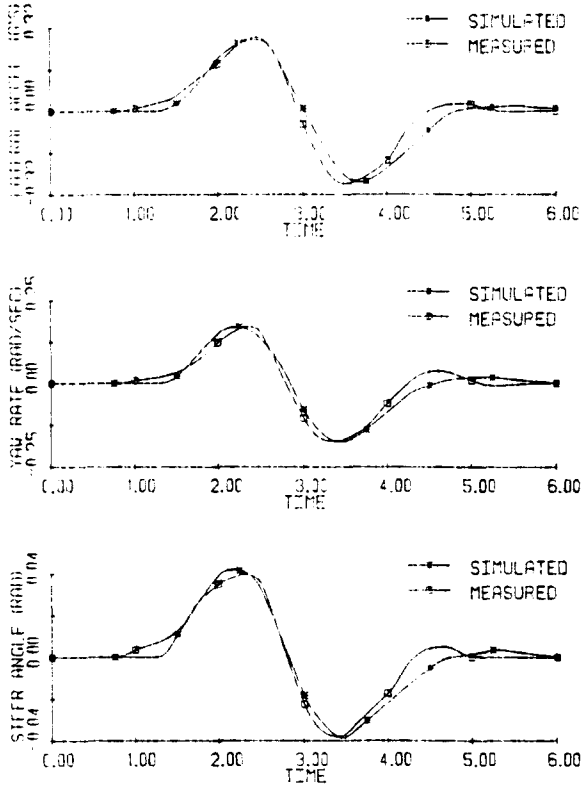

Fig. 6. Closed-loop simulation/test result comparison.

The specific closed-loop maneuver examined here required an automobile driver to perform a standard 3.66 m (12-ft) lane-change within a distance of 30.5 m (100 ft) at a vehicle speed of approximately 26.8 m/s (60 mi/h). The initiation and completion of the lane change was constrained by 3.05-m wide (10 ft) cone-marked lanes (Fig. 5). The test vehicle was a standard American compact with measured parameter values shown in Appendix I-B. A representative test result for this vehicle/driver combination appears in Fig. 6, showing recorded-time histories of lateral acceleration, yaw rate, and front-wheel steer angle [13].

Also shown in Fig. 6 are computer simulation results using the optimal preview control (7) with an assumed human operator transport delay term $e^{-s\tau}$ relating $u^0(t)$ and $u(t)$. The transport lag term is included here, as in the previous section, to approximate the principal human operator lag effects. The calculation of (7), steer angle, seen in Fig. 6 is for values of $\tau = 0.2$ (s) and $T = 1.3$ (s) using ten equally spaced points in the preview interval to approximate the integral. The values of T and τ were selected to closely fit the test measurements. The (F, g) automobile dynamics model is the same two-degree-of-freedom model appearing in Appendix I-A, evaluated for the parameter values identified in Appendix I-B. The previewed input $f(\eta)$ appearing in (7) represents the desired lateral path deviation and was obtained during the simulation using the simple straight-line path segments shown in Fig. 5 as input.

As seen from Fig. 6, excellent agreement can be obtained between the experimental results and simulation predictions using the two numerical parameters (τ, T) and a simple straight-line path input. Variations in the value of τ primarily influenced the closed-loop system damping; larger values producing reduced damping. Variations in the value of T influenced control (steering) amplitude as well as damping; larger values of T producing lower control amplitude and increased damping.

Finally, Fig. 7 shows a comparison of the preview model predictions and measured test results for a modified set of vehicle dynamics (F, g). The same vehicle was employed but with modifications to its mass center and rear tires so as to produce a new set of parameter values listed in Appendix I-C. As shown in Fig. 7 the principal change in the closed-loop response from Fig. 6 is an increased steering gain (lower steering amplitude for the same nominal maneuver) and decreased damping. Larger values of τ (0.3) and T (1.55) were required in the calculation of (7), shown as steer angle in Fig. 7, to better approximate the reduced damping and smaller amplitude steering control. A comparison of computed vehicle path trajectories, corresponding to the baseline and modified vehicle responses shown in Figs. 6 and 7, appears in Fig. 8.

Characteristic roots for each of the closed-loop systems, as calculated from the constant matrix (13), are shown in Fig. 9. The matrix (13) (see Appendix I-D) is similar to that given by (9) but includes the influence of the transport lag term $e^{-s\tau}$ approximated by the first-order Padé polynomial

$$\frac{1 - \frac{\tau}{2}s}{1 + \frac{\tau}{2}s}$$

$$\left[\begin{array}{c|c} F & g \\ \hline c^T\left(F - \frac{2}{\tau}I\right) & c^T g - \frac{2}{\tau} \end{array}\right]. \tag{13}$$

Note that the reduced damping in the driver/vehicle responses, displayed in Figs. 7 and 8, is equivalently represented by the corresponding closed-loop characteristic root locations shown in Fig. 9.

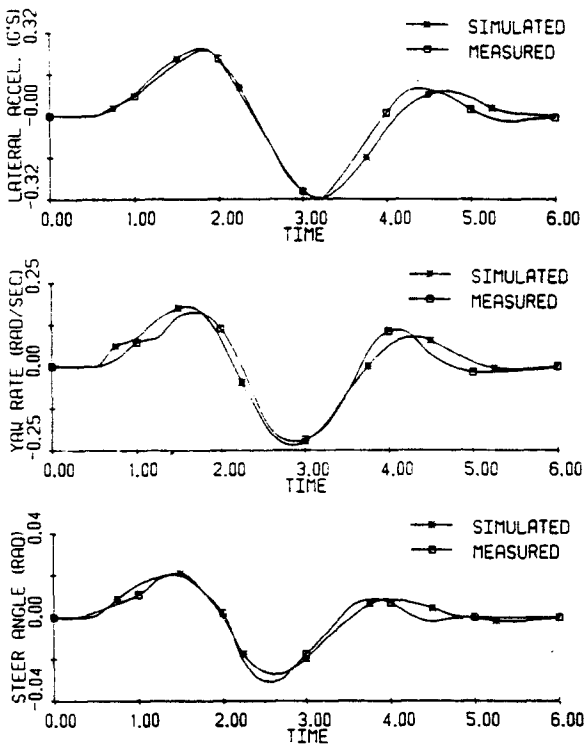

Fig. 7. Closed-loop simulation/test result comparison—modified vehicle.

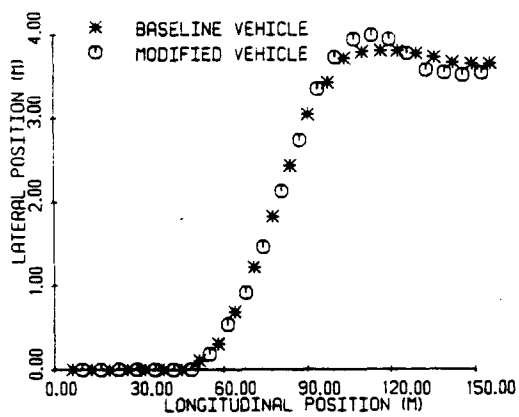

Fig. 8. Simulated path trajectories.

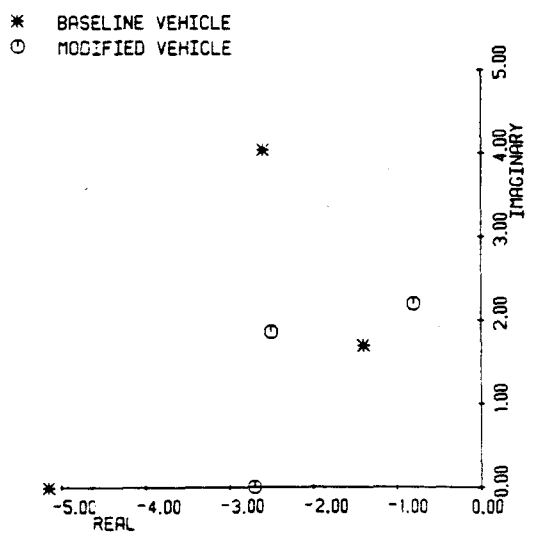

Fig. 9. Characteristic roots of the baseline and modified closed-loop systems.

These results and those of the previous section demonstrate useful application of the optimal preview model in simulation of closed-loop automobile driving. The principal conclusion concerning these results is that driver steering control strategy during path following can be accurately represented as a time-lagged optimal preview control. Similar applications and extensions to problems in other fields are clearly suggested by the results shown here.

Conclusion

The optimal preview control model, applied here to the closed-loop automobile path following problem, offers a useful and direct method for representing closed-loop behavior of linear driver/vehicle systems. It is suggested that driver automobile steering control strategy during path following can be viewed as a time-lagged optimal preview control process.

The general linear system formulation of the preview control methodology, demonstrated here, permits application to a broad range of problems relating to man–machine systems.

Appendix I

A. Vehicle Dynamics

The linear dynamical equations of an automobile for lateral and yaw motions are

$$\dot{y} = v + U\psi \tag{A1}$$

$$\dot{v} = \left[-2(C_{\alpha_F} + C_{\alpha_R})/mU\right]v + \left[2(bC_{\alpha_R} - aC_{\alpha_F})/mU - U\right]r + (2C_{\alpha_F}/m)\delta_{FW} \tag{A2}$$

$$\dot{r} = \left[2(bC_{\alpha_R} - aC_{\alpha_F})/IU\right]v + \left[-2(a^2C_{\alpha_F} + b^2C_{\alpha_R})/IU\right]r + (2aC_{\alpha_F}/I)\delta_{FW} \tag{A3}$$

$$\dot{\psi} = r \tag{A4}$$

where

- y inertial lateral displacement of the vehicle mass center,
- v lateral velocity in the vehicle body axis system,
- r yaw rate about the vertical body axis,
- ψ vehicle heading angle, and
- δ_{FW} front tire steer angle, control variable.

The parameters appearing in (A1)–(A4) are

- U forward vehicle velocity,
- $C_{\alpha_F}, C_{\alpha_R}$ front and rear tire cornering coefficients,
- a, b forward and rearward locations of tires from the vehicle mass center, and
- m, I vehicle mass and rotational inertia.

The above equations can be expressed in matrix notation as

$$\dot{x} = Fx + g\delta_{FW} \tag{A5}$$

where

$$x = \begin{Bmatrix} y \\ v \\ r \\ \psi \end{Bmatrix}$$

$$F = \begin{bmatrix} 0 & 1 & 0 & U \\ 0 & A_1 & B & 0 \\ 0 & A_2 & B_2 & 0 \\ 0 & 0 & 1 & 0 \end{bmatrix}, \qquad g = \begin{Bmatrix} 0 \\ C_1 \\ C_2 \\ 0 \end{Bmatrix}$$

and

$$A = -2(C_{\alpha_F} + C_{\alpha_R})/mU$$

$$B_1 = 2(bC_{\alpha_R} - aC_{\alpha_F})/mU - U$$

$$C_1 = 2C_{\alpha_F}/m$$

$$A_2 = 2(bC_{\alpha_R} - aC_{\alpha_F})/IU$$

$$B_2 = -2(a^2C_{\alpha_F} + b^2C_{\alpha_R})/IU$$

$$C_2 = 2aC_{\alpha_F}/I.$$

The calculation of (11) appearing in Figs. 3 and 4 used the following parameter values identified in [9] for vehicle D

- a = 1.41 m (4.63 ft)
- b = 1.41 m (4.63 ft)
- m = 2016 kg (138 slug)
- I = 4013 m·N·s² (2960 ft·lb·s²)
- U = 22.3 m/s (73.3 ft/s)
- C_{α_F} = 25 266 N/rad (5 680 lb/rad)
- C_{α_R} = 70 933 N/rad (15 960 lb/rad).

The constant observer vector $m^T = (1, 0, 0, 0)$ provided the vehicle lateral position y.

B. Baseline Vehicle Parameter Values

The vehicle parameter values listed below and used in the calculations appearing in Fig. 6 were derived from vehicle wheelbase/weight measurements and steady-state, constant-steer vehicle test results [13]

- a = 1.37 m (4.5 ft)
- b = 1.22 m (4.0 ft)
- m = 1563 kg (107 slug)
- I = 2712 m·N·s² (2 000 ft·lb·s²)
- U = 25.9 m/s (85 ft/s)
- C_{α_F} = 19 438 N/rad (4 370 lb/rad)
- C_{α_R} = 33 628 N/rad (7 560 lb/rad).

The weighting function W appearing in (7) was selected as constant 1.0 over the ten-point preview interval.

C. Modified Vehicle Parameter Values

The vehicle parameters of Appendix I-B were altered to those values shown in this section by a rearward shift in the vehicle mass center and a decrease in rear tire inflation

pressures

a = 1.43 m (4.7 ft)
b = 1.16 m (3.8 ft)
m = 1753 kg (120 slug)
I = 2712 m·N·s^2 (2000 ft·lb·s^2)
U = 25.9 m/s (85 ft/s)
C_{α_F} = 20 906 N/rad (4700 lb/rad)
C_{α_R} = 29 536 N/rad (6640 lb/rad).

The closed-loop calculation using these parameter values appears in Fig. 7.

D. Stability of the Closed-Loop Optimal Preview-Controlled System Including a Transport Time Lag

Given the system

$$\dot{x} = Fx + gu \tag{A6}$$

$$u = e^{-s\tau}u^0 \tag{A7}$$

$$u^0 = -c^T x \tag{A8}$$

where F, g, u^0, and c^T are defined in (1), (4), and (9). If the transport time lag $e^{-s\tau}$ is approximated by the first-order Padé polynomial,

$$\frac{1 - \frac{\tau}{2}s}{1 + \frac{\tau}{2}s}, \tag{A9}$$

(A7) becomes

$$\dot{u} = \frac{2}{\tau}(-u + u^0) - \dot{u}^0. \tag{A10}$$

Substitution of

$$u^0 = -c^T x$$

and

$$\dot{u}^0 = -c^T[Fx + gu]$$

into (A10) produces the closed-loop state equation

$$\left\{\begin{matrix}\dot{x} \\ \dot{u}\end{matrix}\right\} = \left[\begin{array}{c|c} F & g \\ \hline c^T\left(F - \frac{2}{\tau}I\right) & c^T g - \frac{2}{\tau} \end{array}\right] \left\{\begin{matrix} x \\ u \end{matrix}\right\} \quad \text{(A11)}$$

equivalent of (A6)–(A8). For small τ, stability of the time-lagged optimal preview-controlled system is provided by the characteristic roots of the system matrix appearing in (A11).

References

[1] C. C. MacAdam, "An optimal preview control for linear systems," *J. Dynamic Systems, Measurement, Control*, Sept., 1980.

[2] D. T. McRuer, *et al.*, "New approaches to human-pilot/vehicle analysis," Systems Technology, Inc., Tech. Rep., AFFDL-TR-68-150, Feb. 1968.

[3] W. W. Wierwille, G. A. Gagne, and J. R. Knight, "An experimental study of human operator models and closed-loop analysis methods for high-speed autombile driving," *IEEE Trans. Hum. Factors Electron.*, vol. HFE-8, no. 3, pp. 187–201, Sept. 1967.

[4] K. Tanaka, N. Goto, and K. Washizu, "A comparison of techniques for identifying human operator dynamics utilizing time series analysis," in *Proc. Twelfth Annu. Conf. Manual Control*, Univ. of Illinois, Urbana, IL, May 25–27, 1976, pp. 673–693.

[5] D. H. Weir, "Motorcycle handling dynamics and rider control and the effect of design configuration on response and performance," Ph.D. dissertation, Univer. of California, Los Angeles, CA 1972.

[6] S. Ben-Ari and J. R. Ellis, "The control of an articulated semitrailer vehicle," in *Vehicle Safety Legislation—Its Engineering and Social Implications*. London: Mechanical Engineering Publications Limited, 1975.

[7] D. L. Kleinman, S. Baron, and W. H. Levison, "An optimal control model of human response, part I: Theory and validation," *Automatica*, vol. 6, pp. 357–369, 1970.

[8] D. T. McRuer *et al.*, "New results in driver steering control models," *Human Factors*, vol. 19, pp. 381–397, Aug. 1977.

[9] D. H. Weir, R. J. DiMarco, and D. T. McRuer, "Evaluation and correlation of driver/vehicle data," vol. II, Final Tech. Rep., National Highway Traffic Safety Admin., DOT-HS-803-246, Apr. 197[illegible]

[10] R. G. Mortimer and C. M. Jorgeson, "Eye fixations of drivers as affected by highway and traffic characteristics and moderate dose of alcohol," in *Proc. Sixteenth Annu. Meeting, Human Factors Society*, Oct. 17–19, 1972, pp. 86–92.

[11] M. Kondo and A. Ajimine, "Driver's sight point and dynamics of the driver-vehicle-system related to it," SAE Paper No. 680104, Automotive Engineering Congress, Detroit, MI, Jan. 8–12, 1968.

[12] D. A. Gordon, "Experimental isolation of drivers' visual input," *Public Roads*, vol. 33, pp. 266–273, 1966.

[13] "Comparison of vehicle test procedures," Contract DRDA 781433, Highway Safety Research Institute, University of Michigan, 1978.

Journal of Dynamic Systems, Measurement and Control

Technical Briefs

An Optimal Preview Control for Linear Systems

C. C. MacAdam[1]

A technique for synthesizing closed-loop control of linear time-invariant systems during tracking of previewed inputs is presented. The derived control is directly dependent upon the properties of the controlled system and is obtained by minimization of a defined previewed output error.

I Introduction

This paper presents a general method of control synthesis applicable to linear time-invariant systems utilizing preview control strategies for regulation or tracking tasks. A common example of this type of dynamical behavior occurs during normal automobile path following in which drivers "look-ahead" to follow a desired path. A frequent source of preview control strategies in various man-machine systems is, of course, the human operator. It is widely recognized that human operators are capable of controlling and adapting to a wide variety of dynamical systems, many of which are vehicles with preview-oriented control requirements such as automobiles, bicycles, and complex aircraft [1-7]. Although this paper does not offer evidence as to the utility of the proposed control synthesis for man-machine systems involving preview strategies, it is suggested that the method presented here can be applied to such problems. Portions of the work by Tomizuka [8], which treated a similar problem, indicated useful application of optimal preview control methods in representing man-machine dynamical behavior.

The particular method presented in this paper is directly applicable to general linear system representations assumed to incorporate preview control strategies that depend only upon knowledge of the current values of the state and control. The optimal control is derived by minimization of a performance index that is defined as a mean squared preview output error. It will be shown that the derived control function is not arbitrary or independent but depends directly upon the dynamical properties of the controlled system.

II Statement of the Problem

Given the linear system

$$\dot{\mathbf{x}} = F\mathbf{x} + \mathbf{g}u \tag{1}$$

$$y = \mathbf{m}^T\mathbf{x} \tag{2}$$

where,

$\mathbf{x}$ is the $n \times 1$ state vector

y is the scalar output related to the state by the $n \times 1$ $\mathbf{m}^T$ constant observer vector transpose

F is the constant $n \times n$ system matrix

and

$\mathbf{g}$ is the constant $n \times 1$ control coefficient vector

find the control, $u(t)$, which minimizes a local performance index,

$$J \triangleq \frac{1}{T}\int_t^{t+T} \{[f(\eta) - y(\eta)]\, W(\eta - t)\}^2 d\eta \tag{3}$$

over the current preview interval $(t, t+T)$, where,

W is an arbitrary weighting function over the preview interval

and f is the previewed input.

The performance index given by (3) represents the weighted mean squared error between the previewed input and the previewed output as defined below.

The previewed output, $y(\eta)$, is related to the present state, $\mathbf{x}(t)$, by

$$y(\eta) = \mathbf{m}^T\phi(\eta, t)\mathbf{x}(t) + \int_t^{\eta} \mathbf{m}^T\phi(\eta, \xi)\mathbf{g}u(\xi)\, d\xi \tag{4}$$

where,

$$\phi(\eta, t) = \exp[F(\eta - t)]$$

is the transition matrix of the system F [9].

If $u(t)$ is assumed selected on the basis of a constant previewed control, $u(\xi) = u(t)$, equation (4) simplifies to

$$y(\eta) = \mathbf{m}^T\phi(\eta, t)\mathbf{x}(t) + u(t)\int_t^{\eta} \mathbf{m}^T\phi(\eta, \xi)\mathbf{g}\, d\xi \tag{5}$$

and the performance index, (3), can be written as

$$J = \frac{1}{T}\int_t^{t+T} \left\{\left[f(\eta) - \mathbf{m}^T\phi(\eta, t)\mathbf{x}(t) - u(t)\int_t^{\eta} \mathbf{m}^T\phi(\eta, \xi)\mathbf{g}\, d\xi\right] \cdot W(\eta - t)\right\}^2 d\eta \tag{6}$$

The above assumption simply requires the resulting optimization to reflect a control strategy dependent only upon current values of the state and control. This assumption is, in part, motivated by the potential application to those man-machine systems, wherein, it is assumed the human operator is limited in deriving or having knowledge a priori of more complex or optimal control waveforms over the preview interval.

The necessary condition for minimization of J, defined by

[1] Research Associate, University of Michigan, Highway Safety Research Institute, Ann Arbor, Mich. 48109

Contributed by the Dynamic Systems and Control Division of THE AMERICAN SOCIETY OF MECHANICAL ENGINEERS. Manuscript received at ASME Headquarters, July 9, 1980.

equation (6), with respect to the control, $u(t)$, is provided by $dJ/du = 0$, or

$$\frac{dJ}{du} = \frac{2}{T}\int_t^{t+T} \left\{\left[f(\eta) - \mathbf{m}^T\phi(\eta,t)\mathbf{x}(t) - u(t)\int_t^{\eta}\mathbf{m}^T\phi(\eta,\xi)\mathbf{g}\,d\xi\right]\right\} \cdot\left\{\int_t^{\eta}\mathbf{m}^T\phi(\eta,\xi)\mathbf{g}\,d\xi\right\} W(\eta-t)\,d\eta = 0 \tag{7}$$

Equating $\phi(\eta, \xi)$ with $\exp[F(\eta-\xi)] = I + \sum_{n=1}^{\infty} F^n \frac{(\eta-\xi)^n}{n!}$, where I is the identity matrix, and performing the $d\xi$ integrations, (7) becomes

$$\frac{dJ}{du} = \frac{2}{T}\int_t^{t+T} \left\{f(\eta) - \mathbf{m}^T\left[I + \sum_{n=1}^{\infty}\frac{F^n(\eta-t)^n}{n!}\right]\mathbf{x}(t) - (\eta-t)\mathbf{m}^T\left[I + \sum_{n=1}^{\infty}\frac{F^n(\eta-t)^n}{(n+1)!}\right]\mathbf{g}u(t)\right\}\left\{(\eta-t)\mathbf{m}^T \cdot\left[I + \sum_{n=1}^{\infty}\frac{F^n(\eta-t)^n}{(n+1)!}\right]\mathbf{g}\right\} W(\eta-t)\,d\eta = 0 \tag{8}$$

Solving (8) for $u(t)$ yields

$$u^0(t) = \left[\int_t^{t+T}\left\{f(\eta) - \mathbf{m}^T\left[I + \sum_{n=1}^{\infty}\frac{F^n(\eta-t)^n}{n!}\right]\mathbf{x}(t)\right\} \cdot\left\{(\eta-t)\mathbf{m}^T\left[I + \sum_{n=1}^{\infty}\frac{F^n(\eta-t)^n}{(n+1)!}\right]\mathbf{g}\right\} W(\eta-t)\,d\eta\right] \Big/ \left[\int_t^{t+T}\left\{(\eta-t)\mathbf{m}^T\left[I + \sum_{n=1}^{\infty}\frac{F^n(\eta-t)^n}{(n+1)!}\right]\mathbf{g}\right\}^2 W(\eta-t)\,d\eta\right] \tag{9}$$

where $u^0(t)$ represents the optimal solution. For the special case of $W(\eta - t) = \delta(T^*)$, the Dirac delta function for $0 < T^* \leq T$, (9) simplifies to

$$u^0(t) = \frac{f(t+T^*) - \mathbf{m}^T\left[I + \sum_{n=1}^{\infty}\frac{F^n(T^*)^n}{n!}\right]\mathbf{x}(t)}{T^*\mathbf{m}^T\left[I + \sum_{n=1}^{\infty}\frac{F^n(T^*)^n}{(n+1)!}\right]\mathbf{g}} \tag{10}$$

$$= [f(t+T^*) - y_0(t+T^*)]/(T^*K) \tag{11}$$

where

$$K \triangleq \mathbf{m}^T\left[I + \sum_{n=1}^{\infty}\frac{F^n(T^*)^n}{(n+1)!}\right]\mathbf{g}.$$

Equation (11) represents a proportional controller with gain inversely related to the preview interval, T^*, and operating on the error between the previewed input, $f(t+T^*)$, and $y_0(t+T^*)$, that portion of the previewed output deriving from the state vector's current initial condition. Likewise, equation (9) can be interpreted as a proportional controller operating on a similar error averaged and weighted over the preview interval $(t, t+T)$ by the additional terms appearing in equation (9).

The optimal solution, $u^0(t)$, can also be expressed in terms of any current non-optimal $u(t)$ and correspondingly nonzero preview output error, $\epsilon(t)$, by writing equation (9) as

$$u^0(t) = \left[\int_t^{t+T}\left\{f(\eta) - \mathbf{m}^T\phi(\eta,t)\mathbf{x}(t) - u(t)A(\eta)\right\} \cdot A(\eta)W(\eta-t)\,d\eta + u(t)\int_t^{t+T}A(\eta)W(\eta-t)\,d\eta\right] \Big/ \left[\int_t^{t+T}A^2(\eta)W(\eta-t)\,d\eta\right] \tag{12}$$

or

$$u^0(t) = u(t) + \frac{\int_t^{t+T}\epsilon(\eta)A(\eta)W(\eta-t)\,d\eta}{\int_t^{t+T}A^2(\eta)W(\eta-t)\,d\eta} \tag{13}$$

where

$$A(\eta) \triangleq (\eta-t)\mathbf{m}^T\left[I + \sum_{n=1}^{\infty}\frac{F^n(\eta-t)^n}{(n+1)!}\right]\mathbf{g}$$

$$\epsilon(\eta) \triangleq f(\eta) - \mathbf{m}^T\phi(\eta,t)\mathbf{x}(t) - u(t)A(\eta)$$

$$\phi(\eta,t) \triangleq I + \sum_{n=1}^{\infty}\frac{F^n(\eta-t)^n}{n!}$$

For the special case of $W(\eta-t) = \delta(T^*)$, as before, equation (13) reduces to

$$u^0(t) = u(t) + \frac{\epsilon(t+T^*)}{T^*K} \tag{14}$$

The formulation expressed by equation (13) can be useful in describing systems which do not achieve, though closely approximate, the optimal system behavior. Such cases may arise from limitations in achieving the precise optimal control due to time lags or dynamic properties inherent in the controller and not accounted for *a priori* in the optimization.

While equations (9) and (13) are equivalent mathematically, the latter deomonstrates an explicit relationship between the derived optimal control and the previewed output error function appearing in the performance index of the original problem formulation. Simply stated, the current control level is modified only in response to a nonzero function of the previewed output error, and, in this sense, analogous to an integral controller.

Finally, dependence of the derived optimal control upon the system $(F, \mathbf{g})$ properties is clearly demonstrated by the explicit presence of F and $\mathbf{g}$ in equations (9) and (13). Furthermore, information concerning stability of the closed-loop system utilizing the optimal preview control of equation (9) or (13) is provided by the characteristic roots of the constant matrix

$$F - \frac{\mathbf{g}\mathbf{m}^T\int_0^T\left\{\left[I + \sum_{n=1}^{\infty}\frac{F^n(\eta)^n}{n!}\right]\right\}\left\{\eta\mathbf{m}^T\left[I + \sum_{n=1}^{\infty}\frac{F^n(\eta)^n}{(n+1)!}\right]\mathbf{g}\right\}W(\eta)\,d\eta}{\int_0^T\left\{\eta\mathbf{m}^T\left[I + \sum_{n=1}^{\infty}\frac{F^n(\eta)^n}{(n+1)!}\right]\mathbf{g}\right\}^2 W(\eta)\,d\eta}$$

or

$$[F - \mathbf{g}\mathbf{c}^T] \tag{15}$$

where

$$\mathbf{c}^T = \frac{\mathbf{m}^T \int_0^T \left\{ \left[I + \sum_{n=1}^{\infty} \frac{F^n(\eta)^n}{n!} \right] \right\} \left\{ \eta \mathbf{m}^T \left[I + \sum_{n=1}^{\infty} \frac{F^n(\eta)^n}{(n+1)!} \right] \mathbf{g} \right\} W(\eta) d\eta}{\int_0^T \left\{ \eta \mathbf{m}^T \left[I + \sum_{n=1}^{\infty} \frac{F^n(\eta)^n}{(n+1)!} \right] \mathbf{g} \right\}^2 W(\eta) d\eta}$$

resulting from the substitution of (9) into (1). For the special case of $W(\eta) = \delta(T^*)$, (15) becomes

$$F - \left\{ \mathbf{g}\mathbf{m}^T \left[I + \sum_{n=1}^{\infty} \frac{F^n(T^*)^n}{n!} \right] / (T^* \cdot K) \right\} \tag{16}$$

III Summary

The optimal preview control model presented here offers a useful and direct method for representing closed-loop behavior of linear systems utilizing preview control strategies. The derived control is directly related to the properties of the linear system and the previewed input. Further, the method is formulated in terms of general linear system representations, thereby permitting applications to a wide variety of problems.

References

1 McRuer, D.T., et al., "New Approaches to Human-Pilot/Vehicle Analysis," Systems Technology, Inc., Tech. Rept. AFFDL-TR-67-150, Feb. 1968.

2 Wierwille, W.W., Gagne, G.A., and Knight, J.R., "An Experimental Study of Human Operator Models and Closed-Loop Analysis Methods for High-Speed Automobile Driving," *IEEE Trans. on Human Factors in Electronics*, Vol. HFE-8, No. 3, Sept. 1967, pp. 187-201.

3 Tanaka, K., Goto, N., and Washizu, K., "A Comparison of Techniques for Identifying Human Operator Dynamics Utilizing Time Series Analysis," *Proceedings of the Twelfth Annual Conference on Manual Control*, University of Illinois, Urbana, Ill., May 25-27, 1976, pp. 673-693.

4 Weir, D.H., "Motorcycle Handling Dynamics and Rider Control and the Effect of Design Configuration on Response and Performance," Ph.D. thesis, University of California, Los Angeles, 1972.

5 Ben-Ari, S., and Ellis, J.R., "The Control of an Articulated Semitrailer Vehicle," *Vehicle Safety Legislation—Its Engineering and Social Implications*, Mechanical Engineering Publications Limited, London, 1975.

6 Kleinman, D.L., Baron, S., and Levison, W.H., "An Optimal Control Model of Human Response, Part I: Theory and Validation," *Automatica*, Vol. 6, 1970, pp. 357-369.

7 McRuer, D.T., et al., "New Results in Driver Steering Control Models," *Human Factors*, Vol. 19, Aug. 1977, pp. 381-397.

8 Tomizuka, M., "The Optimal Finite Preview Problem and Its Application to Man-Machine Systems," Dissertation, MIT, Cambridge, Mass., Sept., 1973.

9 D'Angelo, H., *Linear Time-Varying Systems: Analysis and Synthesis*, Allyn and Bacon, Boston, 1970.

Asymptotic Theory of Freight Car Hunting

A. M. Whitman[1]

A simple formula is derived for the hunting speed of a freight car from an 8 degree of freedom linear model using asymptotic techniques. A comparison is made between the approximation and exact (numerical) solutions. The two agree within 10 percent for parameter values typical of present designs.

[1] Director of Research, Railroad Dynamics, Inc., Ardmore, Pa.

Present Address: Associate Professor, University of Pennsylvania, Philadelphia, Pa.

Contributed by the Dynamic Systems and Control Division of THE AMERICAN SOCIETY OF MECHANICAL ENGINEERS. Manuscript received at ASME Headquarters, July 9, 1980.

Introduction

The purpose of the present paper is twofold. The first is to obtain an analytic expression for the critical speed of a multidegree of freedom model of a freight car which is simple enough to convey physical insight into the hunting problem while at the same time complex enough to have validity for realistic vehicles. The second is to illustrate the simplification which can be effected in problems of this type by employing asymptotic methods. These methods are model independent and rely on the fact that the creep forces dominate the motion.

Previous work has included analytical studies of simple vehicles [1-2] and numerical solutions for realistic vehicles [3-4]. The present work can be viewed as a generalization and formal mathematical justification of the former, which although cleverly done are ad hoc by nature and seem to be restricted to systems with few degrees of freedom, and a specialization of the latter, giving the same results in the region of validity of the expansion but being restricted by nature to specific regions in parameter space. The utility of the present work is in the simple result which it yields. From this one can obtain physical insight into the phenomenon as well as easily calculable answers.

Model Description

We consider a model of the lateral dynamics of a freight car composed of a rigid car body pinned at either end to a truck. The pin connection transmits a linear damping moment (constant c'_f) between the car body and the truck. Each truck, see Fig. 1, is composed of 2 wheelsets, two rigid sideframes connected by ball joints to each wheelset, and a bolster, which contains the car connection (centerplate) at its midpoint, is constrained to move parallel to each wheelset by means of frictionless slotted pins in each sideframe, and is restrained from moving freely in that direction by 2 linear springs (constant k each) and dampers (constant c each) at each end. In the real system this restraint is provided by the shear stiffness of the bolster springs, whose primary function is to support the car weight, and the sliding of the friction wedges laterally. Further, because the springs and dampers are separated by a distance d, there is a moment tending to square the truck due to both the springs (constant $4kd^2$) and the dampers constant $4cd^2$). In addition, the bolster has mounted symmetrically with respect to the centerplate, constant contact sidebearings (constant k_B each) whose function is to provide a torsional spring restraint for the bolster relative to the car body (constant $2k_B w^2$). Actually the sidebearings also transmit a damping moment between the bolster and the car body (constant $2c_B w^2$); however, this has the same form as the centerplate moment and can be combined with it. There are eight degrees of freedom in this model and we will take as our independent coordinates x^F, ψ^F, β^F, u^F, x^R, ψ^R, β^R, u^R. Here the superscripts represent the front and rear truck coordinates, x is the axial displacement of the truck centroid relative to the track center line, ψ the yaw angle of each wheelset of the truck as a result of the kinematic constraint, β the trail angle of the truck, and u the bolster displacement relative to the truck centroid. The equations of motion, which have been derived elsewhere [5] and which are quite similar to others which have been discussed in the literature [4], are written here in dimensionless form in terms of sum and difference coordinates,

LATERAL STABILITY OF A CONTROLLED ARTICULATED VEHICLE - AN APPLICATION OF BIFURCATION THEORY IN VEHICLE DYNAMICS

Anton Stribersky and Charles C. MacAdam
The University of Michigan Transportation Research Institute
2901 Baxter Road - Ann Arbor, Michigan 48109, U.S.A.

MANY ACCIDENTS OF TRUCK-TRAILER COMBINATIONS are caused by loss of control of the vehicle. Therefore investigations of the dynamic lateral stability of such articulated vehicles are important. In the past, most of the engineering analyses of stability problems have only utilized linear stability theory. However, linear stability theory can be overly generous in identifying regions of stability for dynamic systems containing nonlinearities, such as the articulated vehicle dynamics problem being considered here. In brief, the physical phenomenon of interest in this paper is one in which the lateral stability threshold of the articulated vehicle is reduced and caused to occur at speeds below that ordinarily predicted by a purely linear analysis. For example, if articulated vehicles are driven under high forward speeds, a finite disturbing effect of a steady state straight-line motion can result in a starting of oscillations with catastrophically increasing amplitudes. The experimental results in Fig. 2 (I) show an example (c) of unstable vehicle behavior, caused from a finite steering disturbance, for a speed V much lower then the critical speed V_c. Thus, the need for a nonlinear analysis is clearly evident here. Recent application of nonlinear stability theory [1,2] to vehicle engineering problems is provided in references [4,5,7].

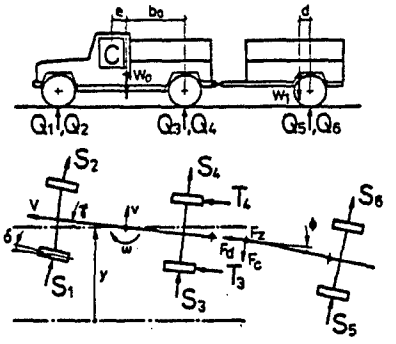

Fig.1: Mechanical model with three degrees of freedom y, γ, and φ.

This paper applies a nonlinear stability investigation to a truck, which is towing a single-axle utility trailer via its rear pintle hook on a flat horizontal road. The geometry of this articulated vehicle is shown in Fig. 1. We consider a symmetric vehicle. The location of the vehicle is described by the variables y, γ, and φ. The constant forward speed, V, and the loading condition of the trailer, measured by d, are the main parameters of the system. The lateral tire forces S_i, which are of particular importance for the stability analyses, are calculated applying an adhesion/sliding approach in the contact area between tire and road [7]. In order to perform an investigation of a vehicle-driver system (closed-loop system) a linear, preview-based driver model [6] is employed in the controlled-vehicle analyses.

In Fig. 2 (I) experimental results from three almost identical field tests are shown, differing only in the amplitude of the initial steering disturbance. Corresponding results from simulations of these transient vehicle responses are also drawn in Fig. 2 (II) for comparision. The simulations were done using the nonlinear Yaw/Roll Program [3]. Shown is the articulation angle, φ, between truck and trailer. Following a short steering disturbance, the vehicle should follow a straight-line path (y = 0).

But this is only possible for a sufficiently small disturbance. If the magnitude of the disturbance becomes too large, the amplitudes of the oscillations following the disturbance increase, and the vehicle behavior becomes unstable (in contrast to stability predicted by a purely linear analysis). Determination of the magnitude of disturbance needed to produce an unstable system response - for different forward speeds - can be performed using a nonlinear stability analysis.

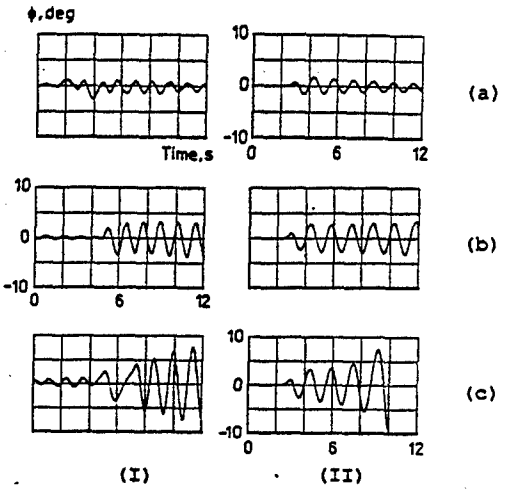

Fig.2: Comparison of measurment (I) and computer simulation (II) of transient vehicle responses of an equally loaded truck-trailer combination (d = - 0.436m) for a driving speed (V=17.9 m/s) much lower then the critical speed (V_c=22m/s).

Applying *Newton's* law, we can write the nonlinear equations of motion

$$W(x)\,\dot{x} = f(x,\delta) \quad , \qquad (1)$$

where $x^T = (y, v, \gamma, \omega, \phi, \dot{\phi})$ is the state vector, δ is the steering angle, and W(x) is a (nonlinear) 6 x 6 matrix. The straight-line motion is given by $\delta_0 \equiv 0$ and $x_0 \equiv 0$. It is obvious that the straight-line motion is an equilibrium position of system (1). After inverting the matrix W(x), which can be done by power series expansion with respect to this equilibrium position, we obtain

$$\dot{x} = F\,x + g\,\delta + n(x,\delta) \quad , \qquad (2)$$

where $n(x,\delta)$ contains the nonlinear terms.

Due to the steering of the driver, any deviation from the straight-line motion of the truck leads to a steering response δ. The position of the driver from the truck c.g. is located by the parameter e. The driver is modelled mathematically by an optimal preview control approach [6], which uses the linear part of equ. (2). The optimal control, $\delta_{opt}(t)$, minimizes the error between the desired straight-line motion and the predicted vehicle position, T seconds ahead in time. The predicted lateral position of the driver, $y_d(t+T)$, T seconds ahead, is derived from the observer vector $m^T = (1,0,e,0,0,0)$, the state vector's current initial condition, x(t), and the state transition matrix.

$$y_d(t+T) = m^T \left[I + \sum_{n=1}^{\infty} \frac{F^n T^n}{n!} \right] x(t) \qquad (3)$$

If the driver delay τ is modelled with a Padé polynomial, the steering input δ applied by the driver can be approximated by (s is the Laplace variable)

$$\delta = \frac{1 - \frac{\tau}{2} s}{1 + \frac{\tau}{2} s} \delta_{opt} \quad . \tag{4}$$

This linear driver model has been shown to be an effective means for representing actual human behavior during driving tasks. A time delay value τ of approximately 0.25 seconds is ordinarily used in this model to represent "average" driver behavior. Equ. (2) together with equ. (4) produces the closed-loop equations of motion:

$$\begin{pmatrix} \dot{x} \\ \dot{\delta} \end{pmatrix} = \begin{bmatrix} F & g \\ c^T(F - \frac{2}{\tau} I) & c^T g - \frac{2}{\tau} \end{bmatrix} \begin{pmatrix} x \\ \delta \end{pmatrix} + \begin{pmatrix} n(x,\delta) \\ 0 \end{pmatrix} \tag{5}$$

where

$$c^T = \frac{m^T \left[I + \sum_{n=1}^{\infty} \frac{F^n T^n}{n!} \right]}{T\, m^T \left[I + \sum_{n=1}^{\infty} \frac{F^n T^n}{(n+1)!} \right] g} \tag{6}$$

With $y^T = (x^T, \delta)$ we can write equ. (5) in the form

$$\dot{y} = A(\lambda)\, y + m(y,\lambda) \quad , \tag{7}$$

where we have now also introduced the parameter vector $\lambda^T = (V,d)$. The stability of the equilibrium position $y_0 = 0$ is guaranteed by a theorem of Liapunov, if all eigenvalues of the matrix $A(\lambda)$ have negative real parts. To find the critical forward speed, V_c, we calculate for a fixed loading condition, d, and a quasistatic increasing speed, V, the eigenvalues of the matrix $A(\lambda)$. The stability boundary is reached, if one or more eigenvalues cross the imaginary axis.

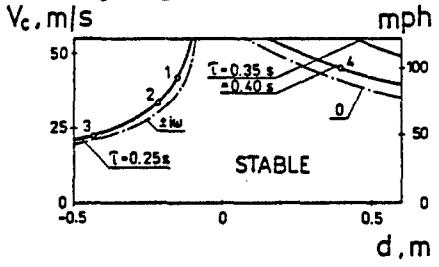

Fig.3: Stability boundary in the parameter space for the open-loop system (— · —) and the closed-loop system (——). See also Fig. 5.

Fig. 3 shows the stability boundaries for the open-loop and the closed-loop system. For the vehicle with a *fixed* steering wheel ($\delta = 0$),

$$y^T = (v, \omega, \phi, \dot{\phi}) \quad ,$$

a rearward located load can lead to an oscillatory type of instability, due to a purely imaginary pair of eigenvalues. The reason is a bifurcation of a limit cycle, which is called *Hopf* bifurcation. On the other side, positive values of d can lead to a divergent type of instability, caused by a simple zero eigenvalue. Fig.4 shows a time history of the articulation angle, ϕ, for a divergent unstable behavior of the vehicle after a steering disturbance.

For the *controlled* vehicle, a *Hopf* bifurcation (oscillatory type) is the only manner in which loss of stability of the straight-line motion can occur. The influence of the driver time lag, τ, upon critical speed is seen to be almost insignificant for the left branch of the stability chart (Fig. 3), indicating that the driver has little control over the oscillatory trailer motion, which dominates during this mode. However, on the right branch, the driver time lag is seen to play a very important role in determining the critical speed.

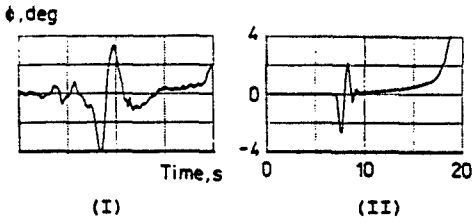

Fig. 4: Divergent time history of the articulation angle for the vehicle with a fixed steering wheel (d = positive) - (I) measurement, (II) computer simulation.

For one to investigate the nonlinear behavior, a change in coordinates $y \rightarrow z$ by $y = Tz$ is necessary as a first step in order to transform the matrix $A(\lambda)$ into diagonal form. The matrix T is given by the eigenvectors of the matrix $A(\lambda)$. *Center manifold theory* [1] allows us to reduce the system (7) to bifurcation equations [7]. (For the controlled vehicle a *Hopf* bifurcation always appears and leads to a two-dimensional bifurcation system.) In the case of a *Hopf* bifurcation, by introducing polar coordinates and applying the *averaging principle* [2], the two-dimensional bifurcation system can be transformed into the *normal form*

$$\dot{r} = v_1 r + K_3 r^3 + O(|r|^5) \quad . \tag{8}$$

Equ. (8) is an equation for the amplitude r of a limit cycle ($\dot{r} = 0$). The mathematical parameter v_1 is proportional to the physical parameter $\lambda_1 = (V - V_c)$, and K_3 is a constant for a given loaded vehicle. Fig. 5 shows amplitudes of the bifurcating unstable limit cycle for different loading conditions (1,2,3, and 4), following from equ. (8). The limit cycles border the attraction domains of the stable straight-line motion. As soon as a disturbance causes a crossing of the unstable limit cycle, an unstable vehicle response occurs. The limit cycles of Fig.5 result from an investigation of the system near the critical equilibrium point (V_c). Interestingly, the theoretical result of Fig.5 (limit cycle 3), when extrapolated to even lower forward speeds, shows good agreement with the corresponding measurements of the transient vehicle responses seen in Fig.2.

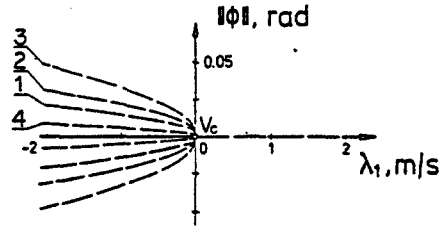

Fig.5: Amplitudes of unstable limit cycle solutions. The numbers correspond to Fig. 3. (——— stable, — — — unstable)

ACKNOWLEDGEMENT

This work has been supported by the Austrian "Fonds zur Foerderung der wissenschaftlichen Forschung" (J0260T), and by the "U.S. Army Tank Automotive Command" (DAAE07-85-C-R069).

REFERENCES

[1] Carr J., Applications of Centre Manifold Theory, *Applied Math. Sciences 35*, Springer-Verlag, New York, Heidelberg 1983.

[2] Guckenheimer J., P. Holmes, Nonlinear Oscillations, Dynamical Systems, and Bifurcation of Vector Fields, *Applied Math. Sciences 42*, Springer-Verlag, New York, Heidelberg 1983.

[3] Gillespie T.D., C.C. MacAdam, Constant Velocity Yaw / Roll Program: User's Manual, UMTRI-82-39, October 1982.

[4] Kacani V., A. Stribersky, H. Troger, K. Zeman, Dynamics and Bifurcations in the Motion of Tractor-Semitrailer Vehicles, *Conference Proceed. Canadian Math. Soc.*, Vol. 8 (F.V. Atkinson, W.F. Langford, A.B. Mingarelli, eds.), 1987, 485-499.

[5] Kacani V., A. Stribersky, H. Troger, Maneuverability of a Truck-Trailer Combination after Loss of Lateral Stability., *Proceed. of the 10th IAVSD-Symposium*, Prague, (M. Apetaur, ed.), Swets and Zeitlinger B.V., Lisse, 1988, 186-198.

[6] MacAdam C.C., Application of an Optimal Preview Control for Simulation of Closed-Loop Automobile Driving, *IEEE Transactions on Systems, Man, and Cybernetics*, Vol. SMC-11, No. 6, June 1981, 393-399.

[7] Stribersky A., P.S. Fancher, The Nonlinear Behavior of Heavy-Duty Truck Combinations with Respect to Straightline Stability, ASME *Journal of Dynamic Systems, Measurement, and Control*, Vol. 111, Nr. 4, December 1989 (to appear)

DISTRIBUTION LIST

	Copies
Commander U.S. Army Tank-Automotive Command ATTN: ASNC-TAC-DIT (Technical Library) AMSTA-CF (Dir. RDE center) AMSTA-CR (Technical Director) AMSTA-R (Dir. Tank-Automotive Technology) AMSTA-RY (System Simulation and Tech. Div.) Warren, MI 48397-5000	 2 1 1 1 20
Commander Defense Technical Information Center Bldg. 5, Cameron Station ATTN: DDAC Alexandria, VA 22304-9990	12
Manager Defense Logistics Studies Information Exchange ATTN: AMXMC-D Fort Lee, VA 23801-6044	2
Commander U.S. Army Operational Test and Evaluation Agency ATTN: CSTE-CS (Combat Support Div.) 5600 Columbia Pike Falls Church, VA 22041-5115	1
Deputy Commander U.S. Army Strategic Defense Command P.O. Box 1500 ATTN: DASD-H-S (Systems Anal./Battle Management Dir.) DASD-H-V (Advanced Technology Dir.) Huntsville, AL 35807-3801	2
Commander U.S. Army Foreign Science & Tech Center 220 Seventh Street NE ATTN: AIAST-RA (Research and Analysis Dir.) Charlottesville, VA 22901-5396	1
Director U.S. Army Cold Regions Research & Engineering Lab P.O. Box 282 ATTN: CECRL-IC (Technical Library) Hanover, NH 03755-1290	1

DISTRIBUTION LIST

	Copies
Director U.S. Army Corps of Engineers Waterways Experiment Station P.O. Box 631 ATTN: WESGV-Z (Geotechnical Laboratory) Vicksburg, MS 39180-0631	1
U.S. Army Laboratory Command Army Research Office P.O. Box 12211 ATTN: SLCRO-EG (Engineering Division) SLCRO-TS (Library Services) Research Triangle Park, NC 27709-2211	2
Director U.S. Army Ballistic Research Lab ATTN: SLCBR-D (Office of Director) Aberdeen Proving Grounds, MD 21005-5066	1
Director Harry Diamond Laboratories ATTN: SLCHD-IT (Eng. & Tech Support Div.) SLCHD-TA (Tech. Applications Div.) 2800 Powder Mill Road Adelphi, MD 20783-1197	2
Director U.S. Army Human Engineering Laboratory ATTN: SLCHE-D (Office of Director) SLCHE-SS-TS (Library) Aberdeen Proving Grounds, MD 21005-5001	2
Commander U.S. Army Material Command ATTN: AMCDE (Development, Eng, & Acqusition) AMCDMA-ML (Library) 5001 Eisenhower Avenue Alexandria, VA 22333-001	2
Commander U.S. Army Armament Munitions and Chemical Command ATTN: SMCAR-MS (Information Management Dir. - Tech Library) Picatinny Arsenal, NJ 07806-5000	1
Commander St. Louis Support Command ATTN: DACL/ASMC-STL-DACL (Library/Information Center) Granite City, IL 62040-1801	1

DISTRIBUTION LIST

	Copies
Director CECOM Research Development & Engineering Center ATTN: AMSEL-RD (Director) Fort Monmouth, NJ 07703-5001	1
Commander U.S. Army Missile Command ATTN: AMCPM (Land Combat Systems) AMSMI-CG (Reference Library) AMSMI-RD (Research, Dev. and Eng. Center) Redstone Arsenal, AL 35898-5000	3
Commander U.S. Army Cold Regions Test Center ATTN: STECR-MT (Materiel Test Dir.) Fort Greenly, AL	1
Commander U.S. Army Combat Systems Test Activity ATTN: Armament Systems Directorate Close Combat Systems Directorate Engineering Directorate Development & Analysis Directorate Aberdeen Proving Grounds, MA 21005-5059	4
Commander U.S. Army Yuma Proving Ground ATTN: STEYP-MT (Material Test Dir.) Yuma, AX 85364	1
Director TRAC-FLVN ATTN: ATRC-F Fort Leavenworth, KS 66027-5200	1
Director TRAC-WSMR ATTN: ATRC-W White Sands Missile Range, NM 88002-5502	1
Commander U.S. Army Center and Fort Knox ATTN: ATZK-DOTD (USAARMS Library) ATZK-CD (Dir. of Combat Developments) ATZK-AE-AO (Library) Fort Knox, KY 40121-5000	3

DISTRIBUTION LIST

	Copies
President U.S. Army Armor and Engineer Board Fort Knox, KY 40121-5470	1
President US Army Aviation Board ATTN: ATZQ-OTC (Technical/Operations Div.) Fort Rucker, AL 36362-5064	1
Director U.S. Army Combat Developments Experimentation Center ATTN: Technical Library; Bldg 2925 Fort Ord, CA 93941-7000	1
Commander U.S. Army Combined Arms Center and Fort Leavenworth ATTN: ATOR-CT (Scientific and Tech. Support Dir.) ATZL-CA (Combined Arms Combat Devl. Activity) Fort Leavenworth, KS 66027-5130	2
Commander TRADOC Combined Arms Test Activity ATTN: ATCT-MA (Methodology & Analysis Dir.) ATCT-SPT (Technical Library) Fort Hood, TX 76544-5065	2
President U.S. Army Communications-Electronics Board ATTN: ATZH-BDS (Analysis & Tech. Support Div.) Fort Gordon, GA 30905-5350	1
Commander U.S. Army Engineer Center and Fort Belvoir ATTN: ATZA-SS-LIB (Library) Fort Belvoir, VA 22060-5000	1
President U.S. Army Field Artillery Board ATTN: ATZR-BDS (Analysis and Tech. Support Div.) Fort Sill, OK 73503-6100	1
President U.S. Army Infantry Board ATTN: ATZB-IB-PR-T (Tech/Science Dir.) Fort Benning, GA 31905-5800	1

DISTRIBUTION LIST

	Copies
Commander U.S. Army Infantry School ATTN: ATSH-CD (Dir. of Combat Development) Fort Benning, GA 31905-5000	1
Commander U.S. Army Intelligence Center and School ATTN: ATSI-CD (Dir. of Combat Developments) Fort Huachuca, AZ 85613-7000	1
President/Commander U.S. Army Intelligence and Security Board ATTN: ATSI-BD-A (Analysis & Tech. Support Div.) Fort Huachuca, AZ 85613-7000	1
Commander U.S. Army Ordance Center and School ATTN: ATSL-CD (Dir. of Combat Development) ATSL-SE-LI (Library) Aberdeen Proving Ground, MD 21005-5201	2
Commander U.S. Army Ordance Missile and Munitions Center and School ATTN: ATSK-C (Dir. of Combat Developments) ATSK-AB (Library) Redstone Arsenal, AL 35897-6500	2
Headquarters U.S. Army Quartermaster Center and Fort Lee ATTN: ATSM-CD (Dir. of Combat Developments) Fort Lee, VA 23801-500095,96	1
Headquarters U.S. Army Troop Support Command ATTN: AMSTR-B (Systems Analysis Office) AMSTR-E (Research & Development Integration Office) 4300 Goodfellow Blvd. St. Louis, MO 63120-1798	2
Commander US Army Belvoir Research, Development, & Engineering Center ATTN: STRBE-BT (Technical Library Div) Fort Belvoir, VA 22060-5606	1

DISTRIBUTION LIST

	Copies
Commander U.S. Army Natic Research, Development, and Engineering Center ATTN: STRNC-ML (Technical Library) Natick, MA 01760-5000	1
Commander U.S. Army Development and Readiness Command 5001 Eisenhower Avenue ATTN: Dr. R. S. Wiseman Alexandria, VA 22333	1
Commander US Army Soldier Support Center National Capitol Region ATTN: ATNC-NMM-A 200 Stovall Street Alexandria, VA 22332-0400	1
HQDA Office of Dep Chief of Staff for Rsch Dev & Acquisition ATTN: ARZ-A Dr. Lasser - Dir. of Army Research DAMA-AR Washington, D.C. 20310	2
Commander U.S. Army Military Equipment R&D Command ATTN: DRDME-T Fort Belvoir, VA 22060	1
Commandant U.S. Army Engineer School ATTN: ATZA-CDT Fort Belvoir, VA 22060-5281	1
Commander Rock Island Arsenal ATTN: SARRI-LR Rock Island, IL 61201	1
Director U.S. Army Material Systems Analysis Agency ATTN: AMXSY-DD AMXSY-C (Mr. Harold Burke) AMXSY-CM (Mr. Fordyce) AMXSY-MP (Mr. Cohen) Aberdeen Proving Ground, MD 21005-5071	4

DISTRIBUTION LIST

	Copies
Director Keweenaw Research Center Michigan Technological University Houghton, MI 49931	1
Director Defense Advanced Research Projects Agency 1400 Wilson Boulevard Arlington, VA 22209	1
Commander U.S. Army Materials and Mechanics Research Center ATTN: Mr. Adachi Watertown, MA 02172	1
Director U.S.D.A. Forest Service Equipment Development Center 444 East Bonita Avenue San Dimes, CA 91773	1
Engineering Society Library 345 East 47th Street New York, NY 10017	1
Commander U.S. Army Armament Research and Development Command ATTN: Mr. Rubin Dover, NJ 07801	1
Commander USAMC Material Readiness Support Activity ATTN: AMXMD-ED (Equip Develop/Deploy Anal Br) Lexington, KY 40511-5101	1
Commander U.S. Army Logistics Center ATTN: ATCL-M Fort Lee, VA 23801-6000	1
Director TRADOC Systems Analysis Activity ATTN: ATOR-TF White Sands Missile Range, NM 88002-5502	1

DISTRIBUTION LIST

	Copies
Commander U.S. Army Test Evaluation Command ATTN: AMSTE-BB AMSTE-TA AMSTE-TE AMSTE-TD-T Aberdeen Proving Ground, MD 21005-5055	4
Commanding General U.S. Marine Corps Mobility & Logistics Division Development and Education Command ATTN: Mr. Hickson MCOTEA Quantico, VA 22134	2
Commander U.S. Air Force Tactical Air Warfare Center ATTN: TE Eglin AFB, FL 32542	1
Commandant U.S. Army Armor School ATTN: ATSB PERI-IK Fort Knox, KY 40121-5000	2
Commander US Army Transportation School ATTN: ATSP-TD Fort Eustis, VA 23604-5361	1
Commander US Army Training Support Center ATTN: ATIC-DM Fort Eustis, VA 23604-5166	1
President CDED Test Board ATTN: ATEC-B Fort Lewis, WA 98433-5000	1
Superintendent U.S. Military Academy ATTN: Dept. of Engineering West Point, NY 10996	1